Measuring and Modelling of Landfill Gas Emissions

by

April Lee Gowing

A thesis
presented to the University of Waterloo
in fulfilment of the
thesis requirement for the degree of
Doctor of Philosophy
in
Civil Engineering

Waterloo, Ontario, Canada, 2001

The University of Waterloo requires the signatures of all persons using or photocopying this thesis. Please sign below, and give address and date.

Abstract

Landfills start emitting landfill gas (LFG) shortly after waste placement and can continue for more than twenty years after the placement of the final cover and landfill closure. The concentration of LFG components will vary significantly over this period; therefore, in order to evaluate long-term impacts on the landfill workers, the surrounding public and the environment, a means to measure and model these emissions were developed in this research.

Flux chambers have been utilized for several years to measure the flux of various gases from soil surfaces. Many of the flux chambers have had problems with the pressure differential between the chamber and the atmosphere that has resulted in underestimation or overestimation of the true flux. The flux chamber developed in this research minimizes the pressure differential with a pressure transducer, process controller and peristaltic pump in a feedback loop. Laboratory evaluation of the system found that the pressure differentials were minimized with an average range of –0.036 to 0.009 mm H_2O over five experiments with nearly complete gas recovery (99%).

Flux measurements with the flux chamber performed at 3 different landfills exhibited excellent pressure control. The flux measurements of CH_4, TCE, PCE and H_2S obtained at the various landfills were dependent on the cover condition. The flux of CH_4 was 1 to 3 orders of magnitude lower from an intact cover than the equivalent flux measured at holes in the cover.

The Landfill Emission Simulation (LES) model, developed in this research simulated the production, transport and emission of CH_4, CO_2, vinyl chloride and H_2S from the landfill surface. The model evaluated the emission during the landfill construction until a user defined length after landfill closure. Contributions of holes and CH_4 oxidation in cover on the flux of these gases were also simulated. Oxidation in the top 0.3 m of the final cover was found to reduce the methane flux and increase the carbon dioxide flux.

Concentrations of vinyl chloride and H_2S at off-site points (100 m, 200 m, 500 m, 1000m) were predicted using the Gaussian Plume model and the emissions of vinyl chloride and H_2S generated from the LES model. These concentrations for the site investigated did not exceed the MOE ½ hour point of impingement standard.

Acknowledgements

I would like to acknowledge the invaluable assistance I received from Bruce Stickney, Mark Sobon, and Terry Ridgway during the laboratory and field component of my research. I would like to thank my supervisor Grahame Farquhar for his assistance, cooperation and understanding over the many years of my research. I would also like to thank Neil Thomson and Peter Slawson for their assistance and time to help with my research. NSERC, University of Waterloo and Region of Waterloo deserve thanks for providing the funds for this research. To all the Water Resources graduate students during my stay, thanks for your support and the good times. Finally, I would like to thank my husband Duncan Millar, for his love, support and encouragement through all the good and bad times.

Table of Contents

List of Tables

List of Figures

Chapter 1

1.0 Introduction

1.1 Background and Problem Definition

The production and release of gas from municipal solid waste landfills continues to generate strong environmental concerns. Historically, the focus of these concerns was on odours in the immediate region of the landfill and the risk of explosions in structures caused by the migration of landfill gas (LFG) through soil and buried infrastructure. While these are still important environmental issues, health risks associated with volatile organic compounds (VOCs) in LFG and harm to the atmosphere through the emission of greenhouse and ozone depleting gases, have also become prominent (Reinhart *et al.*, 1992).

The composition of LFG produced during the decomposition of municipal solid waste consists of approximately 50% V/V methane (CH_4), 50% V/V carbon dioxide (CO_2) and less than 1% V/V of other components including non-methane organic compounds (NMOCs) and hydrogen sulphide (H_2S). The potential for explosion is due to CH_4, the contribution to the greenhouse effect comes from CH_4 and CO_2, and the risk to health is associated with NMOCs and H_2S even though their concentrations are small relative to CH_4 and CO_2.

In 1994, 715 kilograms per person of waste were generated and landfilled in Canada (CCME, 1998). In 1996, approximately 432,900 tonnes of CH_4 were emitted from Canadian landfills, accounting for an estimated 26% of anthropogenic CH_4 emissions for that year (Neitzert, 1999). In 1995, it was estimated that Canadian landfills released an estimated 5,140 tonnes of VOCs based on the total concentration of 144 target VOCs emitted from six Ontario landfills ranging from 12 to 1,600 mg/m^3 (Mortazavi & Williams, 1995). Trichloroethylene (TCE), vinyl chloride (VC) and benzene, the most frequently detected VOCs, are toxic in sufficiently high concentration and are generally regarded to be carcinogenic, mutagenic and/or

teratogenic. Although the connections between LFG emissions and incidents of public health impact are difficult to document, concern over public health issues remains strong, particularly in situations of long-term, chronic exposure.

Human health risk estimates vary between landfills, Crouch *et al.* (1990) found that the average risk exposure for an individual living within 50 km ranged from 0.003 to 0.04 in a million for the eight landfills examined. In the worst-case, which corresponds to an individual living his or her entire lifetime 100 m from the edge of the landfill, Crouch *et al.* (1990) found that the maximum risk increased to 20 in one million. Goldberg *et al.* (1999) suggested that men living near a landfill are exposed to a higher risk of contracting cancer of the liver, kidney, pancreas, and non-Hodgkin's lymphomas than men who lived at more remote locations.

The United States Environmental Protection Agency (USEPA) requires that any new landfill with a waste capacity exceeding 2.5 million tonnes of waste or any landfill observed or expected to emit in excess of 50 tonnes NMOCs per year, install a LFG collection and treatment system. The Province of Ontario has similar requirements and recommends that a version of the Scholl Canyon model be used to estimate NMOCs emission rates (MOE, 1992). However, smaller landfills and many landfills existing prior to the imposition of the regulations may have no effective LFG control systems in place. In addition, LFG collection systems are seldom 100% effective in capturing LFG particularly during the years when the landfill is active and final cover is not in place. Consequently, current regulations have not completely eliminated the concerns related to LFG emissions.

Gases will be emitted from a landfill soon after initial waste placement and well before the placement of final cover; as well emissions can continue for more than twenty years after closure. The concentrations of the LFG components will vary significantly over this period, as will environmental conditions that affect the transport of the components off-site. These variable conditions make the long-term risk analysis of LFG exposure a highly uncertain process. There are no standard procedures available to estimate changing LFG component concentration over the evolution of a landfill and beyond the placement of final cover (Zeiss & Atwater, 1993).

1.2 Objectives of the Research

The primary objective of this research was to examine and model the emission and transport of LFG components to a receptor. The receptor concentrations would be input for the determination of the risk of exposure to LFG for the landfill workers, the surrounding public and the environment.

To achieve this primary objective, the following tasks were undertaken:

- Development of an accurate flux chamber suitable to monitor CH_4 and NMOCs emissions from landfill surfaces;
- Evaluation of the performance of the flux chamber under laboratory and field conditions;
- Measurement of the flux of CH_4 and selected NMOCs from the surface of three landfills;
- Assessment of the impact of intermediate cover and cover imperfections on LFG emissions;
- Development of a model that integrates the production and transport of LFG components from within the landfill through the surface and into the atmosphere over the lifetime of the landfill; and
- Determination of the NMOCs concentration at several points beyond the landfill boundary through the use of a Gaussian plume model.

1.3 Scope of Thesis

The measuring and modelling of landfill emissions was accomplished through the completion of the research activities listed above. Chapter 2 provides the theoretical background and standard practice in use to measure and model the landfill emissions and evaluate the risk of landfill gas emissions.

The first phase of the research involved obtaining accurate flux measurements from the landfill surface. To accomplish this, a flux chamber design was modified to provide more accurate estimates of landfill gas emissions. Chapter 3 presents the design and laboratory evaluation of the flux chamber used to measure emissions from the landfill surface.

Chapter 4 presents the evaluation of the flux chamber under field conditions and the flux measurements obtained from the three landfills. Landfill gas emissions from a landfill will be influenced by the conditions of the landfill surface. To evaluate the overall effect that this variation in emission will have on the public and environment, flux measurements were obtained from various landfill conditions. These conditions involved different waste age and cover conditions. The cover conditions examined consisted of intermediate and final cover and imperfections such as holes and cracks in the cover material.

These field flux estimates were used as a comparison to the flux estimates obtained from the model developed in this research. Chapter 5 develops and presents the fate and transport of the landfill gas emissions from within the landfill, to the landfill surface and beyond the landfill boundary. The model was developed to predict the flux of landfill gas components from the beginning of landfill construction to a user defined simulation period after landfill closure. Atmospheric dispersion of these flux estimates under various wind conditions were made to estimate the concentration of these NMOCs at several locations beyond the landfill boundary.

Finally, Chapter 6 presents the conclusions and recommendations of the research.

Chapter 2

2.0 Literature Review

2.1. Landfill Gas Production

2.1.1 Characteristics of Landfill Gas

Decomposition of emplaced MSW results in the initiation of production of LFG within a period of weeks to months. The composition of the gas shows a characteristic change in composition with time (Farquhar and Rovers, 1973) consisting of four distinct phases. The phases, shown in Figure 2.1, are: Phase I Aerobic; Phase II Anoxic, Non-methanogenic; Phase III Anaerobic, Methanogenic, Unsteady; and Phase IV Anaerobic, Methanogenic, Steady. Several factors will affect the rate, composition, and duration of each phase. Some researchers have added a fifth phase known as the Maturation Phase (Pohland & Harper, 1986).

The aerobic phase lasts only until all the oxygen in the refuse is depleted. During this stage, the aerobic microbes utilize the oxygen to produce carbon dioxide and generate significant amounts of heat. The LFG composition in this phase consists mainly of N_2 and CO_2. The next phases of biodegradation take place in the absence of oxygen. Phase II is characterized by a rapid rise in the carbon dioxide content and a fall in the nitrogen content. An increase in the hydrogen content can also be observed in this phase. In the last two phases, methanogenic bacteria generate methane from the primary products of acidogenic decomposition. These phases are characterized by an increase in methane and a decrease in carbon dioxide to a steady state in the final phase. The final composition of the landfill gas results in approximately 50 to 60 % V/V CH_4 and 40 to 50 % V/V CO_2 with a small quantity of NMOCs. Moisture content has not been included in this however most landfill gas is close to moisture saturation. The production of NMOCs will be discussed in Section 2.1.4.

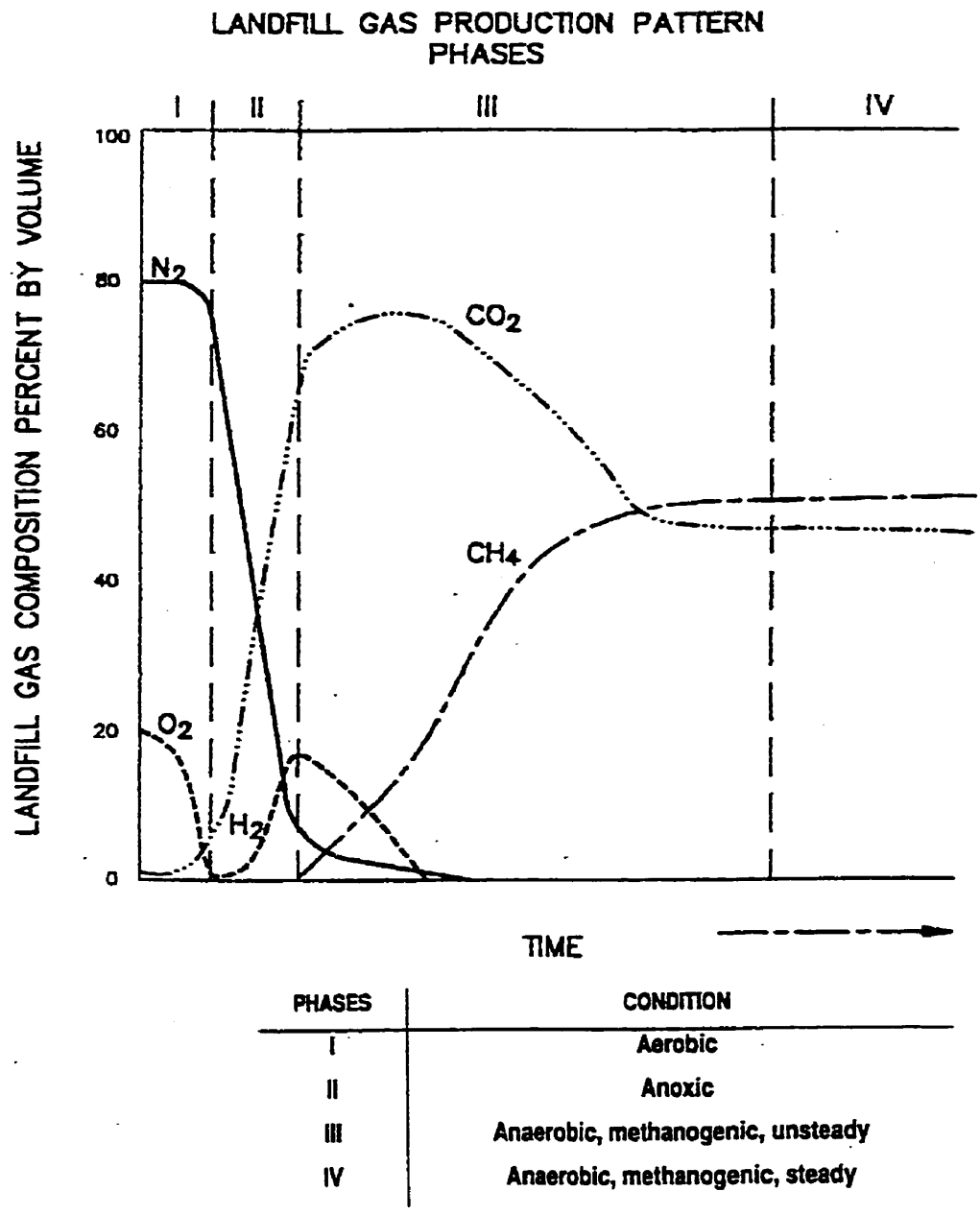

Figure 2.1: Landfill gas production patterns (adapted from McBean *et al.*, 1995)

2.1.2 Factors Affecting Production

Biological decomposition of MSW with LFG production can last for decades but the actual duration is dependent on many factors. Factors such as moisture content, nutrient content, pH, temperature, and density of the waste will affect the production of LFG. The moisture content of the waste provides a pathway for the necessary nutrients to become accessible to the gas producing organisms. The nutrient content of the waste is the second most essential parameter because the nutrients are required for the methanogenic bacteria to metabolize and grow. The quantities of available nutrients will determine the length of gas production. Other environmental parameters such as pH and temperature will also affect the activity of the bacteria. The methanogenic bacteria produce more effectively within an optimal range of pH (6.7-7.5) and temperature (mesophilic 30°C to 35°C, thermophilic bacteria 45°C to 65°C). Waste characteristics such as particle size and density can also affect the gas production rates. Figure 2.2 contains possible factors that affect gas production and their interactions. McBean *et al.* (1995) and Christensen *et al.* (1996) both provide more detail on the effects of these factors on methane production.

2.1.3 Characteristics of NMOCs in LFG

The main classes of trace gases found in LFG include the following (Brosseau & Heitz, 1994):

- Saturated and unsaturated hydrocarbons,
- Acidic hydrocarbons and organic alcohols,
- Aromatic hydrocarbons,
- Sulphur compounds, and
- Inorganic compounds.

Table 2.1 contains some of the NMOCs found in LFG based on a survey of 46 Californian landfills. Some of the landfills in the survey accepted hazardous and municipal solid waste into the landfill. This co-disposal of waste will result in higher emissions of NMOCs than municipal solid waste alone. The NMOCs shown in Table 2.1 are either known or suspected carcinogens; also the Ministry of Environment (MOE) recommended that the LFG be tested for these NMOCs (MOE, 1992). The quantity and types of NMOCs in LFG will vary among landfills depending on the waste content and age of the landfill.

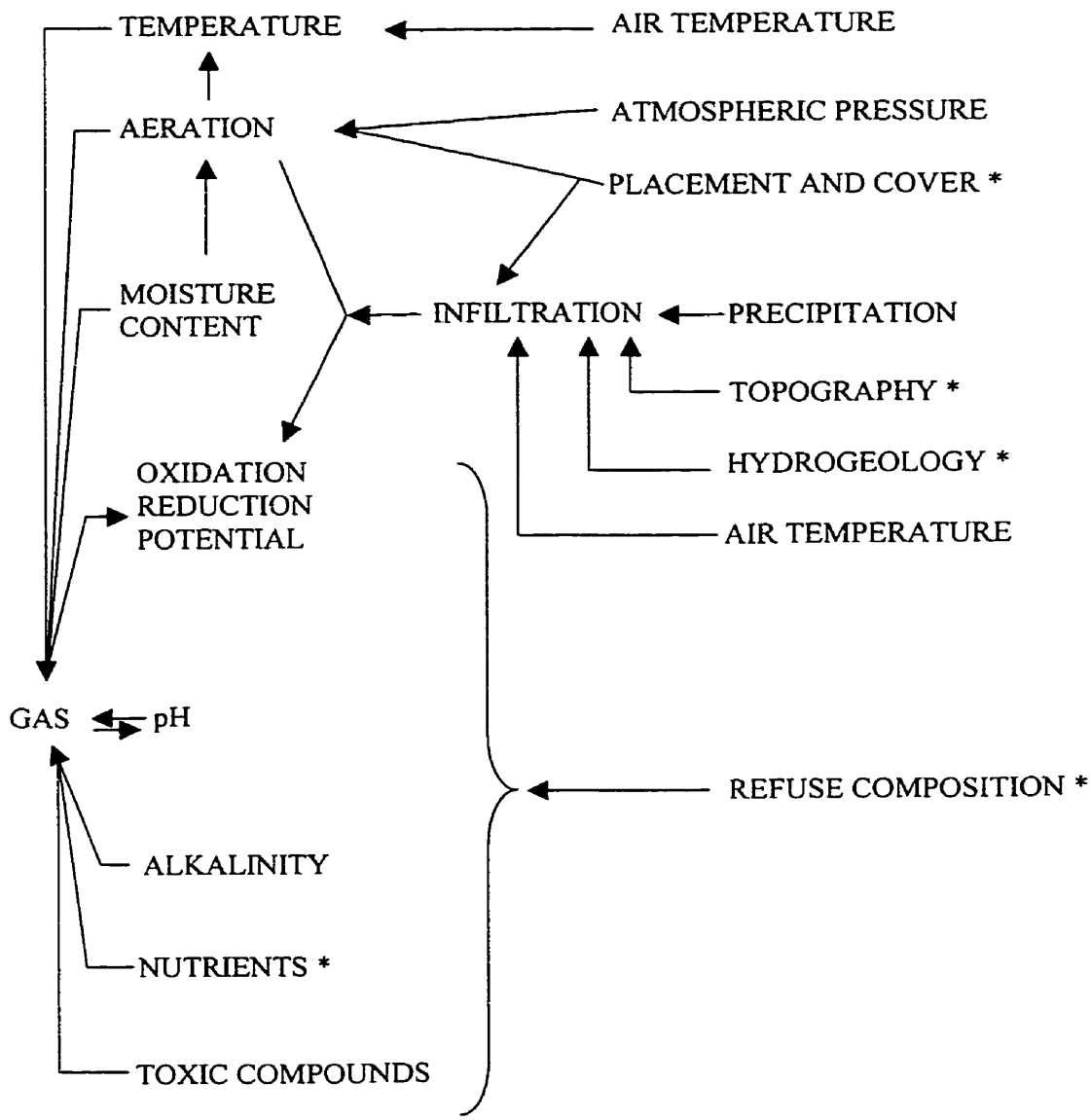

* FACTORS OVER WHICH SOME CONTROL MAY BE EXTERED DURING SANITARY LANDFILL DESIGN AND OPERATION.

Figure 2.2: Factors affecting gas production (adapted from McBean *et al.*, 1995)

Table 2.1: Summary of Non-methane Organic Compounds Found in Landfill Gas in a Survey of 46 California Landfills (USEPA, 1991)

Chemical Name	Average Concentration ($\mu g/m^3$) (ppm)	Range of Concentrations ($\mu g/m^3$)	
		Low	High
Toluene	214,431 (51.6)	841	3,188,660
Methylene Chloride	74,655 (19.7)	ND	659,390
Tetrachloroethene	52,906 (7.15)	ND	569,753
Vinyl Chloride	19,630 (7.05)	ND	134,124
1,2-Dichloroethene	22,016 (5.09)	ND	366,363
Trichloroethene	22,277 (3.8)	58.6	199,322
Benzene	12,267 (3.52)	ND	181,911
Hexane	11,572 (3.01)	ND	96,112
Carbon Tetrachloride	10,227 (1.49)	ND	473,586
1,2-Dichloroethane	4,636 (1.05)	ND	132,894
1,1,1-Trichloroethane	4,107 (0.69)	ND	53,573
1,1-Dichloroethene	692 (0.16)	ND	13,409
Chloroform	320 (0.06)	ND	8,309

ND – Not Detected

2.1.4 Production of NMOCs

Several studies have reported hazardous volatile organic compounds (VOCs, a subset of NMOCs) in emissions from municipal solid waste landfills. These materials originate from the vaporization of the hazardous materials brought into the landfill or from the biological and/or chemical decomposition of the materials deposited in the landfill. The chemicals that most readily vaporize are the compounds with low water solubility and high vapour pressure (*i.e* high Henry's law constants). These organic compounds will vaporize until vapour equilibrium is reached within the landfill. Any changes in temperature or confining pressures within the landfill will affect the equilibrium concentration of these compounds. Biological decomposition, the second process of NMOC production, takes place when microbes break down organic compounds for metabolic change. For example, vinyl chloride can result from

the biological decomposition of trichloroethene and dichloroethene (Vogel & McCarty, 1985; Kromann *et al.*, 1998). Biological decomposition depends on the structure of the compound, the metabolic requirements of the microbes, and the site-specific environmental conditions (Shen *et al.*, 1990). Trace concentrations of NMOCs make them more susceptible to biodegradation (Lang & Tchobanoglous, 1989). A third possible mechanism for the formation of NMOCs is the chemical reaction of waste materials or degradation products present in the landfill (USEPA, 1991); however, the extent to which this mechanism leads to NMOC emissions is not well defined. Figure 2.3 provides a schematic of the pathways and fate of hazardous pollutants in U.S. MSW.

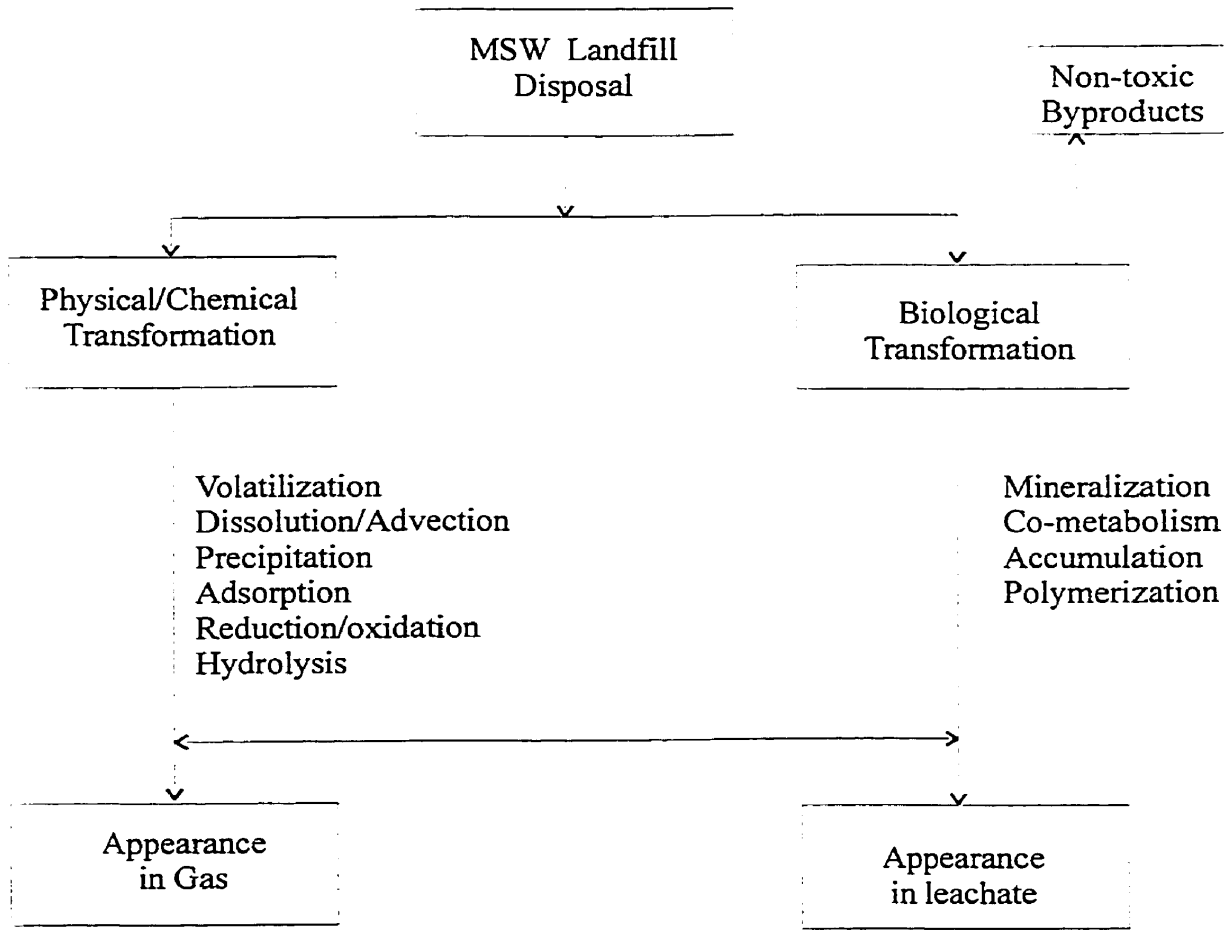

Figure 2.3: Pathways and Fate of Hazardous Pollutants in U.S. MSW (adapted from Reinhart, 1993)

2.1.5 Potential Sources of NMOCs

Production of NMOC emissions by all the above mechanisms is dependent in part on the composition of the waste. Young and Parker (1983) indicated that the origins of many of the NMOCs were uncertain although compounds such as halogenated carbons are present in the waste at deposition and compounds such as benzene, toluene and vinyl chloride appear to be derived from a placed waste source and decomposition products. During a laboratory scale study, Thomas and Barlaz (1999) indicated that the volatization of hazardous organic compounds were not the sole source of NMOCs in landfill gas and that anaerobic biodegration intermediates also contributed to NMOCs. Several potential sources of NMOCs in MSW are as follows: (Reinhart, 1993)

- household hazardous waste,
- illegally disposed regulated hazardous waste,
- waste disposed by small quantity hazardous waste generators,
- hazardous waste disposed prior to enactment of hazardous waste regulations, and
- innocuous waste transformed during normal stabilization process.

Where residential waste contributes to the majority of the MSW, household hazardous wastes have been estimated to represent less than 0.5% of the MSW in landfills (Reinhart, 1993). These potential sources have resulted in up to 100 NMOCs being detected in landfill gas emissions. Many major compounds detected in landfill leachate and gas are produced during the biotransformation of less mobile organics. Several phenolic compounds are biodegradation products of lignin, a major component of plant tissue. Many halogenated aliphatic compounds are transformed under anaerobic conditions.

2.1.6 LFG Production Models

LFG production is dependent on the amount of degradable organic waste present in the landfill. It is possible to predict the total production of CO_2 and CH_4 from specific MSW components; however, the complexity and variability of MSW makes it very difficult to predict LFG production rates based on detailed analysis of MSW. This has led to the development of more general models to simulate the production rate of LFG. The majority of the LFG generation models in landfills are based on first-order kinetics; the four "classic" models are: the constant rate model, the Sheldon-Arleta model, the Scholl Canyon model and the EMCON

MGM model. The four models are illustrated in Figure 2.4 (Richards *et al.*, 1992). One limitation of all the models is that each considers a batch of waste at time zero, although two of the models have a time lag due to the early aerobic phase (Lamborn, 1997). This limits practical use of these models as the waste is placed over a considerable time, often years.

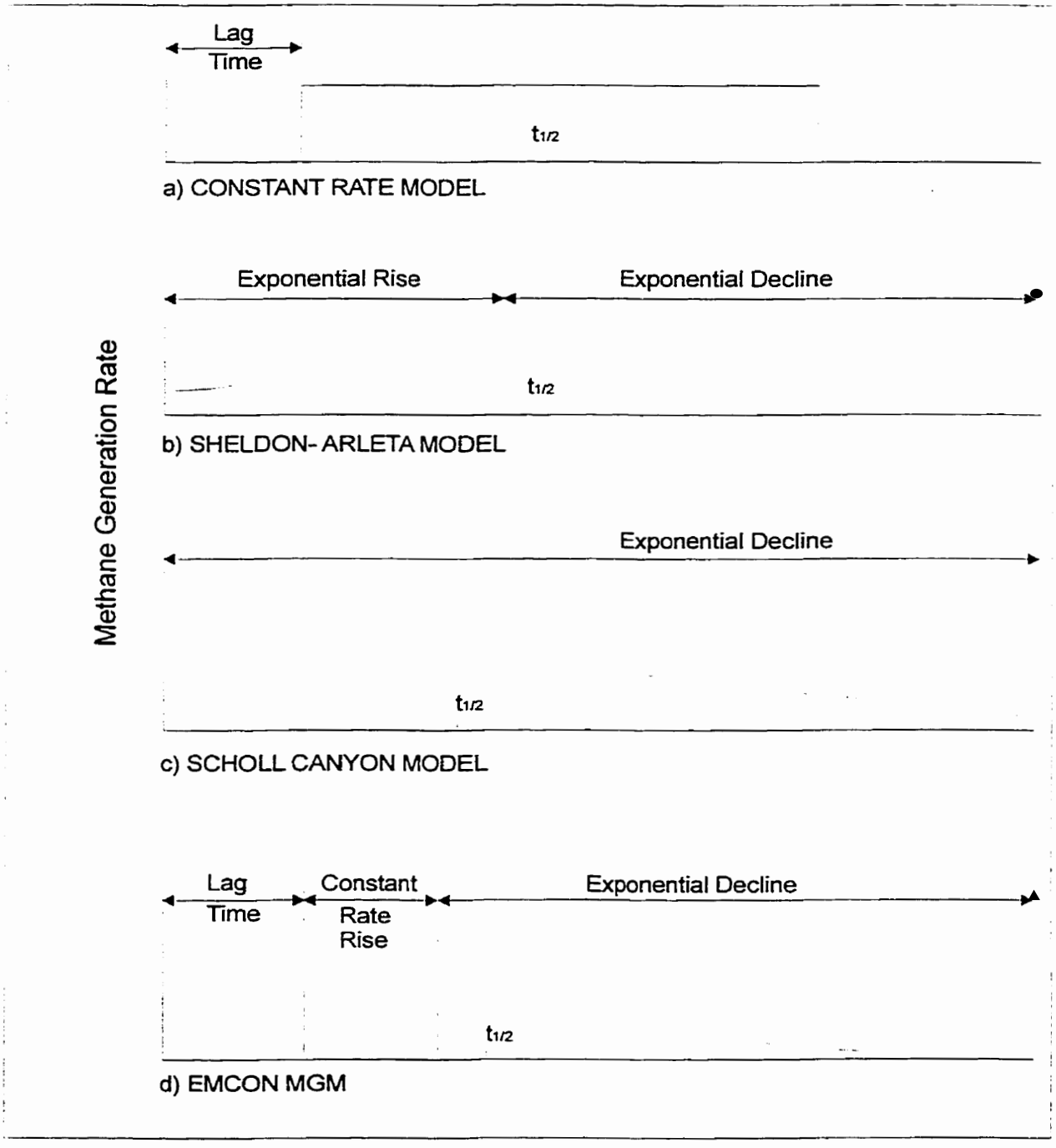

Figure 2.4: Landfill Gas Generation Models (adapted from Richards *et al.*, 1992)

The model which has received the majority of the attention, is the Scholl Canyon model because it has been adapted for use by the USEPA into its tiered approach for estimating the NMOC emissions from landfills. The Scholl Canyon model was developed to predict the quantities of CH_4 produced at a landfill in order to size utilization facilities (EMCON, 1980). The production of CH_4 is estimated using a first-order kinetic equation with the following assumptions:

- After a limited duration, during which anaerobic conditions are initiated, the gas production is assumed to be at its peak, and
- Thereafter, the gas production is assumed to decrease exponentially as the organic fraction of the landfill decreases (RWDI, 1993).

The MOE also utilizes this model to estimate the emissions of NMOCs in the Interim Guide to Estimate and Assess Landfill Air Impacts (MOE, 1992).

2.2 Emission of NMOCs from Landfills

The physical/chemical characteristics of NMOCs and the reactive processes in a landfill will determine the mobility, fate, and quantity of the NMOCs present in the waste (Reinhart, 1993). Table 2.2 contains a brief list of estimated emission rates of NMOCs from landfills found in the literature.

Table 2.2: Summary of VOC emissions from landfills found in the literature

Source	VOCs	Emission Rate
Shen *et al*, 1990	total VOCs	4×10^{-5} to 1×10^{-3} kg/m^2/ d
USEPA, 1991	total VOC (emission factor)	13.6 tonnes/10^6 tonnes/yr. (dry) to 35.4 tonnes/10^6 tonnes/yr. (wet)
Bennett, 1987	Subsurface total VOC	35 tonnes/10^6 tonnes

Note: Emission rate units are in various forms due to the different methods of reporting. The values were obtained from secondary sources and it is difficult to convert the values without the original USEPA documents

2.2.1 Methods of Transport

Air quality at the receptor location is a critical factor in assessing the effects of the NMOC emissions from landfills. The air quality is dependent on the emission rate and the atmospheric

transport of the NMOCs. Major gas emissions at landfills are from surfaces such as the working face and intermediate covered sections particularly through cracks in the surfaces. from various on site structures, and from gas collection and venting systems. The rate of emission of LFG is affected by convection, displacement, and molecular diffusion. Convective flow is considered to be the dominant flow mechanism. The production of CH_4 and CO_2 during decomposition increases the internal gas pressure, which results in the convective transport of all gases towards the surface. The displacement of the gas occurs due to the compacting and settling of the waste, ambient pressure changes and fluctuations in the moisture content of the cover. Thibodeaux *et al.* (1982) found that fluctuations in atmospheric pressure can enhance movement of benzene by approximately 13%. Molecular diffusion is the dominant transport mechanism for NMOCs when convective flow is small such as through an engineered cover with a flexible membrane liner.

Significant factors affecting the emission rate of NMOCs are site conditions (type of cover, depth of cover, compaction of cover), presence of decomposition gas, weather conditions (wind speed, temperature, relative humidity, barometric pressure, precipitation, solar radiation) and soil/waste characteristics (physical state of contaminants, sorption properties of the soil, soil moisture content, volatile fraction of the waste, microbial activity) (Shen *et al.*; 1990). Thomas and Barlaz (1999) found that NMOC concentration in synthetic and MSW reactors peaked before the onset of active gas production. This suggests that volatilization may be the dominant factor for NMOC production in the early stages of refuse decomposition. Table 2.3 summarizes these factors and which transport mechanism they affect.

The site conditions can contribute to the control of NMOC releases. The cover may act as a "bio-filter", although this mitigative effect may not apply to all NMOCs. Field studies indicate that 10-20% of the methane permeating a landfill cover is consumed by CH_4 oxidizers and levels up to 60% have been reported in laboratory simulations (Humer & Lechner, 1999). The presence of oxygen and methane and adequate soil moisture and ambient conditions contribute to the existence of the obligate methanotrophic microorganisms (Börjesson & Svensson, 1997a). The effectiveness of methane oxidation is dependent on the status of the cover; the presence of cracks or holes provides an alternative path for landfill gas escape without oxidation (Scharff & Hensen, 1999). The possibility exists that some of the NMOCs could

Table 2.3: Factors affecting transport mechanisms (USEPA, 1991)

Mechanism	Factors affecting mechanism
Molecular diffusion through soil cover	- Soil porosity - Concentration gradient - Diffusivity of Constituent - Soil thickness
Molecular diffusion through boundary layer	- Wind speed - Concentration gradient - Diffusivity of constituent
Biogas convection	- Nutrient availability for bacteria - Refuse composition - Moisture content - Age of landfill - Oxygen availability - Industrial waste acting as biological inhibitor - Temperature - PH - Presence of gas collection system
Displacement due to compaction and settlement	- Amount of compaction practiced - Compatibility of waste - Overburden weight (settlement)
Displacement due to barometric pressure changes	- Changes in atmospheric pressure
Displacement due to moisture content fluctuations	- Rate of precipitation - Rate of evaporation - Horizontal versus vertical permeability - Presence of a liner

also be oxidized in a similar manner. Slow degradation of TCE and TCA in the presence of methane has been observed during batch experiments (Kjeldsen *et al.*, 1996). Also, the soil cover may retard the release of the gases to the atmosphere but it will not contain the LFG permanently (MOE, 1992). The cover is anticipated to have a finite capacity for filtering the NMOCs that may be exceeded by their production from the landfill. Karimi *et al.* (1988) found that the soil matrix did not have a significant effect on the emission of benzene from a simulated landfill.

The presence of a collection system will also affect the emission rate of the NMOCs. A collection system often consists of vertical wells extending into the landfill. A negative

pressure then applied to the wells will extract the LFG out of the waste and into the collection system. A collection system results in changes in the vertical and horizontal movement in the LFG. It provides a reduction in the lateral movement of the LFG off-site. The controlled movement of the LFG will also result in reduced emissions through the cover; although, the degree of reduction is dependent on the collection efficiency of the system. The collection efficiency of the system is dependent on the coverage of the system, integrity of the final landfill cover and other factors. Based on a study of four landfills, Cook *et al.* (1991) concluded that the collection system could reduce not only gaseous VOCs but also the VOC contamination of the leachate. While monitoring methane emissions at nine US landfills, Mosher *et al.* (1999) found that 100% areal coverage of a gas collection system was effective at reducing atmospheric emissions. Börjesson and Svensson (1997a) found that the average methane emissions rose from 0.16 g $CH_4/m^2/h$ to 0.90 g $CH_4/m^2/h$ during an interruption in activity of the horizontal gas extraction system.

2.2.2 Models of Transport Emission

A summary of the major models that have been developed to date to simulate emission of NMOCs from landfills is presented in Table 2.4. The first three models are based on Fick's Law and involve steady-state diffusion, therefore ignoring the effects of bio-gas production on the movement of the VOCs. The models by Thibodeaux (1981), Thibodeaux *et al.* (1982) and El-Fadel *et al.* (1989) considered the effects of biogas production on the movement of the NMOCs to the surface of the landfill (Seigneur *et al.*, 1989), although, they ignored the sorptive process in the landfill. During the transport to the surface, NMOCs can be adsorbed/desorbed by the surrounding solid/liquid phases. Seigneur *et al.* (1989) developed a model to account for the release of NMOCs from landfill sites with and without biodegradation processes, using material balance and thermodynamic considerations. The model describes the transport of gases in the presence of liquid and gaseous phase in the porous spaces. Popov and Power (1994) developed a two dimensional model that accounts for gas movement in the multi-layers of a landfill. El-Fadel *et al.* (1995) incorporated the effects of temperature (heat generation during production) on the movement of gas through a 1-D multi-layered landfill. Lin and Hildemann (1995) developed a 1-D nonsteady-state analytical model to predict the

Table 2.4: Summary of Major Models of Volatile Toxic Emissions from Landfill Sites (Seigneur *et al.*, 1989)

Reference	Application	Model Formulation
Farmer *et al.*, 1980*	Volatile emissions from covered landfills	Fick's Law of steady state diffusion One dimensional No landfill gas production
Shen, 1982 & Farino *et al.*, 1983*	Worst case volatile emissions from covered landfills with a variety of chemical wastes	Fick's Law of steady state diffusion One dimensional No landfill gas production All pore space is available for diffusion Chemical is at saturation equilibrium wrt vapour
Thibodeaux, 1981	Volatile emissions from covered landfills with internal gas generation	One cell, one dimensional Diffusion Mean internal gas velocity (advection) Prandtl's mixing length theory
Thibodeaux *et al.*, 1982	Volatile emissions from covered landfills with internal gas generation	One cell, one dimensional Diffusion Gas generation term (advection) Atmospheric pressure fluctuations
El-Fadel *et al.*, 1986	Internal gas production	One dimensional Diffusion & Advection Gas generation
Seigneur *et al.*, 1989	Volatile emission from landfills with & without gas generation	One dimensional Diffusion & Advection Gas generation Adsorption/Absorption
Popov & Power, 1994	Emission of gases from a multi-layer landfill	Two dimensional Diffusion & Advection Gas generation
El-Fadel *et al.*, 1995	Internal gas production	One dimensional Diffusion & Advection Gas & heat generation
Lin & Hildemann, 1995	VOC emission from landfill	One dimensional nonsteady state Diffusion & Advection Degradation & Absorption in 3 phases (gas, liquid & solid)
Bogner *et al.*, 1997a	Methane flux from surface	Three dimensional Mass transport (diffusion, convection, microbial composition or production, aqueous solubility of individual gases)

* original source Seigneur *et al.*, 1989

emission of VOCs from the landfill. Degradation and absorption of the VOCs into the liquid or soil were incorporated into the model. Bogner *et al.* (1997a) developed a 3-D model to evaluate the methane flux from the landfill cover surface. The movement of methane is evaluated by mass balance that considers the diffusion, convection, microbial composition or production and aqueous solubility in the soil matrix.

These emission transport models have contributed to the 1-D model developed in Section 5.

2.2.3 Atmospheric Transport of NMOCs in LFG

Once the emissions of the NMOCs have been estimated the next step is to determine the effects of atmospheric conditions on the concentration of the NMOC. The atmosphere will transport and disperse the NMOCs to the point of exposure. In most cases of landfill risk assessment the point of exposure is a receptor (*i.e.* residence) close to the landfill; the boundary of the landfill or the receptor can be considered by the MOE to be the point of impingement (POI).

The atmospheric dispersion of gaseous emissions is dependent upon many interrelated factors such as the physical and chemical nature of the contaminant, the meteorological characteristics of the environment, the nature of the release (*i.e.* stack or surface release) and the terrain downwind of the release point.

The topography of a landfill, which simulates a hill, will affect the mean flow of the wind. The change in flow will affect the dispersion of the pollutants in the area (Taylor *et al.*, 1987). The flow generally speeds up over the crests of hills and slows down on the lee and backs of hills. On the leeward side of "steep" hills, a wake region may form and vortex shedding may occur (Crooks & Ramsay, 1993). The change in flow over hills affects dispersion in the following ways: the streamlines of the mean flow converge and diverge, which leads to increases and decreases, respectively, in concentration gradients, and to decreases and increases respectively, in plume widths; the distance between mean streamlines and the ground decreases, leading to higher ground level concentration; the turbulence is distorted causing changes in turbulent entrainment, leading to changes in concentration, gradients of concentration, plume widths, mean plume position and surface deposition (Crooks & Ramsay, 1993). These perturbations in mean flow and dispersion may be small enough to be ignored in a simple model. The effects

of flow over hills was examined in the research to determine if they are significant enough to alter a simple modelling approach.

One of the most important meteorological characteristics is atmospheric stability; this will determine the amount of dispersion that will occur to the NMOCs prior to the POI. There are three general classes of stability: unstable, neutral and stable. A stable atmosphere is one, which does not exhibit much vertical mixing or motion. As a result, pollutants emitted near the earth's surface tend to remain there. Whether much mixing occurs on a significant scale in the lower atmosphere is primarily dependent upon the temperature gradient and the mechanical turbulence due to the shearing action of the wind (Wark & Warner, 1981). The wind speed, solar radiation and cloud cover have been used to classify the stability of the atmosphere into six stability classes as shown in Table 2.5. Appendix I contains figures that define the spread of the contaminant plume away from the centreline as a function of the downwind distance and stability class.

Table 2.5: Key to Stability Categories (Wark & Warner, 1981)

	Day			Night	
	Incoming Solar Radiation			Cloud Cover	
Surface Wind Speed at 10 m (m/s)	Strong	Moderate	Slight	Mostly Overcast	Mostly Clear
Class [a]	(1)	(2)	(3)	(4)	(5)
<2	A	A-B	B	E	F
2-3	A-B	B	C	E	F
3-5	B	B-C	C	D	E
5-6	C	C-D	D	D	D
>6	C	D	D	D	D

[a] The neutral class, D, should be assumed for overcast conditions during the day or night. Class A is the most unstable and class F is the most stable, with class B moderately unstable and class E slightly stable.

2.2.4 Dispersion Modelling of LFG

Current models of short range dispersion of airborne pollutants from area sources are generally based on modifications of the Gaussian plume model (Chitgopekar *et al.*, 1990). The model assumes a Gaussian or normal spread of the pollutant from its source that is symmetrical about the mean. The model neglects diffusion in the direction of plume travel, which is a valid assumption if the release of the chemical is continuous (McBean *et al.*, 1990). The modified Gaussian Plume Model that determines the concentration for an elevated source is

$$C(x,y,z,H) = \frac{Q}{2\pi u\sigma_y\sigma_z}\exp\left[-\frac{1}{2}\left(\frac{y^2}{\sigma_y^2}\right)\right]\left\{\exp\left[-\frac{1}{2}\left(\frac{(z-H)^2}{\sigma_z^2}\right)\right]+\exp\left[-\frac{1}{2}\left(\frac{(z+H)^2}{\sigma_z^2}\right)\right]\right\} \quad (2.1)$$

where:

C = concentration ($\mu g/m^3$)

Q = emission rate ($\mu g/s$)

u = mean velocity of wind in x direction (m/s)

σ_y = standard deviations of plume concentration in the horizontal direction (m)

σ_z = standard deviations of plume concentration in the vertical direction (m)

y = distance centre line (m)

z = distance above centre line (m)

H = vertical mixing height of plume (m)

This equation assumes that the origin is at ground level with the x-axis extending horizontally in the mean wind direction. The y-axis and z-axis are perpendicular to the x-axis horizontally and vertically. The standard deviations of the plume concentration in the horizontal and vertical directions are functions of the distance downwind (x) and the stability of the atmosphere. Atmospheric conditions including wind speed and solar radiation or cloud cover are used to determine a stability category.

Baker & Mackay (1985) used four dispersion models to estimate ambient vinyl chloride concentrations around a landfill. They recommended the use of virtual point source models based on the Gaussian plume model, although they found the accuracy of the dispersion calculations were affected by the emission rates. The virtual point source approach is potentially subject to significant inaccuracy very close to the source. Chitgopekar *et al.* (1990) developed a model based on K-theory for describing the short range air dispersion from area sources of non-buoyant toxics. The K-theory model was evaluated against the four models used by Baker & Mackay (1985). The K-theory model was found to best reproduce the observed vinyl chloride concentrations near a southern Californian landfill. Venkatram & Seigneur (1993) reviewed several atmospheric models for estimating chemical concentration in health risk assessment. They made recommendations for the selection of models suitable for

screening and refining risk assessments. The models reviewed included commercial models such as the Industrial Source Complex model.

2.3 Measurement of Landfill Gas Emissions

2.3.1 Landfill Gas Emissions

As indicated in the section below, there are several methods that have been used to measure landfill gas emissions. Table 2.6 presents a summary of the emissions found in the literature. The emissions obtained by the various methods range from an average of –0.001 to 6.144 g $CH_4/m^2/d$. The negative values obtained by the static chamber method were caused by the oxidation of atmospheric methane by the landfill cover soil. The condition of the landfill such as the presence of gas recovery, waste age, and cover material will contribute to the variation in the landfill gas emissions. The following sections will briefly discuss the various methods of flux measurement with an emphasis on flux chamber methods.

2.3.2 Methods of Measurement

Shen *et al.* (1990) and Balfour *et al.* (1987) provide an overview of the direct and indirect methods used to measure surface emissions. The direct methods use flux chambers and head space samplers to monitor emissions from the landfill. The indirect methods involve measurement of the ambient air for the compounds downwind of the landfill. Savanne *et al.* (1997) did a comparison of several of the different methods for measuring landfill methane emissions. They compared two accumulation chambers, two micrometeorological techniques (eddy correlation and mass balance methods), two trace gas methods and an airborne infrared thermography. Mosher *et al.* (1999) measured methane emissions at nine landfill using chamber and/or tracer flux techniques. They compared these techniques at two landfills and found less than 10% difference between the methods. Indirect method cannot be applied in all situations, as the presence of interfering methane sources in the immediate vicinity of a landfill may make it difficult or impossible to adequately separate sources downwind (Mosher *et al.*, 1999). The variability in emissions from the landfill surface can be measured using the more labour intensive flux chamber method.

Emission flux measurements provide an estimate of the amount of a single gas species of a multiple species gas being emitted from a given surface area per unit time (Eklund, 1992).

Table 2.6: Some measurements of methane emissions from landfills

Location	Method	Conditions	Flux (g CH_4/m^2 per day) Min.	Max	Mean (*n*)	Reference(s)
New Hampshire, USA						Czepiel
Site 1	Static	No gas rec.	-0.03	1500	58 (139)	(1996a:Czepiel
Site 2	chamber		0	215	12(92)	unpubl.)
Site3	w/o collar		-0.06	433	14(111)	
Site 4			-0.02	4560	274(106)	
Site 5			-0.01	2050	48(124)	
Site 1	SF6 tracer	No gas rec.			0.68	
Illinois, USA						
Proximal, (6/95-2/95)	Static chamber	Silty clay cover soil	-4.10^{-4}	-0.43	-0.006 (22)[a]	Bogner *et al.* (1997)[#]a
Distal		optimised gas rec.	-6.70^{-4}	-0.092	-0.011 (25)[a]	
Proximal(Spring 94)	Static	Same	-2.50^{-4}	-0.002	-0.001 (5)[a]	Bogner *et al.*
Distal	chamber –c		-0.001	-0.004	-0.002 (6)[a]	(1995)[#]
Proximal(93,transect)	Static	w/gas rec. start-	0	0.007	0.003 (12)[a]	Bogner *et al.*,
Distal	chamber	up phase	3.2	29.8	19.7[b] (29)[a]	(1993)[#]
Proximal(93,transect)	Vert. Conc.	Same- dry			0.012[b]	Bogner *et al.*,
Distal, Dry	Gradient				32.9[b]	(1993)[#]
Distal , Wet					108[b]	
California, USA						
Proximal (1994)	Static chamber –c	Sandy silt cover soil w/gas rec.	0.4	11.7	4.03 (18)[a]	Bogner *et al.*, (1995)[#]
		Clayey silt cover soil w/gas rec.	2.00^{-4}	1	0.004 (9)[a]	
Same area, no wells (1988)	Static chamber	Sandy silt cover soil	320	1910	1120 (8)[a]	Bogner *et al.*, (1995)[#]
	Vert. Conc. Gradient	(dry) w/o gas rec.	1670	1880	1730 (8)[a]	Bogner *et al.*, (1992)[#]
UK (26 sites)	Static chamber	Winter	6.10^{-4}	4.3	0.48 (16)	Gregory &
		Summer	0.003	29.3	3.6 (10)	Skennerton, (1997
		Clay cover	0.003	4.3	0.7 (11)	unpubl.)[#]
		Sand/LPDE	0.005	0.025	0.01(3)	
		Other soil cover	6.10^{-4}	29.3	2.9 (12)	
		Age < 10 y	6.10^{-4}	4.3	0.39 (17)	
		Age > 10 y	0.002	29.3	4.1 (9)	
		No gas rec.	6.00^{-4}	5.2	1.3 (9)	
		Partial gas rec.	0.002	29.3	2.9 (11)	
		Full gas rec.	0.003	0.03	0.01 (6)	
Tennessee, USA	Eddy correlation	No gas rec.			6.5	Myers *et al.* (1992)[#]
Moscow, Russia	Static chamber	No gas rec.			34	Nozhevnikova *et al.* (1993)[#]
Sweden						
Hökhuvud	Static				0.33	Börjesson &
Hogbytorp	chamber				-0.003	Svensson (1993)[#]
Netherlands						
VAM site	Dynamic		2.6	746		Verschut *et al.*
AURI site	chamber		6.9	3000		(1991)[#]
ARN site			0.1	214		
VAM site	Micromet.		51.4	398		
AURI site	(gradient)		17.1	386		

Table 2.6: (continued)

Location	Method	Conditions	Flux (g $CH_4/m^2/d$) Min.	Max	Mean (*n*)	Reference(s)
Japan						
H-1	Static chamber	Dense veg			0	Tanaka *et al.* (1997) [-]
		Sparse veg.			0	
		No veg.			9.3	
H-2		Dense veg			0	
		Sparse veg.			2.2	
		No veg.			235	
H-3		Cover soil			7.7	
		Slope cover soil			20.7	
		Waste no cover			0.6	
Luleå ,Sweden						Maurice &
Mar 7/96	Static	No gas rec	0.088	3.156	0.745 (9)	Lagerkvist. (1997)
May –Dec /96	chamber				<0.044 (59)	[-]
France						
	Static chamber				89	Savanne *et al.* (1997) *[-]
					82	
	Tracer gas				63 ± 22	
					52 ± 17	
	Eddy correlation				1.5 ± 0.5	
	Mass balance				23 ± 7	
Italy						
Pecantia Landfill	Static	No gas rec.	1.89	443		Cossu *et al.* (1997)* [+]
	Dynamic		962	1,132		
Netherlands						
Naurena	Plume	No gas rec.			9	Scharff & Henson (1999) [+]
Hollandse Brug	transect				7	
Ontario, Canada						
Ridge Road ,E. Hill	Dilution	No gas rec.	0	10,344	137	Williams & Williams (1995)* [+]
Ridge Road ,W. Hill	tube		0	9,023	219	
Brockville			17	86	39.3	
Florida, USA						
Central Florida		No gas rec.				
Site 1-green	Dynamic				29	Walker (1991) [+]
Site 1-brown	Flux				6144	
Site 2- A1	chamber				6.8	
Site 2- A2	w/o collar				162	
Site 2- A1-1	Dynamic		BDL	158	33.9	Rash (1992) [+]
Site 2- A1-2	Flux		BDL	1578	239.8	
Site 2- A1-3	chamber w/		6.03	1206	266.1	
Site 2- A1-4	collar		BDL	305	84.9	
Site 2- A2			BDL	509	108.9	
Alachua County LF	Flux tube		9.8	159	74.5	Paladugu (1994)[+]
Sweden						
Hagby	Static chamber	Gas rec.	-0.023	335		Börjesson & Svensson (1997a) [+]

[a] *n* values are for daily means (2-6 flux measurements per day). [b] Based on geometric mean of conc in profile w/: with; w/o without; gas rec.: pumped gas recovery in operation; proximal: near gas rec. well; distal: between wells; -c: with collar; LPDE: low density polyethylene; veg.: vegetation; BDL: below detection limit; * data reported as normalized volume converted to mass by multiplying by density of methane at 25 °C and 1 atm. (# Original source, Bogner *et al.*, 1997b;+ with additions)

Flux chamber techniques consist of trapping the gas as it leaves the soil surface. either by allowing the gas to build up in a closed enclosure (closed or static chamber technique). or by removing and measuring the gas as it leaves the enclosure (open or dynamic chamber technique) (Perera *et al.*, 1999). The main drawback of the closed chamber technique is the influence of the chamber itself on the flux rate. The method tends to underestimate the gas fluxes by as much as 55% due to the increase in concentration as the gas accumulates in the chamber (Matthias *et al.*, 1978). The dynamic flux chamber eliminates the problem due the concentration build up by passing an inert sweep gas through an inlet at the base of the chamber. The disadvantage of this process is that an increase or decrease in the internal pressure of the chamber above ambient pressure (Kanemasu *et al.*, 1974) will lead to significant underestimation or overestimation of emissions from the surface.

2.3.3 Dynamic Flux Chamber Theory and Operation

There have been several models of flux chambers (Eklund *et al.*, 1985; Reinhart *et al.*, 1992; Gao *et al.*, 1997; Sadek *et al.*, 1998) used to monitor many types of emissions from all types surfaces (Millison *et al.*, 1991; Roelle *et al.*, 1999; Guo *et al.*, 2000). The use of an enclosed chamber for the measurement of the gases released from soil and plant surfaces has widely been practiced in the soil and biological sciences (Roelle *et al.*, 1999), has only recently been applied to the investigation of volatile hazardous emissions from land treatment facilities (Dupont, 1987; Reinhart *et al.*, 1992; Bogner *et al.*, 1997c).

The USEPA published a user's guide for the measurement of emission rates from land surface using a flux chamber (Kienbusch, 1986). An evaluation of the method indicated that a negative bias problem exists in the measurement of emission by flux chambers (Gholson *et al.*, 1989). Although a dynamic flux chamber tends to underestimate or overestimate the emission rate from the surface, the method still provides the only direct means of measuring the emission rates. Reinhart *et al.*, (1992) suggested that a bigger opening for the outlet reduces this effect. This research also examined the bias aspect of flux chambers and the results are presented in Chapter 3.

The general theory behind the operation of a flux chamber is as follows. Clean dry sweep air is added to the chamber at a fixed controlled rate that is selected based on site conditions (Eklund *et al.*, 1985). This sweep air mixes with the LFG emanating from the surface and

transports these gases through an exit port. The concentration of the emitted species of interest are measured in the exit gas, which are then used to calculate the emission rate of each species. The emission rate is expressed as

$$E_i = \frac{C_i R}{A} \tag{2.2}$$

where:

E_i = emission rate of component i, ug/m^2/sec

C_i = concentration of component i in the effluent air flow, ug/m^3

R = flow rate of air through the chamber, m^3/sec

A = surface area enclosed by the chamber, m^2.

All parameters in the above equation are measured directly.

The size and volume of the chamber should enclose a surface area as large as is feasible so that the observed emission flux is not unduly biased by relatively small areas of unrepresentative emissions. This is also needed so that the areas perturbed by the chamber edge or seal are a small percentage of the total sampling area, and that wall effects are minimal. The optimal chamber geometry is one that promotes the most complete mixing of the chamber atmosphere in the briefest possible time.

The standard protocol specifies the following generic sampling procedure: (Eklund, 1992)

- Establish a grid system over the area to be sampled
- Randomly select six or more points to be sampled
- Begin sweep air flow
- Record time, meteorological conditions and temperature
- Place clean enclosure on emitting surface and insert into ground
- Monitor emissions and note when steady-state concentrations are reached
- Record air and surface temperatures inside the chamber
- Collect samples
- Remove enclosure

The residence time, τ, is defined as the chamber volume divided by the sweep air flow rate. It typically takes three to four residence time before steady-state concentrations are reached inside the camber and sampling can be initiated. The sweep air flow rate can be varied to

achieve the desired analytical sensitivity. The slower the flow rate, the lower the detection limit, but the longer it takes to reach steady-state concentrations within the chamber (Eklund. 1992).

2.4 Regulations on Air Emission from LFG

Although, there is no direct regulation of emissions from landfills in Canada, it does fall under the general regulations of the Environmental Protection Act (EPA). The federal government establishes ambient air quality objectives and encourages the provinces to adopt them as binding standards (Phyper & Ibbotson, 1991). Control of air pollution sources falls under the provincial jurisdiction of the EPA.

2.4.1 Ontario Provincial Regulations on Air Emissions

The Environmental Protection Act of 1971 is a broadly worded piece of legislation directed toward the protection and conservation of the natural environment (Phyper & Ibbotson, 1991). Air quality and atmospheric emissions are addressed specifically in the EPA by Regulation 337 (formerly 296) and Regulation 346 (formerly 308). Regulation 337 contains ambient air quality criteria for 23 compounds. Regulation 346 relies on dispersion to dilute the contaminants so that they do not exceed the values set out in Schedule 1 at prescribed locations called point of impingements. Point of impingement (POI) is defined as the closest place where discharges from one property can affect others, usually a place on the boundary of the property on which the discharge occurs. Section 6 of the regulation requires that no person shall cause or permit to be caused the emission of any air contaminant to extent or degree as may: (Phyper & Ibbotson, 1991)

- cause discomfort to persons,
- cause loss of enjoyment of normal use of property,
- interfere with normal conduct of business, or
- cause damage to property.

The MOE has also introduced the Clean Air Program (CAP) to eliminate the use of dispersion as a way of dealing with air pollution. The CAP will require that:

- The primary means of controlling emissions will be at the source rather than allowing their dilution in the air

- Emissions of toxic pollutants would be virtually eliminated
- Atmosphere would not be used as a disposal facility for pollutants.

Landfill air emissions are required to comply with the above regulations and meet the Ambient Air Quality Criteria (AAQC) at the points of impingement. Table 2.7 contains the AAQC of selected contaminants found in landfill air emissions. Regulation 232/98 fills in the gaps of previous legislation on atmospheric emission of landfill gas. The regulation requires the mandatory collection of landfill gas for new or expanding sites with a total waste disposal

Table 2.7: Ambient Air Quality Criteria and Point of Impingement Limits for Air Contaminants. (Taken from Summary of Point of Impingement Standards, Ambient Air Quality Criteria (AAQCs), and Approvals Screening Levels (ASLs) Standards Development Branch, MOE, June 1994a)

Contaminant Name	CAS No.	Point of Impingement Standard		Ambient Air Quality Criteria (AAQC)	
		Half Hour Point of Impingement Limit ($\mu g/m^3$)	Status	24 Hour ($\mu g/m^3$)	Annual ($\mu g/m^3$)
Benzene	71-43-2		CARC		
Carbon tetrachloride	56-23-5	1800	IS	600	
Chloroform	67-66-3	1500	IS	500	
Dichloroethylene, cis-1,2-	156-59-2	315	ASL	105	
Ethylene dibromide	106-93-4	9	ASL	3	
Ethylene dichloride	107-06-2	1200	IS	400	
Methylene chloride	75-09-2	5300	IS	1765	
Perchloroethylene	127-18-4	10000	IS	4000	
Trichloroethane, 1,1,1-	71-55-6	350000	S	115000	
Trichloroethylene	79-01-6	85000	S	28000	
Vinyl chloride	75-01-4	3	IS	1	0.2
Vinylidene chloride	75-35-4	70	IS	35	

Notes:
IS - Interim Standards- (guidelines, provisional guidelines tentative standards & interim standards)
S - Standards
ASL- Approvals Screening Level
CARC- Carcinogen- no assigned standard or interim standard (emissions to environment prevented or limited)

capacity greater than 3.0 million cubic meters (approx. 2.5 million tonnes of waste) (MOE, 1998). With global warming concerns, the advent of greenhouse gas credits will be implemented in the near future which will make it prudent for all landfills to minimize all forms of landfill gas emissions.

2.4.2 Interim Guide to Assess Impacts of Landfill Air Emissions (MOE, 1992)

The purpose of the interim guide is to present MOE's recommended approach to estimating emission rates and environmental impacts from landfill gas emissions to the atmosphere. Procedures to estimate the emissions of landfill gas contaminants, landfill odours and dust impacts are contained within the document. The guideline produced by the Air Resources Branch of MOE in 1992 is utilized to model the gas emission from a landfill and determine if the site is of significant concern and therefore should follow the requirement in O.Reg 232/98 for gas collection.

The MOE's recommended emission estimating procedure is based on the USEPA's three tiered assessment program. All three tiers utilize a first-order kinetic LFG production model. The first tier utilizes the first-order kinetic model based on the Scholl Canyon Model, landfilling history, and default parameters selected by the MOE to estimate the landfill gas generation rate and NMOC emissions. Table 2.8 contains the default values suggested by the MOE for use in the model.

Table 2.8: Default Values for the Scholl Canyon Model (MOE, 1992).

Constant	Default Value	Reference
k	0.04 1/year (based on wet climate ≥ 23 inches)	USEPA memo dated April 15/92, revision from Federal Register
L_o(methane)	125 m^3/tonne	same as above
C_{NMOC} (vinyl chloride)	18.7 ppm-volume	see note below

Note:
Default value of C_{NMOC} is based upon a 95-percentile value from a compilation of vinyl chloride concentration data in LFG from 46 MSW landfills in the US emission estimates

Tier 2 and 3 require field investigation to replace the default values suggested by the MOE. The default NMOC parameter in the model is replaced in both the second and third tier. The landfill gas generation rate constant default is also replaced in the model in Tier 3.

The first-order kinetic NMOC Emission model is

$$Q_T = \sum_{i=1}^{n} 2 * 3.595E-09 * k * L_o * M_i * C_{NMOC} * \exp(-k * t_i) \qquad (2.3)$$

where:

Q_T = Total emission of specific NMOC (tonnes/year)
k = Landfill gas generation rate constant (1/year)
L_o = Methane generation potential (m^3/tonne)
M_i = Mass of refuse in the i^{th} section (tonnes)
C_{NMOC} = Concentration of specific NMOC (ppm-volume)
t_i = Age of the i^{th} section (year)
n = number of sections of waste
3.595E -09 = conversion factor based on Hexane as the average NMOC

Since, the conversion factor uses hexane as the average NMOC; emissions of a specific NMOC are obtained by multiplying Q_T by a ratio of the molecular weights (molecular weight of specific NMOC to molecular weight of hexane). If the deposition history is not known. an alternative equation is available to estimate the emissions of specific NMOCs.

The next step in the assessment process is to determine the dispersion concentration for comparison to the Ministry Point of Impingement Limits. The dispersion models recommended by the MOE are the Air Resources Branch CAP Model, the Industrial Source Complex Model and the Fugitive Dust Model. These are commercial models which can be utilized for different emitting sources such as ground sources or stacks in several different environments (*i.e.* urban, coastal situations).

2.4.3 US Regulations on LFG Emissions

Presently, 27 states have laws regulating the air emissions from MSW landfills. However, these laws generally deal only with the concentration of methane not NMOCs in or near the landfill. California is the only State to implement air emission regulations for landfills under the state's air pollution control authority; all other states regulate emissions under solid waste laws. The Clean Air Act (CAA) promulgated by the USEPA regulates NMOC emissions for existing and new landills (Federal Register, Vol. 61, No. 49 March 12, 1996). The New Source Performance Standards in the CAA requires that sites containing more than 2.5 million megagrams (Mg) and 2.5 million m^3 or more of waste must collect and control LFG it their estimated emission of NMOCs are 50 Mg or more per year.

The implementation of this regulation in the States may introduce further restriction on the LFG emissions from Ontario landfills.

2.5 Risk Analysis

The previous section discussed the regulations imposed on the hazardous emissions from MSW landfills. The air quality standards used by the MOE are selected based on the risk associated with the inhalation exposure to these compounds. This section will deal with defining and describing risk and the risk assessment process for landfill air emissions.

2.5.1 Risk and the Risk Assessment Process

Risk may be considered as the probability of an adverse effect, or an assessed threat to persons, the environment, and/or property, due to some hazardous situation (Asante-Duah. 1993). In a generic sense, risk assessment is defined as a systematic process for making estimates of all the significant risk factors that prevail over an entire range of failure modes and/or exposure scenarios due to the presence of some type of hazard (Asante-Duah, 1993). It is the determination of the probability that an adverse effect will result from a defined exposure. It may be expressed as the product of the probability of occurrence, (p) and the consequences or severity of occurrence, (S)

$$\text{Risk} = p * S. \qquad (2.4)$$

A hazard may pose risk to people through several possible pathways, therefore the risk assessment process was developed in order to quantify all the risk associated with all pathways for all particular hazards.

The risk assessment process will generally help identify and quantify risks imposed on an individual, the general public, and/or the environment. The U.S. National Academy of Science (NAS) has organized the risk assessment process into four steps (Page & Donahoe, 1993). The four components in a risk assessment are hazardous identification, exposure assessment, dose-response, and risk characterization.

Hazardous identification or data collection and evaluation (as identified by the USEPA) consists of evaluating the potential adverse effects of hazardous situations to which some populations are potentially exposed (Asante-Duah, 1993). In a risk assessment of MSW gas emissions, this will consist of the identification of contaminant emission sources and the selection of the NMOCs of potential concern. In most cases, the compounds identified as carcinogenic or teratogenic are the ones selected.

Exposure assessment consists of developing or identifying realistic exposure scenarios for the specific problem. An exposure pathway analysis examines the ways by which a receptor is exposed to, or impacted by, a source of hazard (Asante-Duah, 1993). Pathways may be direct and immediate or more complex and delayed. The primary pathway of exposure to LFG emission is inhalation of the NMOCs in the ambient air at the receptor location.

Dose-response assessment or toxicity assessment (USEPA, 1991) is the process of quantitatively evaluating the toxicity information and characterizing the relationship between the dose of the contaminant administered or received and the incidence of adverse health effects in the exposed population (Asante-Duah, 1993). It is the process by which the potency of the compounds is estimated by use of dose-response relationships. For carcinogens, this involves estimating the probability that an individual exposed to a given amount of chemical will contract cancer due to the exposure. The majority of the data are derived from toxicological studies performed on animal studies and infrequently, from studies in exposed human populations. The response of a toxicant depends on the mechanism of its action; in the simplest case, the response is directly proportional to its concentration (Asante-Duah, 1993). The response to the toxicant is used to assign potency estimates as "unit risk factor" (in $\mu g/m^3$ or ppm) or as "potency slopes" (in units of $[mg/kg/day]^{-1}$). Uncertainty in identifying the risk for each chemical is directly related to the extent and quality of the data available. The conservative assumption that humans are at least as sensitive as the most sensitive animal species in the toxicological studies introduces a lot of the uncertainty in this step of the process.

Risk characterization is the final step in the risk assessment process that integrates the information gathered in the three previous steps to arrive at an estimate of risk to the exposed population. It is the process of estimating the probable incidence of adverse impacts to potential receptors under various exposure conditions, including an elaboration of uncertainties associated with such estimates (Asante-Duah, 1993). Uncertainties and the main assumptions used to complete the whole risk assessment process are also evaluated during the risk characterization stage in order to quantify the risk estimate obtained in this step. For known or suspected carcinogens, acceptable exposure levels are generally concentration levels that represent as excess upper-bound lifetime cancer risk to an individual of between 10^{-4} and 10^{-6}

(Page & Donahoe, 1993). Cancer risk below 10^{-6} will generally not trigger a remedial response whereas cancer risks that exceed 10^{-4} may trigger some type of remediation or institutional controls.

2.5.2 Risk Assessment of Landfill Gas Emissions

In the past, the risk associated with landfill gas emissions dealt mainly with the explosive hazard of methane gas and its migration into adjacent structures. Many cases have been documented with respect to the destructive results of methane migration off-site. However, it is now the chronic toxicological concerns over the NMOC emission in LFG that are the driving force for limiting air emission from landfills. Section 2.1.3 presented a list of 13 of the many possible NMOCs found in LFG emissions.

Only a few studies have calculated risk values for exposure to the NMOCs in landfill gas. Crouch *et al.* (1990) performed health risk analysis on landfill gas emissions utilizing the four steps in the risk assessment process identified earlier. They investigated two different classes of exposure. The first case considered the "average" individual who lives within a circular region 50 km in radius, centered at the landfill. The second case was the "worst-case, neighbor" who lives at a fixed point located a nominal 100 m from the edge of the landfill. The average individual was found to have an average risk of 2×10^{-8} (range of 3×10^{-9} to 4×10^{-8}) of exposure to landfill gas. The maximum risk for the worst case individual, found at a co-disposal landfill, was 2×10^{-5}. Crouch *et al.* (1990) concluded that the excess carcinogenic risk induced by landfill emissions is significantly smaller than the current risk of cancer from all other cases.

Thoits (1989) found a range of cancer risk in excess of 2.5×10^{-3} to less than 1×10^{-6} from eight different landfills which were classified as mainly residential. In a comparison of landfills and waste to energy (WTE) plants, Jones (1994) indicated that the total cancer risk for the uncontrolled benzene and vinyl chloride emissions exceeded 1×10^{-5}, the acceptable threshold inhalation risk in many States. Young and Parker (1983) indicated quantitatively that the minor components in the landfill do not represent any significant hazard. They indicated that the greatest contributions to the risk were from surface emissions of vinyl chloride and 1,1-dichloroethene. Assmuth and Kalevi (1992) also indicated that carbon tetrachloride, dichloromethane, toluene, and benzene pose the most severe toxicological risks due to their

concentrations and acute toxicities or carcinogenicities. Goldberg *et al.* (1999) suggested that men who lived near the Miron Quarry MSW landfill in Montreal, Quebec may have been and may continue to be at excess risk of cancer of the liver, kidney, pancreas, and non-Hodgkin's lymphomas.

2.5.3 Summary

Presently, limited risk assessments of NMOC emissions have been performed based on a constant emission of a chemical over the lifecycle of the landfill. The major shortcomings inherent in this type of risk assessment approach are that it provides a limited amount of useful information to the risk manager and the public (Finley & Paustenbach, 1994). Modelling the landfill system to accommodate the changes in emissions over the whole life of the landfill and integrate effects such as changes in landfill size and shape would provide more information than the point estimate method. Variability among the risk estimates was observed; part of this may be due to the heterogeneous nature of the landfills or possibly from the methods used in the estimation process. The estimation process requires the use of concentration data; is it appropriate to use average concentrations or the 95th percentile concentrations suggested by the MOE to obtain realistic estimates of the risk?

This research will examine and model the production, emission, and transport of the NMOCs to a receptor as input to the determination of the risk of exposure to LFG. A model that estimates the production, emission and transport of the methane, carbon dioxide, and NMOCs over the lifetime of the landfill will be developed.

Chapter 3

3.0 Flux Chamber Design and Laboratory Evaluation

3.1 Specific Objectives

Researchers have reported that flux chambers have both over and under estimated the actual emission rate of gas from liquid and soil surfaces. Simulated VOC emission source testing was conducted by Kienbusch (1986) under controlled laboratory conditions to determine the flux chamber's precision and accuracy. Kienbusch's test indicated that the flux chamber technique is repeatable (± 5% variability between flux chamber measurements) but tends to underestimate the true emission rates by 22 to 45 percent. Gholson *et al.* (1989) reported similar negative bias (25 to 87 percent) during an emission study to measure 1,1,1-trichloroethane emissions from a liquid surface. They found that increasing the sweep flow rate could reduce the higher negative biases (78 to 87 percent) thereby reducing the concentration buildup or diffusion gradient above the liquid surface. Although further increases in sweep flow rate did not reduce the negative bias below the 25 to 54 percent range. Altering the emission sources environment such as the diffusion gradient has been observed as one of the reasons behind the poor performance of the flux chamber. Other environmental conditions that can be altered by the flux chamber are wind, soil disturbances, pressure, moisture and air turbulence. As indicated by Gholson *et al.* (1989) the diffusion gradient can be minimized by operating the flux chamber under optimal conditions. Reinhart *et al.* (1992) performed several tests using a flux chamber to determine the optimal operation parameters of the flux chamber for measurement of MSW LFG emission rates. They found a bias shift from positive to negative (50% to –20%) as the sweep air velocity was increased. The higher flow rate increased the internal chamber pressure resulting in the negative bias. They selected a sweep flow rate that would minimize both effects.

Operation of the flux chamber under optimal conditions will increase the accuracy of the flux measurements. However, the differential pressure between the flux chamber and atmosphere will still contribute significantly to the error associated with the flux measurements. A pressure of 1.5 mm H_2O in the Reinhart *et al.* (1992) study resulted in an approximately 30% underestimation of the true methane flux. Denmead (1979) found that a pressure deficit of 10 mm H_2O caused a 10-fold increase in measured N_2O emission by diffusion alone. The flow of sweep gas into the chamber tends to increase the pressure within the flux chamber, which in turn would tend to divert the landfill gases away from the chamber (Williams & Williams, 1995). Municipal wastes can produce significant amounts of methane under pressure and therefore these emissions will not be controlled by diffusion alone (Eklund, 1992). It is clear that some of the bias introduced into measured gas flux rates has been due to the pressure differential between the chamber pressure and the ambient air pressure. Therefore, minimizing the pressure differential between the flux chamber and atmosphere can increase the accuracy of the emission flux measurements.

The flux chamber developed in this research was designed to minimize the errors by equipping it with a feed back system involving a pressure transducer and process controller so as to minimize pressure differentials between the ambient air and the inside of the flux chamber.

3.2 Design and Construction

The 30.5 cm (12 in) diameter stainless steel model flux chamber developed in this research is shown schematically in Figure 3.1. Its smaller size was selected to minimize the economic and labour requirements in the movement of the flux chamber between field locations. It was felt that, if a chamber producing accurate flux measurements could be designed at a small scale, the same design parameters could be applied to larger scale units.

The chamber is fitted with a 0.95 cm (3/8 in) ID sweep gas inlet ring (stainless steel) with perforations at approximately 7.62 cm (3 in) on center. Two inlet ports are provided for the sweep gas to provide a consistent pressure and gas flow throughout the sweep gas ring. The chamber is also equipped with an exit port, soil and chamber gas temperature probes, and a pressure transducer. The temperature probes are stainless steel YSI 400 series thermistors with an operating range of -40°C to 150°C. The pressure transducer manufactured by Omega

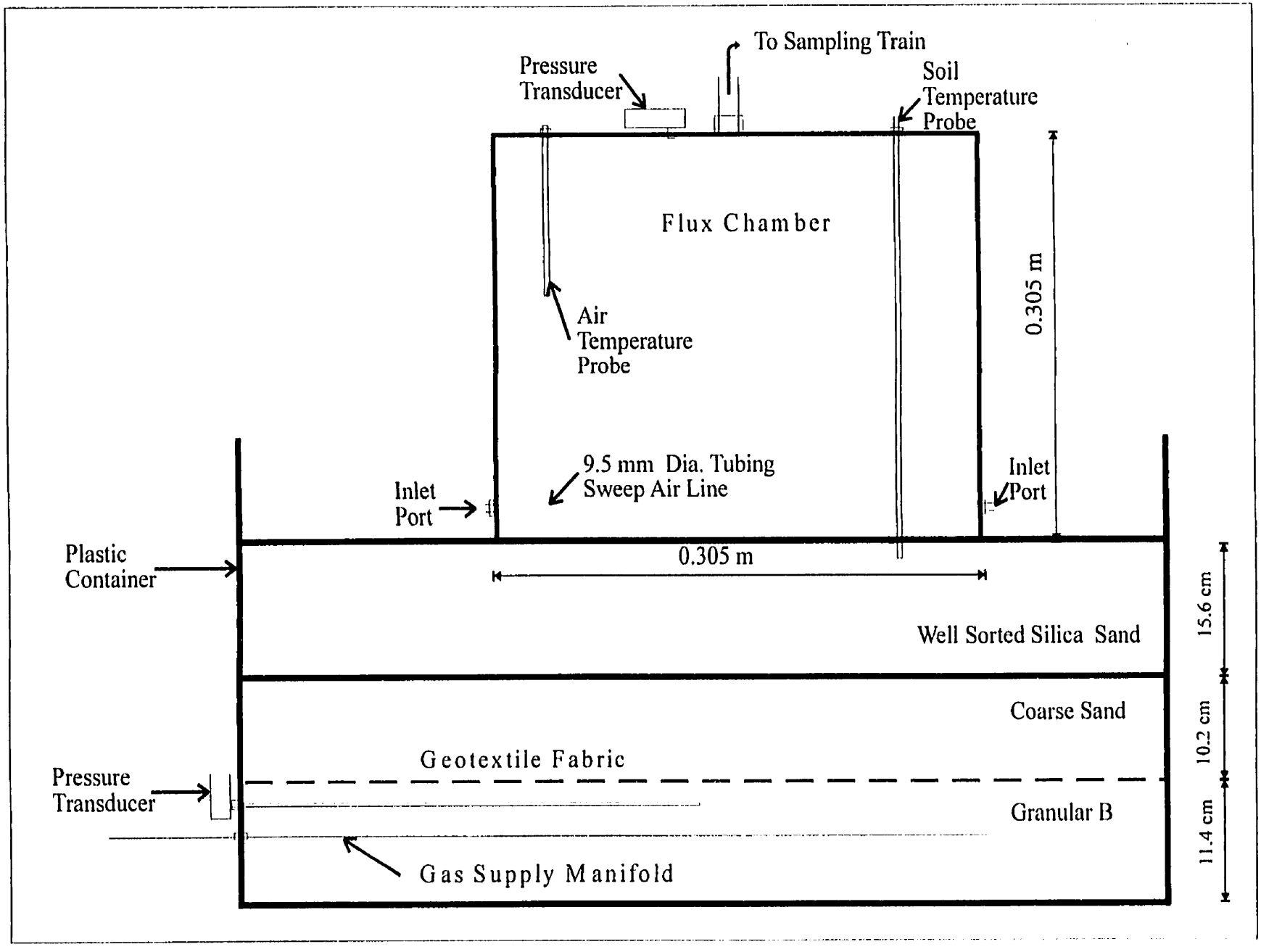

Figure 3.1: Laboratory setup of flux chamber and simulated landfill surface

(PX163-005BD5V) is rated for a maximum pressure differential of ± 12.7 cm (5 in) H_2O. It is attached to a process controller (Omega CN76000) to minimize the pressure differential between the chamber and the external atmosphere (see following section for further detail). The pressure transducer is calibrated to a range of ± 1 cm (0.4 in) H_2O with the use of a Betz manometer which is accurate to 316 Pa (± 0.05 mm H_2O) (see Appendix A for calibration curves). The controller is connected to a variable speed peristaltic pump (Master Flex 7529-30) which increases or decreases the rate of gas removal from the chamber to minimize the pressure differential. The pressure and temperatures are recorded at 10 minute intervals with the use of a data-logger (Ultra-logger by Lakewood Systems). Based on the 12 bit accuracy of the logger, the resolution of the pressure transducer and logger is 0.053 mm H_2O allowing it to detect any change in pressure at or above the indicated resolution.

During preliminary laboratory testing, the flux chamber was placed on a simulated landfill surface consisting of three layers of soil. The bottom layer (11.4 cm) was a coarse aggregate, which surrounded and supported the gas supply manifold. A layer of geotextile fabric was placed over the coarse aggregate and under a layer (10.2 cm) of coarse sand to prevent mixing of the two aggregate types. A 15.6 cm deep layer of fine well sorted silica sand made up the top layer of the simulated landfill cell. All the soil layers were contained within a plastic container that eliminated the lateral loss of gas. A second pressure transducer monitored the pressure differential in the coarse aggregate above the gas supply manifold. A schematic diagram of the laboratory setup is shown in Figure 3.2. The flux chamber did not penetrate the well sorted silica sand but rather was situated on top of it.

3.2.1 Pressure Control Feedback System

The pressure control feedback system consists of the pressure transducer inside the chamber, linked with a process controller and the peristaltic pump controlling the effluent flow rate. The pressure transducer is attached to the top of the flux chamber and it registers the pressure differential between the chamber and the atmosphere. If the differential pressure within the chamber becomes positive, the process controller increases the pumping rate of the peristaltic pump. The pumping rate increases until a zero pressure differential is obtained. As the atmospheric pressure changes throughout the day, this feedback mechanism ensures that the pressure differential in the chamber is minimized.

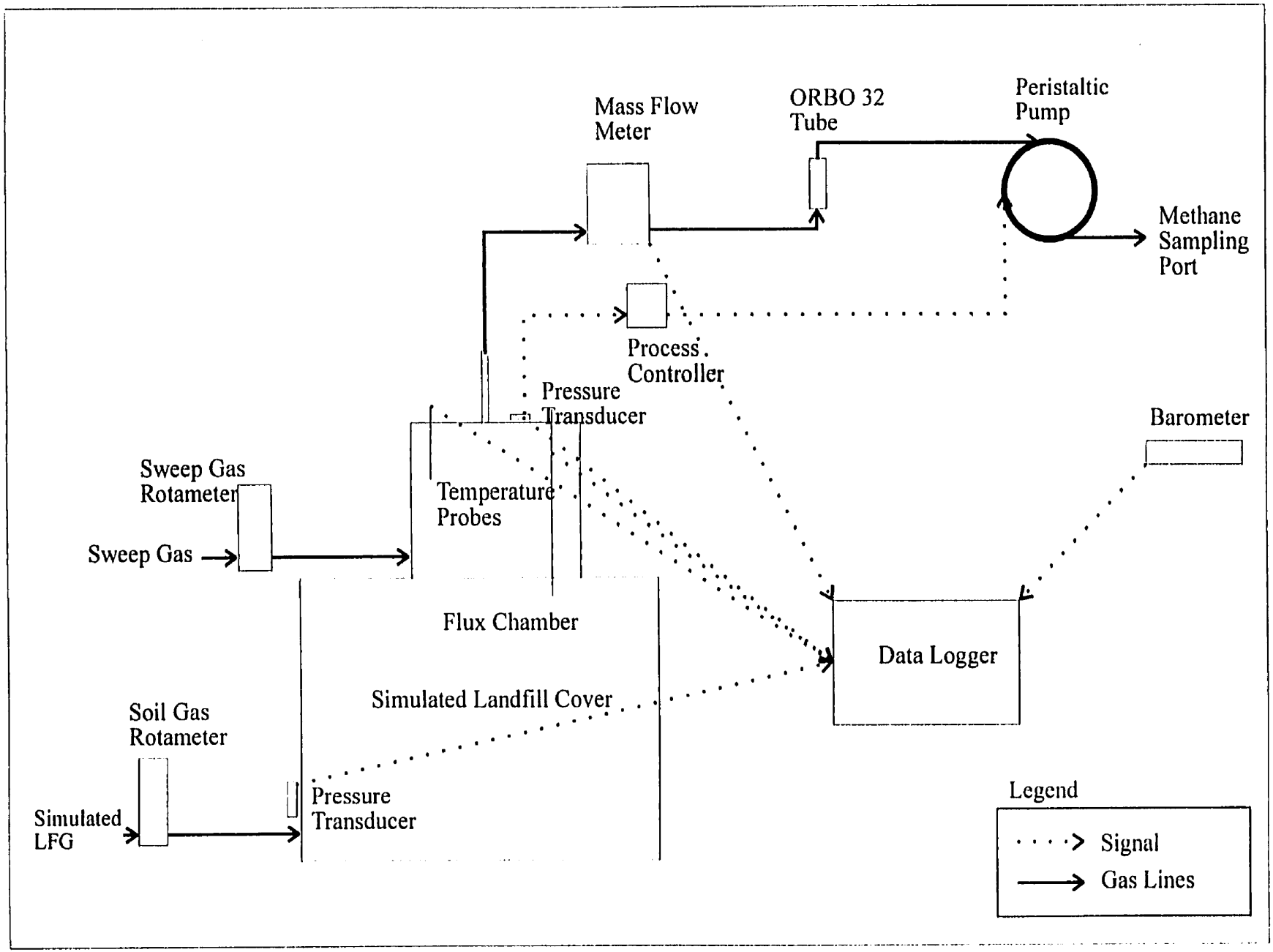

Figure 3.2: Schematic of laboratory setup of flux chamber experiments

3.3 Analytical Methods for Analyses of Methane and VOC

3.3.1 Determination of Methane Concentrations

Methane concentration measurements during the experiments were determined using a gas chromatograph with a flame ionization detector (GC-FID) (Shimadzu GC-9A). The GC was calibrated using a two-point calibration procedure. The method detection level (MDL) was established using the method outlined in Standard Methods (20^{th} edition). Volumetric glass bulbs were used to dilute the gas standards until no significant response was obtained from the GC-FID. The MDL was determined to be 10,200 $\mu g/m^3$ at 1 ATM and 20 °C (1.53×10^{-3} %V/V) (as shown in Appendix B).

After the calibration, the methane concentration in the laboratory experiments was determined by injection of 200 µl of gas into the GC-FID. The methane concentration in the flux chamber was monitored by removing a sample of the effluent gas with a gas tight syringe (Hamilton) downstream of the peristaltic pump. The syringe was purged three times with the effluent gas flow prior to obtaining a gas sample. The background methane concentration was determined by sampling the air supply into the flux chamber.

3.3.2 Determination of VOC Concentrations

The TCE and PCE concentration measurements during the laboratory experiments were determined by procedures outlined by ASTM Standards. Activated charcoal tubes (ORBO 32 supplied by Supleco) were used to trap the TCE and PCE vapour. Figure 3.3 shows a typical ORBO absorbent tube.

ASTM Method D 3687-95 was used to analyse the exposed ORBO tubes for TCE and PCE. A desorption efficiency for each batch of tubes was determined. The percent recovery or desorption efficiency was established as outlined in the ASTM method. The exposed ORBOtubes were desorbed in carbon disulfide (CS_2). Analysis of the tube contents was performed by breaking it open and separating the front and back portions and placing each into a 2 ml vial. The TCE and PCE sorbed onto the charcoal were extracted by adding 1 ml of CS_2 to the vials. The vials were then shaken for 10 minutes. Analysis of the extraction liquid was performed on a Hewlett Packard GC (Series II 6890) with a HP624 VOC (0.53mm ID, 30 m)

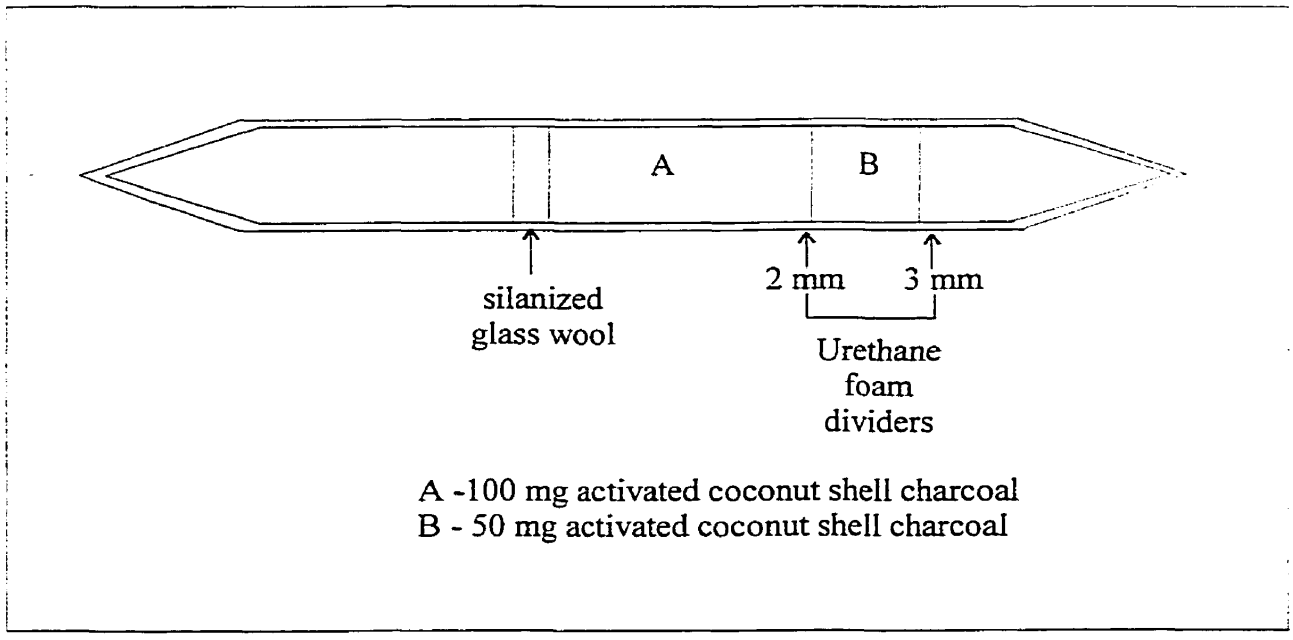

Figure 3.3: Typical absorbent tube for collection airborne compounds

column. The analysis program involved an initial temperature of 50 °C for 7 minutes to obtain optimum peak separation and then increasing the temperature to 220 °C at a rate of 20 °C/min. The final temperature was maintained for 12.5 minutes to ensure no interference with following samples. An autosampler processed the samples using 2 µl injections as suggested in the ASTM method.

TCE and PCE concentrations in the effluent flux experiments were determined by placing the ORBO tubes in the effluent stream from the flux chamber between the flow meter and the peristaltic pump. The flow rate through the ORBO tubes was monitored with the rotameter (Cole Parmer). Time of exposure of the tubes to the effluent stream was recorded. Analysis of the exposed tubes was done using the same procedure outlined above. The air concentration was determined using the procedure outlined in the ASTM method.

3.4 Laboratory Evaluation of the Flux Chamber Performance

The general procedure for operating the flux chamber involved the following steps:

1. Place flux chamber on soil surface.
2. Connect the sweep gas to the inlet ports of flux chamber.
3. Attach pressure transducer to port on top of flux chamber and temperature probes on to flux chamber.

4. Purge flux chamber for approximately six times the fluid residence time of the chamber.
5. Reset dataloggers.
6. Turn on power supply for pressure transducer.
7. Check voltage output of power supply and adjust to 8 VDC (calibration voltage of the pressure transducer).
8. Turn on peristaltic pump and process controller.
9. Adjust flow rate of rotameter to selected sweep flow rate.
10. Determine background methane concentrations.
11. Start and set soil gas flow rate.
12. Monitor methane concentration in effluent of flux chamber hourly.
13. Continue to monitor methane concentration for approximately 24 hours after the methane concentrations stabilized in the flux chamber.
14. At the end of the experiment download the dataloggers and turn off gases.

The sweep gas (air in these experiments) flow into the chamber was regulated with a rotameter (Cole Parmer). A mixture of 50% V/V methane and 50% V/V carbon dioxide was the gas introduced into the gas soil supply manifold in all the following experiments (see Figure 3.1). The soil gas flow rate was also regulated by a rotameter (Cole Parmer). The effluent flow rate from the chamber was monitored with a mass flow meter (Sierra 820 Top-Trak, 1-5 L/min) which was also connected to the datalogger. The methane concentration in the flux chamber was monitored by removing a sample of the effluent gas with a gas tight syringe (Hamilton) downstream of the peristaltic pump. This sample was then immediately injected into a GC-FID (Shimadzu GC-9A) for analysis.

The expected flux through the soil surface was determined by dividing the gas flow rate from the supply manifold (into the soil) by the soil surface area. Assuming that the chamber is gas tight and that it behaves as a completely mixed reactor, a mass balance developed around the chamber was used to determine the expected flux; this was calculated by multiplying the effluent flow rate exiting the chamber by the gas concentration in the effluent and dividing by the influent gas concentration and the surface area of the chamber.

Preliminary tests were performed to determine the most efficient operating parameters for the flux chamber system over a range of landfill emission rates. Two different flow rates of 2.8 ml/min and 12.9 ml/min were selected to simulate low and high emission rates from a landfill

surface. These flow rates would correspond to a flux of rate of 20 and 93 ml/min/m^2 (39 and 180 g/m^2/d) respectively. These flux rates are typical of rates that have been found at landfills (Bogner *et al.*, 1997b).

The effects of the sweep gas flow rate and pressure differential on the flux chamber's capture efficiency were examined. Seven experiments were performed using either the low or high simulated LFG flux rates. The parameters used in each of the seven experiments are shown in Table 3.1. Two replicate experiments were performed at each of the low (1 and 2) and high (3 and 4) LFG flux rates to examine the repeatability of the trial results. The remaining three experiments were run at the high LFG flux rate. Experiment 5 examined the impact that increasing the sweep gas flow rate would have on the efficiency of the flux chamber system. The sweep gas flow rate was increased from 1658 to 2140 ml/min. Experiments 6 and 7 examined the effect of negative and positive pressure differentials in the chamber on capture efficiency. Changing the set-point on the process controller used normally to minimize the pressure differential between the chamber and atmosphere created the pressure differentials.

Table 3.1: Description of experimental parameters for flux chamber experiments.

Experiment Number	Gas Supply Flow Rate[(1)] (ml/min)	Sweep Gas Flow Rate (ml/min)	Design Pressure Differential (mm H_2O)	Purpose
1	2.85	1658	0	Low flux
2	2.85	1658	0	Low flux
3	13.09	1658	0	High flux
4	13.09	1658	0	High flux
5	13.09	2140	0	Increase Sweep
6	13.09	1658	-1.8	Negative bias
7	13.09	1658	1.8	Positive bias

Notes: [(1)] 50% methane V/V and 50% carbon dioxide V/V

3.5 Results of the Performance Evaluation

Table 3.2 contains a summary of the data that were collected from the data-logger and GC analyses of these seven experiments. In experiments 1 to 4, the average pressure differential ranged from -0.035 to 0.009 mm H_2O with standard deviations that ranged from ± 0.153 to

Table 3.2: Summary of data from flux chamber experiments

Experiment Number	Average Flow Rate Gas Supply (ml/min)	Effluent (ml/min)	Methane Concentration Average Influent (% V/V)	Average Effluent (% V/V)	Average Pressure Chamber ($mm H_2O$)	Chamber Std Dev ($mm H_2O$)	Soil ($mm H_2O$)	Barometric ($mm H_2O$)	Average Temperature Chamber (C)	Soil (C)	Ambient (C)
1	2.81	1.74E+03	50	0.034	-0.001	± 0.173	0.967	9988	19.1	18.8	--
2	2.83	1.73E+03	50	0.036	-0.005	± 0.153	0.228	10126	18.8	18.5	18.4
3	12.9	1.75E+03	50	0.165	-0.035	± 0.202	0.967	9988	18.9	18.5	--
4	12.9	1.72E+03	50	0.162	0.009	± 0.193	0.291	9984	18.6	18.1	17.7
5	12.9	2.29E+03	50	0.130	-0.036	± 0.142	0.273	9963	19.0	18.8	17.9
6	12.9	2.86E+03	50	0.265	-1.792	± 0.096	-0.614	10008	19.2	19.1	18.1
7	12.9	7.26E+02	50	0.026	1.773	± 0.144	1.242	9943	19.2	19.0	18.2

± 0.202 mm H_2O. The chamber pressures in the negative and positive pressure experiment were maintained –1.792 ± 0.096 mm H_2O and 1.773 ± 0.144 mm H_2O respectively. Table 3.2 also shows the trends in temperature and barometric pressure during all the experiments. The soil and chamber effluent flow rates were corrected to account for changes in the barometric pressure and chamber air temperature from the standard conditions for each of the experiments. This correction minimizes differences between the experiments. The average pressure differential of -0.035 mm H_20 in experiment 3 resulted in a 4.73% error in the flux measurement as shown later in Table 3.3.

Figure 3.4 shows the gauge pressure of the chamber (obtained from the pressure transducer attached to the chamber) versus the elapsed time of Experiment 3. This was typical of all the other experiments. Appendix C contains all the data from the seven experiments with the data from experiment 3 shown as examples to represent the data from all experiments. The pressure fluctuated around an average differential of -0.035 mm H_2O. Effluent flow rates recorded from the mass flow meter in Experiment 3 are shown in Figure 3.5; the effluent flow rate was relatively constant with an average of 1.75 L/min for the entire experiment. The effluent flow rate data indicate that the system had the potential to achieve steady average operating conditions not withstanding considerable variation about the average. The methane

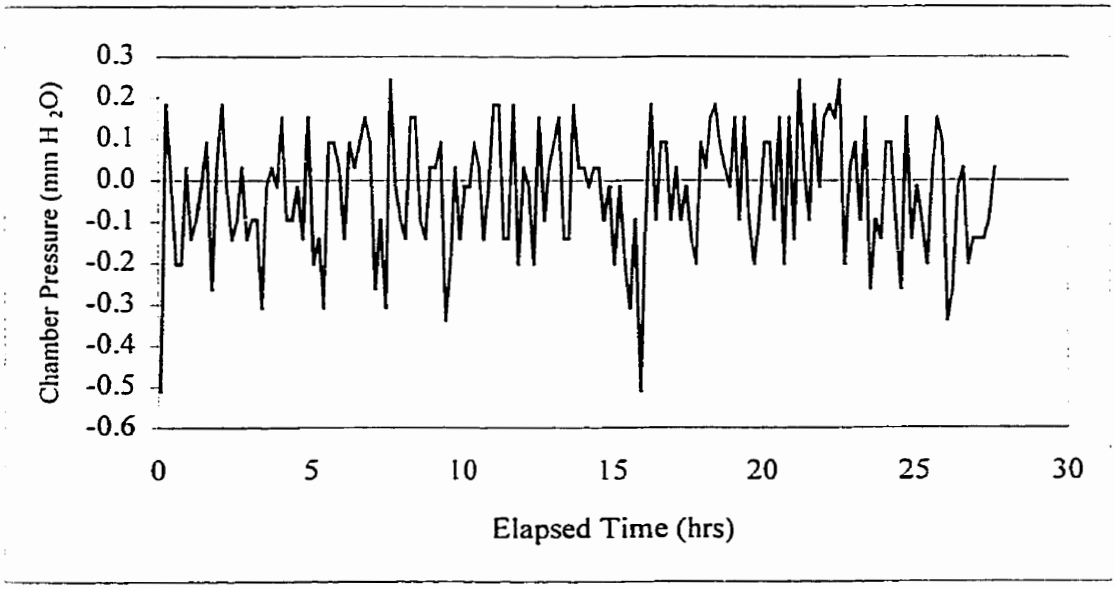

Figure 3.4: Chamber pressure transducer data from experiment #3 versus elapsed time (Time zero corresponds to start of gas flow into gas manifold).

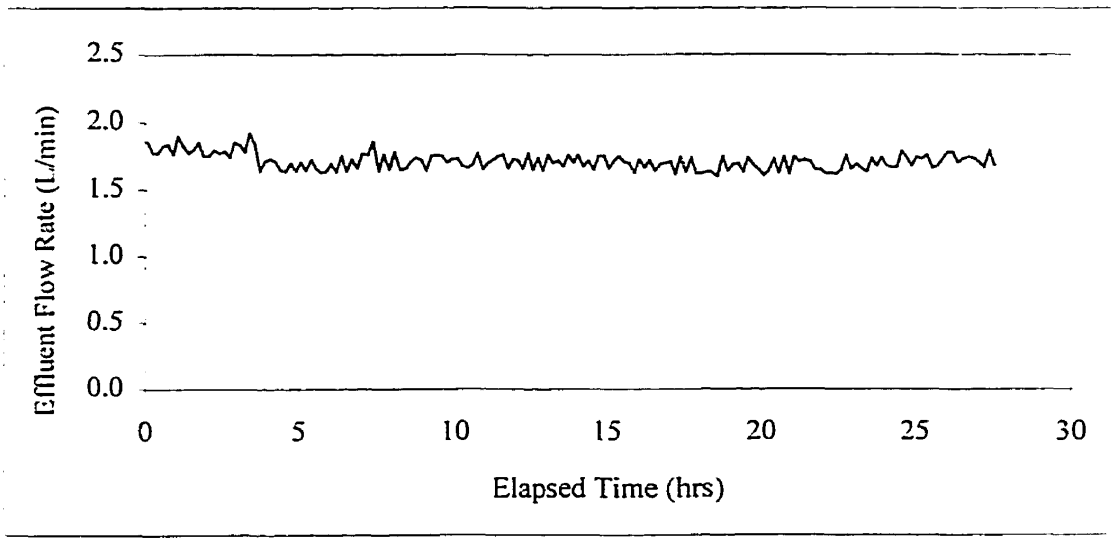

Figure 3.5: Effluent flow rate from flux chamber versus elapsed time in experiment #3 (Time zero corresponds to start of gas flow into gas manifold).

concentration in the chamber effluent over the duration of Experiment 3 is shown in Figure 3.6. The methane concentration builds until it reaches a steady state over a period of about 5 hours. The fluid residence time of the chamber was 0.2 hr assuming a completely mixed condition; the data in Figure 3.6 begins with the start of the experiment (*i.e.* as gas starts to enter the gas manifold) therefore the equilibrium within the soil and the volume beneath the soil would required much more time. The average concentration of the methane was determined after the system had reached a constant methane concentration. The data gap seen

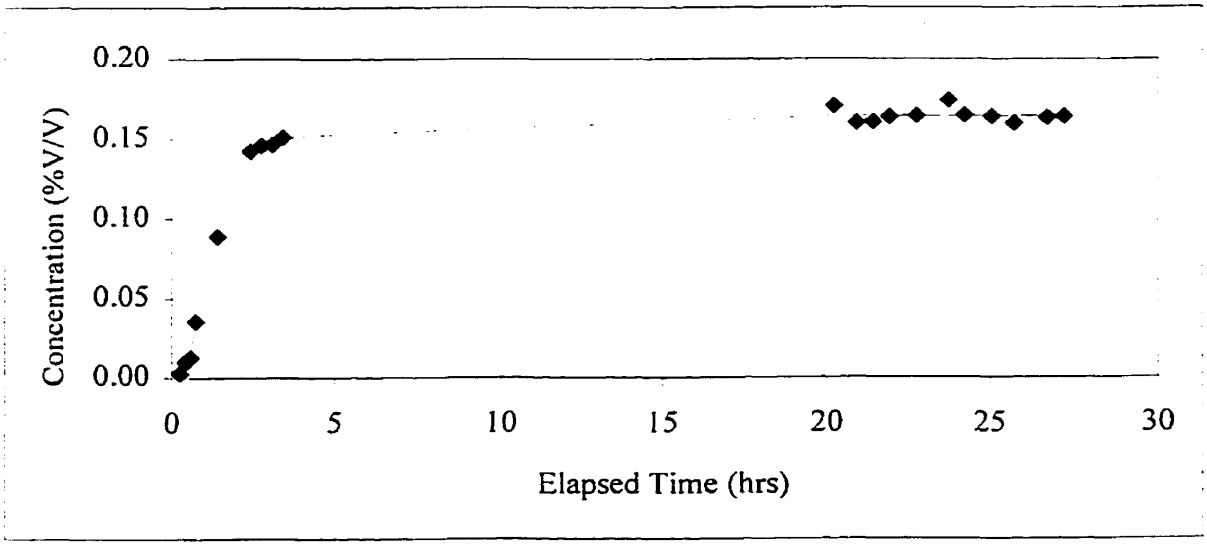

Figure 3.6: Methane concentration in the chamber effluent versus elapsed time in experiment #3 (Time zero corresponds to start of gas flow into gas manifold).

in Figure 3.6 is a result of the methane being monitored manually with the gap occurring during the night.

Table 3.3 presents a comparison of the measured flux with the expected fluxes. This table also contains a capture ratio of the measured flux to expected flux. In Experiments 1 and 2, the capture ratios were 0.99 and 1.02 respectively. At the higher flux flow rate, the ratios were 1.05 for Experiment 3 and 1.01 for Experiment 4. These experiments were conducted to determine the repeatability of the tests and indicate that there is excellent reproducibility in the experimental results under lab conditions. These results show that the experimental system has the potential to produce very accurate measurements of gas emissions from landfill surfaces.

Table 3.3: Comparison of expected to measured flux from the flux chamber experiments

Experiment Number	Expected Flux ($ml/cm^2/min$)	Measured Flux ($ml/cm^2/min$)	Capture Ratio Measured/ Expected
1	2.03E-03	2.00E-03	0.99
2	2.04E-03	2.09E-03	1.02
3	9.30E-03	9.74E-03	1.05
4	9.31E-03	9.36E-03	1.01
5	9.29E-03	1.01E-02	1.08
6	9.31E-03	2.55E-02	2.74
7	9.28E-03	6.27E-04	0.07

The sweep gas flow rate was changed from 1.66 L/min in Experiment 3 and 4 to 2.14 L/min in Experiment 5 to determine its effect on the measured gas emission rate. Increasing the sweep gas flow rate in this way resulted in a capture ratio of 1.08 in comparison to 1.05 and 1.01 capture ratios obtained in experiments 3 and 4 respectively. In experiment 5, the pressure differential of -0.036 ± 0.142 mm H_2O was comparable to the pressure differentials observed in experiments 3 and 4 (-0.035 ± 0.202 mm H_2O and 0.009 ± 0.193 mm H_2O). The change in sweep flow rate did not change the effectiveness of the system to minimize the pressure differential in the flux chamber. It was apparent from these results that the pressure feedback system designed for this research could operate effectively over a range of sweep gas flow rates. It was therefore concluded that a change in sweep flow rate of this magnitude (up to 29%) did not result in any significant bias of the measured emission rate.

The expected flux was obtained by dividing the experimental soil gas flow rate by the soil surface area (1388 cm^2). The simulated landfill soil was contained within a plastic container, which prevented any gas from escaping laterally. Therefore, the gas could only travel vertically out of the soil surface. The chamber's surface area (592 cm^2) covered approximately 43% of the soil surface therefore the gas could travel into the chamber or out the uncovered portion of the surface. In order to get a true estimate of the gas flux from the surface; the pressure inside the chamber must be identical to the atmospheric pressure.

Evidence of this is seen in the results of Experiment 6 where decreasing the average pressure differential to -1.8 mm H_2O increased the capture ratio to 2.7 (Experiment 6). A positive pressure differential of 1.8 mm H_2O in the chamber reduced the capture ratio to 0.07 (Experiment 7). A comparison of these two experiments to Experiments 3 and 4 indicates that they were conducted under nearly identical conditions except for the pressure differential.

Figure 3.7 shows the relationship between the gauge pressure (x) of the chamber from the 7 experiments and their respective capture ratios (y) ($y = -0.75x+1.13$, $R^2 = 0.95$). This relationship indicated that small pressure differentials such as these would result in large errors in the flux measurements obtained by the flux chamber, a positive pressure resulting in an underestimation of the emission flux. This is due to imposing a pressure on the soil beneath the chamber and forcing more gas to be emitted outside of the chamber. An overestimation of the emission flux was obtained when a negative pressure (vacuum) occurred within the chamber. These conditions caused more gas than expected to be drawn into the chamber. The pressure differentials are very small but resulted in major errors in the LFG flux measurements. Thus, maintaining near zero differentials was essential to the flux chamber success. The design developed in this research was shown to have this capability. The inability to maintain pressure differentials near zero is likely to have been the cause of many faulty flux chamber experiments reported in the past. Denmead (1979) reported a 10 mm H_2O deficit would result in a 10 fold increase in N_2O emissions.

The permeability of the soil beneath the chamber was calculated using the soil gas flow rate and the gauge pressure of the soil in each experiment. Table 3.4 presents the permeability calculated for each experiment. The density and viscosity of the gas were corrected for the pressure and temperature on the day of the experiment. The permeability ranged from

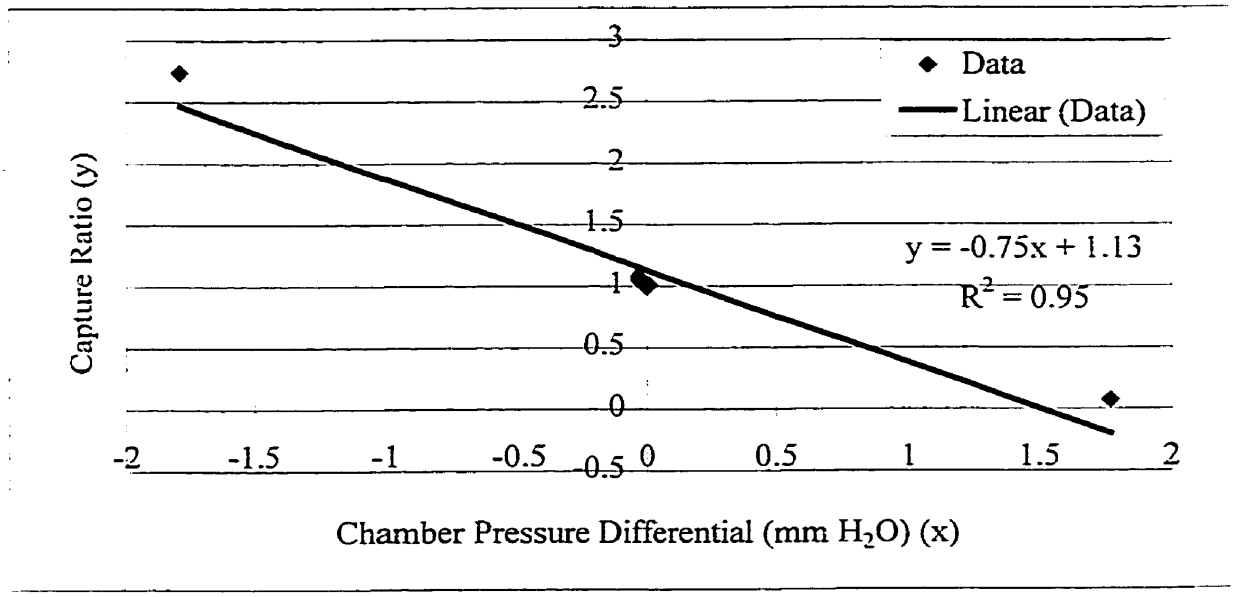

Figure 3.7: Relationship between chamber pressure and capture ratio.

1.03 x10^{-6} to 1.67 x 10^{-5} cm^2 with an average of 8.5 x 10^{-6} cm^2 (standard deviation of 7.2 x 10^{-6} cm^2) for the five experiments. These permeabilities are consistent with the published data for clean sand, which has a permeability range of 10^{-7} - 10^{-5} cm^2 (Freeze & Cherry, 1979). Van Geel (1994) found a permeability range of 1.0 x 10^{-7} to 2.0 x 10^{-7} cm^2 using the same well sorted silica sand (Barco No. 70). The permeabilities for experiments 6 and 7 also fall within the range established by the other five experiments. The moisture content of the soil beneath the chamber was considered to be less than the wilting point.

Table 3.4: Permeability of the simulated landfill soil obtained from soil pressures.

Experiment Number	Soil Flow Rate (ml/min)	Chamber Δ Pressure (mm H_2O)	Soil Δ Pressure (mm H_2O)	Density (kg/m^3)	Viscosity (Pa·s)	Permeability (cm^2)
1	2.8	-0.001	0.967	1.21	1.36E-05	1.03E-06
2	2.8	-0.005	0.228	1.23	1.36E-05	4.33E-06
3	12.9	-0.035	0.967	1.21	1.36E-05	4.72E-06
4	12.9	0.009	0.291	1.21	1.36E-05	1.56E-05
5	12.9	-0.036	0.273	1.21	1.36E-05	1.67E-05
6	12.9	-1.792	-0.614	1.21	1.36E-05	7.43E-06
7	12.9	1.773	1.242	1.21	1.36E-05	3.68E-06

3.6 Evaluation of Flux Chamber to Detect VOC Emissions

Preliminary experiments to evaluate the flux chamber's ability to measure NMOC emissions were performed according to the experimental procedure explained in the following section. The results of these experiments are also given in the following sections.

3.6.1 Methods of VOC Studies

The flux chamber's ability to measure NMOC was evaluated using the equipment and setup used in the previous section with the addition of ORBO tubes to monitor the concentration of VOC in the flux chamber effluent. The experiment involved 10 days of continuous injection of a constant soil gas mixture of methane, carbon dioxide, TCE, and PCE. The longer duration of the experiment was required to ensure that TCE and PCE reached a steady state in the flux chamber effluent.

A mixture of 50% methane and 50% carbon dioxide was placed in a gas sampling bag; measured volumes of PCE and TCE dissolved in methanol were then injected into the bag. The PCE and TCE concentrations in the bag were determined by removing a 100 µl syringe sample for analysis on a Hewlett Packard GC (Series II 6890) with a HP624 VOC (0.53 mm ID, 30 m) column. The concentration of TCE and PCE used in the experiment with the flux chamber was approximately 5×10^{-3} mg/L. This concentration level is typical of the range of TCE and PCE found in LFG at the Waterloo Region Landfill (Waterloo Region, 1994). The gas mixture was then pumped from the sample bag into the gas supply manifold. The flow into soil was monitored with a rotameter. The TCE and PCE in the chamber effluent were monitored using adsorption on to ORBO 32 (Supelco), activated charcoal tubes incorporated into the effluent flow. The ORBO 32 tubes were subsequently desorbed using carbon disulfide as indicated in Section 3.3.2. A flow rate of only 50-100 ml/min was passed over the ORBO tube as recommended in ASTM 3686 to ensure that the tubes were not overloaded and that breakthrough would not occur. Therefore the effluent flow was split with the excess flow being diverted and rejoined with the ORBO tube flow just prior to the peristaltic pump. A rotameter in-line after the ORBO tube monitored the flow rate through the ORBO tube. Over the length of the experiment, the ORBO tubes continuously monitored the effluent at 2 different time intervals (4 and 20 hours). The two different time intervals were used to ensure that breakthrough did not occur on the ORBO tubes. Also the 4 hour sample length was used

to evaluate the samples for field use. The methane in the system was monitored as previously discussed in Section 3.3.1.

3.6.2 Results of VOC Studies

Table 3.5 summarizes the flow rates, methane concentration, pressure and temperature data monitored during the VOC steady state experiment. This table shows a daily average as well as an overall average for the entire experiment. The average chamber pressure was 0.003 mm H_2O with a standard deviation of ± 0.076 mm H_2O over the length of the experiment. Figure 3.8 shows the effluent methane concentration measured over the length of the experiment. The methane rose to near steady concentration by the end of the first day and dropped to near zero on the last day after the soil gas was replaced with ambient air. Table 3.6 shows the methane fluxes (expected and measured) and capture ratios for the experiment. After the system had reached steady state (Day 8), the capture ratio of approximately 1 was achieved for the duration of the experiment indicating that the experiment had very good control of the pressure

Table 3.5: Summary of the data from VOC steady state experiment

Day	Average Flow Rate		Average Methane Concentration		Average		Temp
	Gas Supply (ml/min)	Effluent (ml/min)	Influent (% V/V)	Effluent (% V/V)	Chamber Δ Pressure (mm H_2O)	Barometric Pressure (mm H_2O)	Ambient (°C)
1	14	2009	50		0.006	9914	20.1
2	14	1699	50	0.1671	-0.032	9996	20.3
3	14	1611	50	0.1826	-0.065	10034	20.7
4	17	1644	50	0.2257	-0.075	10066	21.0
5	14	1599	50	0.1815	-0.059	10076	21.6
6	14	1584	50	0.1769	-0.076	10021	22.6
7	16	1668	50	0.2044	-0.085	9977	23.2
8	16	1708	50	0.1989	-0.060	10032	22.7
9	17	1704	50	0.2067	0.032	10105	23.0
10	16	1699	50	0.1975	0.059	10116	23.4
11	15	1724	50	0.1800	0.090	10065	23.6
12	15	1691	50	0.1858	0.113	10022	23.0
13	14	1676	0	0.0001	0.087	10021	23.3
14	14	1705	0	0.0001	0.104	10010	23.1
Average	15	1694		0.1621	0.003	10032	22.2

differential with an excellent methane capture ratio providing a good experimental basis to test the system for measuring VOC emissions. The accuracy of each system component was not assessed. It was felt that capture ratios close to 1.0 would be a sufficient indication that the overall system was providing accurate results.

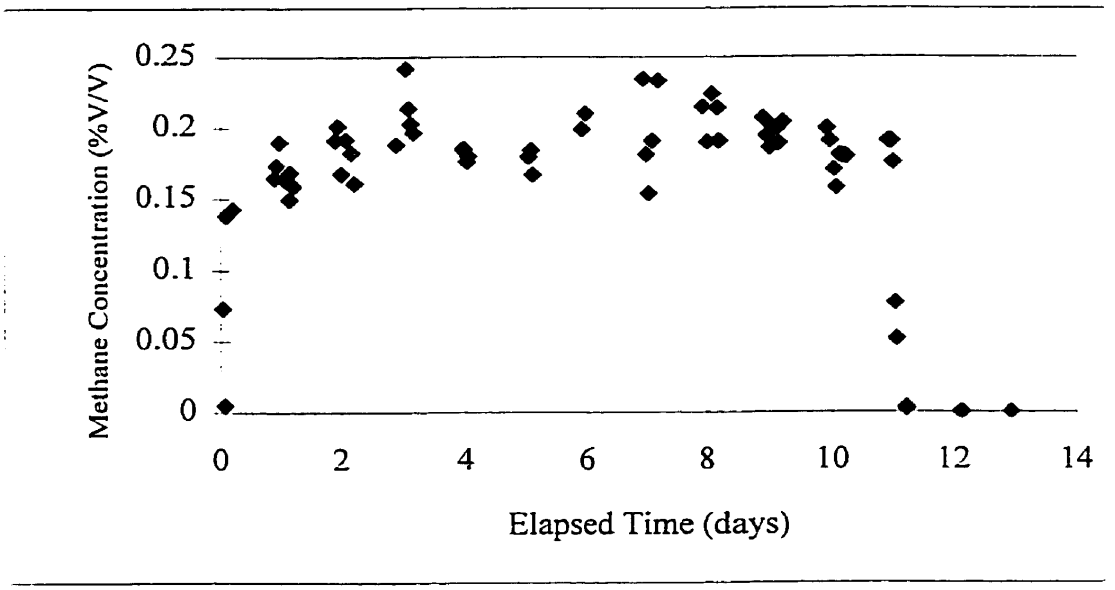

Figure 3.8: Methane concentration in effluent from flux chamber during long term PCE and TCE test.

Table 3.6: Expected and measured methane flux from long term VOC experiment

Day	Expected Flux ($L/cm^2/min$)	Measured Flux ($L/cm^2/min$)	Capture Ratio Measured/ Expected
8	1.01E-05	1.11E-05	1.10
9	1.15E-05	1.16E-05	1.00
10	1.01E-05	1.1E-05	1.09
11	1.01E-05	1.01E-05	1.00
12	1.01E-05	1.02E-05	1.01

Figure 3.9 shows the influent TCE and PCE in the soil gas indicating that their concentrations were reasonably stable throughout the experiment. Table 3.7 shows the measured and estimated concentrations of TCE and PCE in the flux chamber effluent. The capture ratios are also shown in this table. The capture ratio for TCE and PCE increased to near 1 as the

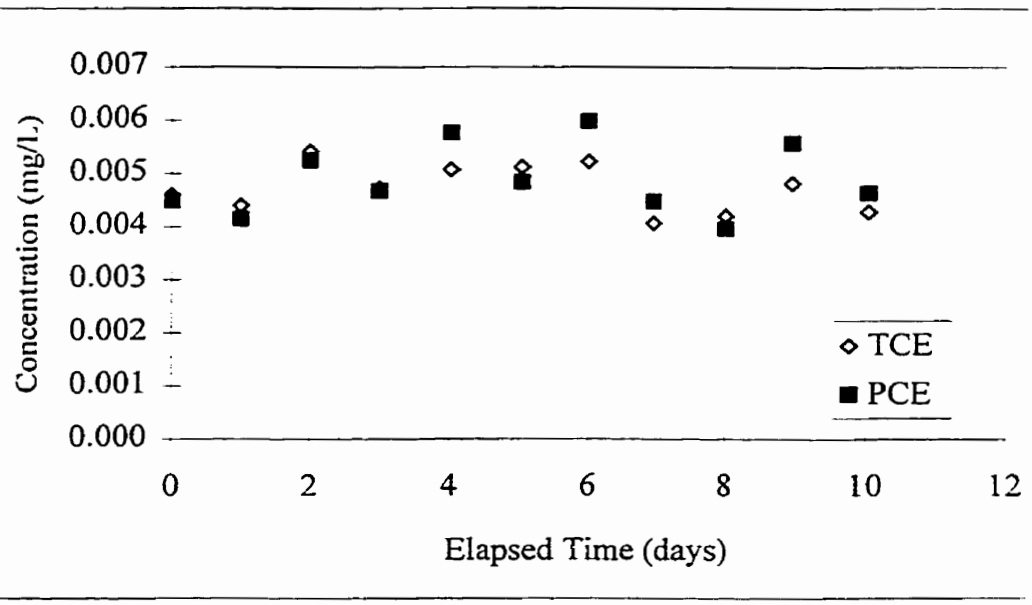

Figure 3.9: Influent TCE and PCE concentration versus time in the VOC steady state experiment.

Table 3.7: TCE and PCE concentrations (expected and measured) from the long term VOC experiment.

Date	Measured concentration (μg/L)		Estimated concentration (μg/L)		Capture Ratio Measured/Expected	
	TCE	PCE	TCE	PCE	TCE	PCE
8*	0.006	0.012	0.019	0.019	0.35	0.60
8#	0.010	0.012	0.016	0.018	0.63	0.64
9*•	0.011	0.015	0.017	0.019	0.63	0.79
9#	0.013	0.012	0.017	0.017	0.75	0.75
10*	0.012	0.014	0.017	0.016	0.71	0.90
10#	0.016	0.027	0.019	0.022	0.87	1.20
11*	0.019	0.023	0.017	0.020	1.08	1.15
11#	0.018	0.020	0.017	0.018	1.06	1.16
12@	0.019	0.022	0.017	0.018	1.10	1.19

Note: * sample taken collected over 4 hours, # sample taken collected over 20 hours, @ sample taken collected over 2 hours

experiment proceeded. The TCE concentration reached a steady state in the effluent as indicated by the increase in the ratio. The TCE and PCE concentrations collected over 4 hours versus 20 hours were consistent with each other indicating the 4 hour samples will provide an accurate estimate of the average VOC emissions in the field. The VOC concentration buildup in the system with time is indicated by the increase in capture ratio with time. The observed

capture ratios for the VOCs were very good but not as good as the methane capture ratio. Figure 3.10 shows a plot of the capture ratios of the methane, TCE and PCE over the length of the experiment. The VOCs should have performed as the methane if no reaction was occurring but the VOCs lagged the methane at first as seen in Figure 3.10. Then the VOCs capture ratio exceeded the methane's capture ratio later in the experiment. The lag of the VOC is likely due to some combination of sorption of the VOCs onto the tubing, flux chamber surfaces, and soil and dissolution into traces of soil moisture. The subsequent higher capture ratio might then be due to the desorption from these surfaces and the release from solution later in the experiment.

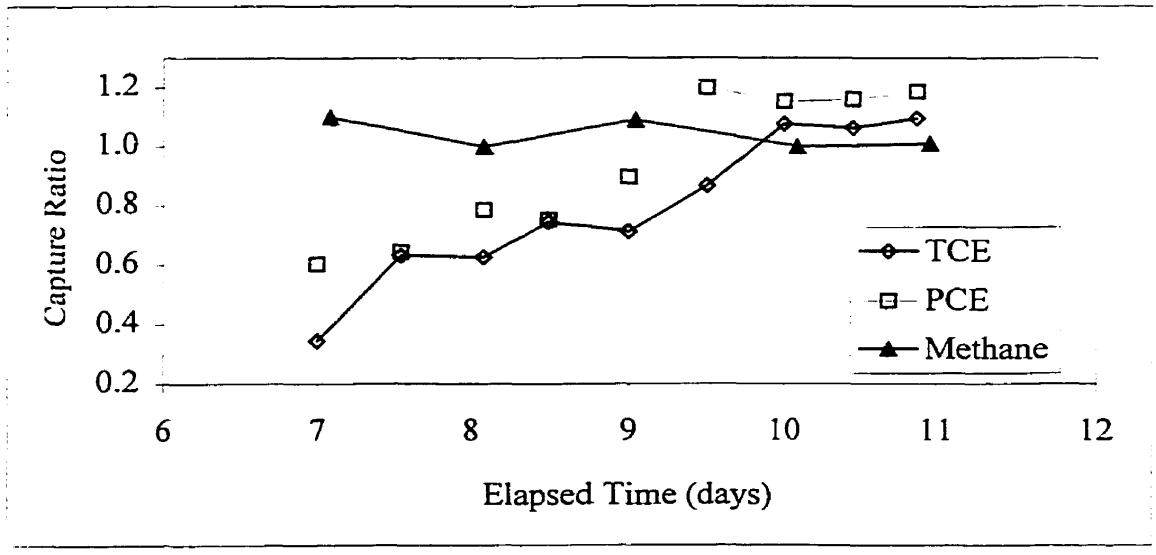

Figure 3.10: Capture ratios for TCE, PCE and methane versus the elapsed time.

3.7 Discussion

The flux chamber approach was originally developed by soil scientists to measure biogenic emissions of inorganic gases. In the early 1980's, the USEPA became interested in this technique for estimating rates from hazardous wastes (Eklund, 1992). An early evaluation by the USEPA of the flux chamber for measuring volatile organic emissions from a liquid surface concluded that the method would provide emission rates with very good precision, and that operational and environmental parameters have only minor effect on the precision and accuracy (Gholson *et al.*, 1989). But, they discovered a negative bias ranging from 40 to 80 percent in the emission rate. The results of this study indicated that pressure differentials in the chamber will have a large effect on the measurement of LFG emission from the surface. A positive pressure differential will result in an underestimation of the expected emission flux.

Overestimation of the emission flux occurs when a negative pressure differential was imposed on the chamber. Similar results were observed by Reinhart *et al.* (1992) during the development of their dynamic flux chamber.

The flux chamber designed and tested under the controlled laboratory conditions of this research was capable of maintaining the average pressure differential between the atmosphere and the chamber at very low levels, less than 0.036 mm H_2O over periods of excess in twenty four hours. This represents excellent control within the chamber environment notwithstanding standard deviations on the order of 0.2 mm H_2O, resulting in methane gas recovery ratios of 0.99 to 1.08 (measured/expected). Similar differential pressure control was exhibited over changes in sweep gas flow rates of up to 30% and likely beyond although this was not tested.

Experiments were performed in which the pressure differential was allowed to reach and remain at approximately 1.8 mm H_2O while this amount is small in terms of the changes in daily barometric pressure that ranged from 9,943 mm H_2O to 10,126 mm H_2O. These represent major deviations from the expected gas flux through the soil and explain in part why some previous researchers have had difficulty in obtaining accurate measurements with gas flux chambers.

The chamber was also used to measure the flux of VOCs carried in the simulated landfill gas. Recovery ratios for TCE and PCE were very good but the build up of these two contaminants within the chamber lagged that of the methane. This was assumed to be the result of adsorption and dissolution with system materials. Nonetheless, the recovery was good after steady state had been reached.

While the focus of this work was on landfill gas, it is likely that the system would work equally well to measure other gases from other surfaces with similar accuracy.

It is to be expected that more representative gas flux measurements from soil and landfill cover surfaces could be obtained with a larger chamber surface area. A larger prototype was however not constructed and tested in this research because of resource and time limitations. However, it is expected that the principles and equipment configurations used in this design could be scaled up to successfully control pressure differentials in larger units.

Chapter 4

4.0 Evaluation of Gas Release at a Landfill

The previous chapter revealed that the flux chamber design could effectively monitor gas emissions from a laboratory surface. To evaluate the flux chamber under field conditions and obtain estimates of LFG emission, a field study using the flux chamber was conducted at three local landfills. Emission from the landfill surface were evaluated based on the cover condition (presence of holes or intact cover), age of underlying waste and heterogeneity of emission from the surface. These flux measurements were to be used for comparison with a model developed in Chapter 5.

4.1 Method of Field Evaluation

4.1.1 Equipment Setup

A schematic diagram of the equipment setup based on the flux chamber used in the laboratory experiments is shown in Figure 4.1. A Porta-Air supply compressor (Model #2067 P113A-G552X) provided the supply of ambient air for the chamber sweep gas. The intake for the compressor was elevated approximately three meters off the ground to reduce the amount of gas phase contaminants in the sweep gas. The air flow from the compressor into the flux chamber was regulated with a rotameter (Cole Parmer).

The flux chamber was placed on a relatively flat surface of the landfill to minimize the gaps between the ground surface and chamber. Loose dirt was placed around the perimeter of the chamber to ensure a better seal with the surface and to close any gaps between the surface and the chamber. The ambient soil temperature probe was placed in the ground next to the chamber. A tripod fitted with cotton fabric hood was placed over the chamber to shelter it from

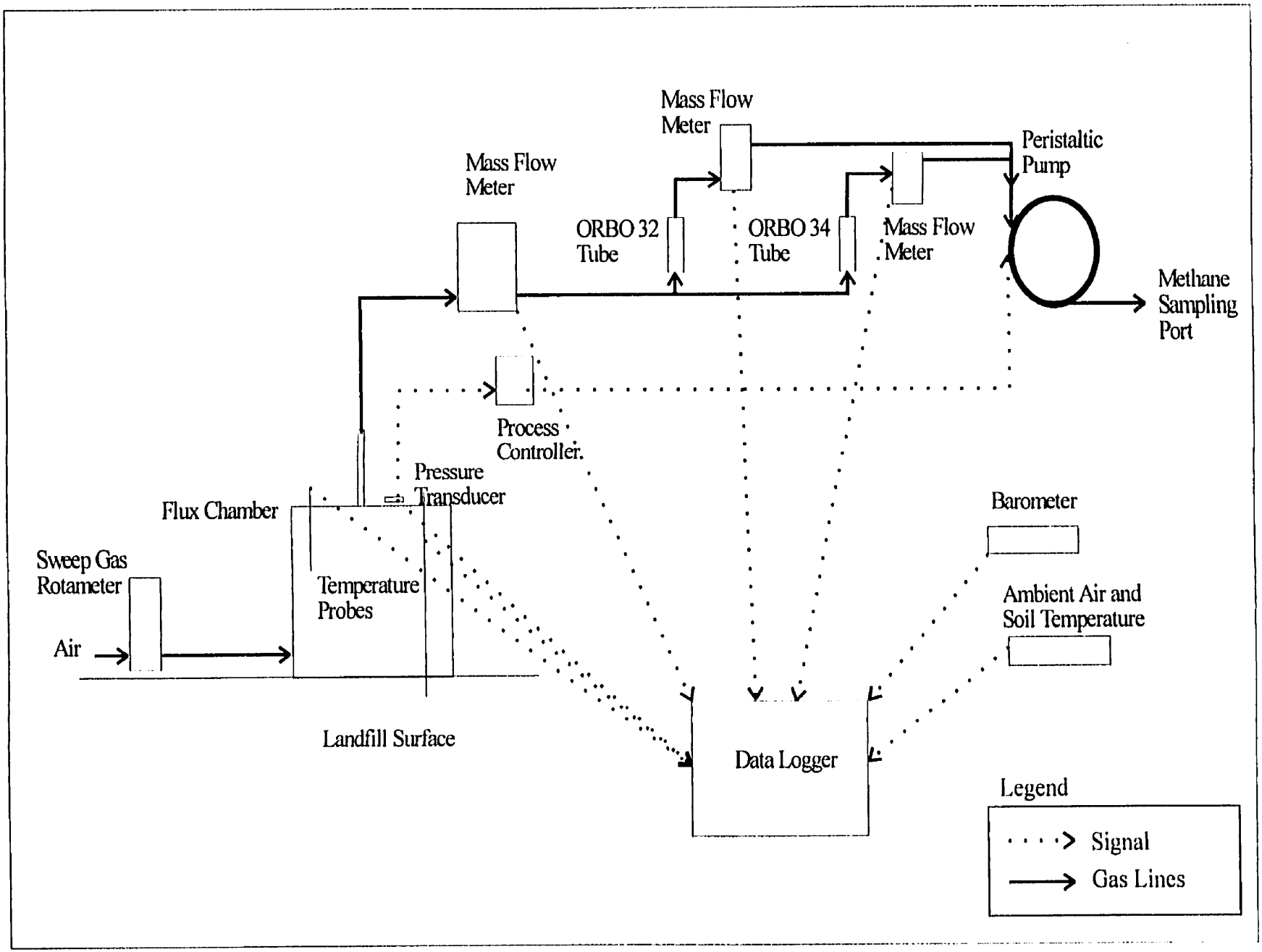

Figure 4.1: Schematic of field setup of flux chamber at landfill

the sun. The ambient air temperature probe was attached to the tripod just above the chamber. Figure 4.2 shows photos of the flux chamber and tripod setup used during the field experiments.

The effluent tube (0.635 cm Teflon) on top of the chamber was connected to the mass flow meter (Sierra Instruments, Top Trak) inside a portable shed which contained the electronic equipment. The four temperature probes were connected to their dataloggers; the pressure transducer was placed on top of the chamber. A HP Harrison 6200B DC Power supply was used to provide the 8VDC required for the pressure transducer. A barometer (Sensotec, EB/2101-01) was placed in the shed. Another HP Harrison 6200B DC Power supply provided power to the barometer. A photo of the shed and its equipment is shown in Figure 4.3. A 3500 W Honda generator (EM3500) was used to supply power for the DC power supplies, peristaltic pump, mass flow meters, and compressor. The generator was placed 9 to 10 meters downwind of the compressor air intake to ensure that the exhaust of the generator was not in the intake of the compressor. Figure 4.3(a) shows the generator and compressor behind the elevated air intake and the samplers used to monitor the intake air.

The effluent from the chamber was connected to the peristaltic pump, which operated on a feedback loop with the pressure transducer on the chamber and the controller that was contained within the shed as shown in Figure 4.3(b). The effluent was split three ways, one for TCE and PCE sampling, another for H_2S sampling and the last as a bypass. The bypass provided a means for the excess effluent flow from the chamber to be routed to the pump downstream. The flows through the sample tubes were regulated with gate valves. After exiting the tubes, the effluent flow passed through mass flow meters (Sierra Instruments, Top Trak), which were monitored at 10 minute intervals with a battery operated datalogger (Chart Pac CP-X, Lakewood). The effluent streams were then rejoined to pass through the final mass flow meter (Sierra Instruments, Top Trak) and into the peristaltic pump.

The four temperature probes (ambient air and soil, chamber air and soil) were monitored by the dataloggers. The chamber pressure differential measured using the pressure transducer and the flows exiting the chamber and passing through the ORBO tubes were also monitored by the dataloggers.

The ambient air was monitored for TCE, PCE, H_2S and methane. An Aircheck sampler (224-

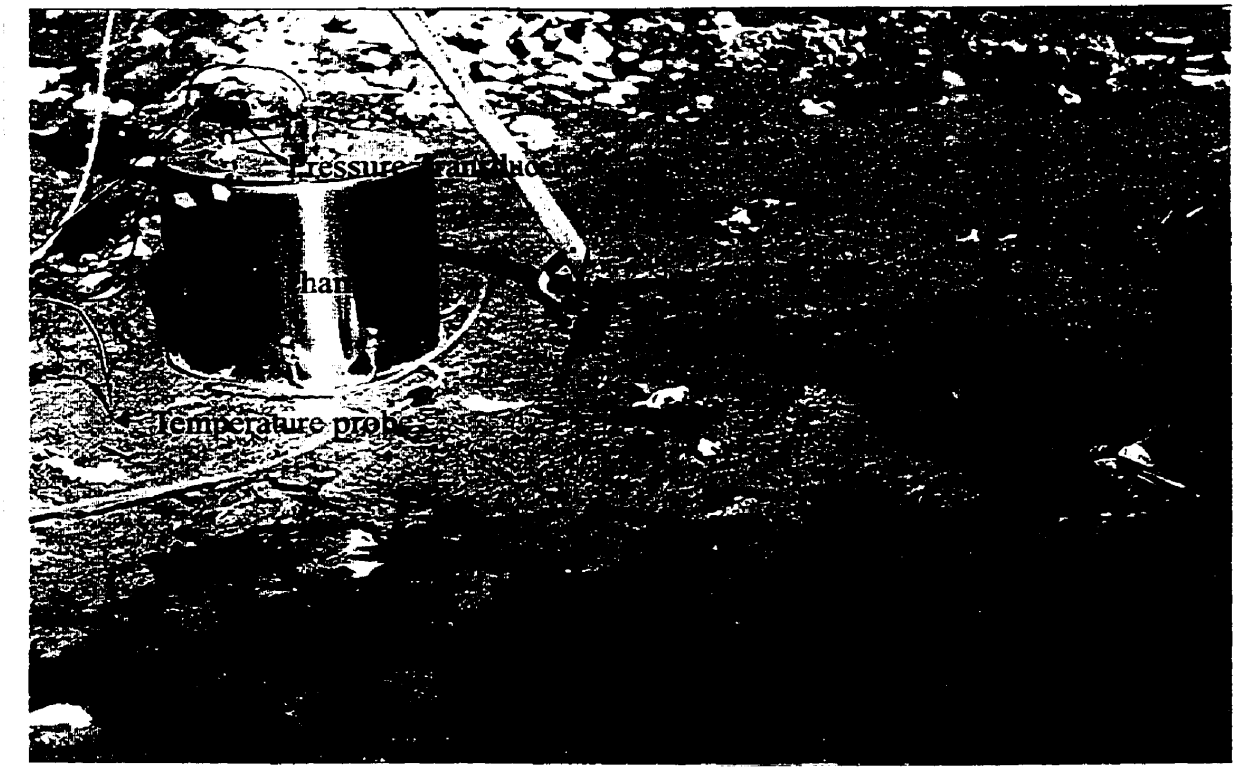

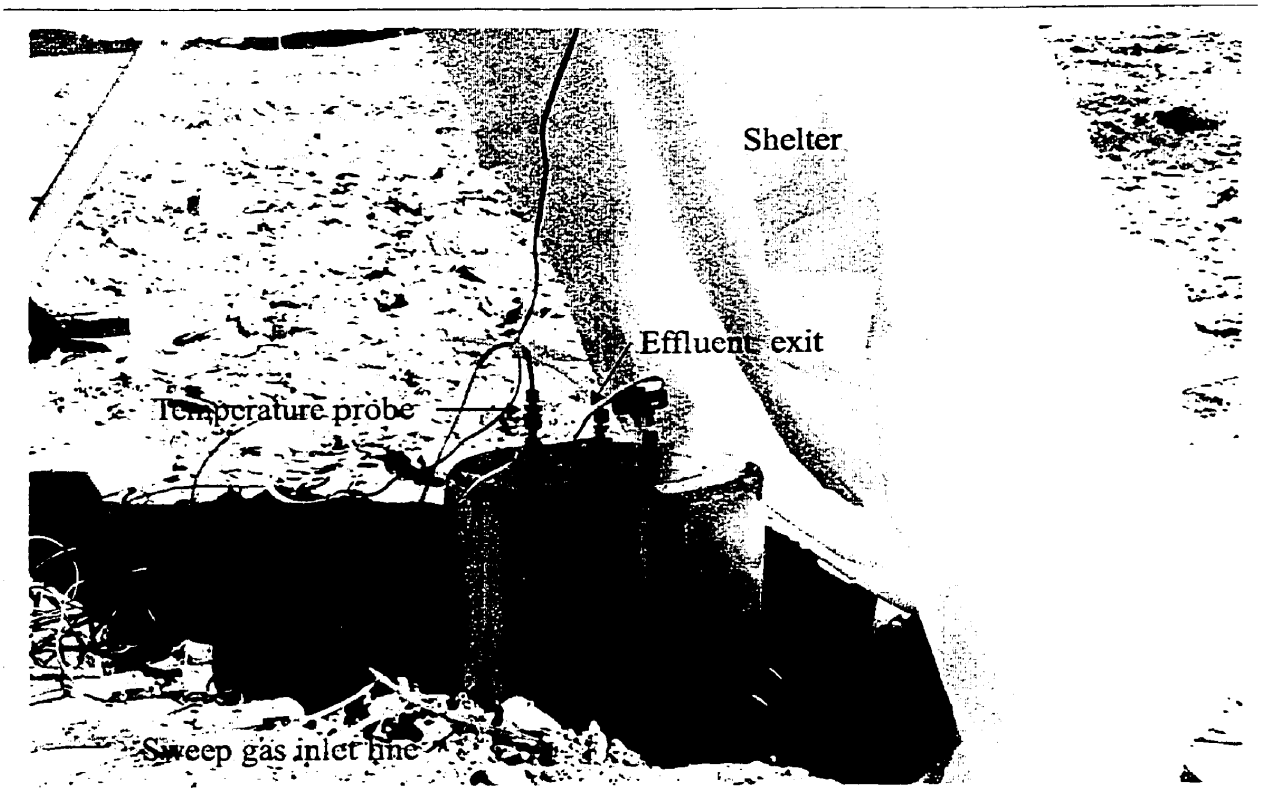

Figure 4.2: Flux chamber with pressure transducer and temperature probes under cloth shelter at the Waterloo Landfill

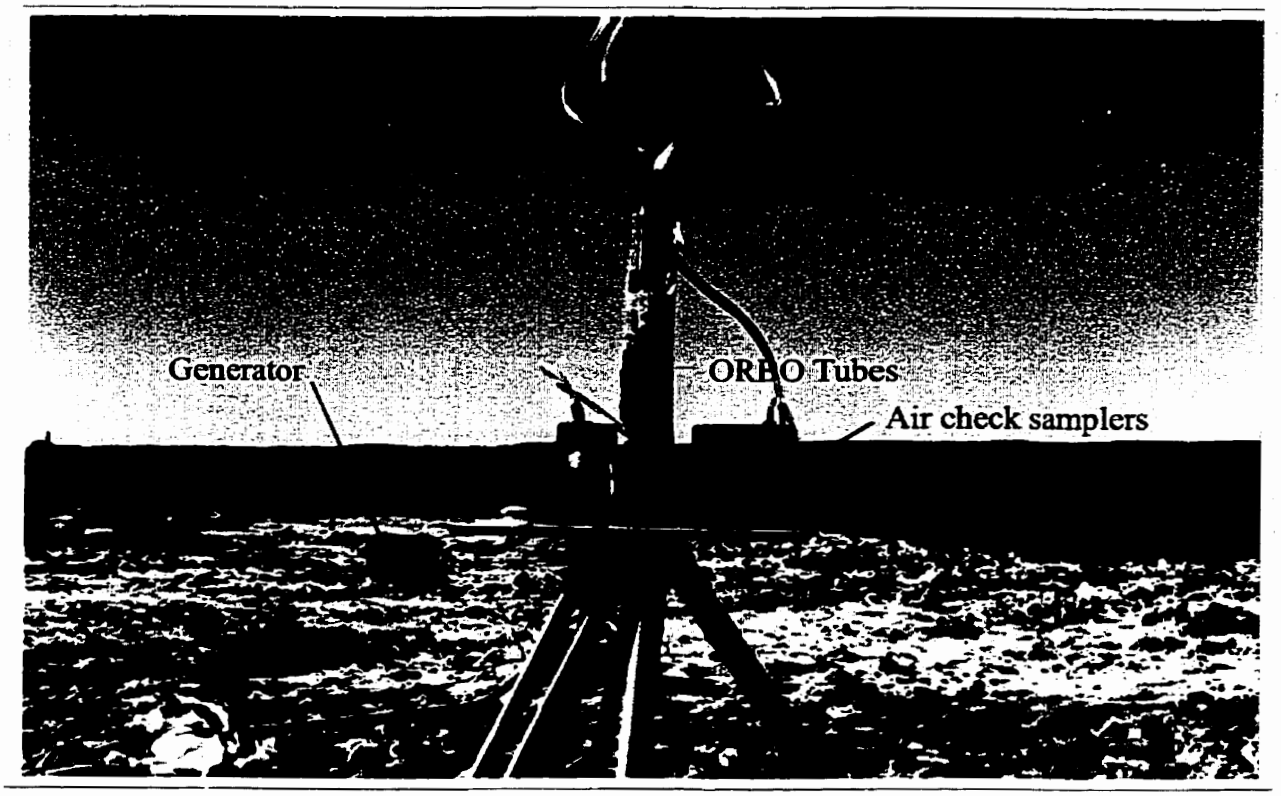

(A)

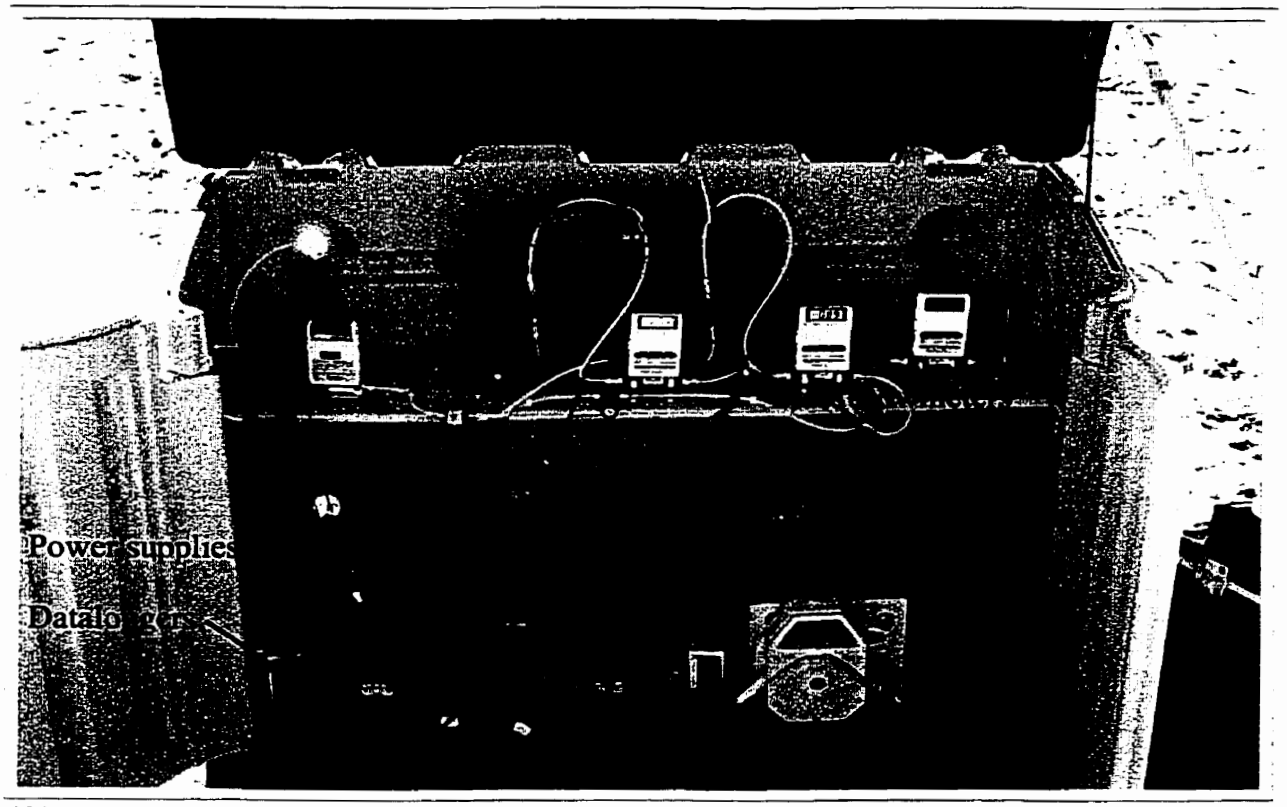

(B)

Figure 4.3: Equipment setup at Waterloo landfill for flux experiments. (A) ambient air sampling equipment for methane and ORBO tubes. (B) pump, mass flow meters, DC power supplies, and effluent ORBO tubes inside shelter used during experiments

PCXR4, SKC Inc.) was fitted with a double adapter to monitor the VOCs and H_2S simultaneously as shown in Figure 4.3(a). The intake for the sampler was also elevated to the same level as the compressor intake. Methane in the ambient air was monitored on an hourly basis by adapting another of the Aircheck samplers to fill 1 litre sample bags. The chamber effluent was monitored for TCE, PCE, and H_2S using ORBO sample tubes. The tubes were placed in the effluent streams as indicated above and shown in Figure 4.3(b) as the two vertical tubes attached to the grey plastic board.

4.1.2 Setup Procedure for Flux Chamber Operation

The procedure used in the field for the flux chamber involved the following steps.

1. The sampling equipment was set up as described previously.
2. The voltage output on the power supplies was checked and adjusted to 8VDC and 28 VDC for the pressure transducer and barometer respectively.
3. The sweep air flow into the chamber was established and allowed to purge the chamber for approximately one hour prior to sampling the effluent. The one hour stabilization period is approximately six times the mean fluid residence time of the chamber.
4. The dataloggers were reset at the beginning of each sample day.
5. After the chamber was purged, the ORBO tubes were placed into the effluent stream and Aircheck air sampler.
6. Samples of ambient air and chamber effluent were taken on an hourly basis to determine the methane concentration.
7. At the end of the sampling period, the ORBO tubes were removed and capped.
8. Dataloggers were downloaded at the end of the sampling period.

During the five months from June to October 1997, a total of 24 locations were sampled. These locations were selected based on their accessibility, compatibility with on-going landfilling activity, cover type and conditions, age of refuse and proximity to the active gas collection system. Three landfills, the Waterloo, Cambridge, and Stratford Landfills, were examined during the study period. Waterloo and Cambridge have active gas collection systems in operation on the slopes of the landfills. Stratford Landfill has only a passive vent system in operation at the perimeter of the existing landfill. Waterloo has an expansion cell to the North of the existing landfill that was considered to be outside the influence of the gas collection system. Table 4.1 indicates the dates, site description, and estimated age of last waste lift at each of the sites sampled at each of the landfills. Twenty of the tests were performed at the

Waterloo Landfill with 7 of these done on the expansion cell. The sites were labelled either by a NE for the North Expansion cell or ML for the main landfill. A "B" behind the site location indicates the flux measurement was made over a "bubble". In a situation, where a puddle of water after a rain was covering a hole or a fracture in the intermediate cover a bubble of gas would form. Figures 4.4 and 4.5 show the sample locations at the Waterloo Landfill and Cambridge Landfill respectively.

A typical experiment lasted approximately 6 hours with the first hour being used to flush the monitoring system. The experiments performed while at the landfill were used to examine the flux of gas from the landfill surface. The gas release from the surface or gas flux would be expected to increase until the waste was approximately one year old after placement at which point there would be a decline in flux emissions. The amount and type of cover will also affect the gas flux. A thin and highly permeable cover will likely have a higher gas flux than a thick and low permeability cover. A 30 cm interim cover of clay was present on the waste at the Waterloo and Cambridge Landfills where the flux measurements were made. A greater distance to gas collection wells would likely result in an increase in the flux of gas from the landfill surface. The variability in emission within an area larger than the flux chamber's surface area was evaluated by determining the emissions from 3 different locations within a half a meter of each other. Only the ambient and effluent methane concentrations were monitored for these experiments. The flux chamber was set up at the first location for 2 hours, 1 hour for equilibration and one hour of sampling. Two samples were taken with one at the beginning and one at end of the hour. The flux chamber was then moved approximately half a meter over into a new location and the process was repeated.

4.2 Analytical Methods for Analyses of Methane, VOC, and H_2S

4.2.1 Determination of Methane Concentrations

During field experiments, the methane concentrations of the flux chamber effluent and ambient air were monitored by taking grab samples of the air in 1 L sample bags. The flux chamber effluent was sampled by attaching a 1 L sample bag to the effluent of the peristaltic pump. An

Table 4.1: Location, site description, and age of waste at each flux experiment at the Waterloo, Cambridge and Stratford Landfills

Date	Site Location*	Site Description	Age of Last Waste Lift
Waterloo Landfill			
19-Jun-97	NE1-1	Interim cover with sparse vegetation	1-2 yrs
25-Jun-97	NE1-2	Interim cover with sparse vegetation	1-2 yrs
26-Jun-97	NE1-2	Interim cover with sparse vegetation	1-2 yrs
3-Jul-97	NE1-2	Interim cover	2-3 yrs
9-Jul-97	ML-1	Interim cover	2-3 yrs
10-Jul-97	ML-2	Interim cover	6 mons
15-Jul-97	ML-3	Interim cover	2-3 yrs
22-Jul-97	ML-4	Interim cover	6 mons
23-Jul-97	ML-5	Interim cover	6 mons
30-Jul-97	ML-6	Interim cover	6 mons
31-Jul-97	NE1-3	Interim cover	1-2 yrs
6-Aug-97	ML-7	Interim cover	2-3 yrs
7-Aug-97	ML-8	Interim cover	2-3 yrs
12-Aug-97	ML-9	Interim cover	2-3 yrs
14-Aug-97	ML-10	Interim cover	6 mons
19-Aug-97	NE1-4	Interim cover	1-2 yrs
20-Aug-97	NE1-5a	Interim cover with sparse vegetation	1-2 yrs
20-Aug-97	NE1-5b	Interim cover with sparse vegetation	1-2 yrs
20-Aug-97	NE1-5c	Interim cover with sparse vegetation	1-2 yrs
26-Sep-97	NE1-6	Interim cover	2-3 yrs
1-Oct-97	MLB-1	Interim cover -ground very wet (gas bubble)	2-3 yrs
8-Oct-97	MLB-1	Interim cover -ground very wet (gas bubble)	2-3 yrs
9-Oct-97	MLB-2	Interim cover -ground very wet (gas bubble)	2-3 yrs
15-Oct-97	MLB-1	Interim cover -soil drier than Oct 1/97	2-3 yrs
16-Oct-97	NE1-7	Interim cover w/sparse vegetation	1-2 yrs
17-Oct-97	ML-11	Interim cover	2-3 yrs
21-Oct-97	MLB-1	Interim cover -soil cracking	2-3 yrs
Cambridge Landfill			
16-Sep-97	CL-1	Interim cover	3-5 yrs
18-Sep-97	CL-2	Interim cover	3-5 yrs
Stratford Landfill			
22-Sep-97		final cover with vegetation	10 yrs
29-Sep-97		clay cover	1/2-1 yrs

Notes:* - See Figures 4.4 & 4.5

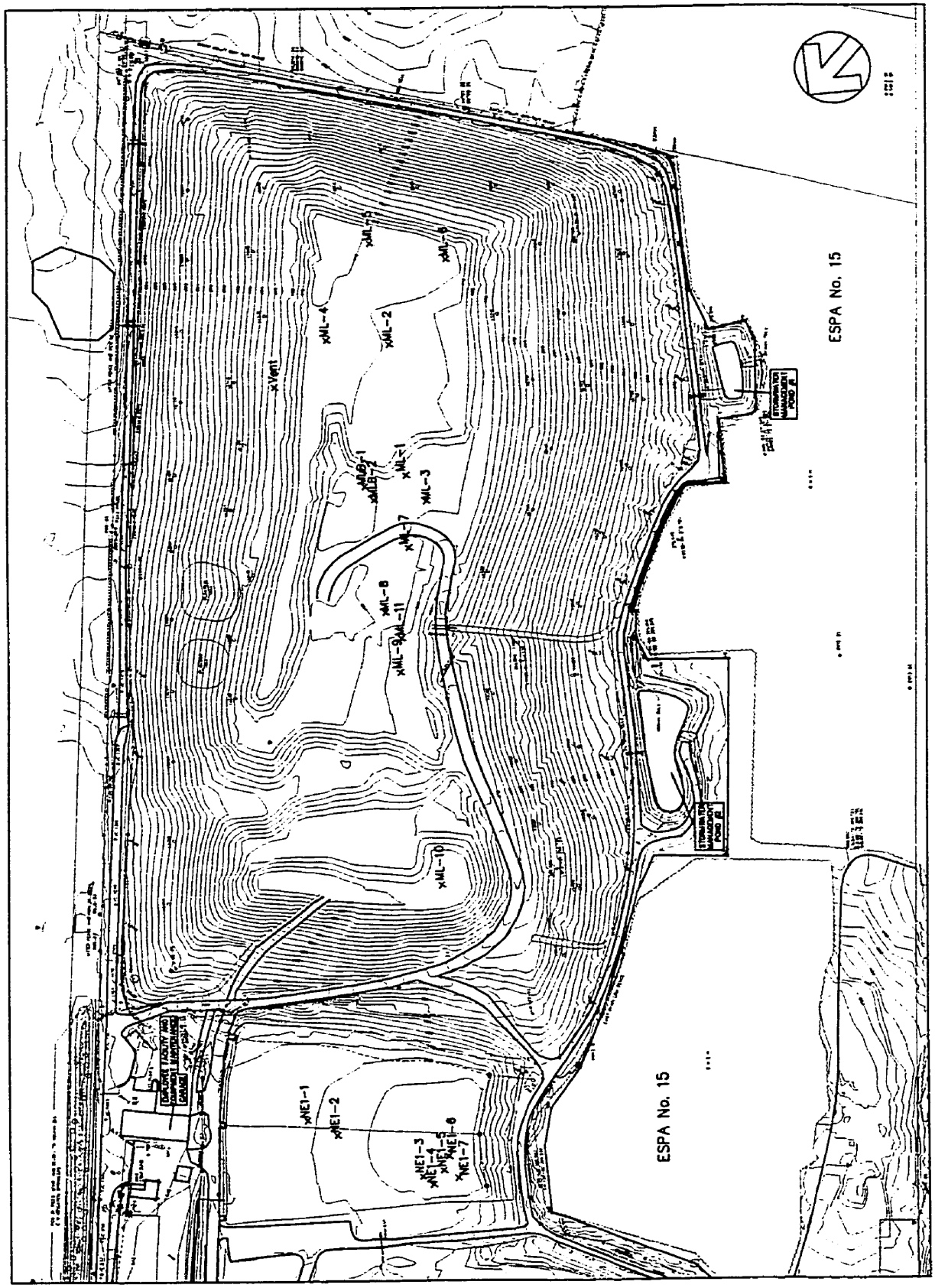

Figure 4.4: Location of sampling points for flux experiments at the Waterloo Landfill

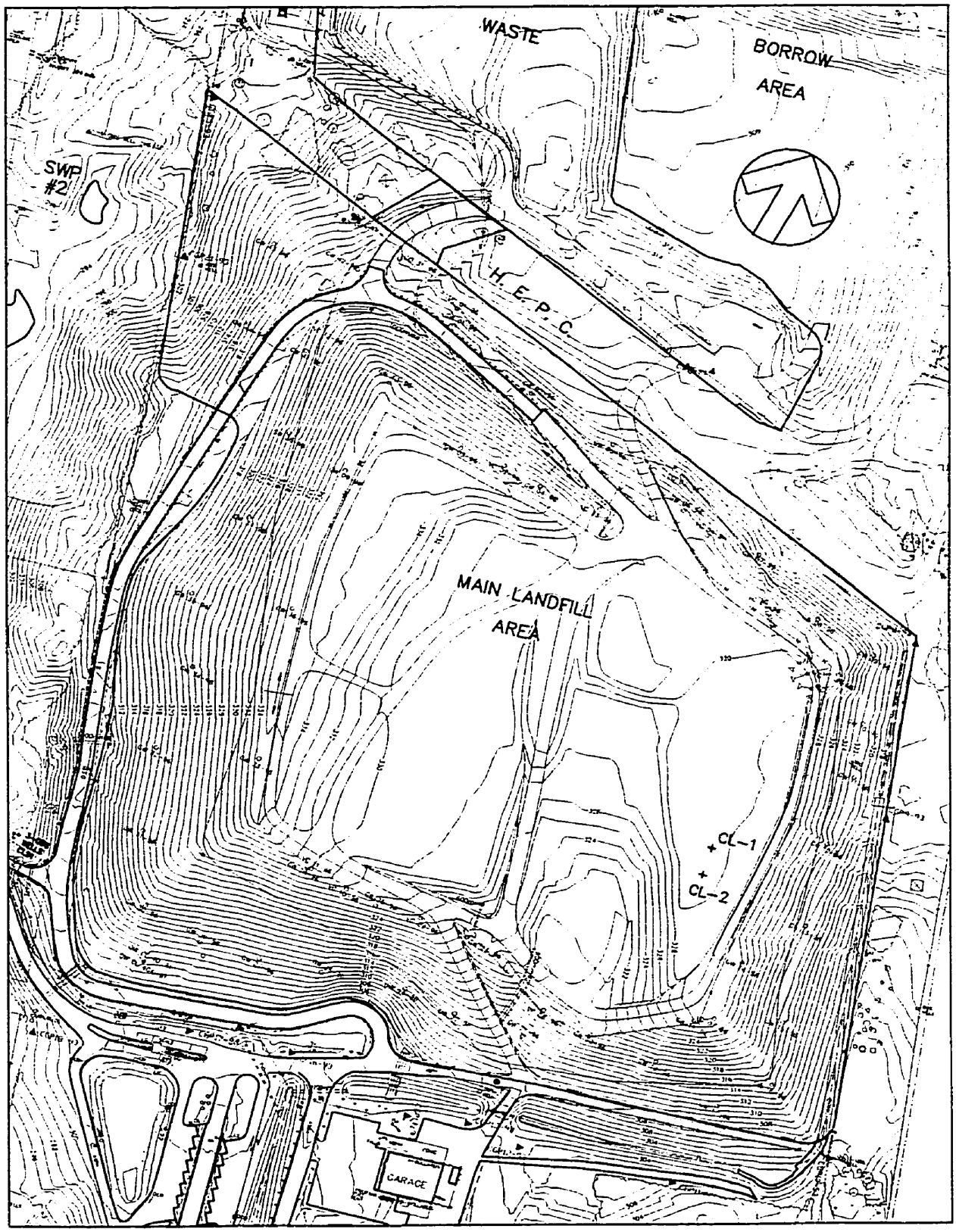

Figure 4.5: Location of sampling points for flux experiments at the Cambridge Landfill

Aircheck air sampler was converted to collect ambient air samples into 1 L tedlar bags. Both the flux chamber and ambient air were monitored hourly. The tedlar bags were stored in a cooler until analyses of the gas samples were performed in the University of Waterloo's Civil Engineering laboratories later that day. The analysis procedure involved removing a sample from the gas sample bag with a gas tight syringe (Hamilton). This sample was then injected into a GC-FID (Shimadzu GC-9A) for analysis.

4.2.2 Determination of VOC Concentrations

The ambient and effluent concentrations of TCE and PCE were monitored using ORBO tubes during the field experiments. Figure 4.3(a) shows the ambient air sampling equipment (SKC Aircheck Sampler Model 224-PCXR4) used along with the ORBO tubes to determine the ambient air concentrations. The SKC sampler recorded the length of time the sample tubes were in contact with ambient air. A bubble calibrator was used to calibrate the flow rate in the SKC sampler before and after each use in the field. A flow rate of 100 ml/min was maintained for all experiments based on the lab calibration studies.

TCE and PCE concentrations in the flux chamber effluent were determined by placing the ORBO tubes in the effluent stream ahead of the peristaltic pump. The average flow rate (designed for 100 ml/min) through the ORBO tubes was determined with the mass flow meters. The flow rate through the mass flow meters was recorded at ten minute intervals by a datalogger (CP-X, Lakewood systems). Figure 4.3(b) is a photo of the ORBO tubes in place with the electronic equipment (*i.e.* dataloggers and flow meters) used during the field experimentation.

The ambient and effluent ORBO tubes were put in place after approximately one hour, the time required to purge the flux chamber. At the end of the sampling period, the ORBO tubes were removed and capped and returned to University of Waterloo laboratory where they were stored at 4°C for analysis at a later date. Analyses of the tubes were performed by the procedure outlined in Section 3.3.2.

4.2.3 Determination of H_2S Concentration

The H_2S concentration was determined during the field experiments with the procedure outlined by NIOSH (Method 6013, Issue 1, 15 August 1994). Activated charcoal tubes

(ORBO 34, Supleco) were used to trap the H_2S vapour (Figure 3.3 shows an example of a typical ORBO tube).

A desorption efficiency for each batch of tubes used was determined. The percent recovery or desorption efficiency was established as outlined in the NIOSH method. The desorption efficiency for H_2S was determined using a gas standard of 1010 ppm H_2S that was diluted with a zero H_2O gas to the desired concentration. The exposed ORBO tubes were desorbed in a mixture of ammonium hydroxide solution (25%) and hydrogen peroxide (30%). Analysis of the tube contents was performed by breaking the tube open and separating the front and back portions and placing each into a 40 ml vial (sample preparation is outlined in the NIOSH method). The desorption procedure resulted in the sorbed H_2S being converted to sulfate ion. Analysis of sulfate ion in solution was performed on a Dionex Ion Chromatography with a Ion-Pac AS4A separator column and AG4A guard column. The sulfate ion concentration was then converted to H_2S by a factor of 0.3548 (MW H_2S/MW SO_4^{2-}).

The ambient air concentration of H_2S was determined by placing a dual adapter on the air sampler to accommodate the two ORBO tubes. The dual adapter allows different flow rates to pass through the ORBO tubes. The calibration of the adapter was checked prior to and after use to ensure that the required flow was maintained during the experiment. A flow rate of 200 ml/min was maintained through the tubes during the experiments.

The flux chamber effluent gas was also monitored for H_2S concentration. The same procedure used to monitor for TCE and PCE was followed to determine the H_2S concentration. An average of 200 ml/min through the ORBO tube was maintained throughout the experiments.

Both the ambient air and effluent gas ORBO tubes were put in place approximately one hour after startup, the time required to purge the flux chamber. At the end of the sampling period, the ORBO tubes were removed and capped and returned to University of Waterloo laboratory where they were stored at 4°C for analysis at a later date. The air concentration was determined using the procedure outlined in the NIOSH method.

4.2.4 Calculation of Flux Measurements for Methane, VOC and H_2S

The concentration within the flux chamber was obtained by the monitoring the effluent for the various gases of interest. The ambient air concentrations were taken at the same height and

position as the air intake for the flux chamber. Therefore, the ambient air concentration was assumed to be equivalent to the influent concentration to the flux chamber. The methane concentration was measured at hourly intervals whereas the average TCE, PCE, and H_2S concentrations were obtained as total accumulation over the experiment duration. Based on the assumption that the flux chamber was a continuous stirred reactor (well-mixed), the concentration of the effluent was the same as in the chamber. The gas flux measurements were calculated by subtracting the influent mass flow rate from the effluent mass flow rate (mass concentration times the flow rate). The difference in mass flow rate was divided by the surface area of the flux chamber. In the case where the ambient air concentrations were below the detection limit of the analytical equipment, the detection limit was used as the influent concentration for further calculations. The gas concentration emitted from the landfill surface was determined by taking the difference between the effluent and influent mass flow rates and dividing by the difference in the influent and effluent volumetric flow rates.

4.3 Results of *In-situ* Flux Chamber Measurements

Table 4.2 presents a summary of the operating parameters recorded during the field operation of the flux chamber. All flow rates were adjusted to the operating temperature and pressure from the standard calibration temperature and pressure.

4.3.1 Pressure Control Under Field Conditions

Figure 4.6 shows the flux chamber effluent flow rate on August 6, 1997 at the Waterloo Landfill. The flux chamber effluent flow rate for October 8, 1997 is shown in Figure 4.7. Both figures show the consistency of the effluent flow rate over the sampling period.

Appendix D contains graphs of all the data collected during the field flux measurements at the landfills. During the field experiments, the flux chamber gauge pressure was found to range from –0.086 to 0.622 mm H_2O with an average of 0.023 ± 0.119 mm H_2O. Excluding the single, very high gauge pressure measurement of 0.622 mm H_2O, the range of gauge pressure becomes –0.086 to 0.101 mm H_2O with an average of 0.003 ± 0.044 mm H_2O. The capture ratio estimated using the relationship established in Figure 3.7 results in an average capture ratio for the field experiments of 1.11 ± 0.09 which is less than 12% error. These capture ratios indicate that the flux measurements obtained during the field experiment can provide

reasonably accurate estimates of gas flux from landfill surfaces. Figures 4.8 and 4.9 show the flux chamber gauge pressure variations during the field experiments on August 6, 1997 and October 8, 1997 respectively. Figure 4.10 shows that while barometric pressure on October 8, 1997 fluctuated over a range of approximately 35 mm H_2O, the flux chamber gauge pressure

Table 4.2: Summary of data recorded during field flux chamber experiments.

Date	Average Chamber Flow Rate		Average Flow Rate		Average Chamber Transducer Δ Pressure	Average Barometric Pressure	Average Ambient Air Temperature
	Influent (ml/min)	Effluent (ml/min)	ORBO 34 (ml/min)	ORBO 32 (ml/min)	(mm H_2O)	(in Hg)	(°C)
Waterloo Landfill							
3-Jul-97	1419	1421	235	120	-0.005	28.5	21
9-Jul-97	1606	1791	225	106	-0.060	28.8	17.2
10-Jul-97	1630	1826	209	102	-0.007	29.1	24
15-Jul-97	1646	1650	221	113	0.006	28.8	29.3
22-Jul-97	1646	1732	223	111	0.058	29	25.5
23-Jul-97	1644	1648	207	101	-0.005	28.9	25
30-Jul-97	1652	1714	237	113	0.057	29.1	28.1
31-Jul-97	1651	1663	225	90	0.060	29.1	28
6-Aug-97	1637	1956	215	106	-0.022	29.0	24.0
7-Aug-97	1635	1666	203	95	-0.086	29.0	24.2
12-Aug-97	1619	1769	228	109	-0.013	29.0	20.9
14-Aug-97	1611	1663	204	113	0.012	28.8	18.2
19-Aug-97	1589	1601	218	103	-0.052	29.0	24.7
20-Aug-97	1601	1718	245	125	-0.045	28.9	16.4
20-Aug-97	1615	1764	249	122	0.017	28.8	18.6
20-Aug-97	1617	1679	243	127	0.062	28.8	18.9
26-Sep-97	1585	1684	164	99	-0.053	28.9	13.9
1-Oct-97	1557	1664	298	117	0.101	28.9	8.5
8-Oct-97	1469	1560	324	100	0.001	29.0	23.5
9-Oct-97	1638	1676	316	97	-0.008	28.9	23.6
15-Oct-97	1549	1605	274	97	-0.021	29.1	9.3
16-Oct-97	1528	1532	261	90	0.021	29.2	12.1
17-Oct-97	1575	1595	318	95	-0.016	29.0	13.5
21-Oct-97	1557	1643	305	119	0.013	28.7	7.2
Cambridge Landfill							
16-Sep-97	1638	1717	259	109	-0.002	29.1	25.9
18-Sep-97	1623	1656	182	114	0.049	29.1	22.9
Stratford Landfill							
22-Sep-97	1601	1808	211	119	-0.005	29.0	18.4
29-Sep-97	1615	1617	338	119	0.622	28.3	19.3

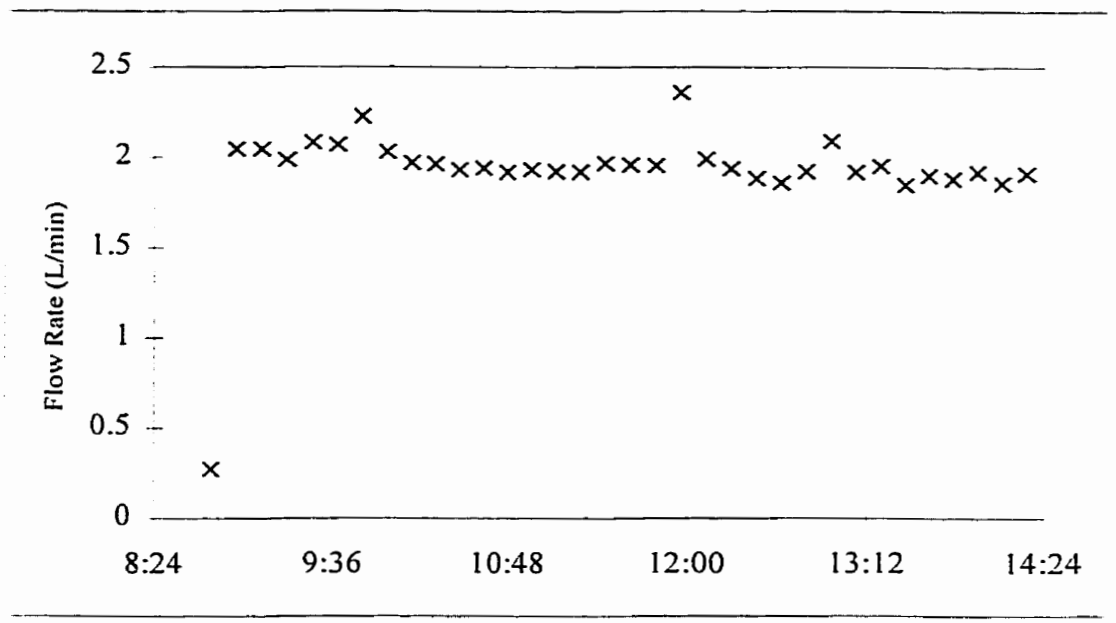

Figure 4.6: Flux chamber effluent flow rate during flux chamber experiment on August 6/97 at the Waterloo Landfill.

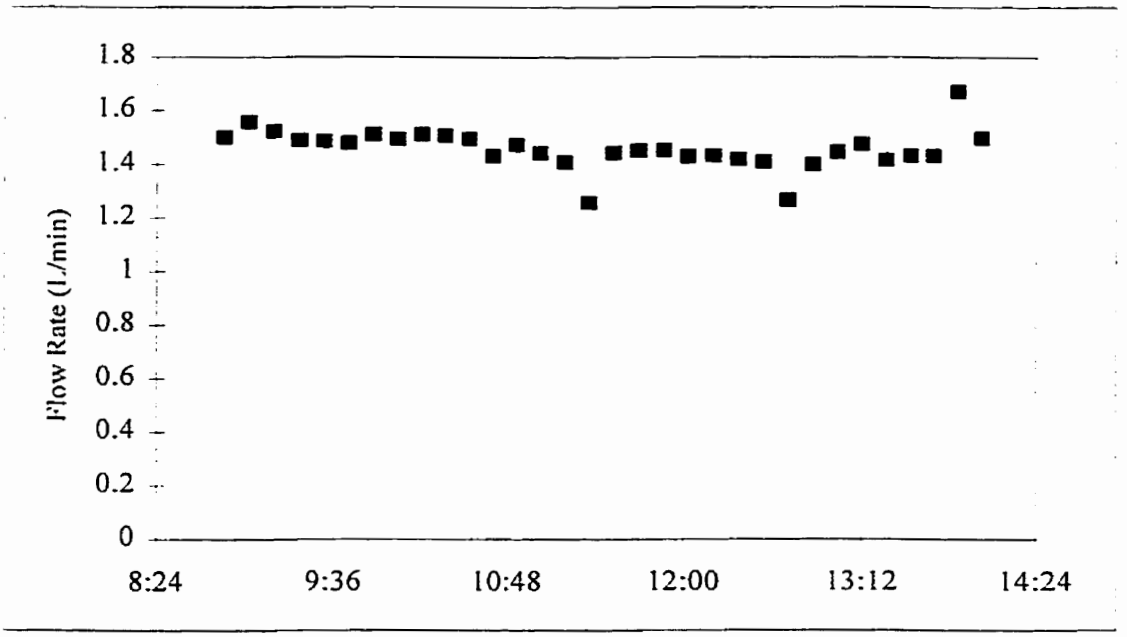

Figure 4.7: Flux chamber effluent flow rate during flux chamber experiment on October 8/97 at the Waterloo Landfill.

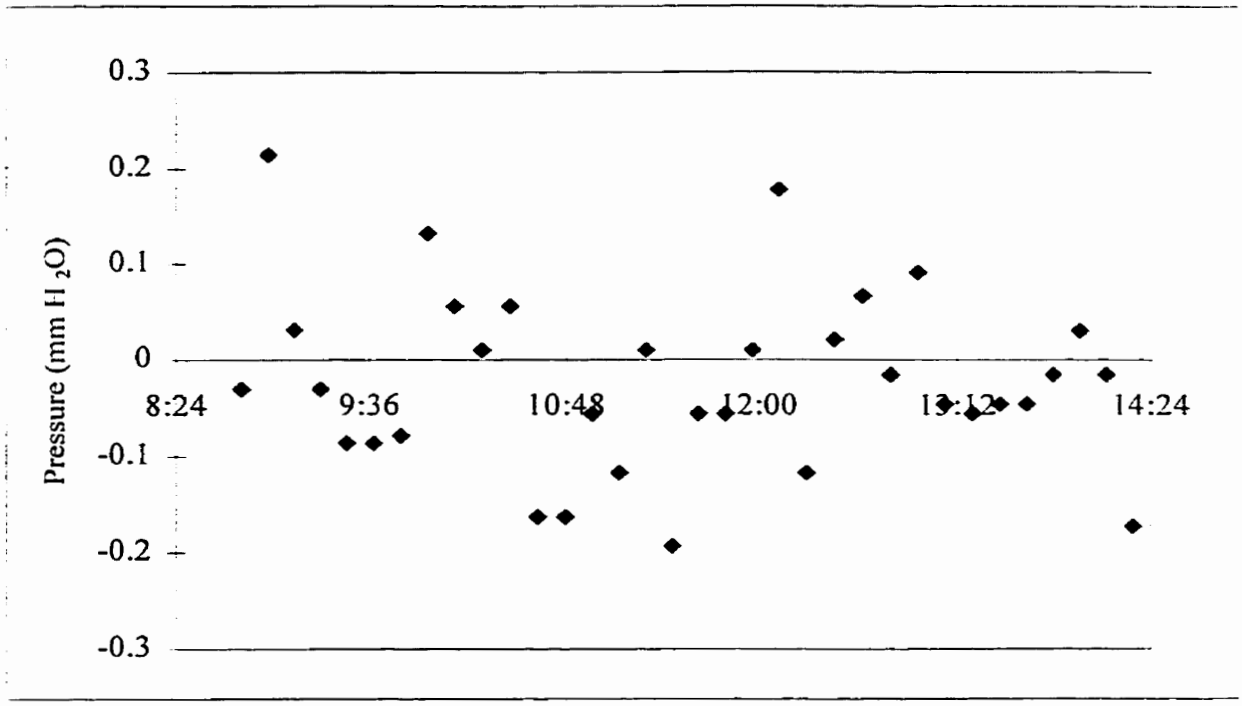

Figure 4.8: Gauge chamber pressure during flux chamber experiment on August 6/97 at the Waterloo Landfill.

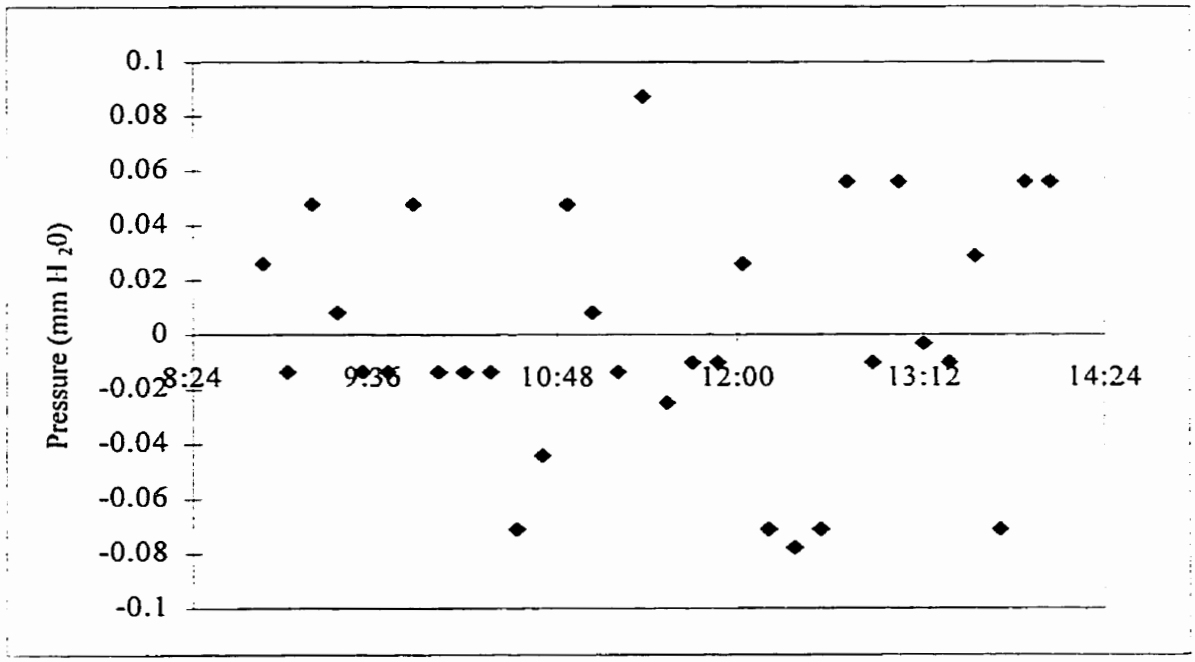

Figure 4.9: Gauge chamber pressure during flux chamber experiment on October 8/97 at the Waterloo Landfill.

was maintained close to zero with most fluctuations less than ± 0.2 mm H_2O. The laboratory analysis presented previously in Section 3.5 quantified the error introduced to flux measurements by small flux chamber gauge pressure and temperature differentials. The need to keep these average differentials near zero to obtain accurate flux measurements was established. These results demonstrate that the equipment functioned well in the field and provided the potential for accurate surface gas flux measurements to be made. This is a significant achievement of the design developed in this research.

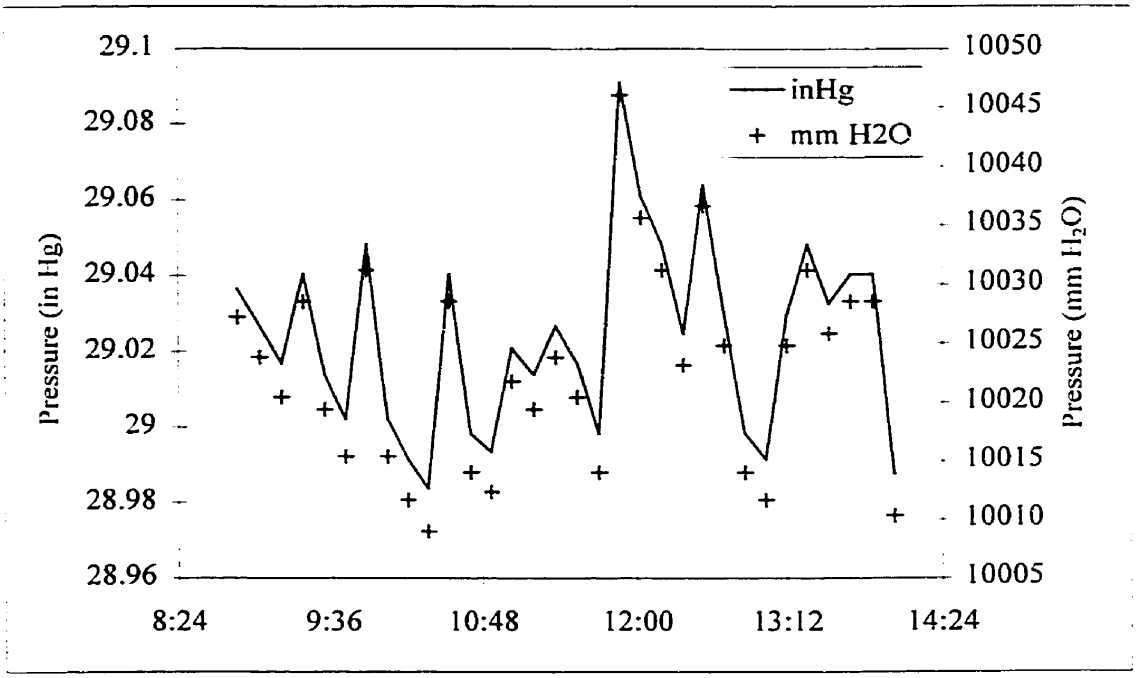

Figure 4.10: Barometric pressure during flux chamber experiment on October 8/97 at Waterloo Landfill.

The temperature of the air and soil within the flux chamber were consistent with the ambient air and soil temperatures as shown in Figure 4.11.

4.3.2 Methane Flux Measurements

Table 4.3 shows the average methane concentration ($\mu g/m^3$) in the ambient air (influent) and flux chamber effluent. As expected the methane concentration was higher within the flux chamber indicating discharge from the landfill surface. It is important to note that at a height of 3 m above the surface, the height of the intake, significant amounts of methane were detectable during most experiments.

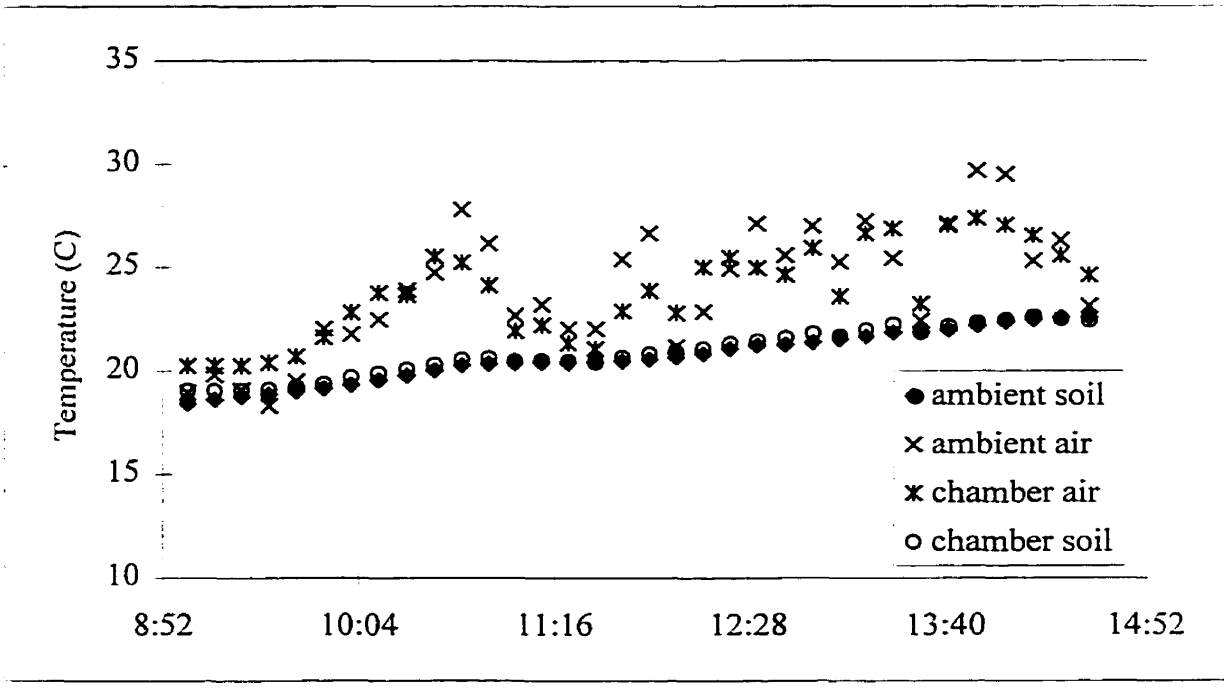

Figure 4.11: Temperature of soil and air within flux chamber and ambient conditions during flux chamber experiment on August 6/97 at the Waterloo Landfill.

Flux measurements were made on holes in the interim cover or gas bubble locations (MLB-1 and MLB-2) as well as on the intact surface (ML, NE1 & CL). The gas bubbles resulted in a much higher methane concentration within the flux chamber. Table 4.4 shows the methane flux ($g/m^2/d$) and methane concentration emitted from the landfill surface (% V/V & $\mu g/m^3$). The methane flux from all surfaces ranged from 0 to 321.48 $g/m^2/d$. Methane flux from the landfill surface with no apparent hole resulted in an average methane flux of 1.86 $g/m^2/d$ whereas an average flux of 172.1 $g/m^2/d$ was found in the presence a hole. In both of these cases, the approximate age of waste below the flux chamber was the same (2.5 years).

The methane concentrations emitted from the landfill surface were found to range from 1.17×10^3 to 1.81×10^8 $\mu g/m^3$. This range included the flux measurements made over small holes in the landfill surface. A range of methane concentration, 2.47×10^7 to 1.81×10^8 $\mu g/m^3$, was found from samples taken over a hole whereas, the methane concentration with no hole ranged from 1.17×10^3 to 6.84×10^7 $\mu g/m^3$ approximately 1 to 3 orders of magnitude lower. The results indicate that small imperfections in the cover such as holes and fissures have a large effect on the amount of landfill gas released.

Table 4.3: Average methane concentrations in the ambient air and flux chamber during each flux experiment at the Waterloo, Cambridge and Stratford Landfills.

Date	Site Location*	Ambient Air Concentration ($\mu g/m^3$)	Measured Concentration within Flux Chamber ($\mu g/m^3$)
Waterloo Landfill			
3-Jul-97	NE1-2	-	-
9-Jul-97	ML-1	-	1.33×10^4
10-Jul-97	ML-2	-	3.82×10^4
15-Jul-97	ML-3	-	-
22-Jul-97	ML-4	-	6.90×10^4
23-Jul-97	ML-5	-	1.31×10^4
30-Jul-97	ML-6	-	-
31-Jul-97	NE1-3	-	5.18×10^5
6-Aug-97	ML-7	1.34×10^4	2.56×10^4
7-Aug-97	ML-8	-	-
12-Aug-97	ML-9	-	7.72×10^4
14-Aug-97	ML-10	2.15×10^4	2.25×10^4
19-Aug-97	NE1-4	-	4.4×10^4
20-Aug-97	NE1-5a	1.97×10^4	2.85×10^4
20-Aug-97	NE1-5b	1.70×10^4	2.07×10^4
20-Aug-97	NE1-5c	-	1.73×10^4
26-Sep-97	NE1-6	-	1.2×10^4
1-Oct-97	MLB-1	2.89×10^4	5.19×10^6
8-Oct-97	MLB-1	4.95×10^4	8.54×10^6
9-Oct-97	MLB-2	4.38×10^4	8.12×10^5
15-Oct-97	MLB-1	4.56×10^4	6.4×10^6
16-Oct-97	NE1-7	1.16×10^4	1.44×10^4
17-Oct-97	ML-11	5.85×10^4	5.78×10^4
21-Oct-97	MLB-1	2.69×10^4	1.32×10^6
Cambridge Landfill			
16-Sep-97	CL-1	-	3.19×10^4
18-Sep-97	CL-2	1.04×10^4	1.21×10^5
Stratford Landfill			
22-Sep-97		-	-
29-Sep-97		1.29×10^4	1.52×10^4

Notes:* - See Figures 4.4 & 4.5

- at or below detection limit of 1.02×10^4 $\mu g/m3$ (at 1 atm and 20°C)

Table 4.4: Methane flux and methane concentration emitted from landfill surface at each flux experiment location at the Waterloo, Cambridge and Stratford Landfills

Date	Site Location*	Methane Flux ($g/m^2/d$)	Estimated Methane Concentration Emitted from Surface (%V/V)	Estimated Methane Concentration Emitted from Surface ($\mu g/m^3$)
Waterloo Landfill				
3-Jul-97	NE1-2	0.00	0.00	9.67×10^3
9-Jul-97	ML-1	0.19	0.01	4.25×10^4
10-Jul-97	ML-2	1.31	0.04	2.75×10^5
15-Jul-97	ML-3	0.00	0.00	9.48×10^3
22-Jul-97	ML-4	2.51	0.19	1.2×10^6
23-Jul-97	ML-5	0.14	0.22	1.41×10^6
30-Jul-97	ML-6	0.01	0.00	9.63×10^3
31-Jul-97	NE1-3	20.5	10.9	6.84×10^7
6-Aug-97	ML-7	0.68	0.01	8.78×10^4
7-Aug-97	ML-8	0.01	0.00	9.73×10^3
12-Aug-97	ML-9	2.93	0.13	8.05×10^5
14-Aug-97	ML-10	0.07	0.01	5.49×10^4
19-Aug-97	NE1-4	1.33	0.74	4.68×10^6
20-Aug-97	NE1-5a	0.42	0.02	1.49×10^5
20-Aug-97	NE1-5b	0.22	0.01	5.95×10^4
20-Aug-97	NE1-5c	6.65	0.68	4.4×10^6
26-Sep-97	NE1-6	0.10	0.01	4.31×10^4
1-Oct-97	MLB-1	209	12.1	8.05×10^7
8-Oct-97	MLB-1	321	22.9	1.46×10^8
9-Oct-97	MLB-2	31.3	5.35	3.39×10^7
15-Oct-97	MLB-1	247	26.9	1.81×10^8
16-Oct-97	NE1-7	0.11	0.14	9.68×10^5
17-Oct-97	ML-11	0.00	0.00	1.17×10^3
21-Oct-97	MLB-1	51.7	3.70	2.47×10^7
Cambridge Landfill				
16-Sep-97	CL-1	0.94	0.08	4.87×10^5
18-Sep-97	CL-2	4.46	0.85	5.43×10^6
Stratford Landfill				
22-Sep-97		0.05	0.00	9.93×10^3
29-Sep-97		0.09	0.29	1.8×10^6

Notes:* - See Figures 4.4 & 4.5

The presence of the gas extraction system and its effects on the flux was examined by plotting the waste age versus the methane flux. Figure 4.12 presents the flux versus the estimated age of the waste with and without gas extraction. The NE1 and Stratford data were taken in the absence of a gas extraction. The other data excluding those data collected at holes and fissures, were collected in the presence of gas extraction wells, although the gas extraction wells were 45 m from the closest sample location. The extraction wells within the gas extraction system were spaced at approximately 45 to 60 meters (with an expected radius of influence of between 25 to 30 m). Although the data are crude, this figure suggests that the gas extraction system had minimal influence on flux emissions measured under the conditions of this research. However, the extraction wells may have been too far away to make a difference. As well, more complex covers including those which use membranes could produce different results.

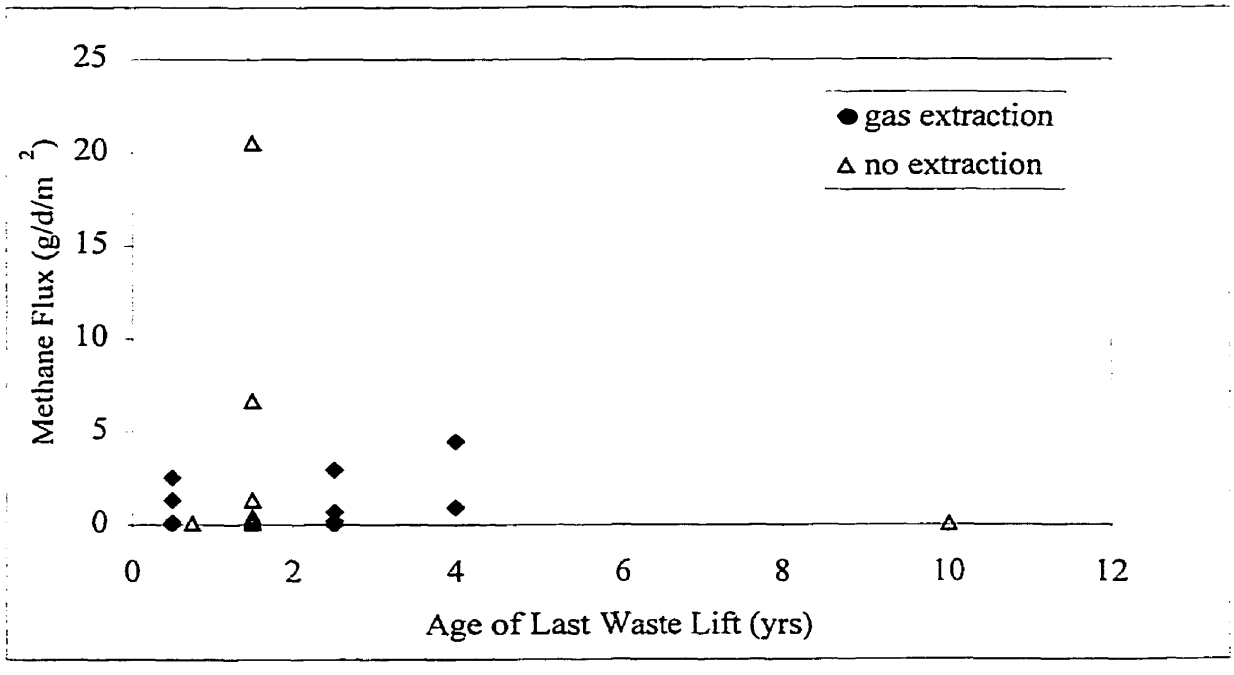

Figure 4.12: Methane flux versus waste age with and without gas extraction.

On August 20, 1997, the spatial variability in flux emissions between site locations within the same time frame was examined. Three different locations within 0.5 meter of each other were examined. The methane flux was found to range from 0.23 to 6.87 $g/m^2/d$. The methane concentration emitted from the surface ranged from 53.6 to 2,472 mg/m^3. This variability over such a short distance is high and is assumed to be the result of variations in intermediate cover soil properties and thickness.

Figures 4.13 and 4.14 show the influent and effluent methane concentration (%V/V) on August 6, 1997 and October 8, 1997 respectively. On August 6, 1997 the landfill surface consisted of a dry clayey soil over the landfilled waste, and in this case the ambient (2.11 x 10^{-3} % V/V) and effluent (4.02 x 10^{-3} % V/V) concentrations were close and resulted in an average methane flux of 0.68 g/m^2/d. Whereas, the flux measurement at a hole in the cover (October 8, 1997) had an effluent concentration (1.34 % V/V) approximately 172 times higher than the influent ambient air concentrations (7.75 x 10^{-3} % V/V) resulting in an average methane flux of 321.48 g/m^2/d. Both sample days had similar ambient air conditions, but ultimately the presence of the hole in the cover resulted in the higher gas flux from the landfill surface.

4.3.3 VOC and H_2S Flux Measurements

The average TCE, PCE, and H_2S concentrations (µg/m^3) in the atmosphere and flux chamber during the experimentation are shown in Table 4.5. The TCE and PCE data for August and the H_2S data for June, July, and August were discarded because of sampling problems. Figures 4.15 and 4.16 show the flow rate through the effluent ORBO 32 tubes (TCE and PCE) on August 6, 1997 and October 8, 1997 respectively. Figures 4.17 and 4.18 show the flow rate

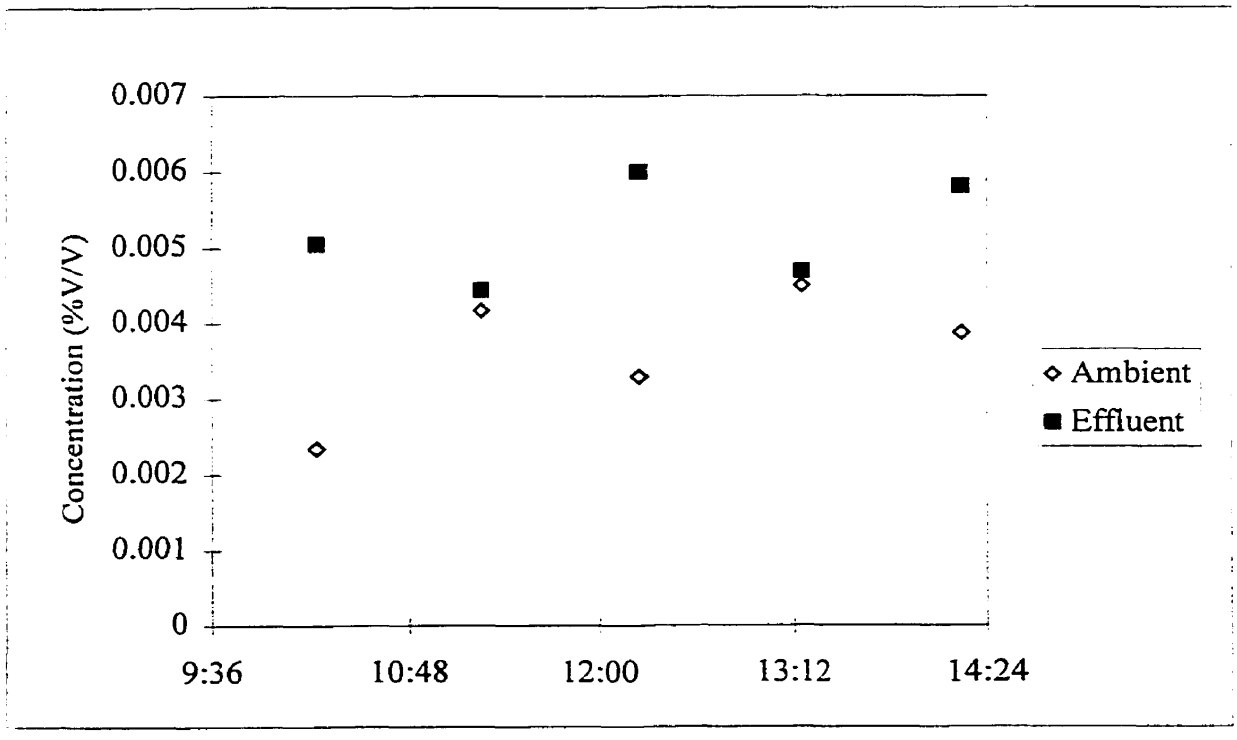

Figure 4.13: Methane concentration (% V/V) in ambient air and flux chamber effluent on August 6, 1997 during flux chamber experiment at the Waterloo Landfill.

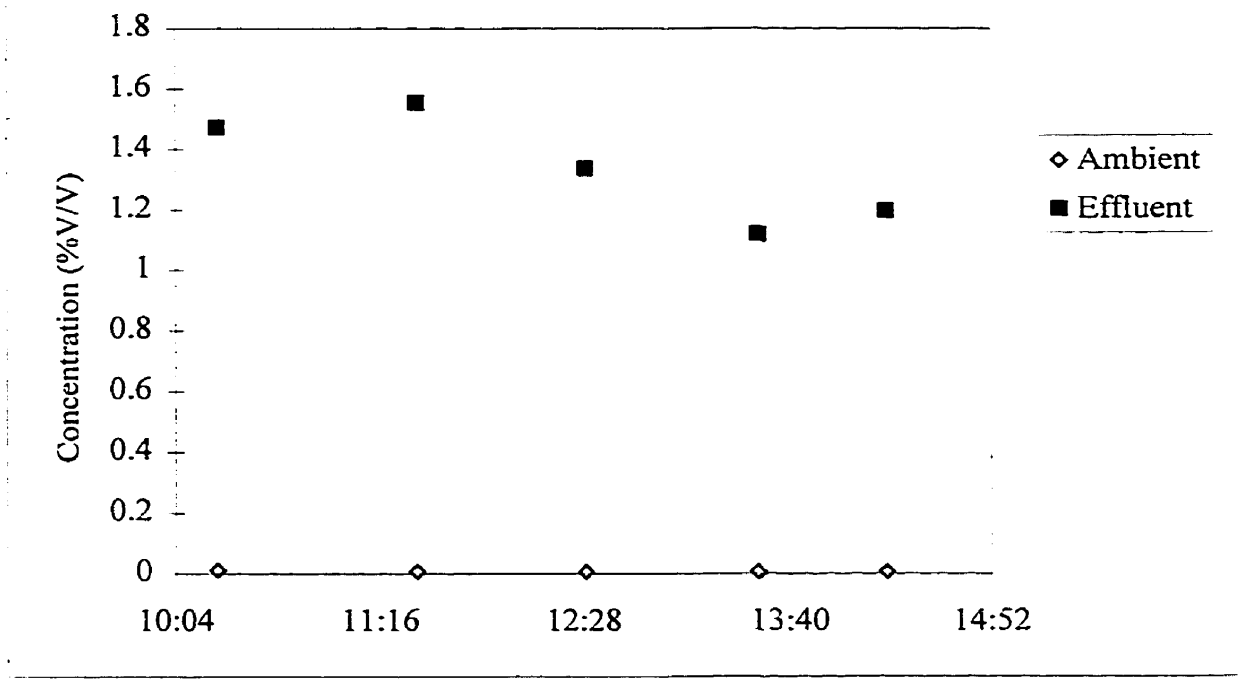

Figure 4.14: Methane concentration (% V/V) in ambient air and flux chamber effluent on October 8, 1997 during flux chamber experiment at the Waterloo Landfill.

through the effluent ORBO 34 tubes (H_2S) on August 6, 1997 and October 8, 1997 respectively. The volume of air passing through the ORBO tubes is affected by the flow rates, therefore a constant flow rate is needed to ensure an accurate estimate of the air volume and ultimately the measured concentration. The fluctuation in the flow rates shown in the Figures over time, was due to the peristaltic pump and the timing of the recording device. The peristaltic pump used to remove the air from the flux chamber has one large head and large diameter tubing. The size of the head and tubing contributed to the fluctuations observed in the flows. The larger pump head has larger spaces between the rollers in the pump resulting in greater time delay between the recovery phase. The data logger recorded every ten minutes. Therefore depending on the phase of the pump head cycle, the flow may have been up or down. These fluctuations would have been smoother with the use of many more smaller pump heads where the distance between the rollers is smaller and off-setting the cycle of the rollers in each pump head. This option was not available because the required flow of approximately 2 litres per minute could not be met with the available smaller pump heads and pumps. The

Table 4.5: Average TCE, PCE and H_2S concentration in the ambient air and flux chamber during each flux experiment at the Waterloo, Cambridge and Stratford Landfills. (3-5 hour samples)

Date	Site Location*	Ambient Air Concentration			Concentration within Flux Chamber		
		TCE ($\mu g/m^3$)	PCE ($\mu g/m^3$)	H_2S ($\mu g/m^3$)	TCE ($\mu g/m^3$)	PCE ($\mu g/m^3$)	H_2S ($\mu g/m^3$)
Waterloo Landfill							
19-Jun-97	NE1-1	0.63	1.14				
25-Jun-97	NE1-2	1.00	1.01				
26-Jun-97	NE1-2	0.77	0.88				
3-Jul-97	NE1-2	1.12	0.77		0.68	2.28	
9-Jul-97	ML-1	0.82	0.68		0.36	2.82	
10-Jul-97	ML-2	0.82	1.11		0.87	0.50	
15-Jul-97	ML-3	1.16	0.83		0.72	0.54	
22-Jul-97	ML-4	0.97	0.66		0.60	1.12	
23-Jul-97	ML-5	0.80	0.65		0.72	0.71	
30-Jul-97	ML-6	3.27	1.38		1.00	0.97	
19-Aug-97	NE1-4	NA	NA	NA	NA	NA	NA
20-Aug-97	NE1-5	NA	NA	NA	NA	NA	NA
26-Sep-97	NE1-6	NA	NA	NA	NA	NA	NA
1-Oct-97	MLB-1	1.79	2.02	55	1.24	2.35	460
8-Oct-97	MLB-1	2.38	1.36	ND	4.15	1.67	625
9-Oct-97	MLB-2	1.38	1.35	ND	1.79	1.60	ND
15-Oct-97	MLB-1	0.68	0.85	ND	2.01	1.35	408
16-Oct-97	NE1-7	0.78	0.85	82	1.45	1.29	ND
17-Oct-97	ML-11	0.91	1.05	ND	1.09	1.11	89
21-Oct-97	MLB-1	0.67	1.22	ND	0.62	1.25	ND
Cambridge Landfill							
16-Sep-97	CL-1	4.70	2.76	ND	2.57	3.59	ND
18-Sep-97	CL-2	2.71	3.58	ND	1.08	3.27	ND
Stratford Landfill							
22-Sep-97		1.32	2.04	ND	1.44	2.16	ND
29-Sep-97		2.53	1.30	12	0.74	2.03	ND

Notes:

* - See Figures 4.4 & 4.5

NA – samples not obtained during these dates

ND- non detect

values shown in Table 4.5 are average concentrations obtained over the 3 to 5 hour duration of experimentation. The TCE, PCE, and H_2S concentrations obtained from the ORBO tubes were based on the total accumulation of these compounds in the tubes over the exposure period. The TCE concentrations ranged from 0.63 to 4.70 $\mu g/m^3$ in the ambient air and 0.36 to 4.68 $\mu g/m^3$ in the flux chamber. The PCE concentrations ranged from 0.65 to 3.58 $\mu g/m^3$ in the ambient air and 0.5 to 6.4 $\mu g/m^3$ in the flux chamber in eleven samples. The H_2S concentration data in the ambient air ranged from ND to 82 $\mu g/m^3$ and ranged from ND to 625 $\mu g/m^3$ in the flux chamber in eleven samples. There was little difference between the ambient air and flux chamber concentration of the TCE, PCE and H_2S indicating very low levels of surface flux of these chemicals through the cover at the points of measurement.

In order to compare this data to the ambient air quality criteria, these values were standardized to ½ hour values and 24 hour values (See Appendix E for conversion equation and procedure). Table 4.6 contains the TCE, PCE and H_2S values converted to ½ hour averages. Comparing these values to the ½ hour Point of Impingement Standard established by the Ontario Ministry of Environment (1994), indicates that H_2S exceeded the established limits in the four samples

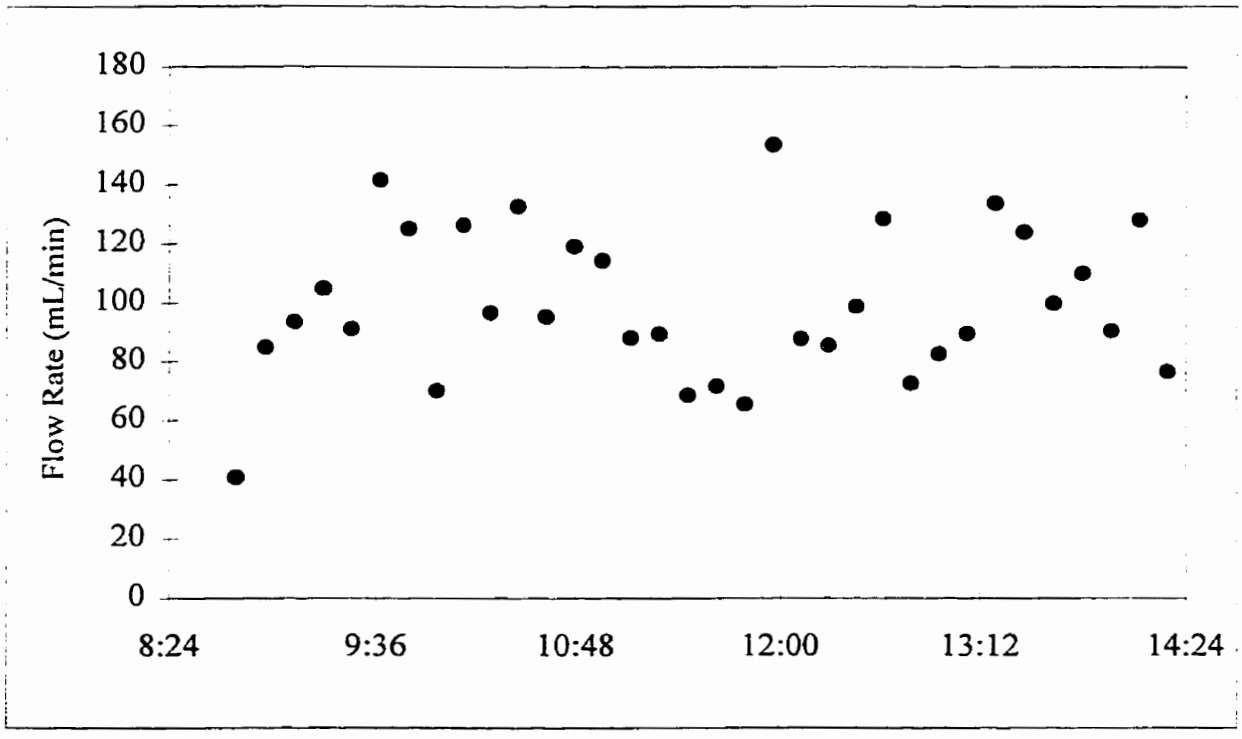

Figure 4.15: ORBO 32 flow rate during flux chamber experiment on August 6/97 at the Waterloo Landfill.

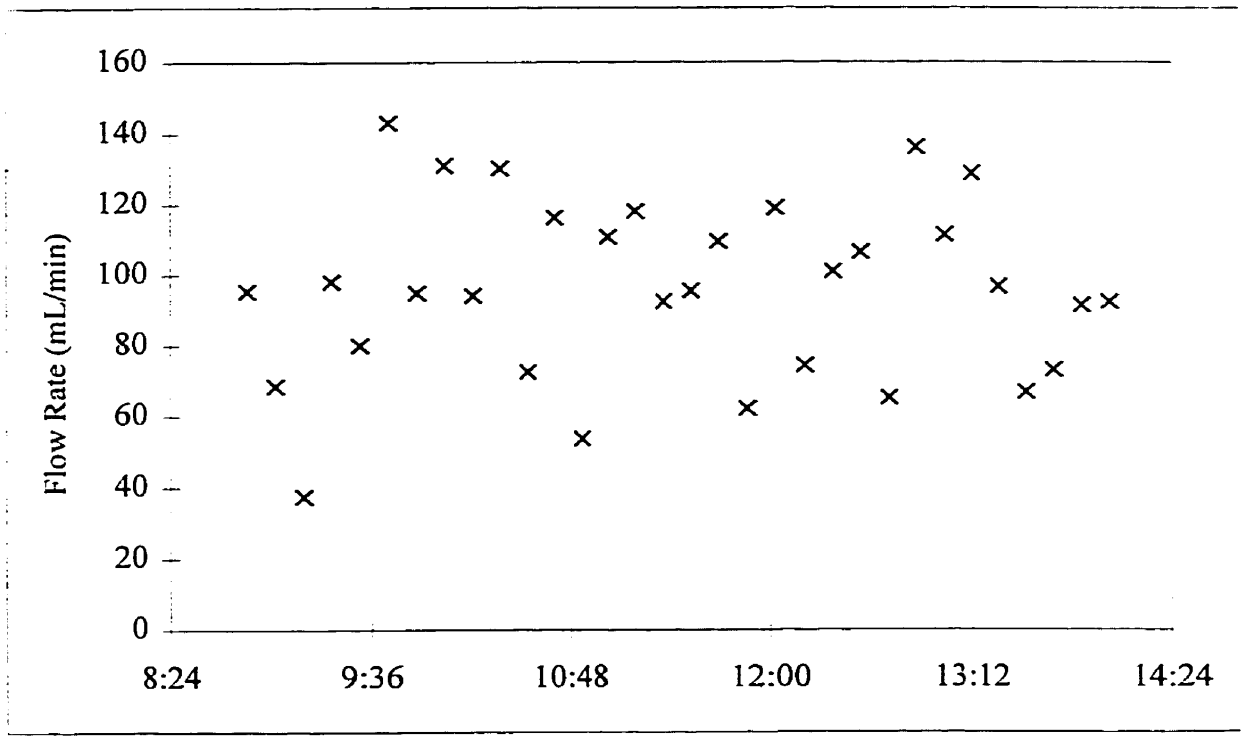

Figure 4.16: ORBO 32 flow rate during flux chamber experiment on October 8/97 at the Waterloo Landfill.

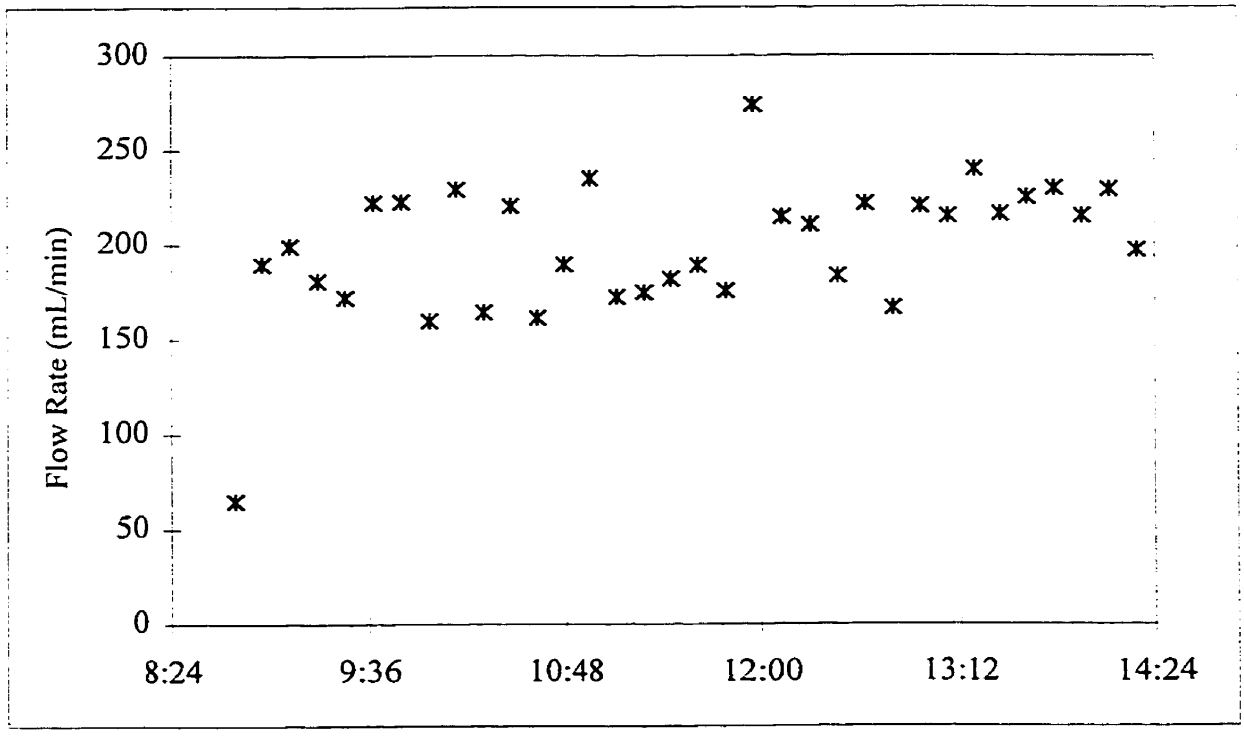

Figure 4.17: ORBO 34 flow rate during flux chamber experiment on August 6/97 at the Waterloo Landfill.

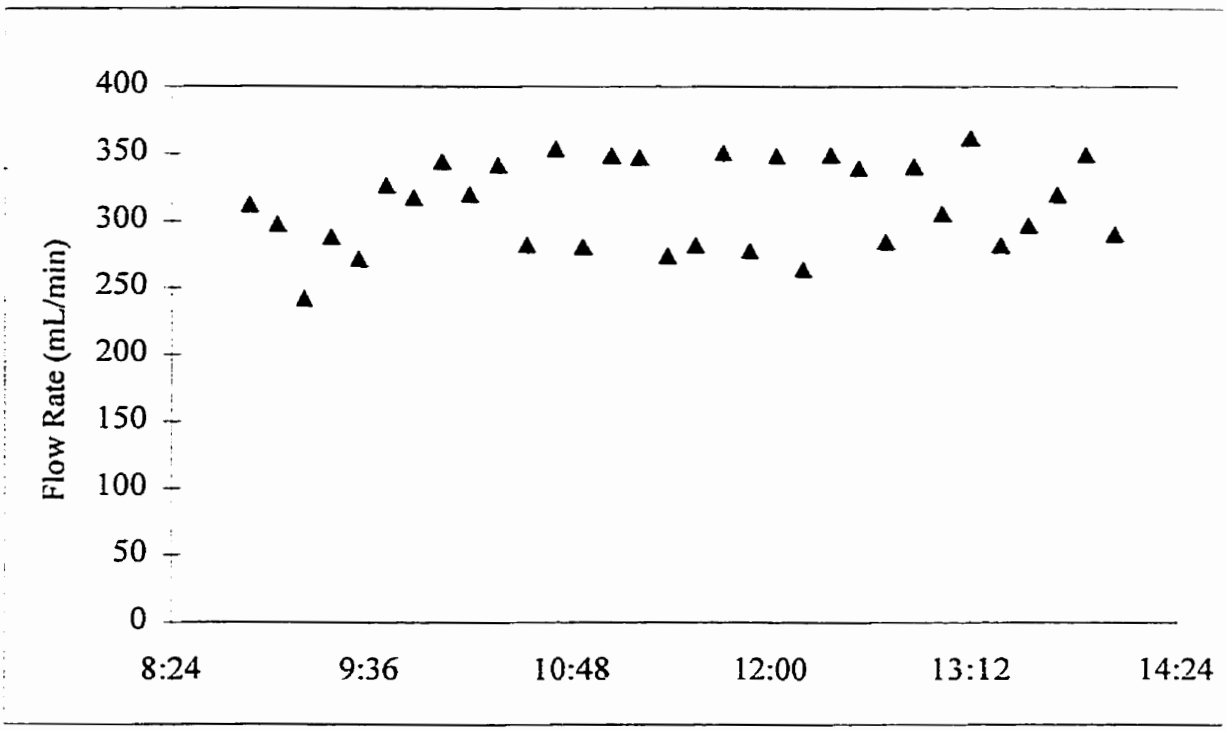

Figure 4.18: ORBO 34 flow rate during flux chamber experiment on October 8/97 at the Waterloo Landfill.

of flux chamber effluent in which it was detected. The 24 hour averages of the TCE, PCE and H_2S are presented in Table 4.7. Again, the H_2S values exceeded the 24 hour National Ambient Air Quality Criteria (NAAQC) in both the ambient air and flux chamber. TCE and PCE concentrations did not.

Table 4.8 contains the flux and concentration data for TCE, PCE and H_2S emitted from the surface. The ambient and flux chamber concentrations as shown in Table 4.5 were almost equivalent during many of the field measurements. However during the flux measurement on the "bubble" (hole), the concentration in the flux chamber exceeded the ambient air conditions. This difference in concentration may have been a result of the intact cover absorbing or oxidizing the VOCs and H_2S therefore removing them prior to emission to the atmosphere. In the case of a hole, transport to the atmosphere is much quicker and does not allow time for these reactions to occur. The rainfall during October and the wet condition of the cover may also have reduced the release of these compounds to the atmosphere. Only the data from October

Table 4.6: Average TCE, PCE and H_2S concentration in the ambient air and flux chamber during each flux experiment at the Waterloo, Cambridge and Stratford Landfills converted to ½ hour values.

Date	Site Location*	Ambient Air Concentration			Concentration within Flux Chamber		
		TCE ($\mu g/m^3$)	PCE ($\mu g/m^3$)	H_2S ($\mu g/m^3$)	TCE ($\mu g/m^3$)	PCE ($\mu g/m^3$)	H_2S ($\mu g/m^3$)
Waterloo Landfill							
19-Jun-97	NE1-1	1.93	3.50				
25-Jun-97	NE1-2	2.06	2.09				
26-Jun-97	NE1-2	2.59	2.96				
3-Jul-97	NE1-2	3.43	2.34		1.95	6.53	
9-Jul-97	ML-1	2.64	2.20		1.10	8.58	
10-Jul-97	ML-2	2.70	3.64		2.82	1.63	
15-Jul-97	ML-3	3.82	2.75		2.29	1.72	
22-Jul-97	ML-4	3.38	2.27		1.98	3.69	
23-Jul-97	ML-5	2.49	2.04		2.29	2.23	
30-Jul-97	ML-6	10.4	4.38		3.07	2.98	
1-Oct-97	MLB-1	3.28	3.70	100	2.14	4.04	790
8-Oct-97	MLB-1	7.54	4.28	ND	12.5	5.03	1.88×10^3
9-Oct-97	MLB-2	2.74	2.69	ND	3.36	2.99	ND
15-Oct-97	MLB-1	2.17	2.71	ND	5.81	3.91	1.17×10^3
16-Oct-97	NE1-7	2.38	2.60	252	3.99	3.55	ND
17-Oct-97	ML-11	2.62	3.03	ND	3.25	3.29	265
21-Oct-97	MLB-1	1.76	3.22	ND	1.64	3.29	ND
Cambridge Landfill							
16-Sep-97	CL-1	15.20	8.93	ND	7.79	10.9	ND
18-Sep-97	CL-2	7.26	9.57	ND	3.34	10.1	ND
Stratford Landfill							
22-Sep-97		4.17	6.43	ND	4.06	6.10	ND
29-Sep-97		4.70	2.42	22	1.31	3.60	ND
½ hour Point of Impingement Limit (MOE, 1994)					85,000	10,000	30

Notes:

* - See Figures 4.4 & 4.5

ND - non detect

Table 4.7: Average TCE, PCE and H_2S concentration in the ambient air and flux chamber during each flux experiment at the Waterloo, Cambridge and Stratford Landfills converted to 24 hour values.

Date	Site Location*	Ambient Air Concentration			Concentration within Flux Chamber		
		TCE ($\mu g/m^3$)	PCE ($\mu g/m^3$)	H_2S ($\mu g/m^3$)	TCE ($\mu g/m^3$)	PCE ($\mu g/m^3$)	H_2S ($\mu g/m^3$)
Waterloo Landfill							
19-Jun-97	NE1-1	0.28	0.50				
25-Jun-97	NE1-2	0.57	0.58				
26-Jun-97	NE1-2	0.37	0.43				
3-Jul-97	NE1-2	0.50	0.34		0.28	0.94	
9-Jul-97	ML-1	0.38	0.32		0.16	1.24	
10-Jul-97	ML-2	0.39	0.53		0.41	0.24	
15-Jul-97	ML-3	0.55	0.40		0.33	0.25	
22-Jul-97	ML-4	0.49	0.33		0.29	0.53	
23-Jul-97	ML-5	0.36	0.30		0.33	0.32	
30-Jul-97	ML-6	1.50	0.63		0.44	0.43	
1-Oct-97	MLB-1	0.91	1.03	28	0.60	1.13	220
8-Oct-97	MLB-1	1.09	0.62	ND	1.80	0.73	271
9-Oct-97	MLB-2	0.76	0.75	ND	0.94	0.83	ND
15-Oct-97	MLB-1	0.31	0.39	ND	0.84	0.56	169
16-Oct-97	NE1-7	0.34	0.38	36	0.58	0.51	ND
17-Oct-97	ML-11	0.38	0.44	ND	0.47	0.48	38
21-Oct-97	MLB-1	0.25	0.46	ND	0.24	0.48	ND
Cambridge Landfill							
16-Sep-97	CL-1	2.19	1.29	ND	1.12	1.57	ND
18-Sep-97	CL-2	1.05	1.38	ND	0.48	1.46	ND
Stratford Landfill							
22-Sep-97		0.60	0.93	ND	0.59	0.88	ND
29-Sep-97		1.31	0.68	6	0.37	1.00	ND
24 hour AAQC (MOE, 1994)					28,000	4,000	
24 hour NAAQO (Environment Canada, 1998) (proposed)							5

Notes:
* - See Figures 4.4 & 4.5
ND – Not Detected

was used to calculate the flux and concentration emitted from the landfill surface since the concentration in the flux chamber was consistently higher than ambient conditions. The equivalent flux of TCE and PCE ranged from 7.46 to 72 $mg/m^2/d$ and 3.56 to 20.7 $mg/m^2/d$

Table 4.8: TCE, PCE and H_2S flux and concentration emitted from landfill surface at each flux experiment location at the Waterloo Landfill.

Date	Site	Flux			Estimated Concentration Emitted from Surface		
	Location*	TCE ($mg/d/m^2$)	PCE ($mg/d/m^2$)	H_2S ($mg/d/m^2$)	TCE ($\mu g/m^3$)	PCE ($\mu g/m^3$)	H_2S ($\mu g/m^3$)
Waterloo Landfill							
1-Oct-97	MLB-1		18.3	16.5		7	6.38×10^3
8-Oct-97	MLB-1	72	14.9	23.7	33	7	1.08×10^4
9-Oct-97	MLB-2	18.1	11.2		20	12	
15-Oct-97	MLB-1	52.7	20.7	15.9	39	15	1.16×10^4
16-Oct-97	NE1-7	25.3	16.6		233	153	
17-Oct-97	ML-11	7.46	2.67	3.43	16	6	7.18×10^3
21-Oct-97	MLB-1		3.56		0	2	

Notes:
* - See Figures 4.4 & 4.5

respectively. The area-based equivalent flux of H_2S ranged from 3.43 to 23.7 $mg/m^2/d$. It is considered to be an area-based equivalent flux rather than a true flux due to the presence of the hole that emitted the gas rather than the cover. The estimated concentration of TCE and PCE emitted from the surface ranged from 0 to 233 $\mu g/m^3$ and 2 to 153 $\mu g/m^3$ respectively. A range of 6.38×10^3 to 1.16×10^4 $\mu g/m^3$ was estimated for the H_2S emitted from the landfill surface. The ½ hour and 24 hour limits set by the MOE are not exceeded by the surface emission of TCE and PCE. However the H_2S emitted from the landfill surface exceeds the both the ½ hour POI limit and 24 hour NAAQO.

4.4 Effect of Cover Imperfections on Gas Release

4.4.1 Field Conditions Involving Holes and Fissures

During the field experiments to evaluate the flux chamber, gas was observed bubbling out of the surface in water puddles after a rain. The gas was also observed to be bubbling out of various stages and conditions of cover. At the Waterloo Landfill, the lower slopes have a gas extraction well system installed and in operation and final cover is in place. However, at several locations, gas bubbles were observed above the lateral connected to a gas extraction well. Gas release from the landfill surface, after a rain was audible as "hissing" indicating the escape of the gas through the landfill surface. Several larger holes with gas bubbles were

found within the expected radius of influence of the gas extraction system. Figure 4.19 shows photos taken of the gas bubbles. The approximate location of the large hole (approximately 5 cm diameter), shown in Figure 4.19(a) is indicated on Figure 4.4 as "vent". This hole is only 15 m away from the nearest extraction well and therefore within the expected radius of influence of the well. This suggests that the gas produced in this region of the landfill exceeds the capacity of the gas collection system.

A sample of the gas emitted from this hole was analysed and the methane content was determined to be 54% (V/V). Using the flux chamber, the flow rate of gas out of this hole was determined to be approximately 19.2 L/min. Another hole was visible under a water puddle due the gas pressure resulting in a small water geyser. The flow rate out of this hole was measured to be approximately 0.5 L/min. The methane content of the gas from this hole was approximately 4.5% (V/V). Also several 5 mm (or less) diameter holes were evident throughout the landfill intermediate cover surface that were emitting landfill gas. Based on these observations further laboratory experimentation was done to evaluate the extent to which such holes contribute to the emission of gas to the atmosphere.

4.4.2 Experiments on Gas Flow through Cover Perforation

During the field evaluation of the flux chamber, the landfill gas flux was observed to be highly variable across the surface and small holes were observed to emit extensive landfill gas to the atmosphere. Figure 4.20 shows photos of gas bubbling through puddles over holes observed in the cover. It was suspected that much of the gas produced in the landfill could pass through these numerous holes. Therefore, further experiments using the flux chamber were performed in order to evaluate the effect that these small holes have on the total flux of landfill gas from the landfill surface.

The simulated landfill cover from the previous laboratory experiments was adapted to evaluate the effects of small holes on flux. A 17 cm clay layer was placed on top of the Ottawa sand. The clay was obtained from the Waterloo Landfill's Upper Till Unit, which is used for daily and final cover on site. The hydraulic conductivity of the Upper Till Unit has been determined to vary between 2.6×10^{-7} to 1.4×10^{-8} cm/sec (ROW, 1990). The clay content of the till unit averages 24 percent by weight and the combined silt and clay content averages 74 percent by

(A)

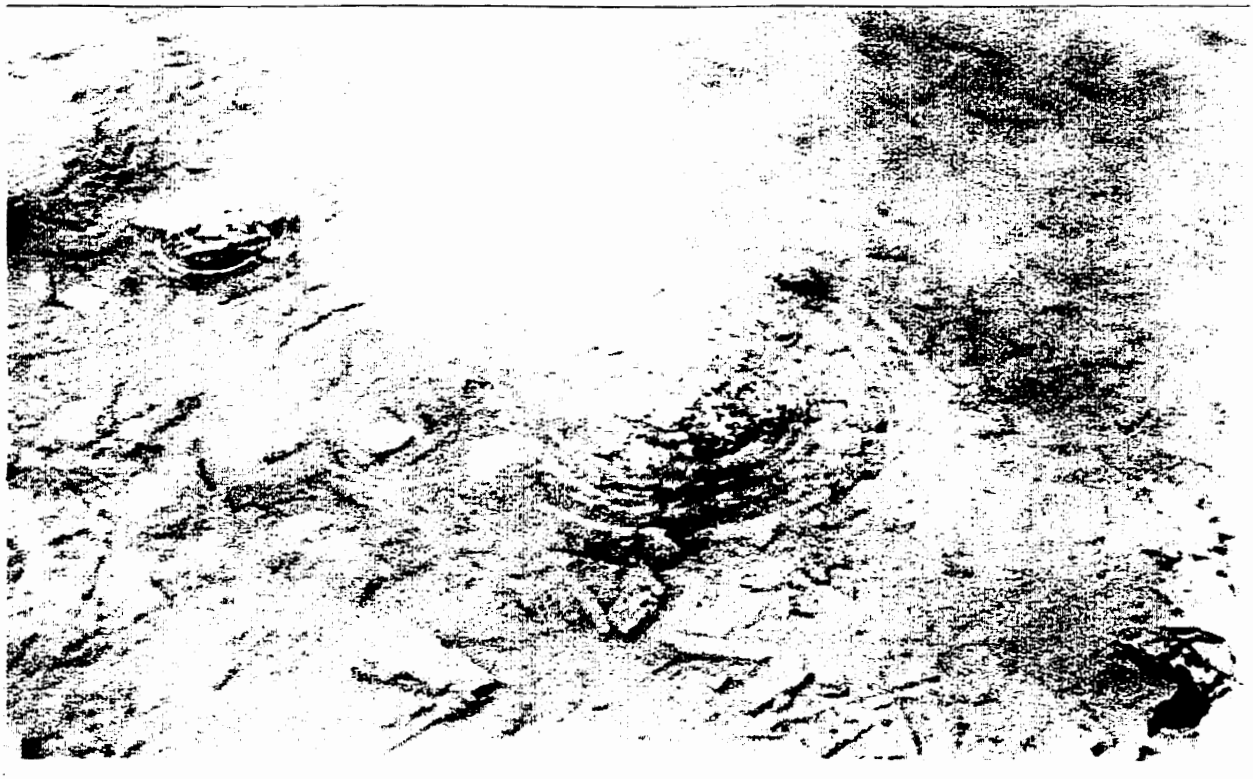

(B)

Figure 4.19: Gas bubbles and vent at the Waterloo Landfill. (A) Gas vent on slope above final cover (B) Gas bubbles in intermediate cover surface of main landfill

(A)

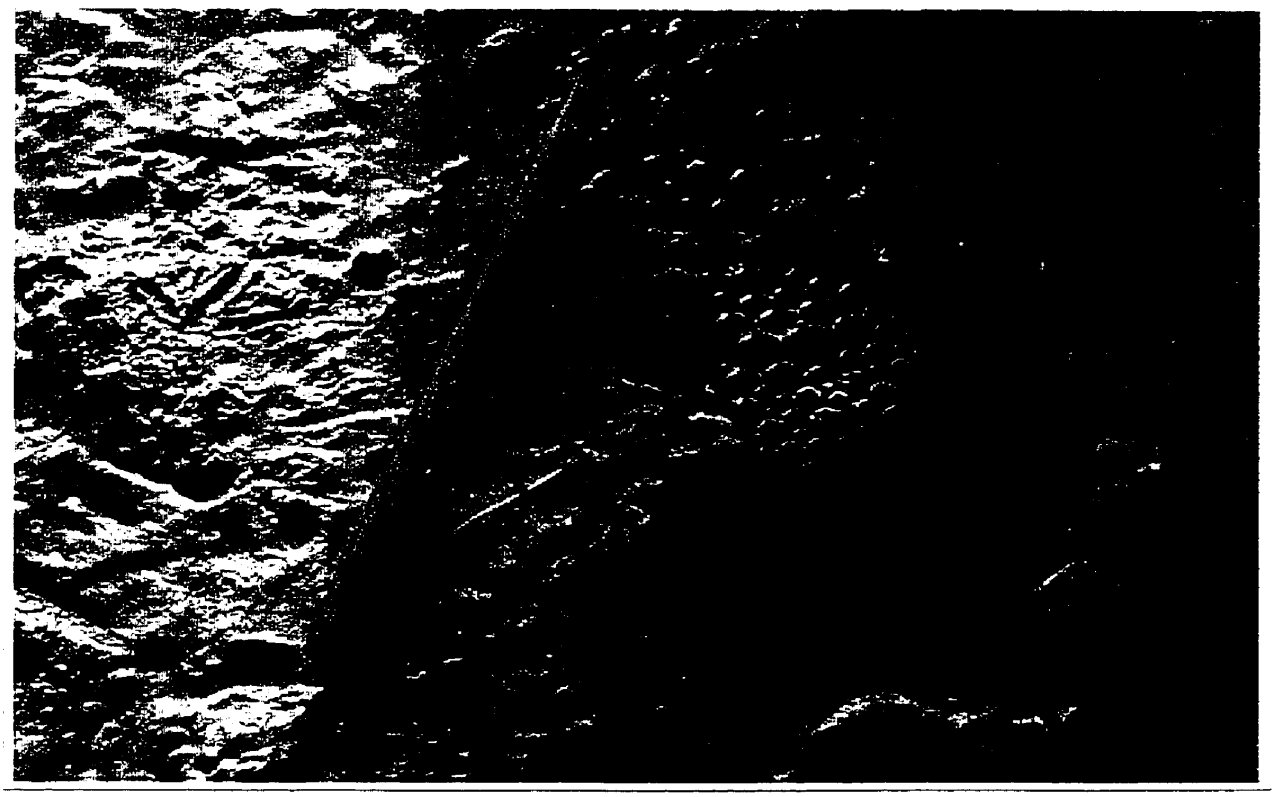

(B)

Figure 4.20: Gas bubbles seen at the Waterloo Landfill. (A) Gas bubbles in final cover between gas wells (B) Gas bubbles adjacent to sample location MLB-1

weight (ROW, 1990). The clay was remoulded and compacted by hand as it was placed on the Ottawa sand layer. A 0.318 cm (diameter) stainless tube was placed on top of the Ottawa sand and under the clay layer (Figure 4.21). One end of the tube was at the center of the sand layer and the other passed through to the exterior of the container and attached to a pressure transducer. A schematic of the setup is shown in Figure 4.22. The pressure transducer was connected to a data logger and monitored on a ten-minute interval. These pressure measurements were utilized to predict the flow rate from a hole that would be later placed in the clay surface.

The volumetric moisture content of the clay was monitored hourly using Time Domain Reflectometry (TDR) (Trase System 1 6050X1). The TDR determines the dielectric constant, Ka, of the soil by measuring the time required for a microwave pulse to travel down a known length of transmission line, referred to as "waveguides", buried in the soil. The Ka value is then converted to the volumetric water percentage of the soil by the factory calibration within the TDR. The buriable waveguide (Model 6005) consists of three 20 cm metal probes, which are connected to the TDR by a cable. The waveguide was placed in the clay layer below the flux chamber.

The moisture content of the clay was maintained by misting water over the surface of the clay. A 2 cm by 2 cm depression in the clay was formed between the perimeter of the clay layer and plastic container. Water was placed in the depression to ensure that the clay remained moist and adhered to the plastic container. The water in the depression also provided a visual indication of any gas escaping around the edge of the container. A continuous supply of 50% V/V methane and 50% V/V carbon dioxide was passed through the gas manifold into the granular B below the sand. A 0.16 cm (1/16 in) diameter hole was created through the clay layer with a stainless steel rod. The flux from this hole was later determined using the flux chamber equipment. The hole was required initially to prevent a gas pressure build up under the clay layer and the resulting escape of gas between the clay layer and the container interface. The system was allowed to equilibrate for 3 days. The equilibration of the system consisted of allowing the methane and carbon dioxide to displace the air within the soil below the clay layer.

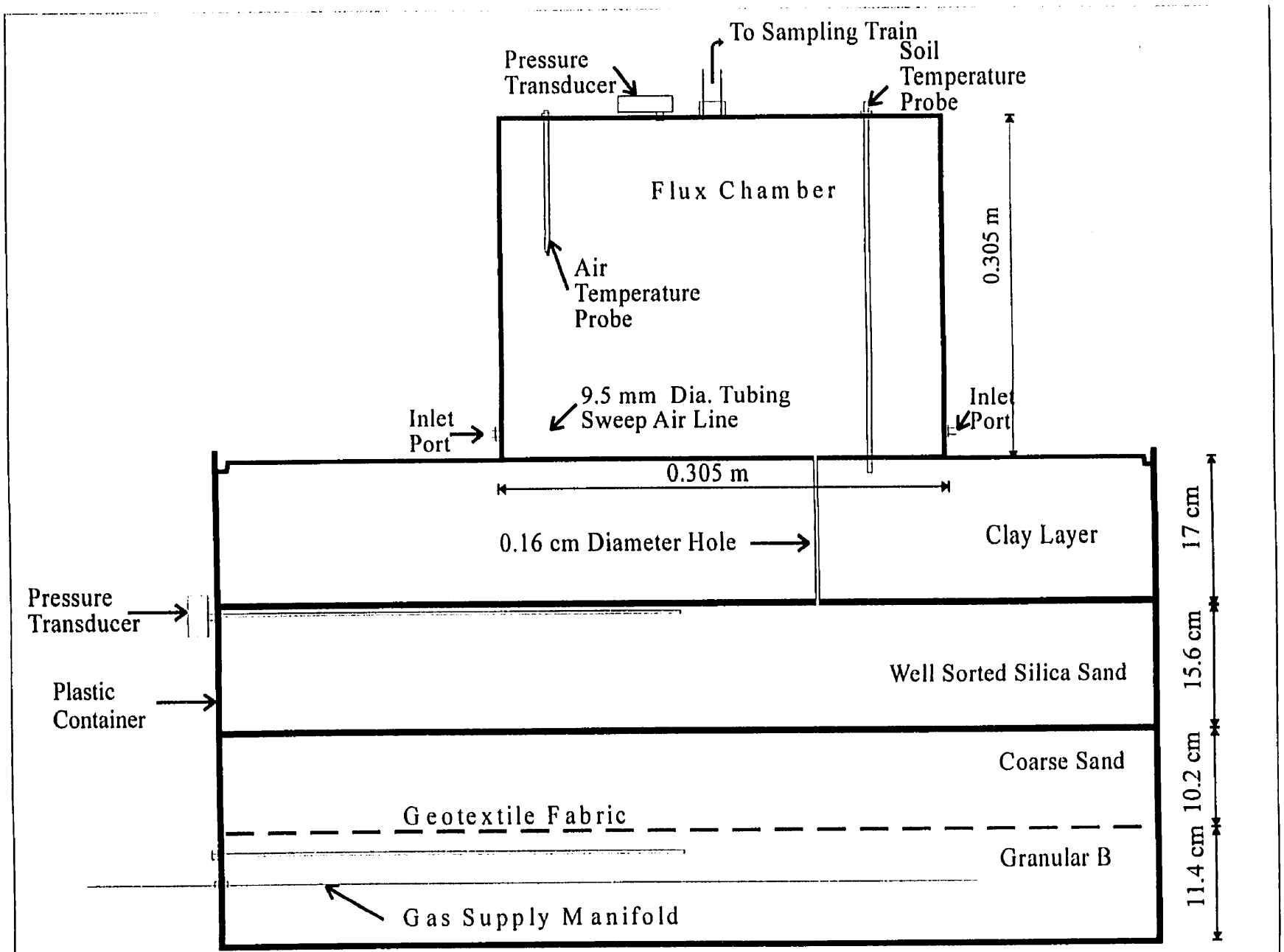

Figure 4.21: Laboratory setup of flux chamber and simulated landfill surface for hole experiments

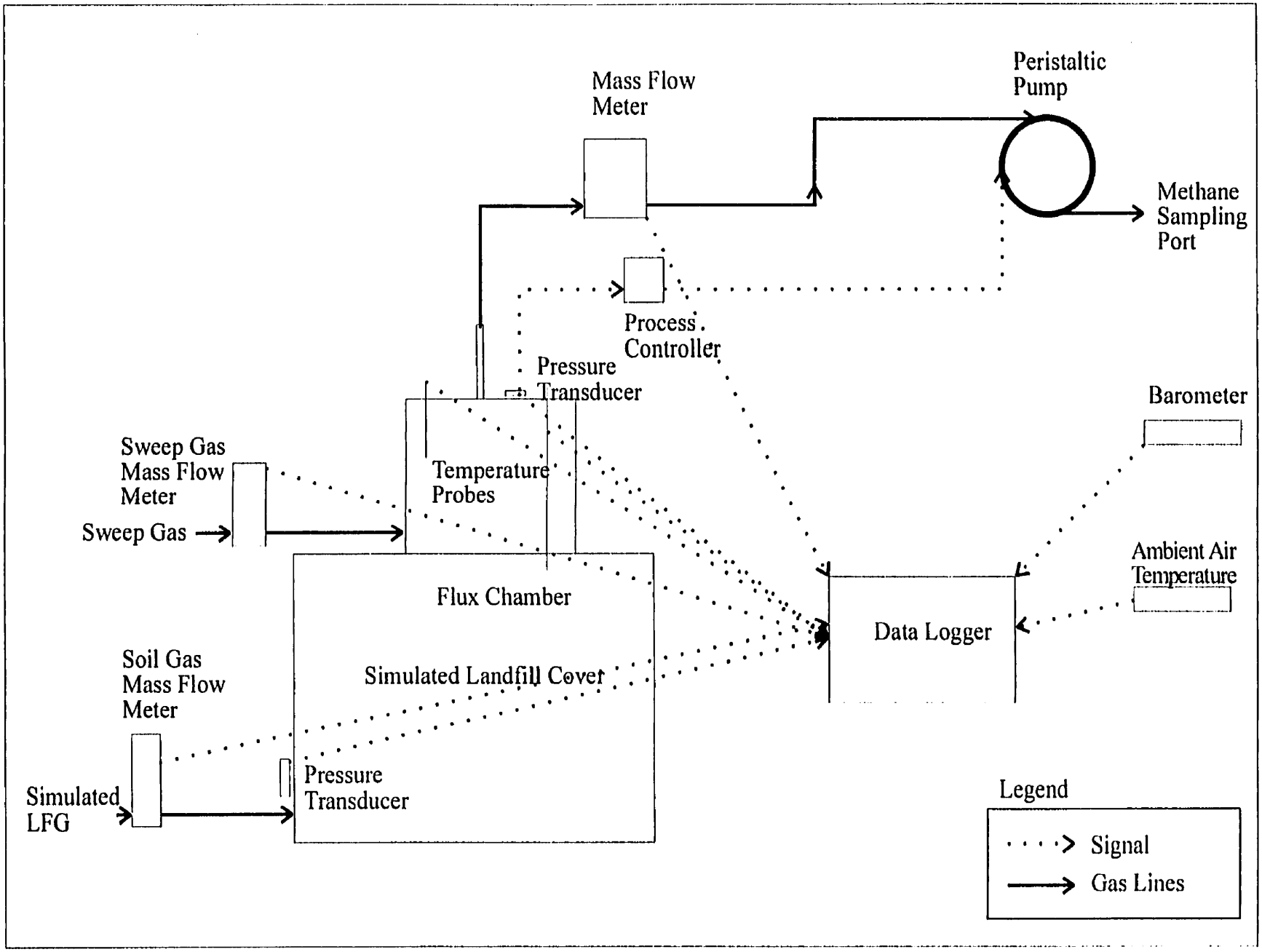

Figure 4.22: Schematic of laboratory setup of flux chamber experiments for hole experiments

The gas emitted from the hole was monitored for methane by sampling with a syringe and injection into a GC-FID.

Once the gas composition in the sand below the clay had equilibrated, the hole experiments were started. First a sweep flow rate of air into the flux chamber was established. The original hole in the clay layer was closed and sealed. The pressure transducer connected to the tube in the sand below the clay layer was attached and logged at 30 sec intervals to measure the pressure build up. Then a 0.16 cm diameter stainless steel rod was pushed through the clay surface into the sand layer below to a depth of approximately 19 cm and removed leaving a small hole in the clay layer with a nominal diameter of 0.16 cm and a length of approximately 17 cm.

The flux chamber was then placed over the hole and sealed to the clay surface with wet clay. During each experiment, barometric pressure, room temperature, chamber air temperature, sand temperature, gas inflow rate to the sand, sweep air flow rate, chamber effluent flow rate, were monitored at 10 minute intervals using a datalogger (ChartPac CP-X, Lakewood systems). The gas inflow rate was monitored by a mass flow meter at the entrance to the gas supply manifold.

Once a steady state methane concentration in the flux chamber was established, the methane content was monitored for a minimum of 8 hours up to 24 hours on an hourly basis. The chamber effluent was monitored for methane by removing 200 µl samples by syringe and injecting it into a GC-FID. At the end of the experiment, the hole was closed and sealed. The experiment was repeated with a new hole in a new location. A total of two experiments were performed in February 1998.

Using one hole in the same location, a total of nine experiments (March 1998) were performed using three different gas inflow rates (17 ml/min, 67 ml/min and 142 ml/min). The experiment was repeated three times at each flow rate. Each experiment lasted 5 hours and the effluent methane was monitored every 30 minutes.

The data obtained from the above experiments was used to model the flow of gas through the hole in the clay layer. Two fluid flow equations, Hagen-Poiseuille and Darcy-Weisbach were examined. These two equations are for incompressible flow and can be used to model gas flow if the change of the gas density within the system is no more than 10 percent (Perry & Green,

1984). Given the pressure and temperatures used during the experiment, the density would change by less than 1%, therefore, the gas could be considered to be an incompressible fluid.

The Hagen-Poiseuille equation is:

$$Q = \frac{\pi(P_o - P_L)R^4}{8\mu L} \tag{4.1}$$

where:

R = radius of pipe (m),
L = length of pipe (m),
μ = viscosity of fluid (Pa·s),
P_o = inlet pressure (Pa),
P_L = outlet pressure (Pa), and
Q = flow (m^3/s) (Bird *et al.*, 1960).

The assumptions behind the Hagen-Poiseuille equation are:

1. The flow is laminar – Re less than about 2100.
2. The density ρ is constant ("incompressible flow").
3. The flow is independent of time ("steady state").
4. The fluid is Newtonian – that is, $\tau_{rz} = -\mu(dv_z/dr)$.
5. End effects are neglected – actually an "entrance length" (beyond the tube entrance) on the order of $L_e = 0.035DRe$ is required for build up to the parabolic profile; if the section of pipe of interest includes the entrance region, a correction must be applied. The fractional correction introduced in either ΔP or Q never exceeds L_e/L if $L>L_e$.
6. The fluid behaves as a continuum – this assumption is valid except for very dilute gases or very narrow capillary tubes, in which the molecular mean free path is comparable to the tube diameter ("slip flow" regime) or much greater than the tube diameter ("Knudsen flow" or "free molecule flow" regime).
7. There is no slip at the wall – this is an excellent assumption for pure fluids under the conditions assumed in 6. (Bird *et al.*, 1960)

Darcy-Weisbach Equation is:

$$\Delta P = \frac{fLV^2\rho}{2D} \tag{4.2}$$

where:

D = diameter of pipe (m),
L = length of pipe (m),
ρ = density of fluid (kg/m^3),
$\Delta P = P_o - P_L$,
P_o = inlet pressure (Pa),
P_L = outlet pressure (Pa),
V = velocity (m/s), and

f = friction factor (Streeter & Wylie, 1985)

The above equation was rearrange and solved for the velocity. The velocity was converted to a flow by multiplying by area of the hole. This value was then compared to the experimental flow. The assumptions associated with the Hagen-Poiseuille equation also apply to the Darcy-Weisbach equation (the Darcy-Weisbach equation will simplify to the Hagen-Poiseuille equation if the flow in the pipe is laminar).

Both equations are considered to be long pipe flow equations. This allows the flow regime and the velocity profile to be established so that any entrance and exit effects on the flow can be ignored. The ratio of length/diameter (L/D = 107) in this experiment was greater than 100; therefore, the error due to neglecting the "end correction" (using the long-pipe formulas) will be less than 2 percent (Perry & Green, 1984).

The Reynold's numbers ranged from 6 to 200, which is considered laminar and justifies the use of the Hagen-Poiseuille equation. The pressure change from the inlet to the outlet of the pipe (hole) ranged from 2 to 76 Pa during the experiment. Therefore there would be less than a 0.1 percent change in the density of the gas that indicates the gas will act as an incompressible fluid.

4.4.3 Results of the Gas Flow Experiments through Cover Perforation

Figure 4.23 presents clay moisture data throughout the experiments. The moisture content stabilized at approximately 25% by volume. Figure 4.24 shows the pressure build up in the sand below the clay layer with no hole in the layer and the pressure drop after the hole was placed in the clay layer prior to the start of the March 5-6, 1998 experiment. In both examples, the gas inflow rate was 17 ml/min. The nearly linear pressure build-up shown in Figure 4.24 (a) and (b) prior to the creation of the hole demonstrated that gas leakage from the system was negligible. In Figure 4.24 (b) pressure spikes were observed after the hole creation. The cause of these spikes is uncertain, although any blockage of the hole such as sand particles shifting with the gas movement would result in a momentary rise in pressure. The hole creation required the removal of the flux chamber. Therefore the actual flux measurements were taken after the flux chamber was re-established on the clay surface. Table 4.9 contains the chamber, soil and ambient temperatures and barometric, chamber and soil pressures for each of the

experiments. The values presented in Table 4.9 are averages obtained over the duration of each experiment. Each experiment performed from February 14 until February 26. 1998 was done using the same size hole but in a different location in the clay layer. The soil gas flow

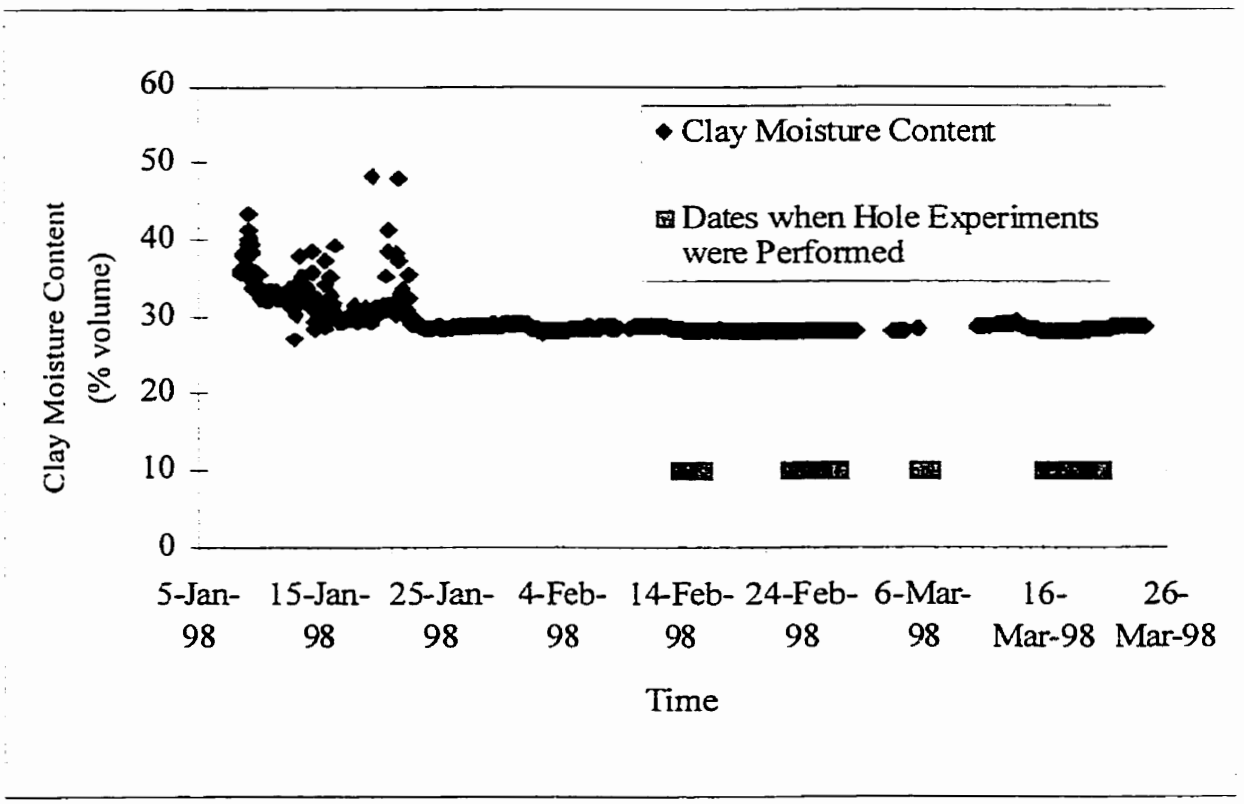

Figure 4.23: Clay moisture measurements provided by TDR during hole experiments

rates for the experiments ranged from 16 to 17 ml/min. The experiments performed in March 1998 were done using one hole in the same location but the gas inflow rates ranged from 17 to 140 ml/min. In all experiments, the percent methane recovery ranged from 85% to 102% as shown in Table 4.10. Table 4.10 contains average values for the gas inflow rate, sweep flow rate, chamber effluent flow rate and methane concentrations in the sand and chamber effluent for each experiment. The percent methane recovery was a mass balance ratio of the measured methane mass inflow rate to the expected or theoretical methane mass inflow rate. The measured methane mass inflow rate was determined based on the difference between the methane mass out and the methane mass in. The methane mass out was equal to the measured methane concentration in the chamber effluent gas times the effluent gas flow rate. The methane mass in was 0.0002% methane V/V (assumed in the air) times the sweep gas flow

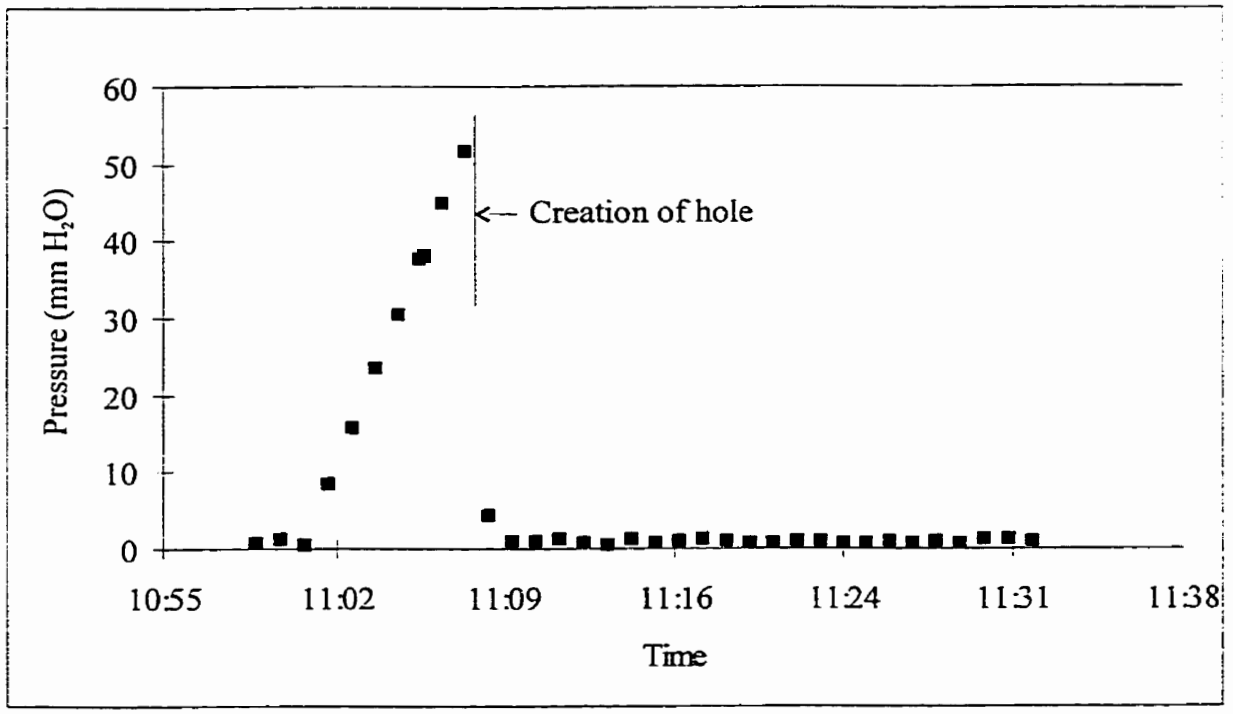

(A)

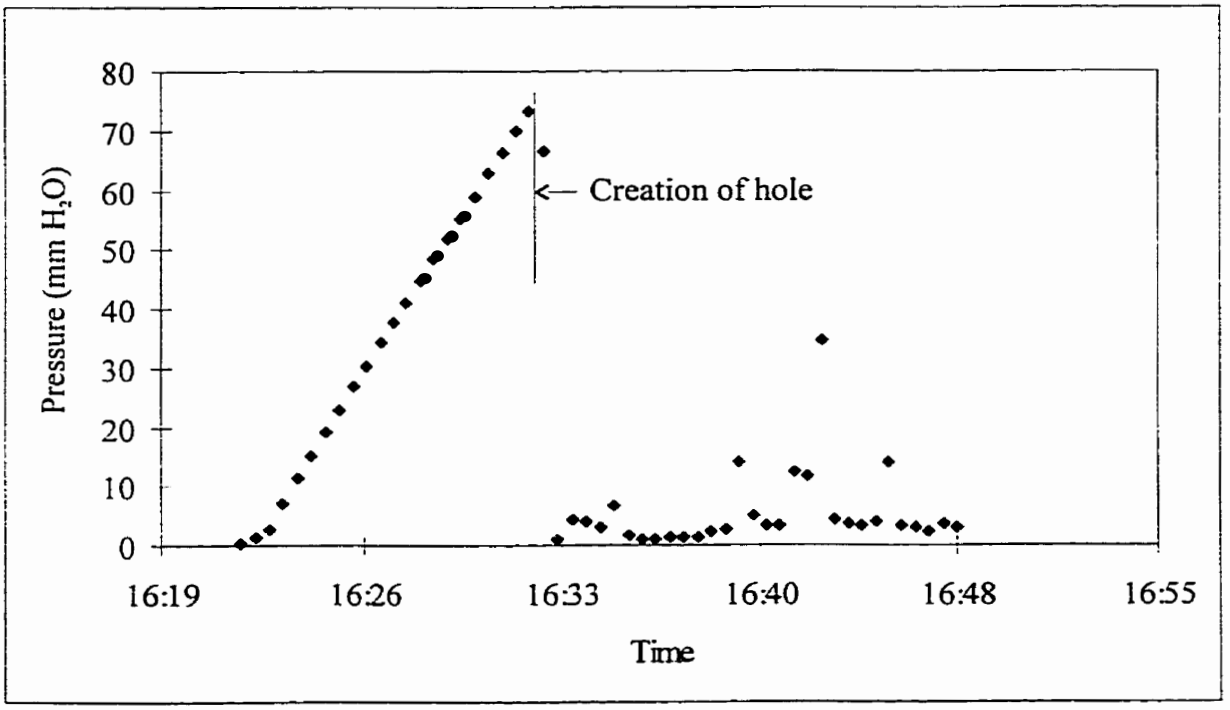

(B)

Figure 4.24: Pressure build up and drop in the sand beneath clay cover prior to and after hole placement for two different experiments. (A) On Feb 26/98 with a gas inflow rate of 17.2 ml/min. (B) On Mar 4/98 with a gas inflow rate of 17.7 ml/min.

Table 4.9: Hole experiment parameters

Date of Experiment	Average Temperature			Average Pressure		
	Chamber Air (°C)	Clay (°C)	Ambient Air (°C)	Barometric (mm H_2O)	Chamber Δ (mm H_2O)	Sand Beneath Clay Δ (mm H_2O)
Feb 14-15/98	17.6	16.9	18.0	10118	0.05	0.88
Feb 23-26/98	19.2	17.8	19.7	9980	0.01	0.74
Mar 5-6/98	18.5	16.5	19.0	10059	0.28	1.60
Mar 16/98	18.1	15.2	18.9	10165	0.16	1.36
Mar 17/98	19.1	15.8	20.0	10123	0.23	1.17
Mar 17-18/98	17.9	16.0	18.7	10049	0.25	3.14
Mar 18/98	18.3	16.0	18.9	10027	0.15	3.03
Mar 19/98	18.4	16.5	18.8	9958	0.27	3.53
Mar 19/98	18.5	16.5	18.9	9952	0.51	7.64
Mar 20/98	18.3	16.6	18.9	9990	0.14	7.43
Mar 20/98	18.5	16.6	18.9	9979	0.30	8.34

Table 4.10: Hole experiment data.

Date of experiment	Average Flow Rate			Average Methane Concentration		% Recovery of Methane
	Inflow (mL/min)	Sweep (L/min)	Effluent (L/min)	Sand (mg/L)	Chamber (mg/L)	
Feb 14-15/98	16.2	1.91	2.10	328	2.4	95
Feb 23-26/98	17.2	1.91	2.01	322	2.3	85
Mar 5-6/98	17.7	1.91	2.07	325	2.6	94
Mar 16/98	17.5	1.89	2.04	329	2.5	90
Mar 17/98	17.9	1.89	1.99	326	2.6	87
Mar 17-18/98	67.0	1.88	2.09	325	9.9	95
Mar 18/98	67.3	1.89	2.01	324	10.0	92
Mar 19/98	66.9	1.87	1.98	322	10.2	93
Mar 19/98	144.6	1.87	2.22	322	21.5	102
Mar 20/98	141.3	1.87	2.15	323	20.8	98
Mar 20/98	143.5	1.87	2.24	323	20.9	101

rate. The expected or theoretical methane mass inflow rate is equal to the measured methane concentration in the sand times the gas inflow rate.

Table 4.11 contains a comparison between the effluent flow rate and the sum of the influent/sweep flow and gas inflow. The data indicate that there is a small gain in volume within the system (2 to 10%). The difference between the effluent and the sum will be due in part to the changes in temperature and pressure within the soil below the clay. Although all the flow rates were monitored with mass flow meters as they enter the system, the drop in temperature and increase in pressure in the soil will result in a compression and then expansion of the soil flow rate as it reenters the chamber at a different temperature and pressure. It was calculated that, for the changes in temperature and pressure recorded, the gain in volume would be less than 0.1%.

Table 4.11: Comparison of effluent flow rate and the sum of gas inflow and sweep/influent flow rates

Date of experiment	Influent/Sweep flow rate (L/min)		Gas Inflow rate (ml/min)		Effluent flow rate (L/min)		Sum gas inflow and influent (L/min)	Difference (L/min)
	Ave	Std	Ave	Std	Ave	Std		
Feb 14-15/98	1.91	0.01	16.2	1.03	2.10	0.24	1.92	0.18
Feb 23-26/98	1.91	0.01	17.2	0.50	2.01	0.13	1.93	0.08
Mar 5-6/98	1.91	0.01	17.7	0.40	2.07	0.09	1.92	0.14
Mar 16/98	1.89	0.01	17.5	0.42	2.04	0.40	1.90	0.14
Mar 17/98	1.89	0.01	17.9	0.49	1.99	0.09	1.90	0.08
Mar 17-18/98	1.88	0.01	67.0	0.17	2.09	0.07	1.95	0.14
Mar 18/98	1.89	0.01	67.3	0.25	2.01	0.46	1.95	0.05
Mar 19/98	1.87	0.01	66.9	0.34	1.98	0.49	1.94	0.04
Mar 19/98	1.87	0.01	144.6	0.43	2.22	0.08	2.01	0.21
Mar 20/98	1.87	0.01	141.3	0.54	2.15	0.08	2.01	0.14
Mar 20/98	1.87	0.01	143.5	0.49	2.24	0.09	2.02	0.22

Note:
Ave – Average
Std – Standard deviation

The presence of the pump on the effluent end of the chamber will also contribute to the difference. The peristaltic pump increases the standard deviation in the flow through the mass flow meter as is shown in the above table when the influent and effluent flow rates are

compared. For the last entry in the table for example, the standard deviation is within 0.5% of the average value for the influent flow rate whereas the standard deviation of the effluent is approximately 4% of the average value. The operation of the peristaltic pump and dataloggers may have resulted in a larger average value if the recording interval of the datalogger and the pumps high flow rate cycle were matched more frequently than with the low flow cycle. A smaller time recording interval and smaller pump head with smaller diameter tubing would have reduced the impact of the peristaltic pump on the variation in effluent flow rates.

Figure 4.25 shows the relationship between the gas inflow rate and the pressure differential between the sand and atmosphere. The experimental data shows a linear relationship of $y=0.05x+0.09$ ($R^2=0.98$). In Figure 4.26, an increase in pressure below the clay surface resulted in an increase in the methane concentration within the flux chamber. A linear relationship of $y=2.74x-0.06$ ($R^2=0.98$) is also observed between the flux chamber methane concentration and the pressure differential between the clay layer and atmosphere.

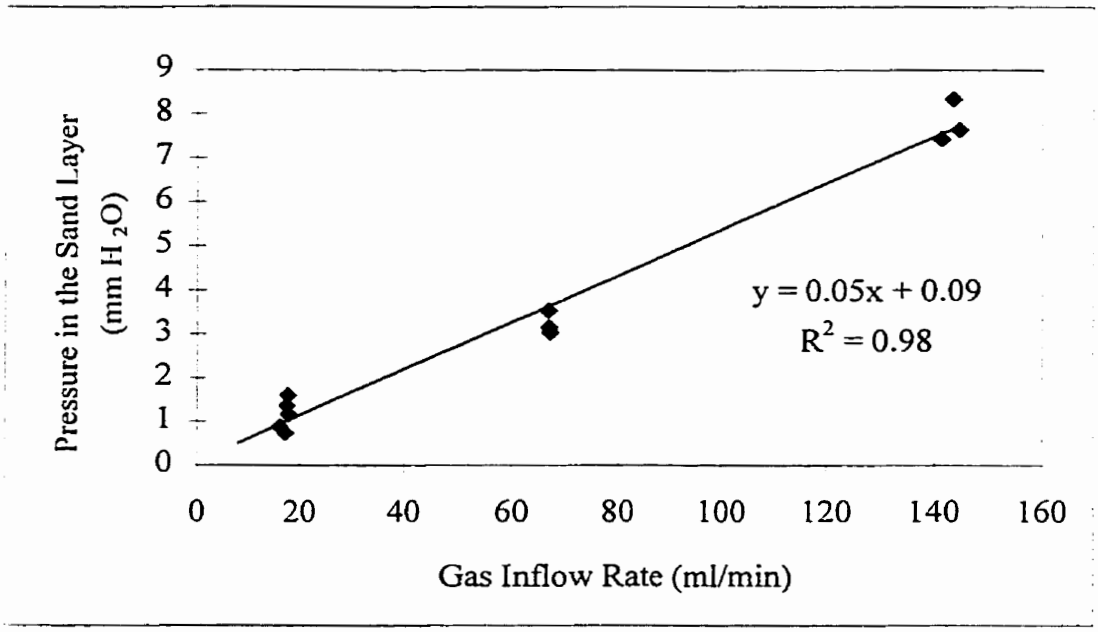

Figure 4.25: Gas inflow rate to gas supply manifold versus pressure measured in the sand layer beneath the cover during hole experiments

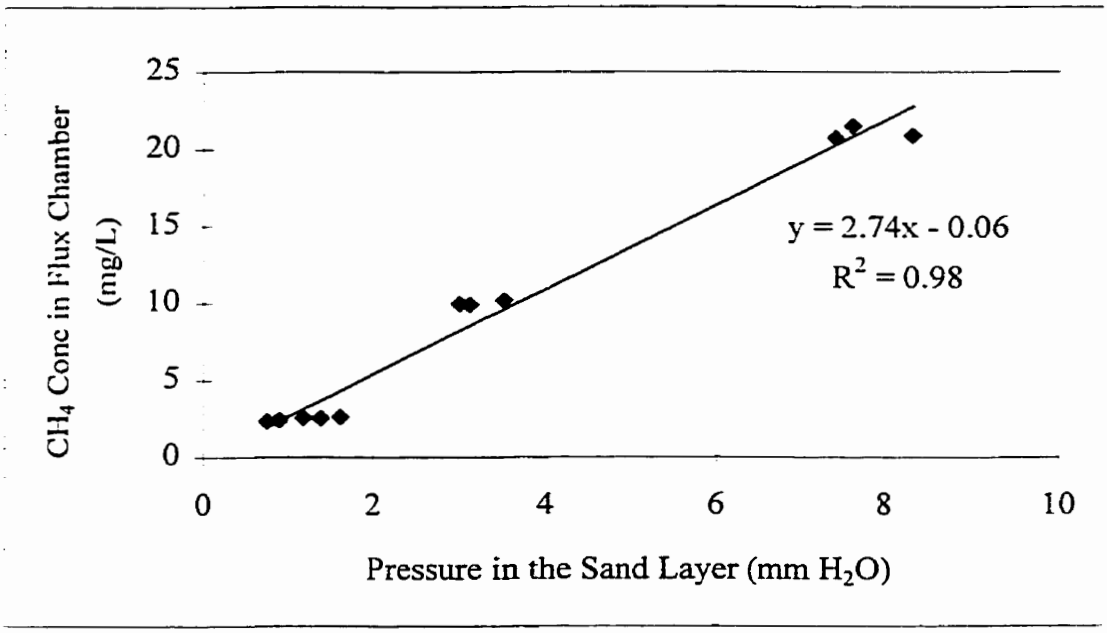

Figure 4.26: Methane concentration versus pressure measured in the sand layer beneath the clay cover during the hole experiments

4.4.4 Modelling of Gas Flow Experiments through Cover Perforation

Flows calculated from the two equations presented previously, were compared to the experimentally obtained flow as is shown in Figure 4.27. The Hagen-Poiseuille equation was adjusted using a factor of approximately 0.45 in order to decrease the mass flow to match the experimental data. In the Darcy-Weisbach equation, the calculated flow values were multiplied by a factor of 0.68 in order to decrease the values to match the experimental data. The Darcy-Weisbach equation contains a friction factor, which is a function of the gas velocity through the hole. The adjustment factor for the Darcy-Weisbach equation could be expected to incorporate friction loss coefficients.

Factors affecting the fit of the models to the data may have included errors in estimating the diameter and length (depth) of the hole. Diameter of the hole was assumed to be 0.16 cm, the outside diameter of the stainless steel tube used to create the hole. However, it is likely that the effective diameter of the hole would be less than 0.16 cm because of uneven sidewalls and particles of clay left after the withdrawal of the rod. If the effective diameter of the hole had been 0.131 cm, an adjustment factor of 0.45 (as determined above from the data) would be needed to make the equation with a diameter equal to 0.16 cm, fit the data. The depth of the

clay layer was used as the pipe length in the equations but this depth may have not been uniform. A 1% error increase the length will result in an approximately 1% increase in the adjustment factor for the Hagen-Poiseuille (0.455) and Darcy-Weisbach (0.687) equations.

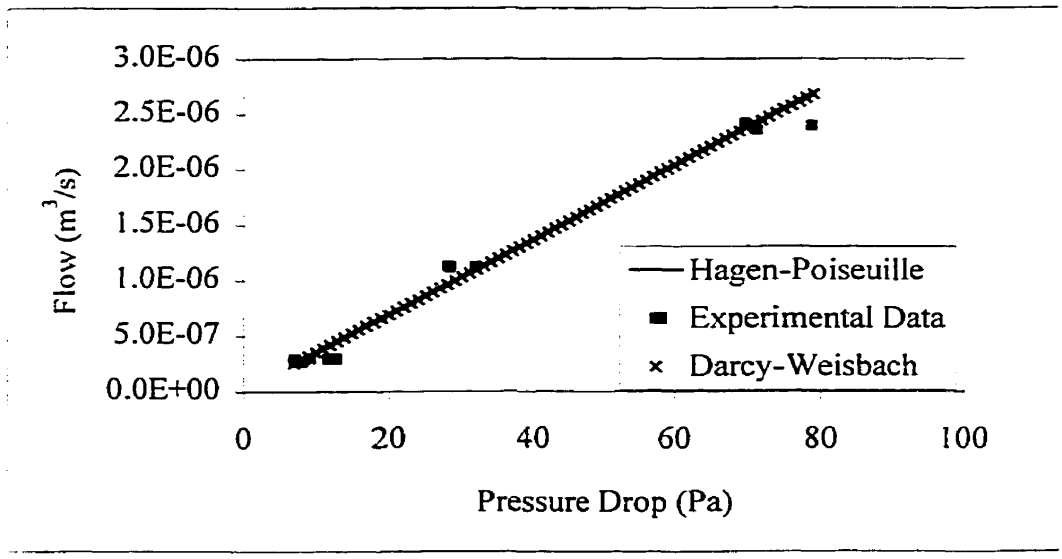

Figure 4.27: Experimental data from hole experiment with modelled data

The variability in pressure measurements will also contribute to the error associated with determining the adjustment factor and ultimately the friction factor for the hole. A 1 percent decrease in the pressure differential used in the Hagen-Poiseuille equation will result in an increase in the adjustment factor to 0.4545 (1%). The Darcy-Weisbach equation adjustment factor will increase by 0.5% (0.6834) due to a 1 percent decrease in the pressure differential.

Therefore, small changes in length and diameter of the pipe as well as the pressure measurements at the inlet and outlet of the pipe will contribute to the fit of equations to the data.

These experiments indicate that traditional pipe flow equations with some adjustment, can be used to fit gas flow data through holes in landfill cover material. In both cases, the equations overestimated the flow rates requiring the application of adjustment factors. The Hagen-Poiseuille equation provided the best fit for the experimental data after the application of the adjustment factor. The factors affecting the magnitude of these coefficients were not fully quantified; further work is required to do so.

4.5 Discussion

The average methane flux of 1.78 $g/m^2/d$ with a range of 0 to 20.5 $g/m^2/d$ measured at the three landfills is within the range of values reported by various authors shown in Table 2.6. The maximum values of 1.03×10^4 $g/m^2/d$ and 9.02×10^3 $g/m^2/d$ reported by Environment Canada (Williams & Williams, 1995) at an Ontario landfill were higher than values obtained in this study. However, the landfill did not have a gas collection system, whereas two of the three landfills in this study had operational gas extraction wells on the slopes of the landfill.

Table 4.12 presents a comparison of VOC flux rates from the literature and the present study. The data for Waterloo (this study) are average values of the data presented in Table 4.8. The results from this study indicated that emissions of TCE and PCE were higher from the cover with a hole than the surface without a hole. Kjeldsen *et al.* (1996) found that LFG affected soils have a large potential for degrading methane, benzene and toluene in the presence of sufficient oxygen. They also found that TCE and TCA were degraded, but only if methane was present. The presence of the hole in the cover limits the ability to degrade the VOCs therefore resulting in higher emissions from the landfill surface.

The average TCE emissions from an intact surface were higher than literature values. The average PCE flux measured from an intact surface in this study was within the range of flux observed in the literature. Walker (1991) found that VOCs emissions were higher in young waste and poor cover (brown area) situations which are comparable to the conditions measured during this study. Therefore, higher TCE measurements might be expected.

The variability in the literature data in Table 4.12 is likely due to the different flux chambers and related procedures used to obtain the VOC flux measurements. Walker's measurements were taken with a dynamic flux chamber whereas Bogner *et al.* (1997c) used a static flux chamber. A dynamic flux chamber uses a sweep gas to dilute the surface flux as in this research. The static flux chamber uses no sweep gas; the change in gas concentration (over 30 minutes to one hour) is monitored by removing small quantities of the gas from the gas confined by the static flux chamber. Based on the results of this research it is unlikely that a static chamber can produce satisfactory flux measurements.

Several authors have reported a change in gas flux measurements due to a shut down in a gas extraction system. Börjesson & Svensson (1997b) observed 333 mmol $CH_4/m^2/h$ (128 g

$CH_4/m^2/d$) in a flux chamber during an interruption in gas extraction whereas no detectable CH_4 was observed in the same flux chamber during the operation of the gas extraction system. Bogner *et al.* (1997b) also reported the mitigating effect of a gas recovery system on the emissions of CH_4. Mosher *et al.* (1999) found that 100% areal coverage of a gas collection system was more effective than partial coverage at reducing atmospheric emissions of the LFG. During the experiments of this study, both Waterloo and Cambridge landfills have vertical gas collection wells installed and operational on the finished portions of the landfills. Also, Waterloo landfill uses a silt clay daily cover that should impede the flow of the gases due to its low permeability. The use of this cover for daily waste lifts may also reduce the radius of influence of the gas collection wells or make it irregularly shaped. Figure 4.12 showed that there appeared to be minimal effect due to the gas collection on the flux measurements obtained during this study. The flux measurements were performed on waste lifts that were above the top elevation of the gas collection wells. The closest well was over 50 m away; it is likely that the sample points were outside the radius of influence of the wells.

Table 4.12: VOC flux rates obtained from literature and present study.

Source & Location		Flux rate ($mg/m^2/d$)			
		Benzene	Trichloroethene	Vinyl Chloride	Tetrachloroethene
Walker (1991)					
Central Florida Landfill					
Landfill 1	Green Area	0.036	0.012	0.115	BDL
	Brown Area	5.88	1.174	25.92	0.96
Landfill 2	Area 1	0.1	BDL	BDL	BDL
	Area 2	5.52	0.624	240	5.95
Bogner *et al.* (1997c)					
Green Valley LF Illinois					
GVN			3.89×10^{-5}	-5.68	0.277
			4.52×10^{-3}	0.83	
		4.64	-0.049		0.035
		-1.2	0.173	2.75	
		-1.57	0.059		0.188
		-11.5	0.268	-8.68	1.06
This study					
Waterloo	Holes in cover		47.6		13.7
	Cover		16.3		9.64

The quality of the cover is also a contributing factor in limiting the emission of the LFG as indicated by the higher emissions from the holes measured during the field experiments. Landfill cover quality can contribute or reduce the amount of LFG emissions. Holes, fissures, and cracks in the cover will increase the atmospheric release of LFG. Methanotrophic CH_4 oxidation can be a natural control to limit CH_4 emissions with oxidation rates as high as 166 $g/m^2/d$ (Bogner *et al.*, 1997b). Oxidation of methane in the cover by the microbes can also provide a means of reducing the emissions of VOCs through oxidation by the methanotrophic microbes. Bogner *et al.* (1997c) reported negative fluxes of benzene, TCE, and vinyl chloride while performing static chamber flux measurements at a landfill. These negative fluxes indicate the possibility of uptake or oxidation by the landfill cover of the atmospheric VOCs. The presence of holes limits the effectiveness of the cover's oxidation potential since the gas passes rapidly into the atmosphere rather than through the cover soil. A hole 0.16 cm (1/16 in ∅) in the cover emitting 5.76 mg/min of methane (flow rate of 17.5 ml/min and 50% V/V methane Mar 16/98 Table 4.10) will produce the same emission as approximately 212 m^2 of competent clay cover (a darcy's velocity of 1.37×10^{-9} m/s and the same pressure differential, 1.36 mm H_2O, as the Mar 16/98 example). However, a competent clay cover will result in a pressure build up under the cover. Therefore, a comparison between the hole and the darcy's velocity from a competent clay cover with a pressure typical of a landfill (15 in H_2O or 381 mm H_2O without a venting system) reduces the equivalent surface area to 0.76 m^2.

Chapter 5

5.0 Model Development for LFG Production, Emission through Cover and Atmospheric Dispersion

To evaluate the emission of gases from a landfill over its lifetime, the Landfill Emission Simulation (LES) model was developed that evaluates these emissions during the construction of the landfill and after closure. Estimating landfill gas emissions required accounting for the production of the gases as well as their transport to the surface from the start of landfill construction to completion. The processes accounted for in the model are complex and have not been quantified for the most part, particularly at full landfill scale. The complexity results from the heterogeneity of the waste and its properties, together with the changes in composition, density and permeability as decomposition proceeds and the size of the landfill increases. Complex decomposition processes are by necessity, simulated by simple first and second order decay equations. Compaction and changes in density and permeability have been simulated only by highly empirical methods. As a result, it was necessary to make many assumptions regarding certain landfill configurations and properties to produce a comprehensive model that would simulate gas production at full landfill scale under evolving conditions from opening through construction to final closure and beyond. The LES model represents a first approximation to simulate a very complex situation. Future research involving the model can adjust its many components as more appropriate information becomes available.

The production of the landfill gas was simulated using the first order equation that comprises the Scholl Canyon Model. The Scholl Canyon Model is accepted and utilized both by the USEPA (USEPA, 1995) and MOE (MOE, 1992) to simulate the production of landfill gas. In order to simulate the heterogeneous nature of the landfill gas emissions, the landfill was

divided into columns of waste while tracking the daily placement within them. Within these waste columns, a 1-D advection-dispersion equation was used to transport the produced gases through the waste layers and cover materials. To simplify the model and avoid the need for 3-D analysis, no lateral transmission of gas to adjacent waste columns was allowed to occur in these simulations. The assumption was justified to some degree since the landfill construction, as simulated by the model, produces waste cells for which the height is much less than their lateral dimensions. The use of several columns in various stages of production and emission generates a 2-D image of the LFG emitted from the landfill surface.

To assess the impact of these emissions off-site, the Gaussian plume equation was used to disperse the emissions to the limits of the landfill boundary.

5.1 LES Model Development

Landfill emissions start with the construction of the landfill. The waste deposited in landfills will emit different gases at different rates based on the phases of decomposition as is discussed in Chapter 2 Section 2.1. The LES model accounts for the various stages in construction and phases of gas production.

5.1.1 Conceptual Landfill Design and Construction

The LES model provides estimates of the emission of CH_4, CO_2, VOCs and H_2S over the lifecycle of the landfill.

The landfill model starts with consideration of the overall length, width and depth of the landfill. Figure 5.1 shows a finished landfill divided into several 100 m x 100 m areas. Each of these areas was filled with lifts of waste and the exploded view in Figure 5.1 shows the conceptual filling sequence used for each area. The length and width parameters for the lifts were selected to ensure that an even number of the lifts would fit into the area. The daily height of the landfilled and compacted waste was selected to be the depth of the lift. A lift consists of approximately one day's waste placement with each lift being divided into 5 equal divisions known as cells. These cells were used to define the production differences between the bottom and the top of the lift. The top of the lift would be aerobic and the bottom anaerobic. Anaerobic production in the top of the lift was delayed until the top cell of the lift

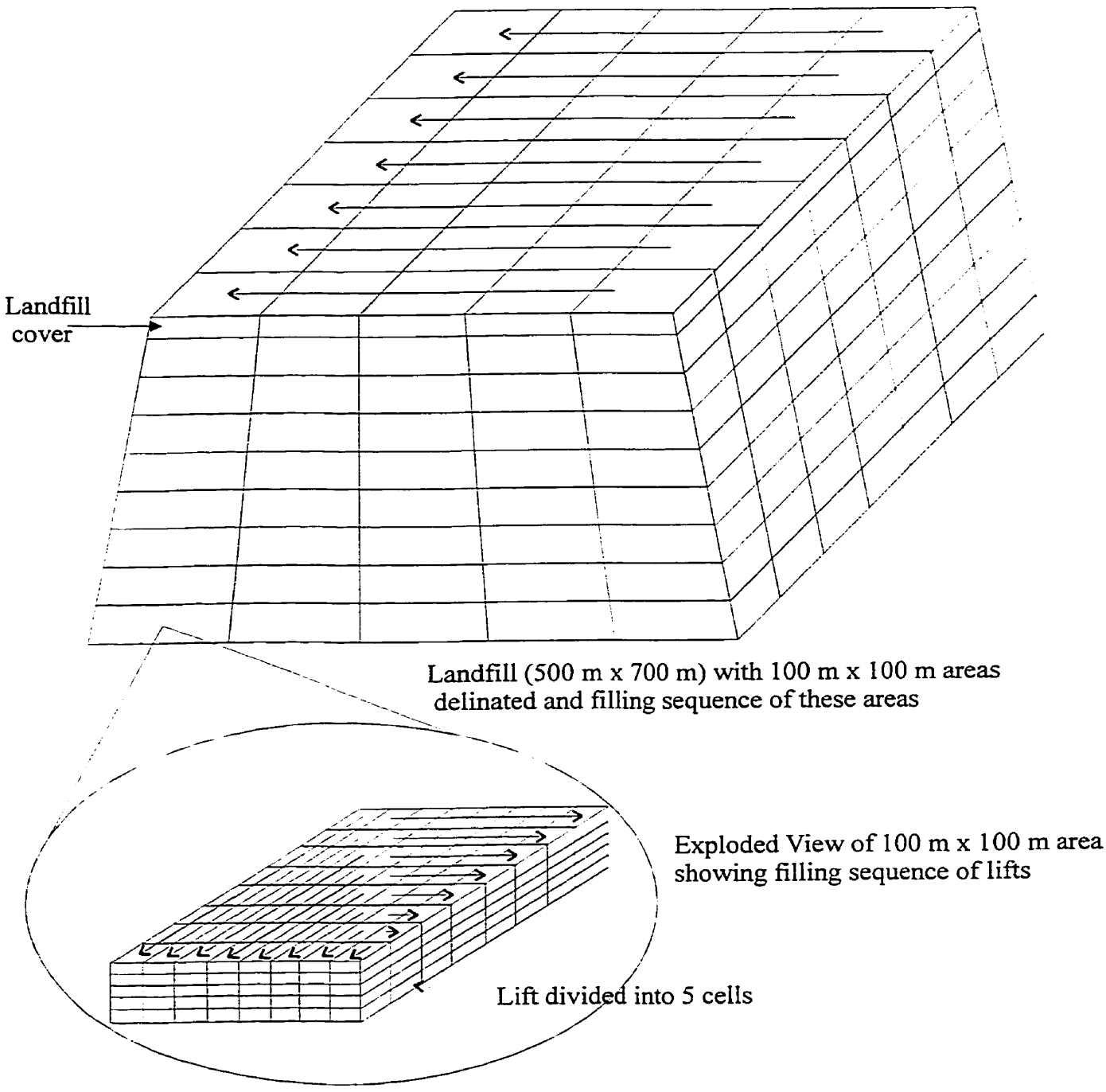

Figure 5.1: Conceptual landfill with filling sequence for the daily lifts and overall landfill filling direction

was covered with intermediate cover. Only 4 out of 5 waste cells placed in each lift started gas production after the lift was placed. The oxygen concentration within the top cell is higher due to greater diffusion from the atmosphere; therefore the anoxic and anaerobic phases would be delayed until the supply of oxygen is reduced due to the placement of another waste cell or cover. Yoshida *et al.* (1999), also incorporated an aerobic decomposition zone above active anaerobic decomposition zones in their simulation of temperature distribution in a landfill. Once the 100 m by 100 m area has been filled, each lift within this area is covered with intermediate cover. After intermediate cover was in place, the top cell (5^{th}) in the waste lift started gas production.

Landfill construction within the LES model is simulated using these lifts to create columns of waste. Figure 5.2 shows the filling sequence or stacking of the 100 m by 100 m areas at approximately 20 months and 64 months. Each column within the landfill was built from several lifts of waste, intermediate cover and landfill cap. Each lift is assigned to a column based on the placement order and lift position. The logical time sequence of each column is checked to ensure that waste age within the column progressively decreases from the oldest lift at the bottom to the youngest at the top of the column. The growth of the landfill was based on the annual waste acceptance rate and the compaction of the waste. These parameters were used to determine the waste's daily placement rate and mass of waste in the lift. The daily placement rate is determined by dividing the annual waste tonnage by the number of days in the year and the compaction rate to determine the volume of waste placed per day. This volume is in turn then divided by the surface area of a column to determine the height of waste per day. If this value is larger than the user prescribed lift depth, the excess height is used to start a new lift at the next location identified in Figure 5.1. The next day's waste placement will start on the top of the previous day until it reaches the prescribed lift height. Once the daily lifts have filled a prescribed area, they are capped with intermediate cover. This process is repeated until all eight lifts of the column have been placed within the prescribed area. The layers of the final cap are then placed. The mass of waste within each cell of the lift was determined by multiplying the cell volume by the compaction rate.

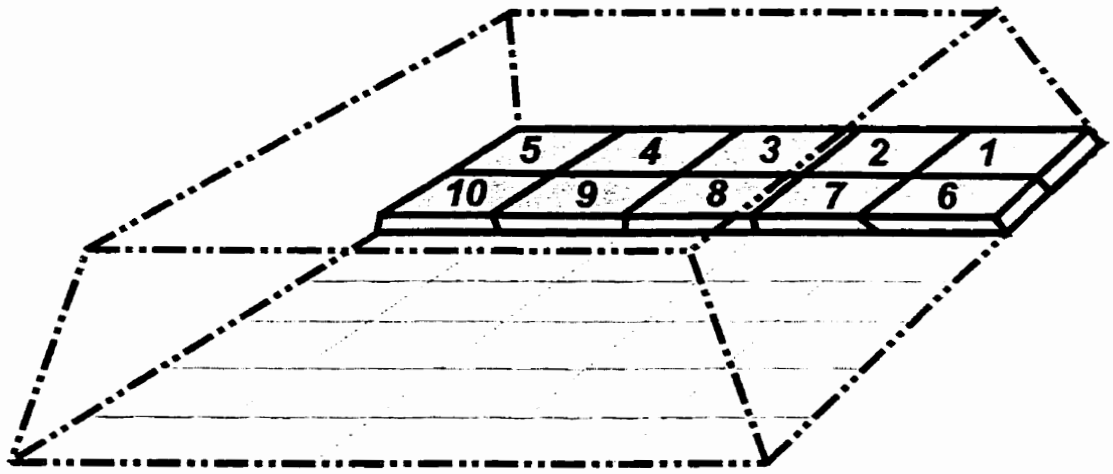

(A) Approximately 20 months in landfill construction

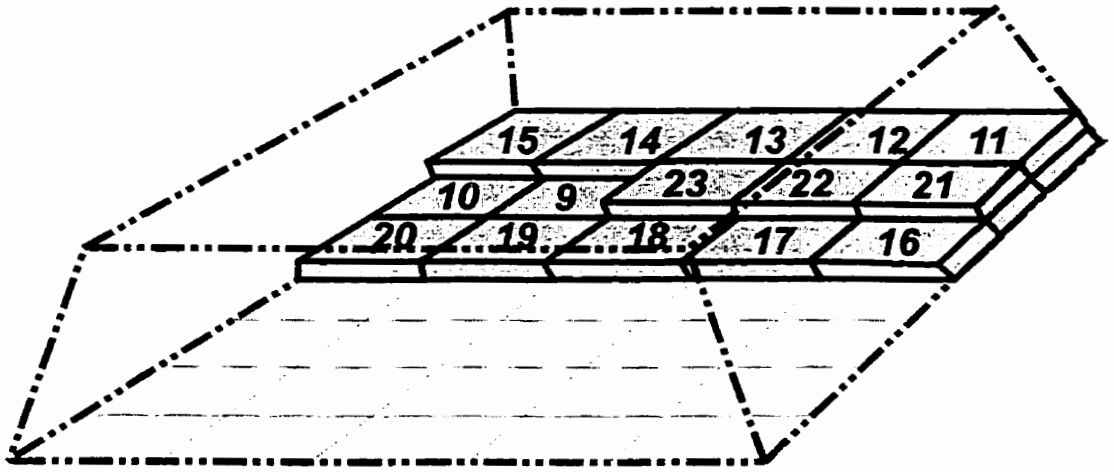

(B) Approximately 64 months in landfill construction

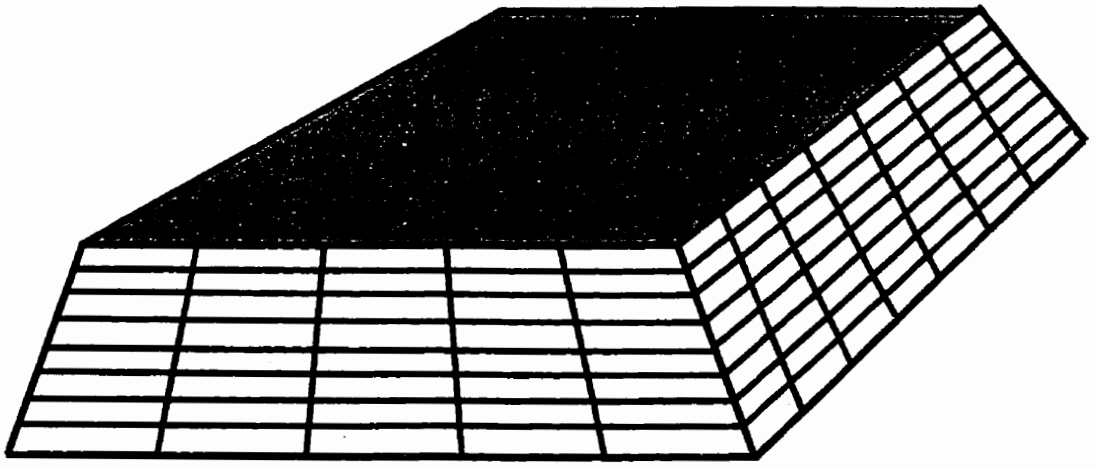

(C) End of landfill construction with final cover in place

Figure 5.2: Illustration of the sequential placement of the 100 m x 100 m areas over time

5.2 Gas Production in a Landfill

Gas production in a landfill starts at the time of the placement of the waste with degradation occurring in four distinct phases as shown in Figure 2.1. Typical time frames for these four phases are summarized in Table 5.1.

Table 5.1: Typical Time Frame in Qualitative Stage Model (Augenstein & Pacey, 1991)

Stage	Time Frame
I	Hours to 1 week
II	1 to 6 months
III	3 months to 3 years
IV	1 to 80 years

Although, many factors such as moisture, temperature, nutrients and microorganisms influence biogas production, most authors believe that first-order kinetics with respect to substrate are the most suitable to model gas production in a landfill (Cossu *et al.*, 1996). The fact that the gas production gradually declines in the long term supports the selection of first-order reactions (Cossu *et al.*, 1996). The first phase or aerobic phase was ignored in the development of this model. The length of the aerobic phase (phase I) is short relative to the other phases and the amount of CO_2 produced is small in comparison (less than 5%) to the following phases. The anoxic or nonmethanogenic phase (phase II) is dominated by the production of CO_2. The next two methanogenic phases, unsteady and steady, (phases III & IV) consist of the production of both CH_4 and CO_2 through the anaerobic degradation of the waste. All phases of the gas production in the model were approximated with first-order reactions.

In phases II and III, the equation with an exponential production component used to simulate the production of CO_2 and CH_4 is

$$Q_T = k * L_o * M_i * (1 - \exp(-k * t_i)) \qquad (5.1)$$

where:

Q_T = Total production of gas (m^3/year)

k = Landfill gas generation rate constant (1/yr)

L_o = LFG generation potential (m^3/Tonne)

M_i = Mass of refuse in the i^{th} cell (tonnes)

t_i = Age of the i^{th} cell (years)

The steady anaerobic methanogenic phase (IV) producing CH_4 and CO_2 is simulated by the Scholl Canyon model

$$Q_T = k * L_o * M_i * \exp(-k * t_i) \qquad (5.2)$$

where:

Q_T = Total production of gas (m^3/year)

k = Landfill gas generation rate constant (1/yr)

L_o = LFG generation potential (m^3/Tonne)

M_i = Mass of refuse in the i^{th} cell (tonnes)

t_i = Age of the i^{th} cell (years)

Figures 5.3 and 5.4 show the production rates used in this research. The production of CO_2 started at 7 days after waste placement and was simulated using equation 5.1. This lag in start time simulates the wait time between placement and the startup of the anoxic phase of the decomposition process. This second phase lasts for approximately 50 days at which time the third phase of decomposition in the model starts. Unsteady anaerobic decomposition (phase III) of the waste is assumed to start just as the anoxic phase is peaking. The model simulates the unsteady anaerobic decomposition as an exponential process (equation 5.1) in the CH_4 production (phase III) until one year after placement of the waste. Production of CO_2 in phase III as presented in Figure 5.3 was produced by subtracting 8.75 times the values obtained in the production equation (5.1) for phase III from production equation (5.1) for phase II. The value 8.75 was required to match the tail of the curve from phase II to meet the start of the production curve in phase IV. CO_2 gas production within phases II and III both used equation 5.1 but with different k and L_o which are shown in Section 5.4.1. At this point, the Scholl Canyon model with a lag of one year simulates the production of CO_2 and CH_4. The USEPA (1995) and MOE (1992) also use a one year lag in the production of CH_4 and CO_2 by the Scholl Canyon Model. The one year lag ensures that the decomposition of the waste has entered the steady anaerobic methanogenic phase (phase IV). The one year lag used for the Scholl Canyon Model was used as the base time line for the timing of the other phases of decomposition. The start times for phases II and III are within the ranges predicted for the qualitative model generated by Farquhar & Rovers (1973). The Scholl Canyon Model requires

input of the mass of the waste in each cell to predict the gas production. During landfill construction, each cell is assigned a mass based on the cell volume and the waste compaction as described previously.

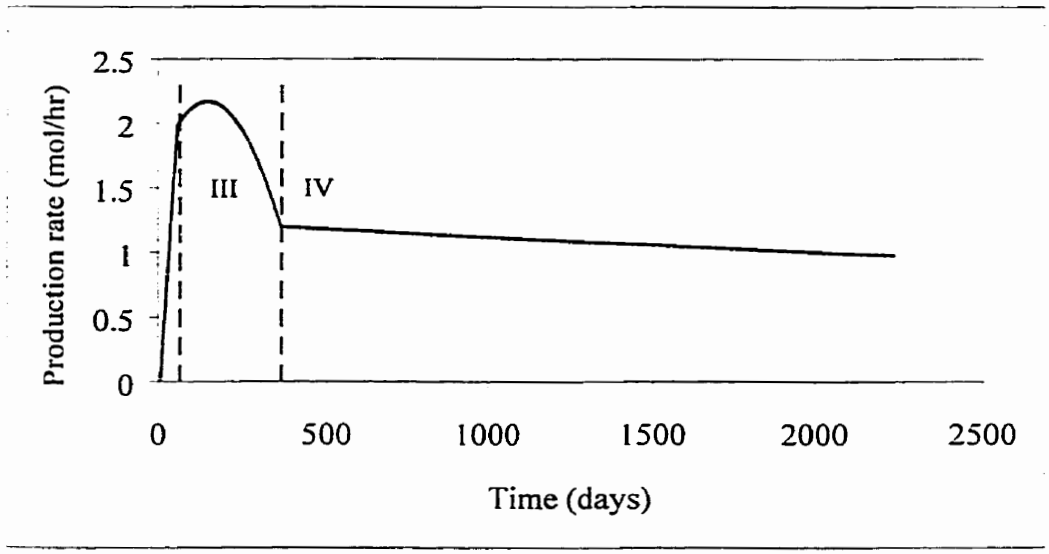

Figure 5.3: Production rate for CO_2 in the LES model

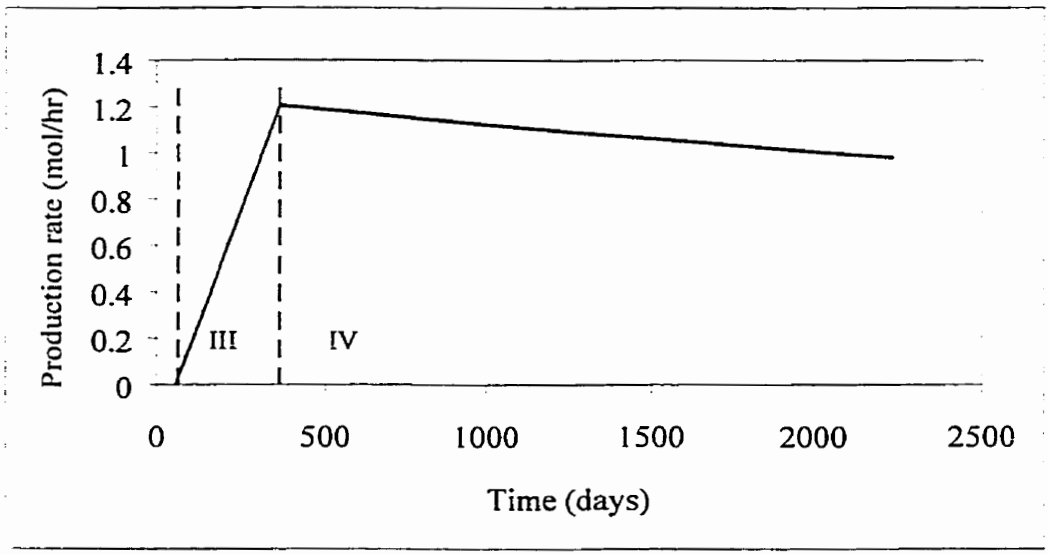

Figure 5.4: Production rate for CH_4 in the LES model

The presence of vinyl chloride in LFG is mainly the result of anaerobic and other decomposition processes. The production of vinyl chloride was assumed to start at two days after placement for 4 cells out of the 5 cells in the lift. The production in the top cell (5^{th} cell) was limited to the volatilization process due to the high levels of oxygen; therefore the

production of vinyl chloride in this cell was arbitrarily set at 10% of the rate predicted by the first-order equation (equation 5.3). The concentration due to the volatilization process was expected to be small and with no other available information the 10% value was chosen. Production of vinyl chloride was simulated using a first-order equation similar to the Scholl Canyon model (MOE, 1992). The equation used to simulate the vinyl chloride (VC) production is

$$Q_T = 2 * 3.595E-09 * k * L_o * M_i * C_{VC} * \exp(-k * t_i) * \frac{MW_{VC}}{MW_{Hexane}} \qquad (5.3)$$

where:

Q_T = Total production of VC (Tonnes /year)

k = Landfill gas generation rate constant (1/yr)

L_o = Methane generation potential (m^3/Tonne)

M_i = Mass of refuse in the i^{th} cell (tonnes)

C_{VC} = Concentration of specific VC (ppm-volume)

t_i = Age of the i^{th} cell (years)

MW = molecular weight (g/mol)

3.595E -09 = conversion factor based on Hexane as the average NMOC

The vinyl chloride production rate used in the model simulation is shown in Figure 5.5.

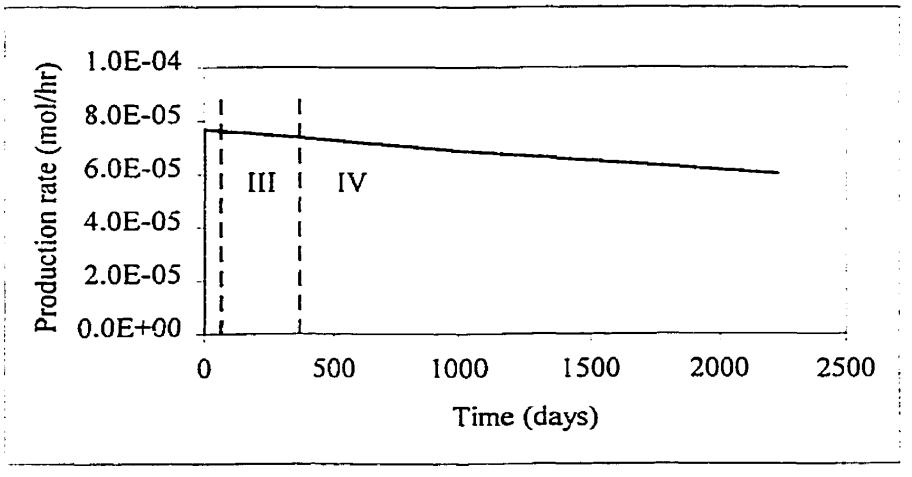

Figure 5.5: Production rate for vinyl chloride in the LES model

H_2S production was assumed to follow a similar cycle as CH_4 production but with the peak in the curve shifted forward due to sulfide production occurring faster than CH_4 production

(Flynn, 1998). The H_2S production rate curve shown in Figure 5.6 uses the same formulation as the CH_4 curve (equation 5.1) with an exponential growth curve starting at 55 days and peaking at 183 days and exponential decline after that (equation 5.2). Given that sheet rock or wall board ($CaSO_4$) is a major source of H_2S through anaerobic decomposition. the equations used to produce CH_4 in phase III and IV were multiplied by 1/10000 to simulate the much slower production of H_2S. This number was selected based on the ratio of methane to H_2S observed at the Waterloo and Cambridge Landfills. The Waterloo Landfill average methane concentration (22.1 mol/m^3) and H_2S concentration (1.9 x 10^{-3} mol/m^3) gives value of 11631 whereas the Cambridge values 15.5 mol/m^3 to 1.7 x 10^{-3} mol/m^3 gives a value of 9118. An average of these two ratios results in a value of 10374. Figure 5.6 shows the resulting production rates with respect to time.

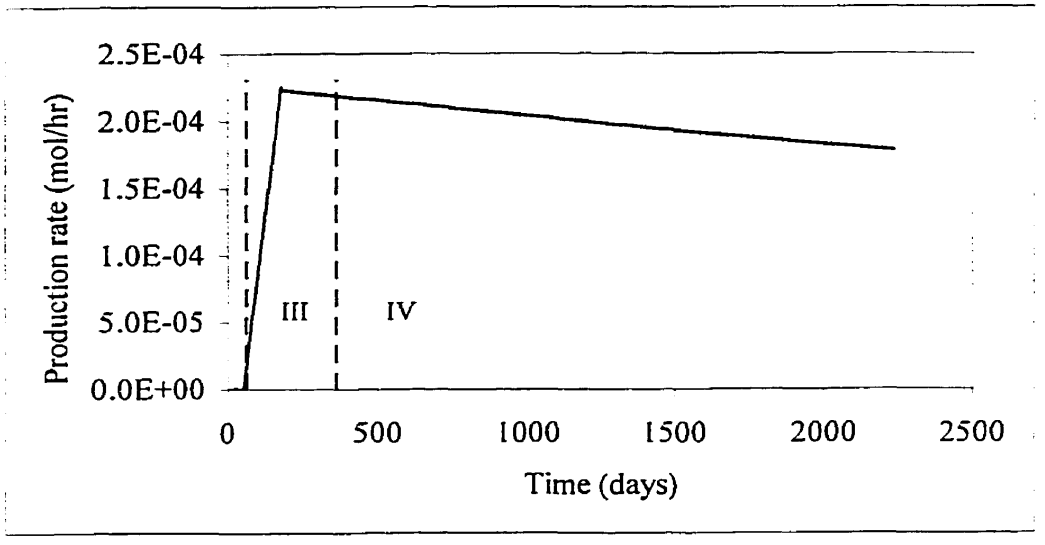

Figure 5.6: Production rate for H_2S in the LES model

5.3 Model for Gas Transport in a Landfill and Emission from the Surface

El-Fadel *et al.* (1995) used a finite difference solution of a 1-D advection dispersion equation to simulate gas transport through several layers of landfill waste in test cells. Using this method, they achieved a good comparison between the simulated results and data collected from the test cells. Landfill gas transport in their model was simulated using a block-centred finite difference solution of a 1-D advection dispersion equation coupled with a pressure

equation based on the gas concentrations. A fully implicit (backward in time) scheme and the Newton-Raphson method were used to iteratively solve the system of nonlinear equations.

The following section briefly discusses the equations used to model the movement of the gas mixture through the landfill. The movement of the gas mixture was dependent on the viscosity and diffusion coefficient for the landfill gas mixture both being dependent on the composition of the gas mixture.

5.3.1 Equations for Gas Mixture

Landfill gas is a multicomponent gas made of approximately 50 percent CH_4 and 50 percent CO_2 with a small percentage of other gases such as H_2S and vinyl chloride. The composition of the LFG within the landfill is dependent on the phase of gas production or waste decomposition. Therefore, to account for the change in composition with time, the LFG was considered to be a mixture of gases each having their individual viscosity and diffusion properties. The LES model used the following set of equations to calculate the viscosity and diffusion coefficient for each individual gas that made up the LFG. The overall flux of the LFG within the landfill is dependent on the viscosity and the diffusion coefficient of the gas mixture. As the gas composition changed within the waste the viscosity and diffusion coefficient was updated using the mixture gas equations shown in the following sections.

Absolute Viscosity

Absolute viscosity is the physical property that characterizes a fluid's resistance to flow. The kinetic theory of Chapman-Enskog has resulted in the following equation for the absolute viscosity of a single gas (Bird *et al.*, 1960);

$$\mu = \frac{2.6693 * 10^{-6} (MT)^{1/2}}{\sigma^2 \Omega_v} \tag{5.4}$$

where:

μ = viscosity, (Pa·s)

M = molecular weight, (g/mol)

T = temperature, (K)

Ω_v = Lennard-Jones viscosity collision integral, (dimensionless)

σ = Characteristic length, (A°).

The collision integral, Ω_v, is unity if the molecules do not attract each other. The Lennard-Jones viscosity collision integral is a slow varying function of the dimensionless temperature and can be approximated using the empirical equation (Neufeld *et al.*, 1972).

$$\Omega_v = \frac{A}{T^{*B}} + \frac{C}{\exp(DT^*)} + \frac{E}{\exp(FT^*)} \tag{5.5}$$

where:

A=1.16145, B=0.14874, C=0.52487, D=0.77320, E=2.16178, F=2.43787,

$T^* = \frac{kT}{\varepsilon}$,

T = temperature, (K)

ε/k = characteristic energy/Boltzmann's constant, (K).

The theory of Chapman-Enskog can be extended to the viscosity of multicomponent gases. The multicomponent viscosity, μ_m, can be approximated using the mole fraction of the mixture, individual viscosities and the Wilke's approximation of ϕ_{ij} (Reid *et al.*, 1977) by

$$\mu_m = \sum_{i=1}^{n} \left[\frac{y_i \mu_i}{\sum_{j=1}^{n} \varphi_{ij} y_j} \right] \tag{5.6}$$

where:

$$\varphi_{ij} = \frac{\left[1 + \left(\frac{\mu_i}{\mu_j} \right)^{1/2} \left(\frac{M_j}{M_i} \right)^{1/4} \right]^2}{\sqrt{8} \left(1 + \frac{M_i}{M_j} \right)^{1/2}} \tag{5.7}$$

μ_m = viscosity of mixture, (μP)

μ_i, μ_j = pure component viscosities, (μP)

M_i, M_j = molecular weight, (g/mol)

y_i, y_j = mole fractions, (dimensionless).

The mole fraction of the gas mixture used to quantify the composition of the mixture is given by

$$y_i = \frac{C_i / M_i}{\sum_{i=1}^{n} C_i / M_i} \tag{5.8}$$

where:

y_i = mole fraction, (dimensionless)

C_i = concentration of gas *i*, (g/m^3)

M_i = molecular weight of gas *i*, (g/mol).

Diffusion Coefficient

Diffusion is the process whereby ionic or molecular constituents move in the absence of mixing (by mechanical means or by convection) in the direction of a decreasing concentration gradient (Freeze & Cherry, 1979). The theory describing diffusion in binary gas mixtures was developed by Chapman and Enskog (Reid *et al.*, 1977). The diffusion of binary gas mixtures is given by

$$D_{ij} = \frac{3}{16}\left(\frac{4\pi kT}{M_{ij}}\right)^{1/2} \frac{f_D}{n\pi\sigma_{ij}^2\Omega_D} \tag{5.9}$$

where:

k = Boltzmann's constant

n = number density of molecules in the mixture

f_D = correction term

$$M_{ij} = \frac{2}{\left(\frac{1}{M_i} + \frac{1}{M_j}\right)}$$

M_i, M_j = molecular weights of gases i and j, (g/mol)

T = temperature, (K)

Ω_D = Lennard-Jones diffusion collision integral, (dimensionless)

P = pressure, (bar)

$$\sigma_{ij} = \frac{\sigma_i + \sigma_j}{2}$$

σ_i, σ_j = Characteristic length of gases i and j, (A°).

The correction term, f_D is near unity. If M_i is of the same order as Mj, f_D lies between 1.0 and 1.02 regardless of composition of the intermolecular forces (Reid *et al.*, 1977). The value of f_D

is significantly different from unity only if the molecular masses are very unequal and the lighter component is present in trace amounts. If f_D is unity and n is expressed by the ideal gas law, the equation (5.9) can be written as

$$D_{ij} = \frac{0.00266T^{3/2}}{PM_{ij}^{1/2}\sigma_{ij}^2\Omega_D} \tag{5.10}$$

Neufeld *et al.* (1972) provided an equation that accurately represents the Lennard-Jones diffusion collision integral for the binary diffusion coefficient as

$$\Omega_D = \frac{A}{T^{*B}} + \frac{C}{\exp(DT^*)} + \frac{E}{\exp(FT^*)} + \frac{G}{\exp(HT^*)} \tag{5.11}$$

where:

A = 1.06036, B = 0.15610, C = 0.19300, D = 0.47635, E = 1.03587, F = 1.52996, G = 1.76474, H = 3.89411,

$$T^* = \frac{kT}{\varepsilon_{ij}},$$

$$\frac{\varepsilon_{ij}}{k} = \left(\frac{\varepsilon_i}{k}\frac{\varepsilon_k}{k}\right)^{1/2}.$$

In binary gases, D_{ij} is normally assumed independent of composition (Reid *et al.*, 1977). With this approximation and theory developed by Maxwell and Stefan, the diffusion coefficient for multicomponent gases, D_{im}, can be approximated by

$$D_{im} = \left(\frac{1-y_i}{\sum_{j=1}^{n}\frac{y_j}{D_{ij}}}\right) \tag{5.12}$$

where:

y_i, y_j = mole fractions of gases *i* and *j*, (dimensionless)

D_{ij} = binary diffusion coefficient of gases *i* and *j*, (m^2/s)

D_{im} = diffusion coefficient of gas *i* in the mixture of *n* gases, (m^2/s)

n = number of gases,

m = indicates a gas mixture.

Fairbanks and Wilke (1950) experimentally verified equation (5.12) and indicated that the equation was a satisfactory representation of the effective diffusion coefficient in multicomponent mixtures.

Appendix F contains the characteristic length and energy and molecular weights to calculate the viscosity and diffusion coefficient for the pure gases.

5.3.2 Equations for Gas Transport

Gas transport through porous media is dependent on the porosity and water content of the porous media. Gas utilizes the larger pore spaces to move through the porous media due to capillary pressure within the porous media maintaining the water phase within the smaller pore spaces. An accurate estimate of the gas transport through porous media must reflect the presence of the porosity and moisture content of the soil.

Diffusion coefficients are expressed in the absence of obstruction although there is tortuosity of path within the porous media caused by water within the pores. To allow for this, the multicomponent diffusion coefficients were corrected for total porosity and water content using (Millington, 1959)

$$D^{'} = D_{im} \frac{\theta_a^{7/3}}{\phi^2} \tag{5.13}$$

where:

ϕ = total porosity, (dimensionless)

θ_a = air porosity, (dimensionless)

D_{im} = multicomponent diffusion coefficient in air, (m^2/s)

D' = effective multicomponent diffusion, (m^2/s).

The movement of the gas through the porous media is dependent on the permeability of the porous media. The presence of water in porous media will limit the movement of the gas and thus the permeability of the porous media must be adjusted to reflect the water content. Kjeldsen (1996) identified a ratio of the air porosity to total porosity has been used to find the gas permeability of the waste

$$k^* = k \frac{\theta_a}{\phi} \tag{5.14}$$

where:

k^* = effective permeability, (m^2)

ϕ = total porosity, (dimensionless)

θ_a = air porosity, (dimensionless)

k = permeability, (m^2).

The effective dispersion of the gas within the porous media is a function of the effective molecular diffusion and the mechanical dispersion. Mechanical dispersion is a result of the mixing that occurs due to the variation in velocity within the porous media. The dispersivity, a geometric measure of the permeability and storage heterogeneities in the porous media (Luckner & Schestakow, 1991) is the result of the gas velocity variation. The effective dispersion of the gas within the porous media is expressed as (Freeze & Cherry, 1979)

$$D^* = \alpha|q| + D' \tag{5.15}$$

where:

D' = effective molecular diffusion (m^2/s)

α = dispersivity (m)

q = Darcy velocity of gas (m/s)

D^* = effective dispersion (m^2/s).

The spatial and temporal concentration and pressure profiles within the landfill columns were simulated using conservation of mass relationships. The theory and derivation of the gas flow equation in porous media are discussed in Bear (1972). The equation of mass transport in a porous media can be written as

$$\frac{\partial \phi S_g C_i}{\partial t} = -\frac{\partial (qC_i)}{\partial z} + \frac{\partial}{\partial z}\left(\phi S_g D_i^* \frac{\partial C_i}{\partial z}\right) + G_i \tag{5.16}$$

where:

ϕ = porosity of the landfill

t = time, (s)

C_i = concentration of gas *i*, (g/m^3)

D_i^* = dispersion coefficient of gas *i*, (m^2/s)

G_i = production rate of gas *i*, (g/s)

q = Darcy velocity, (m/s)

S_g = gas saturation (dimensionless).

Since the Reynolds number characterizing the flow of gases generated in sanitary landfills is typically smaller than 1, the gas velocity can be described by Darcy's equation

$$q = -\frac{k^*}{\mu_m}\left(\frac{\partial P}{\partial z}\right) \tag{5.17}$$

where:

k* = effective gas permeability of the medium (m^2)

μ_m = viscosity of mixture, (Pa·s)

P = pressure (Pa).

The effects of gravity within the Darcy's equation were ignored for gas flow. The total pressure when two or more gases are present is equal to the sum of the individual partial pressures and the individual partial pressures are determined from the ideal gas law. Hence the total pressure can be given by

$$P = RT\left(\sum_{i=1}^{n}\frac{C_i}{M_i}\right) \tag{5.18}$$

where:

R = gas constant

M = molecular weight of gas *i*, (g/mol)

T = absolute temperature, (°K)

C_i = concentration of gas *i* (g/m^3).

The Darcy velocity (5.17) and total pressure (5.18) were substituted into the transport equation (5.16) to yield a nonlinear equation for each gas.

After placement of the waste, the gas concentrations within the waste were assumed to be at atmospheric conditions (79% N_2, 20.964% O_2, O% CH_4, 0.036% CO_2, O% VC, 0% H_2S). These percentages were converted to molar concentrations using the atmospheric conditions at the time of placement and the ideal gas law. The partial pressure of each gas was calculated using the ideal gas law and then summed to determine total gas pressure. The pressure and concentration are linked to create a system of nonlinear equations that must be solved iteratively. A new mole fraction was calculated based on the previously iterated concentrations and used in the next iteration. Using the new mole fraction, the viscosity, dispersion coefficient and pressure values were updated. Landfill gas transport in this model was

simulated using a block-centred finite difference solution of a 1-D advection dispersion equation. A fully implicit (backward in time) scheme and the Newton-Raphson method were used to iteratively solve the system of nonlinear equations. The iterative process was repeated until the conversion criteria was below the selected tolerance level (1×10^{-5}).

The Peclet number and Courant number were checked to ensure that numerical dispersion did not occur during the simulations. The Peclet number formula and criteria (Luckner & Schestakow, 1991) used in the LES model was

$$Pe = \frac{\Delta z|q|}{D_i^*} \leq 2 \qquad (5.19)$$

where:

Δz = depth of cell (m)

D_i^* = dispersion coefficient of gas *i*, (m^2/s)

q = Darcy velocity (m/s).

Courant number formula and criteria used in the LES model was (Luckner & Schestakow, 1991),

$$Cr = \frac{\Delta t|q|}{\phi \Delta z} \leq 1 \qquad (5.20)$$

where:

Δt = time step, (s)

Δz = depth of cell, (m)

q = Darcy velocity, (m/s)

ϕ = porosity (dimensionless).

As the pressure gradient increased within the column, the time step was reduced to minimize the numerical oscillations. The new time step was determined by rearranging equation (5.20) and substituting the criteria of one for the Courant number.

A flow chart of the LES model is shown in Figure 5.7.

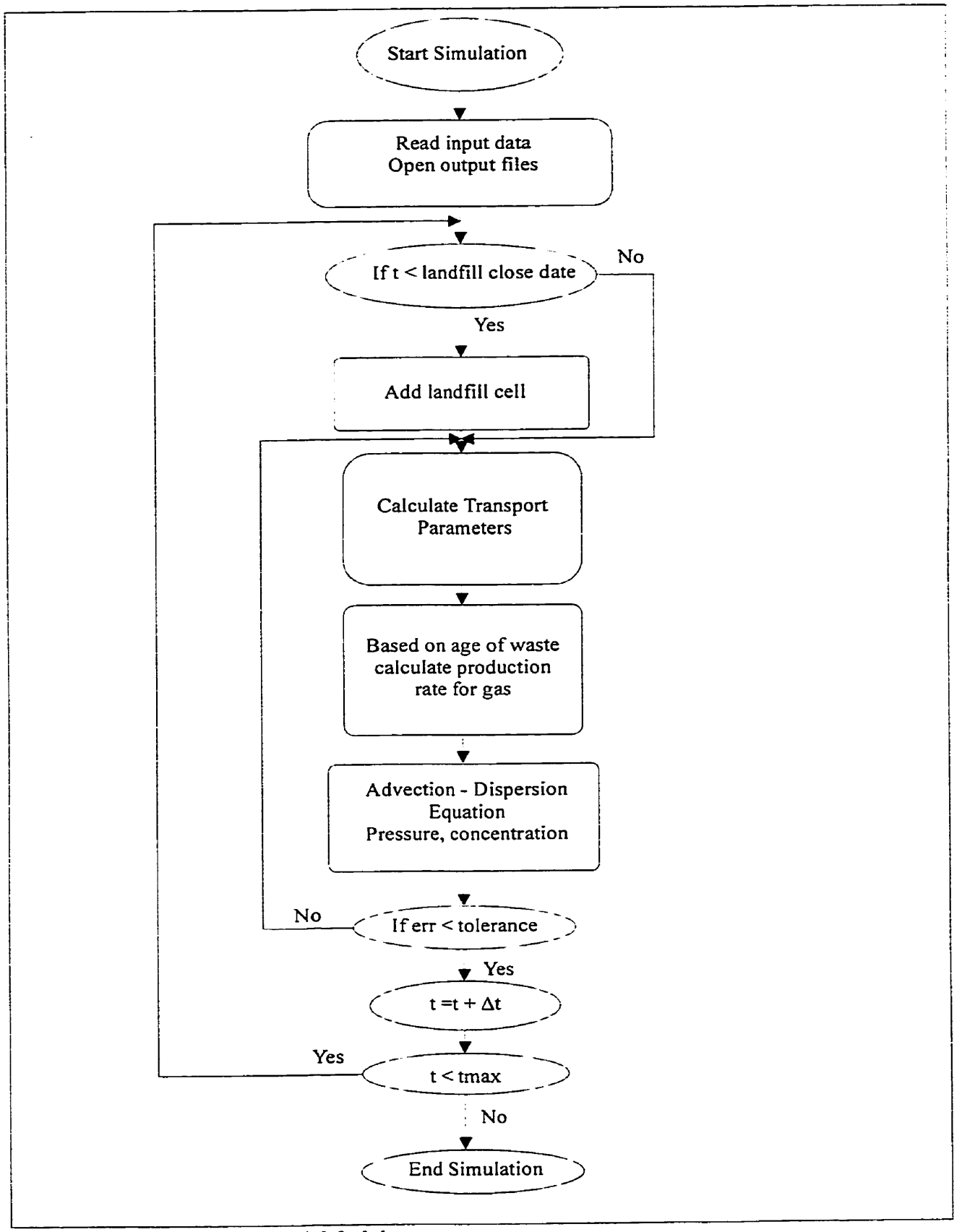

Figure 5.7: Flowchart of LES Model

5.3.3 Boundary Conditions

The model is 1-D and therefore only two boundary conditions are required. An impermeable layer delineates the lower boundary. Neumann boundary conditions are used for both the pressure and concentration at the lower boundary.

A static boundary layer defines the top of the column. The static boundary layer is the result of the atmospheric conditions. The laminar layer is a thin film of the order of 10 cm in thickness (a range of 0.5 to 100 cm is reported) with the horizontal wind velocity and ground cover determining the thickness of the layer. The gas concentration and the pressure were set to the atmospheric gas concentration and atmospheric pressure at the top of the laminar layer above the landfill surface. The laminar layer thickness and the transport coefficient (permeability and viscosity) were selected to approximate the surface layer above the landfill. The diffusion coefficient within the laminar layer was approximated by the free diffusion coefficients of the gases in air.

5.3.4 Gas Transport in Waste Column during Landfill Construction

Construction of the waste column was simulated using an expanding mesh. Figure 5.8 illustrates the process of the expanding mesh to simulate the addition of cover material or waste on top of an actively emitting waste column. The growth rate of the block was determined based on the final depth of the block divided by the number of time steps during the 24 hour period. The example shown in Figure 5.8 had an 8 hour time step and the final block depth was 0.25 m. Therefore, the block would have a growth rate of 0.25 m divided by 24 hours to give a growth rate of 0.0104 m/hr and within each time step the block would grow 0.083 m.

The addition of waste on top of the actively emitting waste column required that the gas flow within the block to be adjusted to account for the movement of the upper surface. Finlayson, (1992) modelled the contaminant in a stream with a moving grid. The contaminant front within the stream is rapidly changing therefore to delineate the change the grid system moved at a velocity different than the velocity of the stream. The advection term within the advection/dispersion equation required that the velocity term be corrected for the movement or

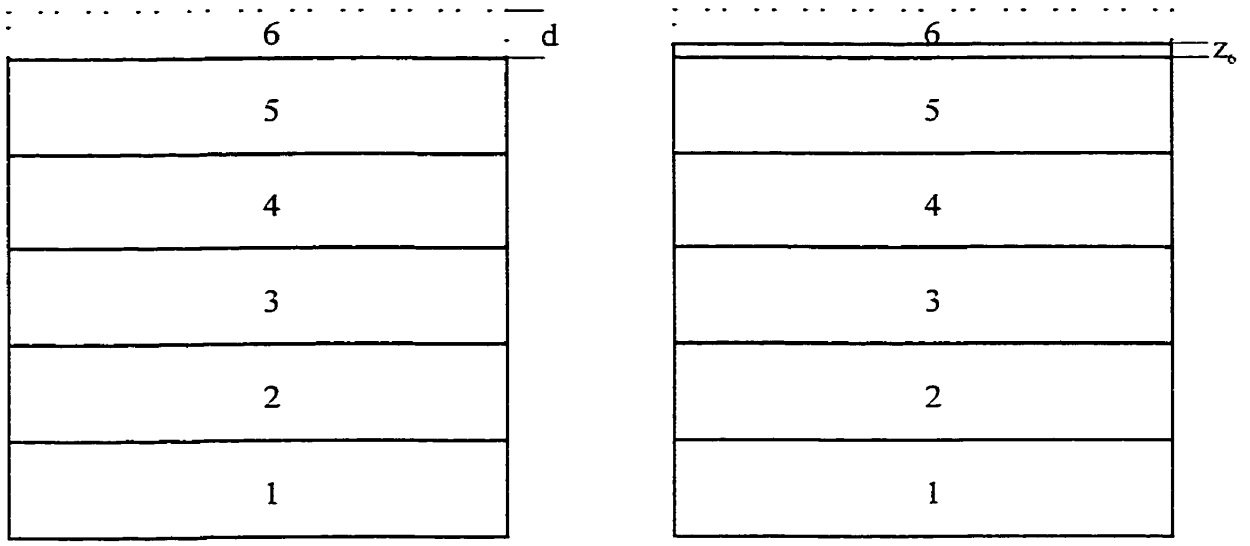

(A) Start of placement day, $z_6 = 0$ m, vz = 0.0104 m/hr

(B) Next time step, $z_6 = 0.083$ m, vz = 0.0104 m/hr

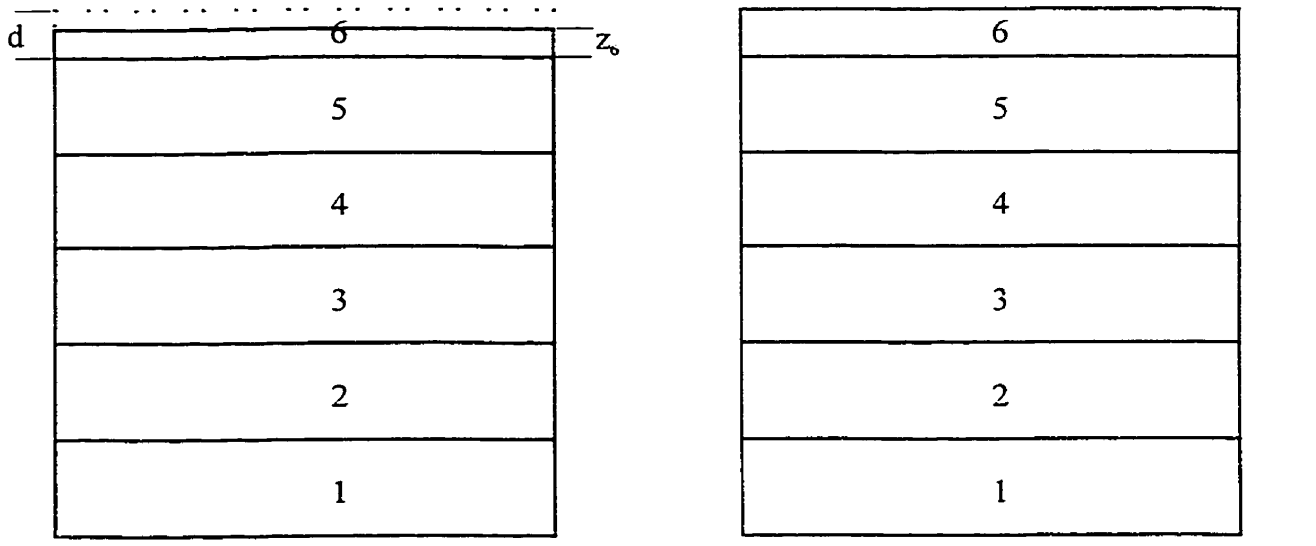

(C) Next time step day, $z_6 = 0.166$ m, vz = 0.0104 m/hr

(D) End of placement day/ start of next day, $z_6 = 0.25$ m, vz = 0 m/hr

Figure 5.8: Conceptual illustration of the expanding mesh to simulate addition of waste or cover material. Example shown the new cell depth (d) = 0.25 m and time step = 8 hrs vz = growth rate of block 6

velocity of the grid. Similiarly, the gas flux of the LES model within the expanding block was adjusted to account for the movement or growth rate of the block to give a new gas flux by.

$$q_{new} = (q - vz) \tag{5.21}$$

where:

q = darcy velocity of gas, (m/hr)

vz = column growth rate (m/hr).

The depth of the new block was adjusted at the end of each time step by

$$z_{new} = (z + vz * dt) \tag{5.22}$$

where:

z = depth of block, (m)

dt = time step (hr).

5.3.5 Permeability Change due to Construction

Bleiker (1992) found that the hydraulic conductivity of waste was much lower at the base of landfill in comparison to the top layers. The change in hydraulic conductivity is a result of the waste becoming compacted from the new lifts of waste applied on top of the existing waste and due to decomposition as well. Therefore, the permeability of the waste in the model was adjusted to account for the new layers of waste added. A relationship between the depth of each cell and the permeability was developed based on the effective stress and hydraulic conductivity data used by Bleiker (1992) in the development of his landfill settlement model. The relationship used was

$$k = k_i * 10^{-0.138*d} \tag{5.23}$$

where:

k_i = initial waste permeability, (10^{-10} m^2)

d = depth at centre of waste cell (m).

Total porosity can decrease as the permeability decreases but in this model the total porosity was assumed to remain constant. The gas porosity of the waste is dependent on the water content of the waste. The change in water content in the waste as a result of leachate movement within the waste was not considered in this model; therefore, a constant gas porosity for the waste was used throughout the model simulations.

5.3.6 Model Testing and Validation

An overall mass balance and time step mass balance for each gas was performed. The error in the overall mass of each gas at the end of the simulation was less than 0.1 percent and significantly less than 0.1 percent for the between time step mass balance.

The concentration profiles of the gases with depth were compared to literature gas concentrations measured at a landfill (Lagerkvist *et al.*, 1997). The concentration profiles were found to compare reasonably well and the results are shown in Section 5.8.1.

For the purpose of validation, the model output was also compared to an analytical equation and the results are shown in Appendix G.

5.4 LES Model Simulations

Three different simulations were performed to determine the flux of CH_4, CO_2, vinyl chloride and H_2S out of the waste columns under different situations. The three simulations consisted of a base case, base case plus methane oxidation in the topsoil, and the base case with a cover perforation. Each simulation was run for 100 years. The first 16 years were used for the construction and capping of the column.

5.4.1 Base Case

The landfill dimensions used for the base case were 700 m (length) by 500 m (width) and 20 m deep. The base case consisted of a column of waste that was built over time as described in the Section 5.1.1. The lift parameters used were 12.5 m by 12.5 m forming the base of one column and a lift depth of 2.5 m. Figure 5.9 provides a schematic of the columns built in the model for the simulations in this research. Each column consists of 8 lifts of waste with an intermediate cover and a final cover that consisted of a gravel layer, clay cap, sand layer and topsoil. Table 5.2 shows the permeability and time of placement of each cell and cover and other default parameters of the column used for the base case simulation. The permeability of the waste shown in Table 5.2 was adjusted using the equation from Section 5.3.5 as each new lift was added to the waste column. This base case column format was adjusted to generate the simulations for the methane oxidation and cover perforation simulations. The modifications are discussed in the following sections.

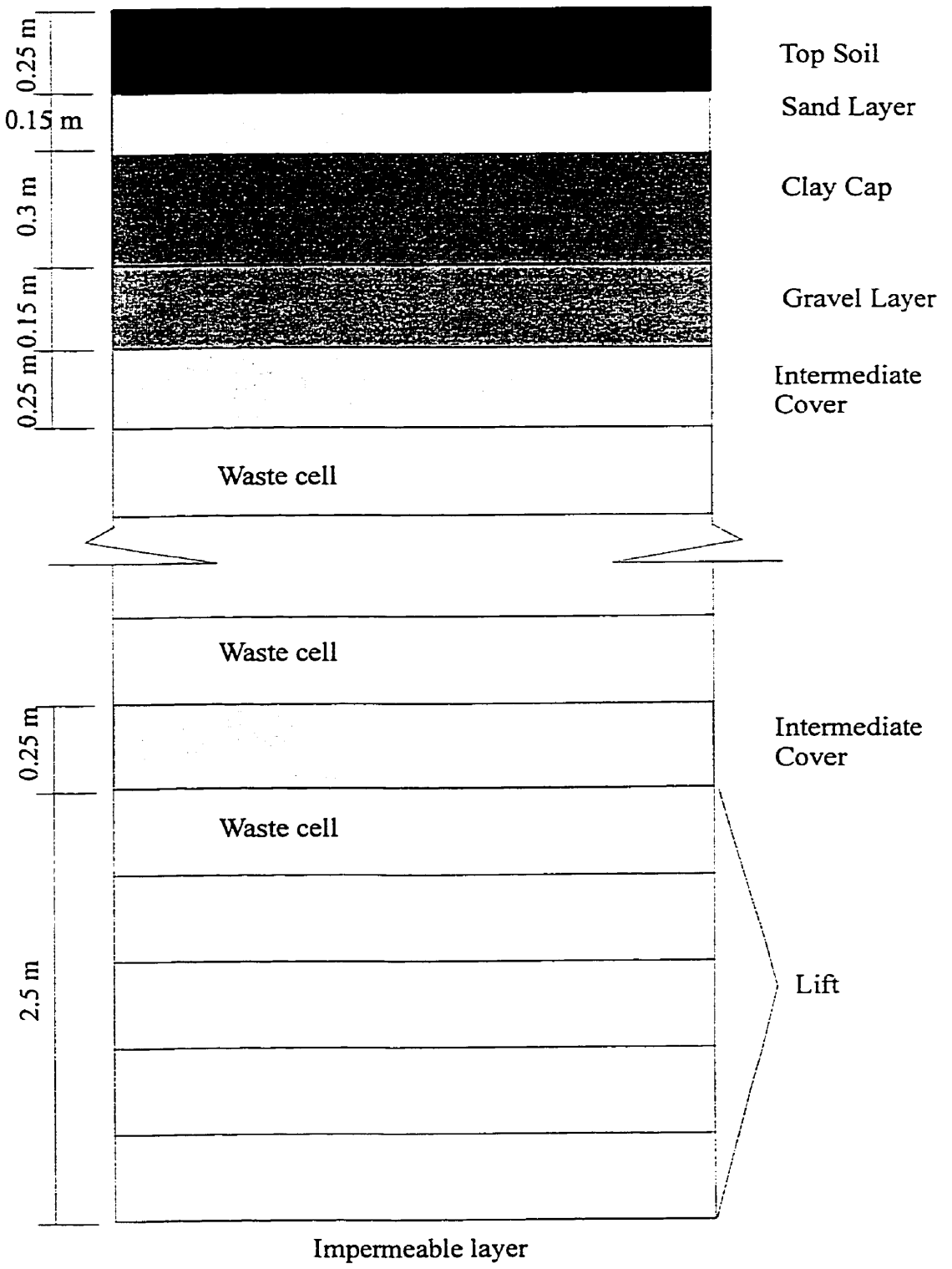

Figure 5.9: Schematic of a landfill column.

Table 5.2: Parameter of waste and cover material within the column

Description	Cell Number	Permeability (m^2)	Placement time (days)	Porosity	Cell Thickness (m)
Waste	1 to 5	10^{-10}	1	0.3	0.5
I cover	6	10^{-13}	65	0.3	0.25
Waste	7 to 11	10^{-10}	604	0.3	0.5
I cover	12	10^{-13}	685	0.3	0.25
Waste	13-17	10^{-10}	1353, 1354	0.3	0.5
I cover	18	10^{-13}	1423	0.3	0.25
Waste	19-23	10^{-10}	2041, 2042	0.3	0.5
I cover	24	10^{-13}	2120	0.3	0.25
Waste	25-29	10^{-10}	2852	0.3	0.5
I cover	30	10^{-13}	2962	0.3	0.25
Waste	31-35	10^{-10}	3957, 3958	0.3	0.5
I cover	36	10^{-13}	4116	0.3	0.25
Waste	37-41	10^{-10}	5127	0.3	0.5
I cover	42	10^{-13}	5262	0.3	0.25
Waste	43-47	10^{-10}	5986	0.3	0.5
I cover	48	10^{-13}	6141	0.3	0.25
Gravel	49	10^{-8}	6144	0.3	0.15
Clay cap	50	10^{-14}	6147	0.3	0.3
Sand	51	10^{-11}	6247	0.3	0.15
Top soil	52	10^{-10}	6250	0.3	0.25

Gas production within the waste column was simulated using the equations outlined and discussed in Section 5.2. Table 5.3 contains the values for each parameter used to simulate the production of CO_2 and CH_4 in the 3 phases of gas production. The k and L_o values for phases II and III were chosen to simulate the production of CO_2 and CH_4 and duplicate the curves shown on Figure 2.1. The default values selected by the MOE (1992) for L_o and k were used to simulate the production of CH_4 and CO_2 in phase IV of gas production for the simulations in this research.

The default parameters recommended for the production of vinyl chloride by the MOE (1992) were used in the model simulations and are shown in Table 5.4. The parameters used for the production of the H_2S are also shown in Table 5.4.

Table 5.3: Values of the k and L_o used to simulate the production of CH_4 and CO_2 within all phases of the

Phase	Gas	k (1/yr)	L_o (m^3/tonne)
II	CO_2	0.5	250
III	CO_2	0.23	125
	CH_4	0.23	125
IV	CO_2	0.04	125
	CH_4	0.04	125

Table 5.4: Values of the k and L_o used to simulate the production of vinyl chloride and H_2S in the model

Phase	Gas	k (1/yr)	L_o (m^3/tonne)
II	Vinyl chloride	0.04	125
III	Vinyl chloride	0.04	125
	H_2S	0.04	125
IV	Vinyl chloride	0.04	125
	H_2S	0.04	125

A dispersivity of 0.01 m was assumed for the calculation of the dispersion coefficient. A temperature of 20° Celsius was used in all calculations requiring temperature. The waste saturation was set to 30 percent during the placement of the waste and cover material. This value remained unchanged throughout the model simulation assuming that no further water entered the system.

5.4.2 Methane Oxidation in Cover

Oxidation of methane by the microbial population in the cover soil has been well documented by several authors (Kightley *et al.*, 1995, Bogner *et al.*, 1997a, Whalen *et al.*, 1990). These authors indicate that moisture content, oxygen supply and methane concentration affect the rate of methane oxidation in the cover. Höring *et al.* (1999) summarized methane oxidation in soil and landfill cover soils from literature sources and found that the methane consumption ranged from 0.01 to 70 L $CH_4/m^2/hr$. Given the wide range of oxidation rates and parameters that affect the oxidation of CH_4 in the cover, it was assumed for this analysis that 40% of the CH_4 in the top cell was oxidized to CO_2. Gregory *et al.* (1999) used the same percentage to simulate CH_4 oxidation in the landfill cap and it produced results that agreed well with observed gas behaviour.

5.4.3 Cover Perforations

A landfill's final cover is applied to minimize water infiltration to the waste below. This cover will also impede gas transport to the atmosphere depending on its thickness and permeability. Imperfections in the final cover will result in the increased emission of the landfill gas to the atmosphere. This component of the landfill model examines the effect that small perforations have on the emissions to the atmosphere. The perforations or holes in the cover can be simulated by a simple pipe flow equation with an adjustment coefficient as shown in Chapter 4. The Hagen-Poiseuille equation provided the best fit for the experimental data in Chapter 4 with an adjustment factor of 0.45 required to match the experimental data. This adjustment factor was not used in the model simulations but the equation was used to approximate the permeability of the cover with a hole. Including the adjustment factor would further reduce the cover permeability by 0.45. The velocity through the hole as determined by the Hagen-Poiseuille equation divided by the area of the hole is

$$q = \frac{(P_o - P_L)R^2}{8\mu L} \tag{5.24}$$

where:

R = radius of pipe (m),

L = length of pipe (m),

μ = viscosity of fluid (Pa·s),

P_o = inlet pressure (Pa),

P_L = outlet pressure (Pa), and

q = velocity (m/s).

This equation is similar in format to the Darcy's equation (5.17) for the velocity of gas through porous media. To simulate the presence of a hole in the clay cap, an effective permeability of the clay cap was obtained from the above equation. The $R^2/8$ from the Hagen-Poiseuille equation (equation 5.24) was used to calculate the effective permeability of the clay cap. In the case of a 1 in (2.54 cm) diameter hole, the permeability would be 2.02×10^{-5} m^2. The permeability of the clay cover was therefore adjusted from 10^{-14} m^2 to 2.02×10^{-5} m^2 over a period of 60 days. The formation of a hole would not occur overnight, therefore an arbitrary selection of 60 days was used to generate the exponential equation used to simulate the

formation of the hole over the 60 days. The effective permeability of the clay cap was used in the Darcy's equation to predict the velocity of the gas within the clay cap.

5.5 Results of LES Model Simulations

5.5.1 Base Case

Figure 5.10 shows the change in the CH_4 concentration profiles with depth in one landfill column at three different times (3000, 9000 and 36500 days) during the simulation. At 3000 days the column is approximately half built; therefore the concentration profile shown does not reach the same depth as the two other time intervals. The second time interval (9000 days) is approximately 3000 days after completion of the waste column (6250 days). The CH_4 profile at the end of the simulation is illustrated by the profile at 36500 days. This figure shows that the gas concentration is at approximately the maximum concentration during construction and that the concentration declines as the production starts to die off well after closure. Profiles of the CO_2, vinyl chloride and H_2S also show similar results and are presented in Appendix H.

Figure 5.11 shows profiles of pressure with column depth. This figure shows how the pressure within the landfill builds as gas production is progressing and that a reduction in the pressure profile occurs as gas production is declining. The pressure profiles at 3000 and 9000 days are discontinuous (or stepping) due to the lower permeability of the intermediate cover layers which restricts gas through it and creates higher pressures below.

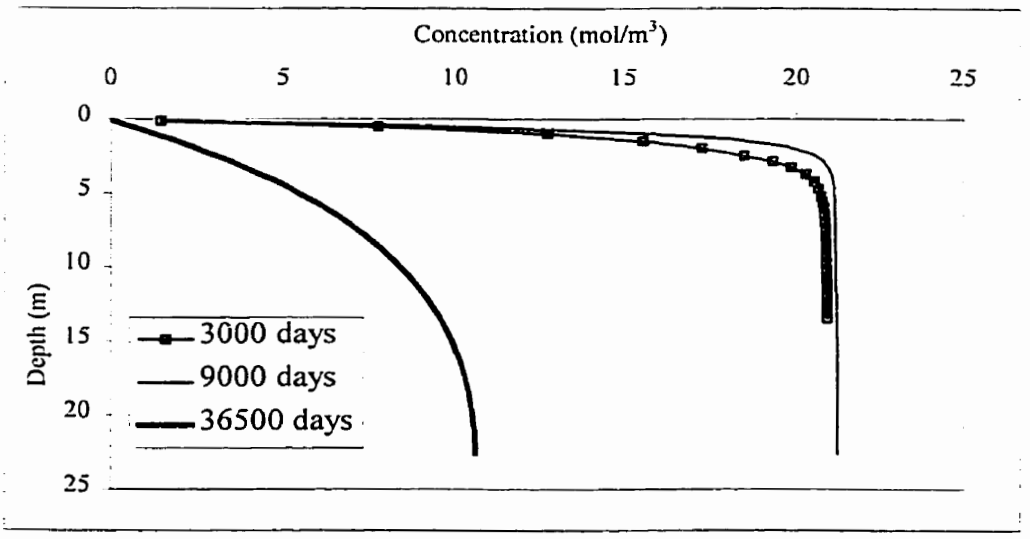

Figure 5.10: Methane profile in waste column for the base case at three different time intervals.

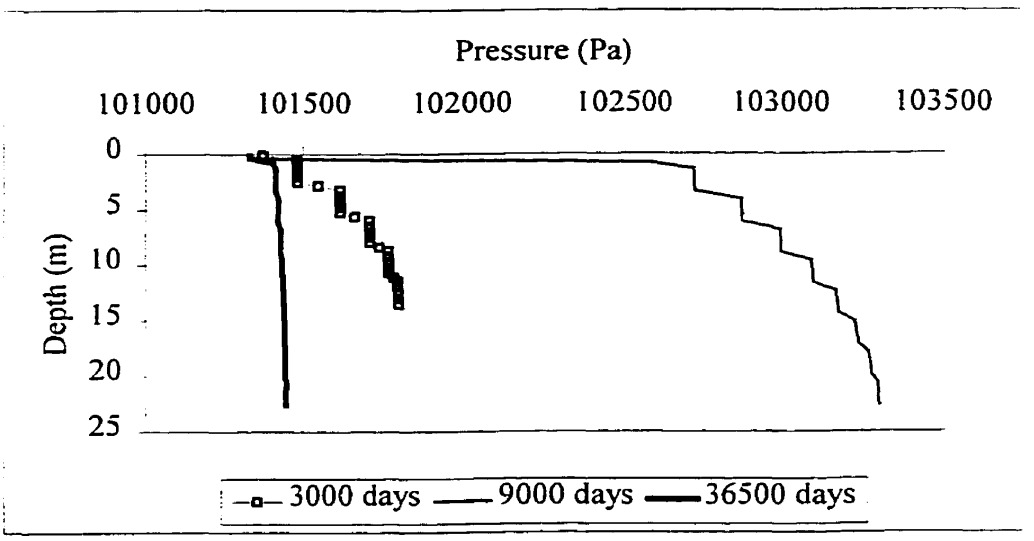

Figure 5.11: Pressure profile in waste column for the base case at three different time intervals.

Figure 5.12 shows the co-existence of O_2 and CH_4 in the bottom cell prior to the placement of the third lift. The heterogeneity of actual conditions in the cell allows anaerobic regions conducive to methogenesis to be adjacent to regions containing O_2. Including an aerobic phase in the model would have lowered O_2 concentration within the cell rather than allowing it to be displaced by the gases produced in the anaerobic phases. However, this was not done because of the very short duration of the aerobic phase and its negligible impact on gas production over the life of the landfill. El-Fadel *et al.* (1996) assumed 20% CO_2 and 80% N_2 for the initial conditions for modeling the gas concentrations in layers of waste rather than include and aerobic phase in their model.

Figure 5.12 shows the concentrations of CO_2, O_2, N_2 and CH_4 in the bottom cell of the column with time. The CH_4 and CO_2 concentrations in this cell increase with the addition of waste lifts (2^{nd} and 3^{rd}) and the gas production in the cells above as shown in the figure. The increase in CO_2 and CH_4 is a result of the increase in pressure due to the addition of the waste lifts and displacement of the N_2. Additional lifts appear to have minimal effect on the gas concentration in the cell. The gas concentration profiles within the bottom cell are very similar to the gas curves produced by Farquhar and Rovers in 1973 as shown in Figure 2.1.

The flux of CO_2 and CH_4 from the top of the column over the length of the simulation is shown in Figure 5.13 and Figure 5.14 respectively. The flux curve shows the stepping up at the additions of each lift for a total of 8 lifts. The rise and fall in the CO_2 production curve is

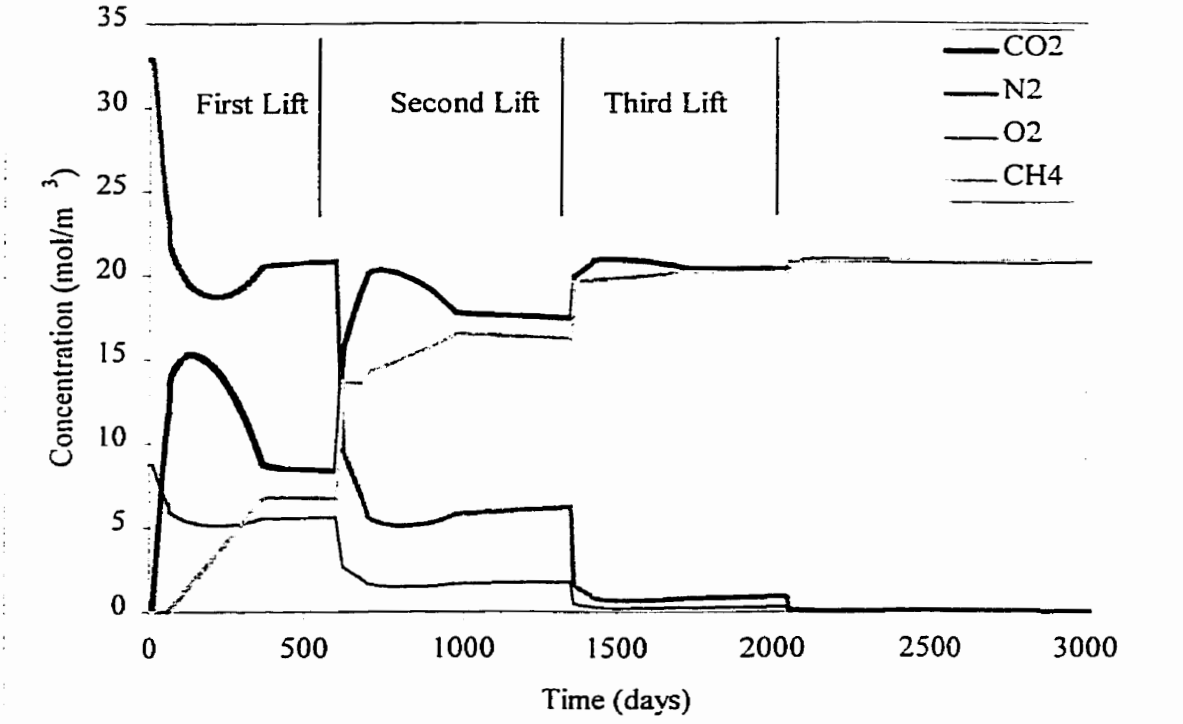

Figure 5.12: Concentration of gases in the bottom cell of the waste column versus time

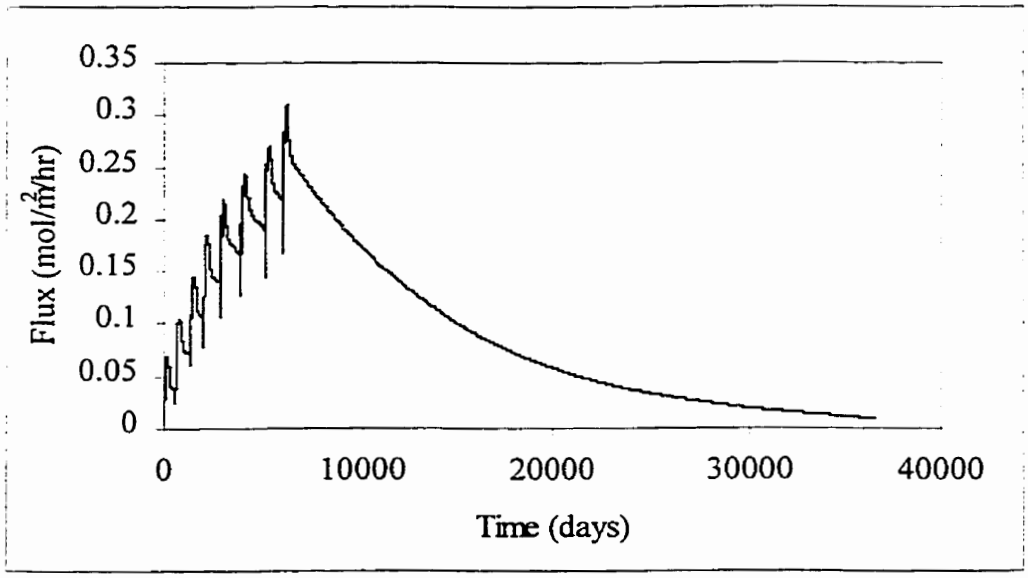

Figure 5.13: CO_2 flux from the landfill surface in the base case simulation

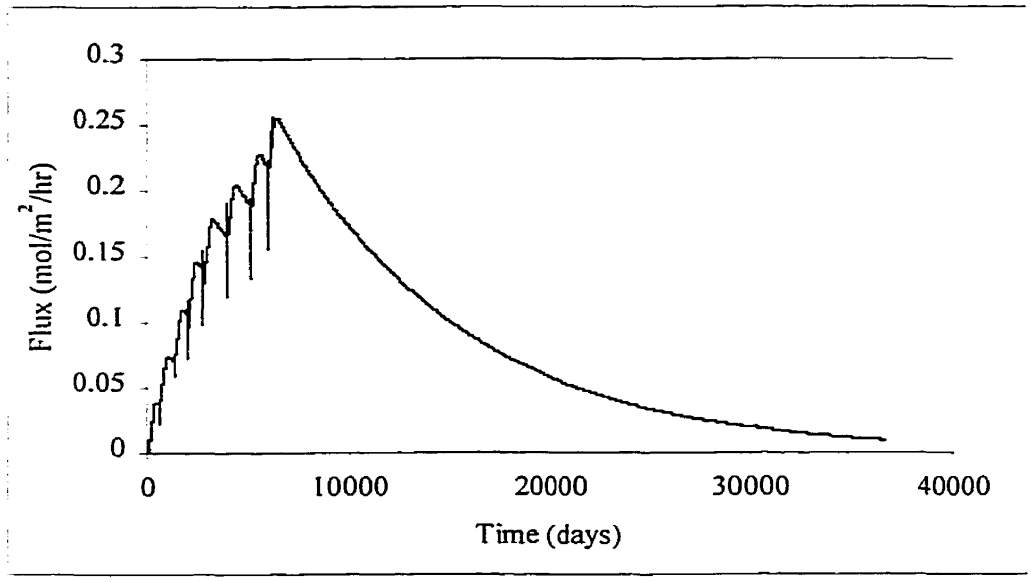

Figure 5.14: CH_4 flux from the landfill surface in the base case simulation

mirrored in the flux curve with a rise above the CH_4 flux and a dip back to the CH_4 flux for each lift as the anaerobic production takes over in the waste cells. The valleys or dips in the flux curve are a result of the addition of more waste and cover being placed on each lift. The addition of the waste and cover impedes the flux out of the surface for a short period of time thus producing a dip in the flux as observed. The peak of the CH_4 flux curve corresponds to a flux of 0.257 mol/m^2/hr (98.8 g/m^2/d).

Figure 5.15 shows the flux curves for vinyl chloride and H_2S. These curves show the same dips due to the addition of waste lifts on top of the existing lifts. The peak of the vinyl chloride curve would correspond to a flux of 1.76×10^{-5} mol/m^2/hr (31.2 mg/m^2/d). The H_2S flux curve peaked at 5.21×10^{-5} mol/m^2/hr (42.6 mg/m^2/d).

The total flux from the total landfill was determined by assuming that the landfill was made up of 2240 columns identical to the waste column modelled above. The number of columns in the landfill was determined as described previously, by dividing the landfill area of 500 m by 700 m by area of a column (12.5 m square). The total flux for each day was determined by summing the flux from all active columns for that day. This was done by assuming that each additional column added was identical to the previous column but one day behind in gas production and emissions than the previous day's column. Figures 5.16 and 5.17 show the landfill's total flux for CO_2 and CH_4 and VC and H_2S respectively. The total flux curves peaked at 527 mol/m^2/hr (8.45 kg/m^2/d) for CH_4 and 555 mol/m^2/hr (24.4 kg/m^2/d) for CO_2.

The vinyl chloride and H_2S curves peaked at 0.033 mol/m^2/hr (2.07 g/m^2/d) and 0.097 mol/m^2/hr (3.31 g/m^2/d) respectively.

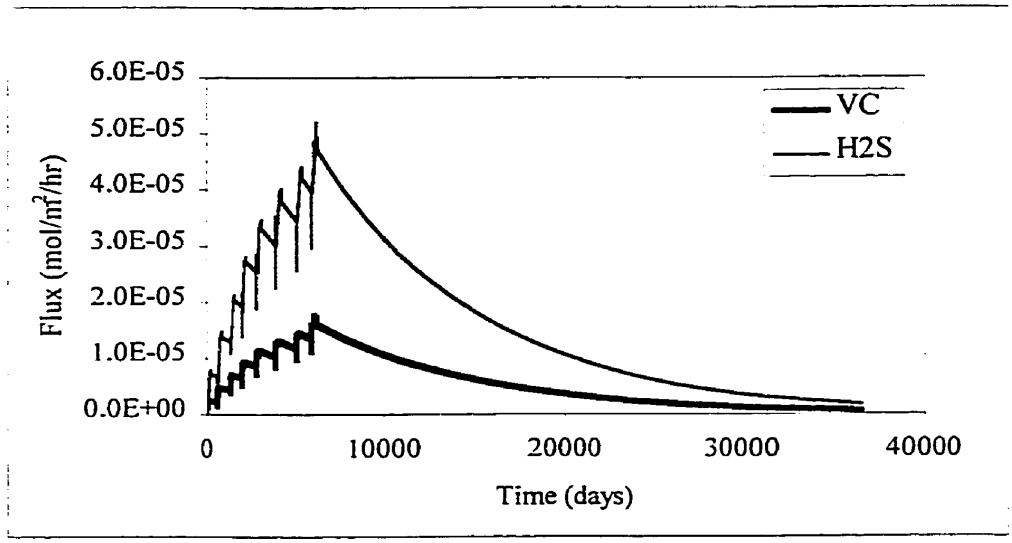

Figure 5.15: Vinyl chloride and H_2S flux from the landfill surface in the base case simulation

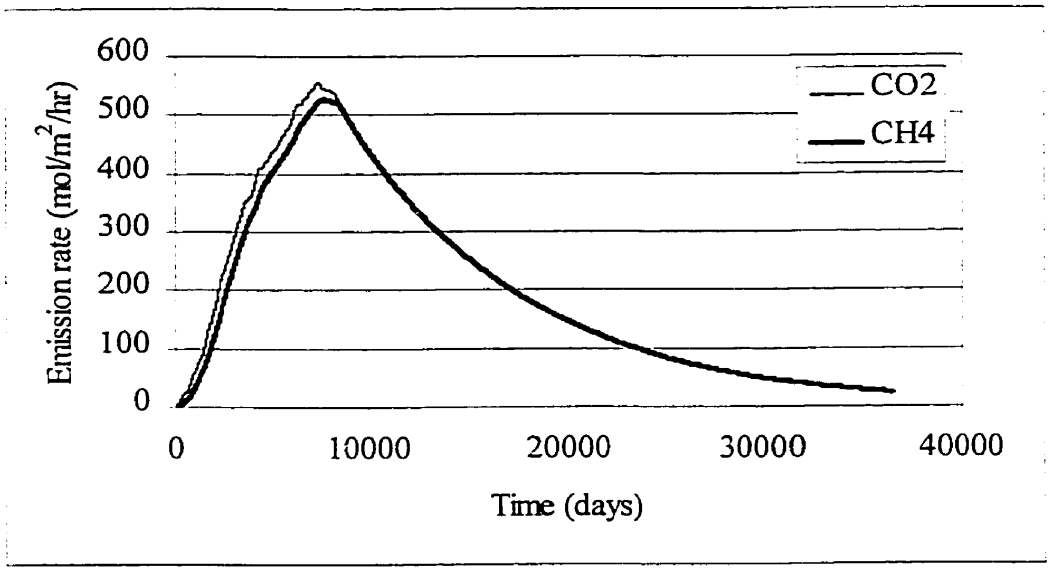

Figure 5.16: Total flux of CH_4 and CO_2 from the entire landfill over 100 years

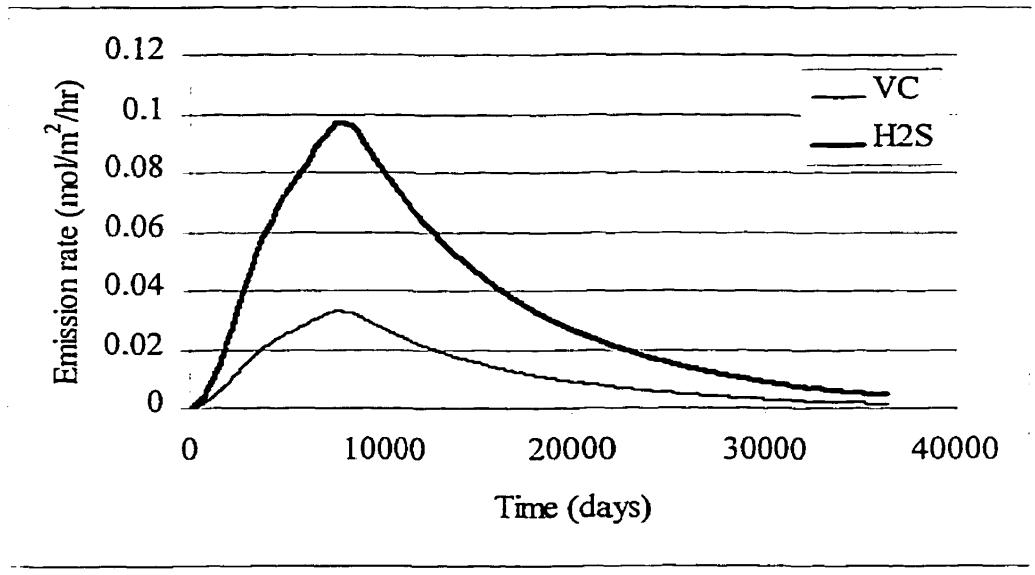

Figure 5.17: Total flux of vinyl chloride and H_2S from the entire landfill over 100 years

5.5.2 Methane Oxidation

Methane oxidation in the model started after the construction of the waste column was completed and the final cover was in place. Therefore, the model up to this point performed identically to the base case discussed above. The presence of methane oxidation in the topsoil in the cover had a dramatic result on the flux of the CH_4 and CO_2 out of the landfill surface. Figures 5.18 and 5.19 show a comparison between the flux with and without methane oxidation for CO_2 and CH_4 respectively for a single column. The oxidation of methane results in a conversion of one mole CH_4 to one mole of CO_2. This ratio was verified at 6380 days where the CO_2 fluxes were 0.263 mol/m^2/hr without oxidation and 0.389 mol/m^2/hr with oxidation indicating a gain of 0.126 mol/m^2/hr. The corresponding CH_4 fluxes were 0.254 mol/m^2/hr and 0.128 mol/m^2/hr with a loss of 0.126 mol/m^2/hr.

Figure 5.20 shows the total flux of CH_4 and CO_2 from all the columns with methane oxidation in the top soil over the 100 years simulation. Methane oxidation in the cover reduces the peak of the methane curve and increases the peak on the CO_2 curve in comparison to the curves without oxidation in the cover (Figure 5.16). Methane oxidation in the cover reduces the peak of the CH_4 curve to 465 mol/m^2/hr (7.46 kg/m^2/d) a 12% decrease from the base case curve. A 40% increase to 775 mol/m^2/hr (34.1 kg/m^2/d) in the peak of CO_2 curve was observed as a result of the methane oxidation in the cover.

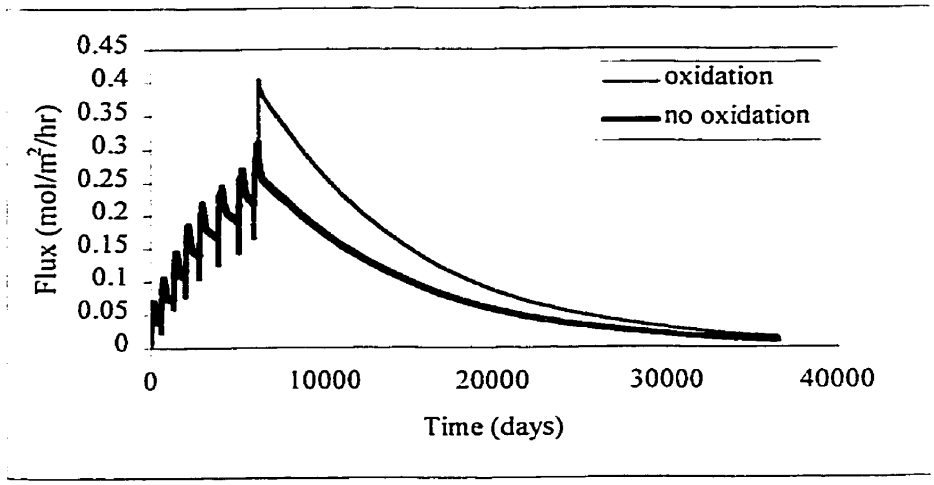

Figure 5.18: Comparison of CO_2 flux from landfill surface with and without CH_4 oxidation

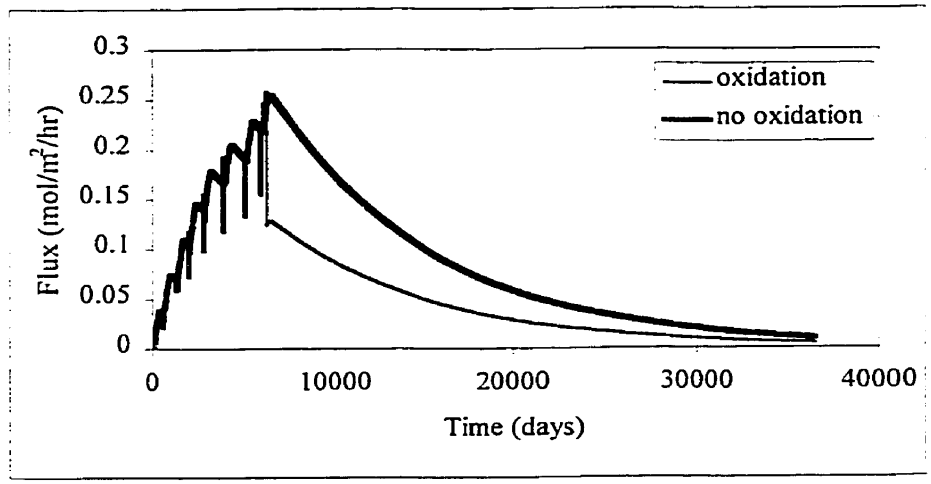

Figure 5.19: Comparison of CH_4 flux from landfill surface with and without CH_4 oxidation

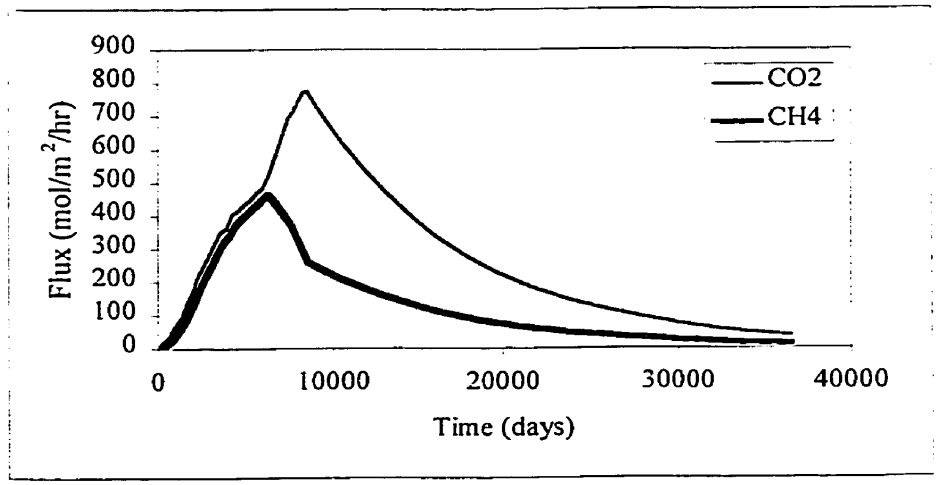

Figure 5.20: Total flux of CH_4 and CO_2 with methane oxidation in cover from the entire landfill over 100 years

5.5.3 Cover perforation

A simulation was performed to accommodate an one inch diameter hole through the clay layer of one column. The effective permeability of the clay cover was adjusted to 2 x 10^{-5} m^2 in order to simulate the presence of the hole equation as described in Section 5.4.3. Figure 5.21 shows a comparison between the pressure in the bottom cell with and without the presence of the hole in the clay layer and no clay layer in the landfill cover (grey line). The pressure in the bottom cell increases during the construction of the waste column until 6141 days. The addition of the clay layer in the landfill cover at 6147 days results in a large jump in the pressure. The pressure jump is not observed when the clay layer is absent from the landfill cover. The presence of the hole results in the pressure dropping off radically to pressures levels as if the cover was not there. Figure 5.22 compares the pressure profile of the waste column at 9000, 20000, and 36350 days with and without the hole in the clay cap. These profiles show the change in pressure throughout the waste column as a result of the hole present in the clay cap. Both cases show a decrease in the pressure profile to approximately atmosphere levels. The difference is that the waste column with the hole progresses more rapidly toward atmospheric levels than the column without the hole in the cover.

Fluxes out of this column were essentially the same as the base case.

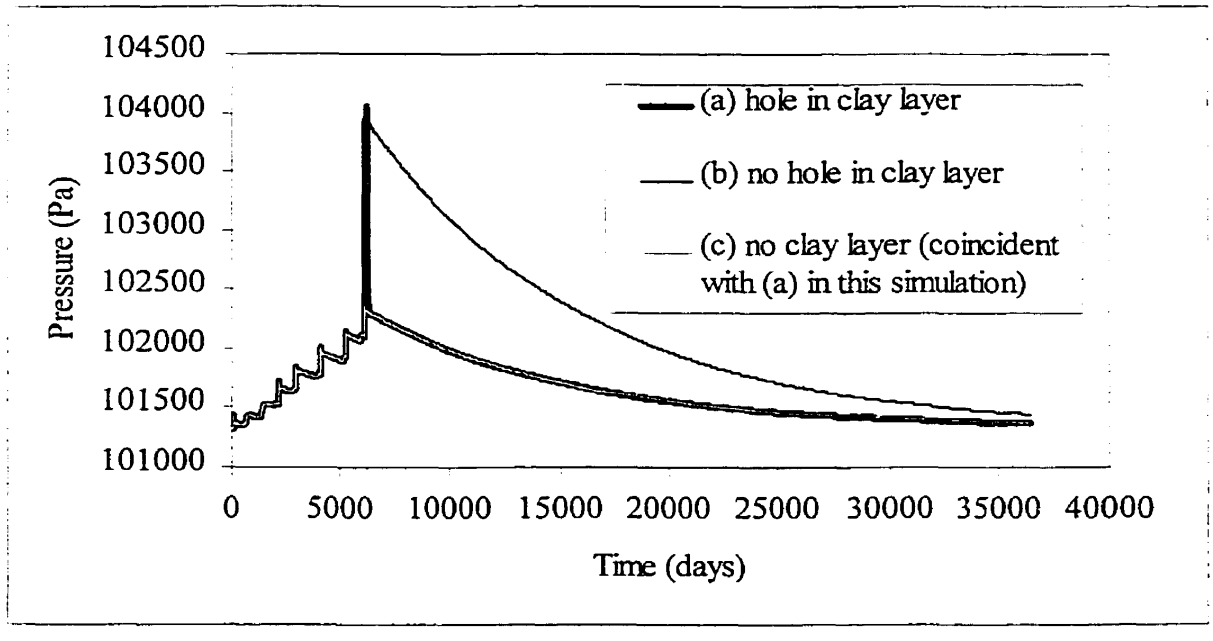

Figure 5.21: A comparison between the pressure in the bottom cell with and without a hole in the clay cap.

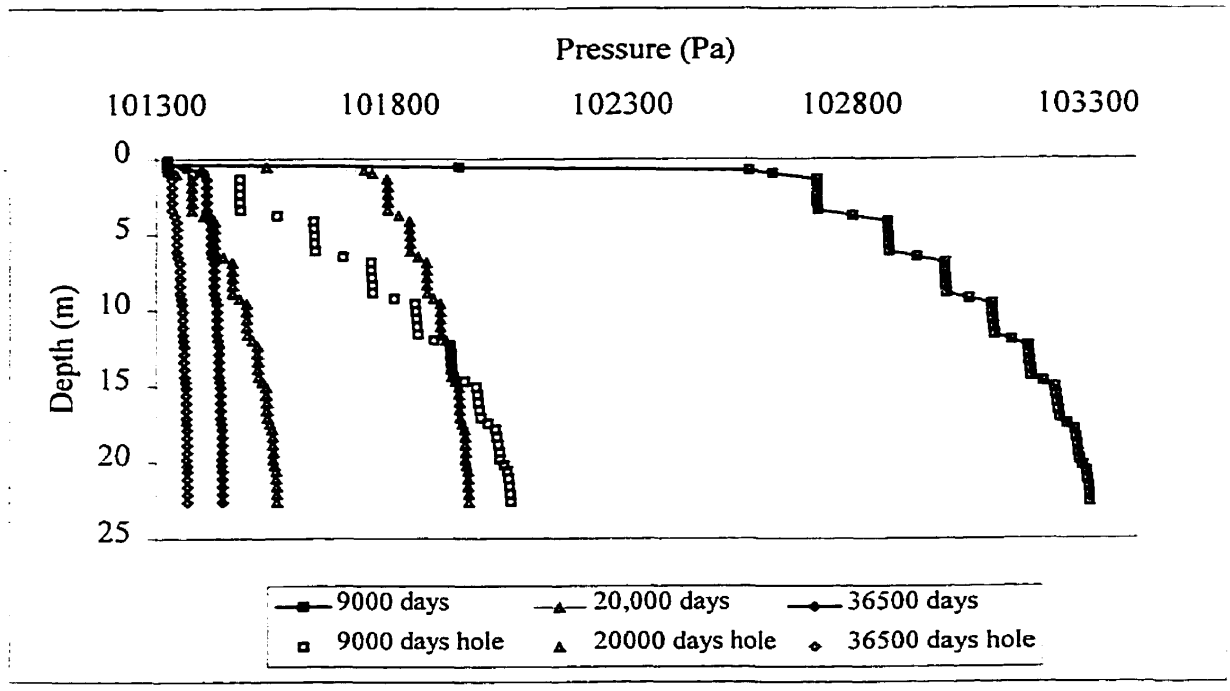

Figure 5.22: A comparison between the pressure profiles in the waste column with and without a hole in the clay cap at different time intervals.

5.5.4 Summary

Table 5.5 shows the total mass of the compounds emitted from the landfill surface over the entire 100 year simulation. The mass emitted was calculated by multiplying the flux emitted from each of the simulation by 24 hours and the surface area of the column. These masses were then summed to give the total mass emitted for the length of the simulation.

The methane oxidation in the cover was able to reduce the methane emitted from the landfill surface by 37% to 2.7 x 10^5 tonnes from 4.3 x 10^5 tonnes.

Over the 100 years, the simulated landfill will emit 105 and 167 tonnes of vinyl chloride and H_2S respectively. Although the recommended MOE equation for vinyl chloride emission was used in this analysis, it seems unlikely that 105 tonnes of vinyl chloride or its' precursors would be present in a landfill.

As expected, the presence of the hole resulted in little change in the total mass of gases emitted of any of the components from the base case but significantly reduced the pressure within a column. In a field situation with several columns, the pressure reduction would be lessened through interflow between adjacent columns.

Table 5.5: Mass of compounds emitted from landfill surface under various conditions

Compound	Mass Emitted (tonnes)		
	No oxidation & no hole	Methane oxidation & no hole	No oxidation & hole
CO_2	1.2×10^6	1.6×10^6	1.2×10^6
CH_4	4.3×10^5	2.7×10^5	4.3×10^5
Vinyl chloride	105	105	105
H_2S	167	167	167

5.6 Model for Atmospheric Transport of LFG Emissions

The emitted landfill gas components will diffuse into the atmosphere and the wind and atmospheric turbulence will transport and dilute these components to impact the surrounding regions. Atmospheric turbulence consists of eddies that mix the pollutants with the surrounding air (Schnelle & Dey, 2000). Wind speed and the characteristics of the atmospheric turbulence are used to classify the stability of the atmosphere into six classes (A to F). The classes range from unstable (A) to stable (F) with D signifying neutral atmospheric conditions. The downwind plume for each stability class varies in the spread in both y and z directions from the plume's centreline. These differences are reflected in the standard deviations obtained from the curves shown in Figures H.1 and H.2 in Appendix H. The standard deviations, wind velocity and emitting source concentration are used to determine the downwind concentrations. The downwind concentrations of the LFG compounds can be simulated using the Gaussian Plume model.

5.6.1 Gaussian Plume Model and Sensitivity Analysis

Gaussian Plume Model

Atmospheric dispersion of the LFG components was modelled using the modified Gaussian Plume Model for an elevated source :

$$C(x,y,z,H) = \frac{Q}{2\pi u \sigma_y \sigma_z} \exp\left[-\frac{1}{2}\left(\frac{y^2}{\sigma_y^2}\right)\right]\left\{\exp\left[-\frac{1}{2}\left(\frac{(z-H)^2}{\sigma_z^2}\right)\right] + \exp\left[-\frac{1}{2}\left(\frac{(z+H)^2}{\sigma_z^2}\right)\right]\right\} \quad (5.25)$$

where:

C = concentration (g/m^3)

Q = emission rate (g/s)

u = mean velocity of wind (m/s)

σ_y = standard deviations of plume concentration in the horizontal direction (m)

σ_z = standard deviations of plume concentration in the vertical direction (m)

y = distance centre line (m)

z = distance above centre line (m)

H = vertical mixing height of plume (m).

This equation assumes that the origin is at ground level but that the source is at a height (H) above the origin. The x-axis extends horizontally in the mean wind direction. The y-axis and z-axis are perpendicular to the x-axis horizontally and vertically. The standard deviations of the plume concentration in the horizontal and vertical directions are functions of the distance downwind (x) and the stability of the atmosphere. The H in the equation accounts for the elevation and rise of the gases from the point source. In the case of emission from a stack, the H would be the sum of the height of the stack plus any buoyancy effects due to temperature and density differences. Further discussion on the use of this equation and dispersion of compounds is available in Chapter 2 section 2.2.4 or Wark & Warner (1981). Atmospheric conditions including wind speed and solar radiation and/or cloud cover are used to determine a stability category as outlined in Wark & Warner (1981). Table 5.6 shows the ranges of wind speeds as well as solar radiation and/or cloud cover that contribute to the determination of the stability of the atmosphere.

Table 5.6: Key to Stability Categories (Wark & Warner, 1981)

	Day			Night	
	Incoming Solar Radiation			Cloud Cover	
Surface Wind Speed at 10 m (m/s)	Strong	Moderate	Slight	Mostly Overcast	Mostly Clear
Class [a]	(1)	(2)	(3)	(4)	(5)
<2	A	A-B	B	E	F
2-3	A-B	B	C	E	F
3-5	B	B-C	C	D	E
5-6	C	C-D	D	D	D
>6	C	D	D	D	D

[a] The neutral class, D, should be assumed for overcast conditions during the day or night. Class A is the most unstable and class F is the most stable, with class B moderately unstable and class E slightly stable.

Sensitivity Analysis

A sensitivity analysis of the Gaussian Plume model was performed to illustrate the effects that changes in stability class, wind speed, and downwind distance (x) have on the atmospheric concentration. An emitting source, 2.5 m (H) above ground level, with a continuous emitting concentration of 1.02×10^{-6} g/s was used to generate the following simulations. Ground level concentrations were used; therefore z was set to zero in the Gaussian Plume Model. Increasing the wind speed from 1 m/s to 2 m/s, a 100% increase, under the same stability condition (A) and 1000 m (x) from the source reduced the centreline concentration by 50% as shown in Figure 5.23. This is consistent with equation 5.25. The change in the concentration distribution curve with distance from the source at a wind speed of 2 m/s and unstable conditions (A) is shown in Figure 5.24. Increasing the distance between the source and receptor reduces the centreline concentration and flattens the distribution curve. Changing the stability class will also change the shape of the distribution curve and centreline concentration. Figure 5.25 shows the change in the distribution curve due to changes in stability classes at 1000 m downwind and a wind speed of 2 m/s.

As stated previously, the stability classification of the atmosphere is determined based on wind speed and atmospheric turbulence. Several methods (USEPA, 1987) employing these two parameters have been developed. Strong turbulence enhances vertical motion that disperses the pollutants more rapidly and is characteristic of an unstable atmosphere. As a result, the

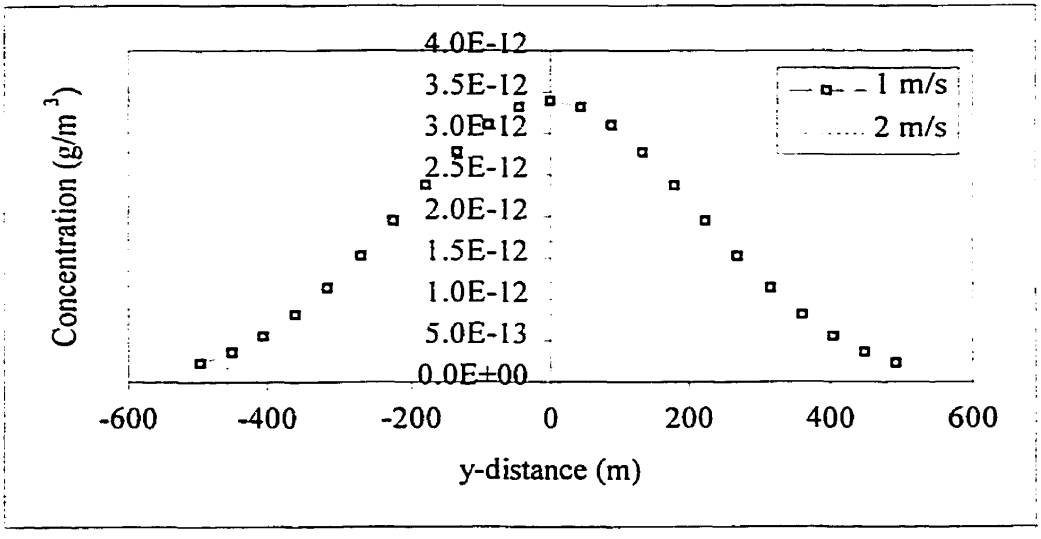

Figure 5.23: Comparison of concentration distribution at two different mean wind speed under unstable conditions 1000 m from source.

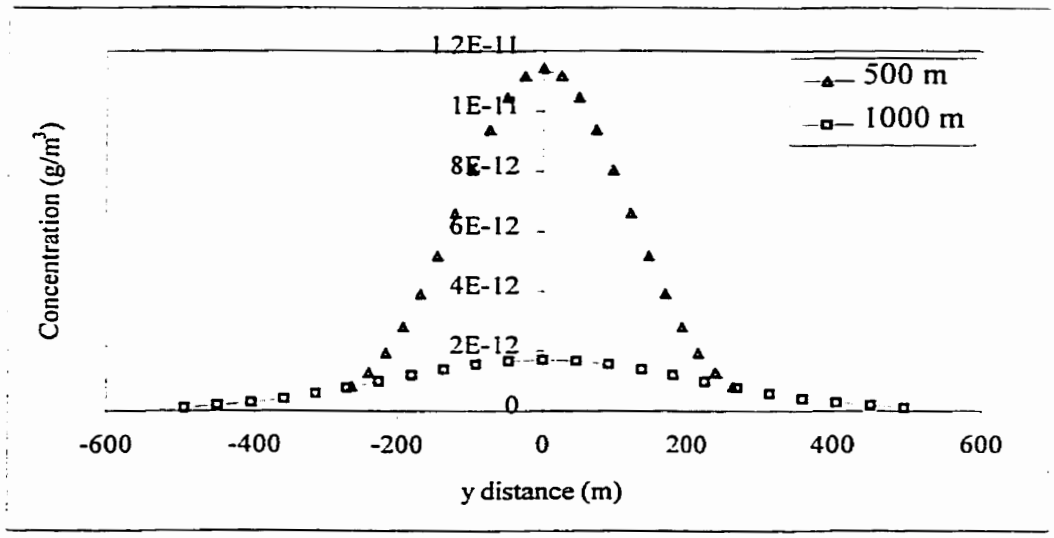

Figure 5.24: Concentration distribution at 500 m and 1000 m from source with a wind velocity of 2 m/s and unstable conditions

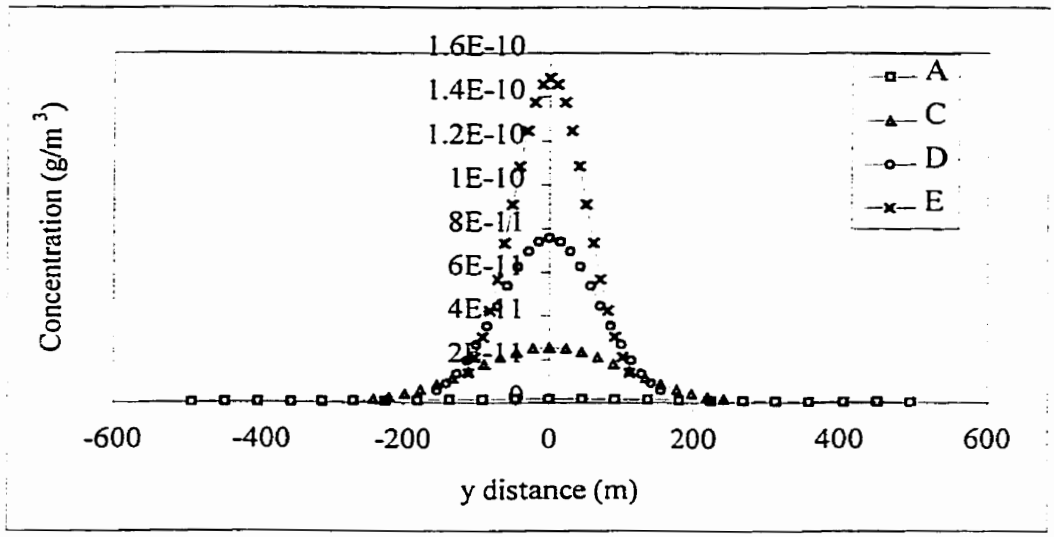

Figure 5.25: Comparison of concentration distribution at four different mean stability classes using the wind speed of 2 m/s and downwind distance of 1000 m.

concentration distribution within the pollutant plume will be much flatter and wider under unstable conditions (stability class A) relative to more neutral and stable conditions (stability class D to F) where the turbulence is weaker (Figure 5.25). The standard deviations, σ, in the y and z directions, are used to reflect the difference in turbulence between the unstable and stable atmospheric conditions. The spread of the contaminant plume away from the centreline along the downwind x-axis is simulated by the σ values in the y and z directions obtained from the graphs in Appendix I. Turbulent conditions (unstable) result in a greater dispersion of the

contaminant plume and therefore larger σ_y and σ_z downwind whereas stable conditions have smaller σ_y and σ_z and therefore narrower and more concentrated contaminated plumes downwind of the source.

Emissions from an area source can be modelled using the virtual point source method or by integrating across the area source. The virtual point source method allows the use of the Gaussian Plume model whereas integrating across the area source would involve a more complex equation. The virtual point source method involves treating an area source as having an initial horizontal standard deviation σ_{yo} (contaminant plume width) with the σ_{yo} equal to 4.3 times the side of the area (assuming the area is square) (Turner, 1994). This initial standard deviation is used to determine a virtual distance, x_y for a given stability by back calculation from the stability curve equation (shown in Figure I.1 in Appendix I). The virtual distance assumes that the point source is x_y distance upwind of the true area source. The stability curve equations for point sources may be used to determine the σ_y as a function of the downwind distance and the virtual distance $(x + x_y)$. Further detail on this method is available in Turner (1994). A comparison between the virtual point source method and point source method was done to evaluate the error in assuming the point source at the centre of each emitting area. The comparison was done using a column with a point source at the centre and a column with a virtual point source upwind of the column. Figure 5.26 shows a comparison between the virtual point source and point source methods at two different downwind distances and the same velocity and stability class. The comparison between the concentration distribution using the point source and virtual point source methods under the same stability class and velocity indicate that the difference between the two methods is small and decreases as the distance from the source increases. Closer to the source the centreline concentration is higher with the point source than the virtual point source as might be expected. Given the distances (500 m and 1000 m) used in the emission modeling in this research, the use of the point source method to simulate the area emissions from the waste columns was considered to be acceptable.

The terrain around an emitting source and surrounding area will affect the dispersion of the emitted compounds. Construction of the landfill places a hill in the path of the dispersing winds. On the downwind side, the presence of the hill will increase the travel distance of the transporting air to the receptor assuming that the wind follows the lay of the land. Assuming

that the landfill has a 3:1 slope on the side and is 20 m high, the landfill will increase the distance to a receptor 100 m away by 3 m or 3%. The 3% increase in distance will reduce the concentration by 4.5% at a receptor 100 m away. The presence of the hill is therefore considered to have minimal affect on the concentration downwind; the effect will lessen the further the receptors are from the landfill. The presence of the hill formed due to the landfill construction was neglected in the simulations.

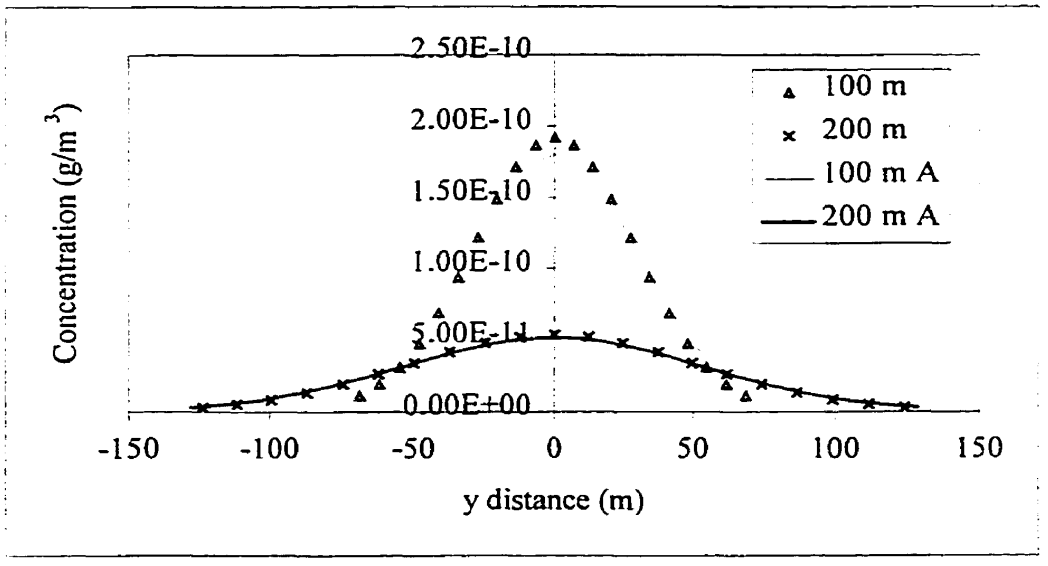

Figure 5.26: Comparison between point source and virtual point source methods for area source at two different downwind distances (A in legend indicates the virtual point method)

5.6.2 Atmospheric Dispersion of Landfill Gas Emissions

Atmospheric dispersion of LFG components emitted from the landfill surface to a receptor downwind was modelled using the Gaussian Plume Model. In order to estimate the effects of dispersion, a grid of sources and receptors was required as well as weather data to determine the downwind concentration of the LFG emissions.

Source & Receptor Grids

The grid of the source consisted of the x-y coordinates of all sources on the landfill. The emitting sources at the landfill were taken to be the centre of the surface area of each of the waste columns, that is the centre of the 12.5 m x 12.5 m waste column.

The receptors were selected to be 100 m, 200 m, 500 m and 1000 m from the edge of the landfill. These distances were selected based on the of MOE (1994b) document on land use on

or near landfills. The document indicates that the landfill boundary must be at least 30 m from the edge of the landfill with the majority of landfills having a boundary that is 60 to 100 m from the edge of the landfill (MOE, 1994b).

The grid systems for the receptors and sources were setup with the X axis positive to the east of the user-specific origin and the Y axis positive to the north as indicated by Schnelle and Dey (2000). The receptors were spread along the boundary lines at a 100 m spacing. Figure 5.27 is schematic of the landfill layout with the 1 km boundary line used to illustrate the dispersion of the LFG flux from the waste column.

Gaussian Plume Model Parameters

The flux values generated from the production and emission model discussed in the previous sections were used as the input concentration Q, to the Gaussian Plume Model. The height of the waste column during and after construction was used as H (height of plume rise) in the Gaussian Plume Model. Temperature and density difference of the emitting gases were ignored in these simulations. The density of gases was assumed to be the same as the atmospheric gases. Any temperature and density differences that would affect the rise of the gases could easily be incorporated into the value of H.

The dispersion model was used to generate a simulation of the ground level hourly concentrations of vinyl chloride and H_2S at receptors downwind of the landfill. The concentration at each receptor location was a summation of the dispersed flux from each of the emitting column sources. At the beginning of simulation the landfill was under construction; therefore the number of emitting sources and height of these sources was changing until the landfill closure. The height of the emitting sources increased due to the addition of waste or cover material. The model was run for a 100 year simulation that corresponds to the simulation length used in the flux emission simulations.

Figure 5.28 shows the steps used in the model to determine the concentration at the receptors due to the different sources.

Weather Data

Weather data obtained from the weather station at the Waterloo Landfill were used to construct a wind rose and atmospheric stability classes. The stability classes were determined using the

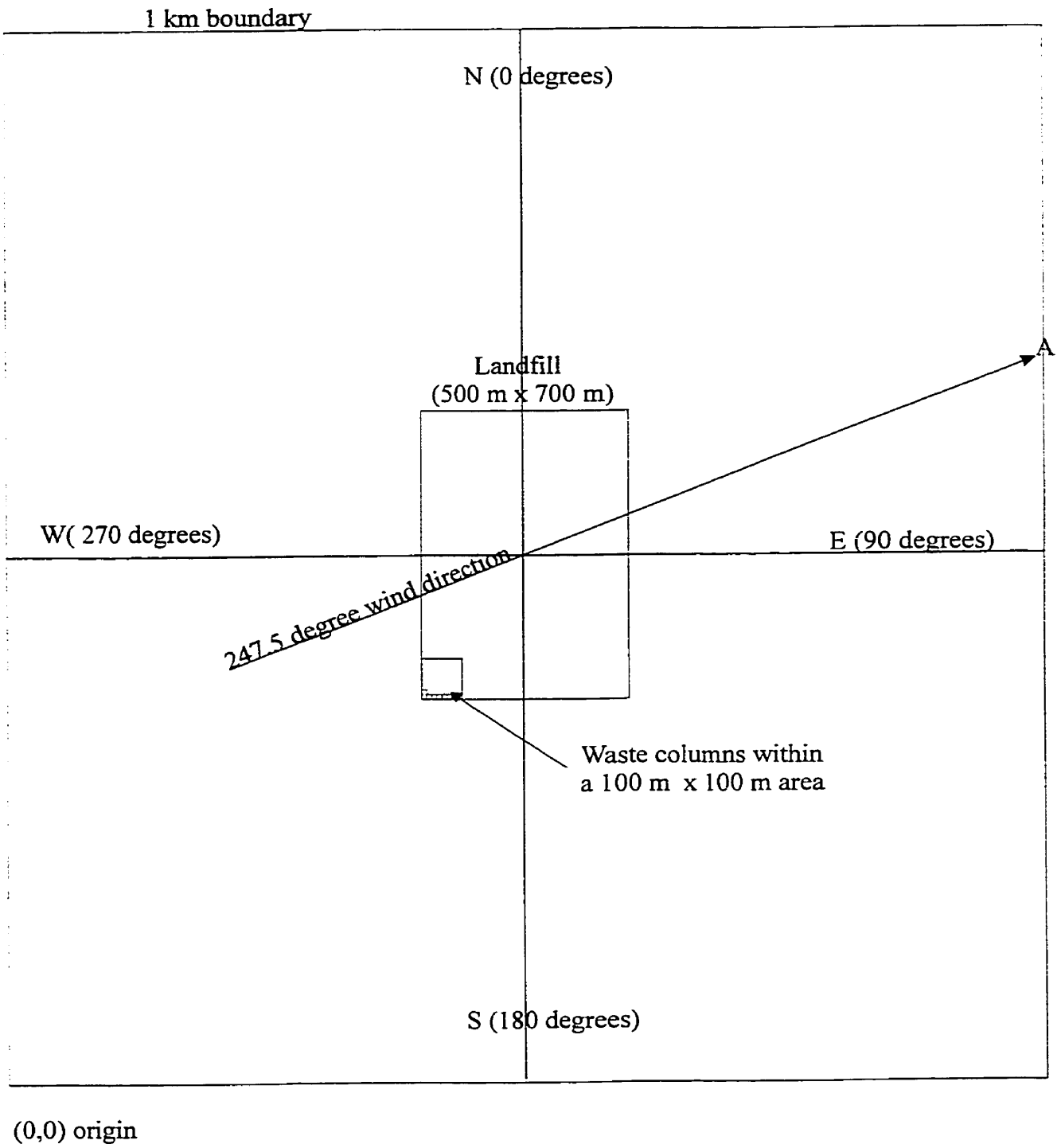

Figure 5.27: Schematic of landfill and 1 km boundary line used in dispersion modelling

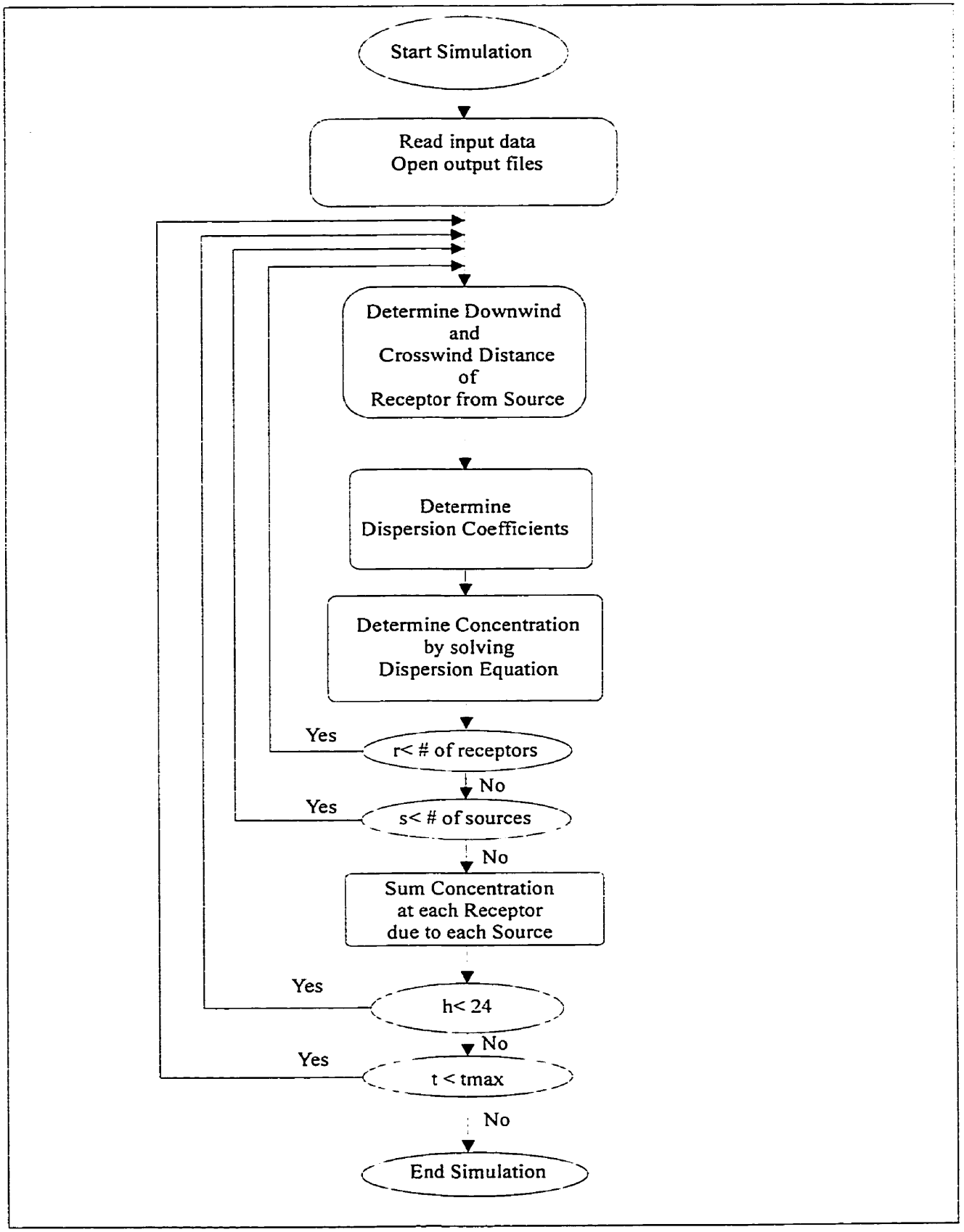

Figure 5.28: Flowchart of Atmospheric Transport Model

horizontal wind velocity and its standard deviation following the procedure indicated by USEPA (1987). Appendix I contains the wind rose and frequency distribution for the wind velocities and stability classes.

The wind rose data indicated that the most frequent wind directions were in the sectors between south and west with most common wind from WSW (247.5 degrees from N). These wind directions are consistent with this area of Southern Ontario. Neutral atmospheric wind conditions (D) with an average velocity of the 4 m/s were most frequently observed atmospheric conditions from 1995-1997.

Simulations

Hourly concentrations of the vinyl chloride and H_2S were generated under different stability conditions and wind velocities to generate a range of possible concentrations that may be observed on any given day over the 100 years of the simulation at the 1 km boundary line. Three wind conditions were selected. Based on the wind rose data, the neutral stability class (D) with a 4 m/s wind speed was the most frequently observed wind condition; therefore it was selected to give the most likely observed concentration along the boundary line. A & F stability conditions with a wind speed of 2 m/s provide the best and worst case concentrations along the boundary line. Each of these three wind conditions was simulated using five wind directions. The other four wind directions selected were N, E, S, and W. Given that the long axis of the landfill was in the N-S direction, the highest concentration would likely be directly downwind of the landfill rather than at an angle to the landfill. These five wind directions with the three wind conditions were used to generate hourly concentrations for vinyl chloride and H_2S at one receptor along the 1 km boundary line in the downwind direction. The flux values for the vinyl chloride and H_2S from the base column case in the previous section were used as the input concentrations for these simulations. The atmospheric concentrations at the 1 km boundary line were predicted for 100 years for all simulations.

Simulations of the hourly concentrations along the 100 m, 200 m, 500 m and 1000 m boundary line were also done. The most frequent wind direction (WSW), wind speed (4 m/s) and stability class (D) observed at the Waterloo Landfill were used to generate these simulations. Each of these simulations was also performed for 100 years. The receptors on the boundary

lines for these simulations were at the intersection between the boundary lines and a line through the centre of the landfill in the downwind direction.

The last simulation consisted of all the six stability classes (A to F) with a wind speed of 2 m/s and a wind direction of 0 degrees at several downwind distances up to 4 km away from the edge of the landfill. This simulation was done to evaluate where the maximum concentration for each stability class would occur. The crosswind concentrations under different stability classes along the 1 km boundary were also evaluated during this simulation in order to evaluate the impact of the contaminant plume along this boundary line.

The provincial standard and criteria used to evaluate the concentration of the vinyl chloride and H_2S at the boundary lines or receptors are shown in Table 5.7.

Table 5.7: Provincial standard and criteria for vinyl chloride and H_2S

Standard/Criterion	Vinyl Chloride ($\mu g/m^3$)	H_2S ($\mu g/m^3$)
½ hour point of impingement (POI) standard	3.0	30
1 hour ambient air quality criterion	-	30
24 hour ambient air quality criterion (AAQC)	1.0	-
Annual ambient air quality criterion	0.2	-

5.7 Results of Atmospheric Dispersion of LFG Emissions

Figure 5.29 and 5.30 show the range of maximum hourly concentrations of vinyl chloride and H_2S over the 100 year simulation using a wind direction of 247.5 degrees, wind velocities of 2m/s (A & F) and 4 m/s (D) and 3 stability classes, A, D & F. The examples show the concentrations at one receptor on the 1 km boundary shown as "A" on Figure 5.28. The best and worst case concentrations along the boundary lines were simulated by the stability classes of A and F respectively. The highly turbulent wind conditions of the stability class A (unstable) result in the mixing and rapid diffusion of the emissions and therefore provide a very flat distribution of the downwind concentration over the 100 year simulation. A very narrow distribution with a high centre line concentration is obtained under very stable (F) or low turbulence wind conditions. Therefore, the worst case concentration had a larger range of concentration values than either of two other cases. Appendix J contains additional examples

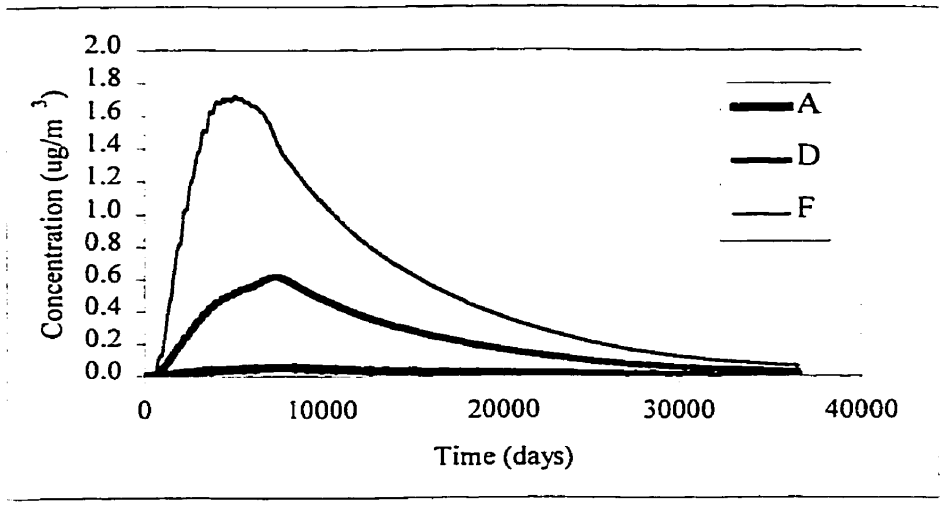

Figure 5.29: Hourly vinyl chloride concentration from 3 different stability classes and wind direction of 247.5 degrees at receptor A.

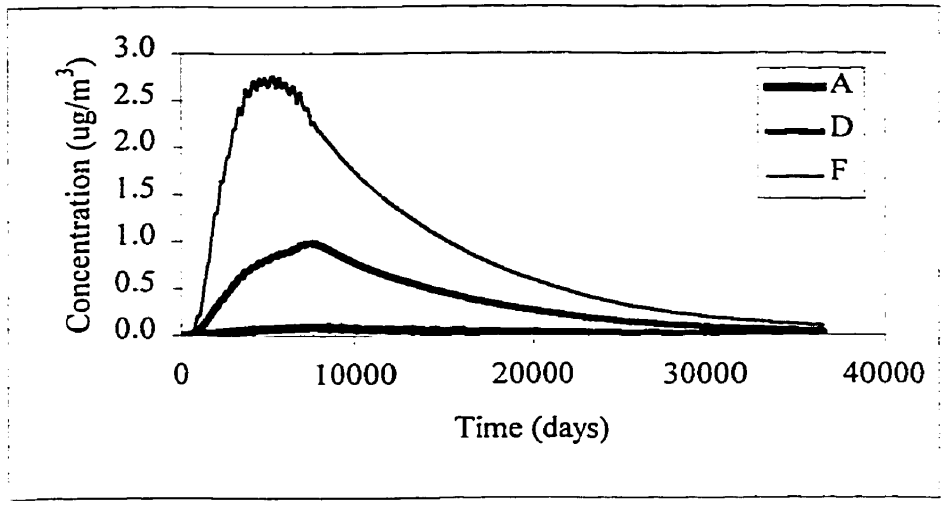

Figure 5.30: Hourly H_2S concentration from 3 different stability classes and wind direction of 247.5 degrees at receptor A.

in other wind directions (N, E, S and W). Table 5.8 contains the 1 hour and 24 hour peak concentrations observed during the 100 year simulation for these three different stability classes. Appendix E contains the equation used to calculate the 24 hour concentrations from the 1 hour peak concentrations.

A 180 degree wind direction (S) resulted in the highest hourly peak concentration for both the vinyl chloride and H_2S. Landfill construction of the simulated landfill started in the SW corner and moved across the south boundary then progressed northerly. This peak concentration along the North 1 km boundary is due to the landfill being filled from the South to the North;

therefore the most recently added waste was closest to the northern 1 km boundary limit. Under these wind conditions, the hourly vinyl chloride concentration will not exceed the ½ hour point of impingement (POI) standard of 3 $\mu g/m^3$ during the simulations shown in Figure 5.29. However the 24 hour AAQC of 1$\mu g/m^3$ would be exceeded under the stable condition (F) for 3 of the wind directions. In the case of H_2S, (Figure 5.30) none of the wind conditions would cause the concentration to exceed the MOE criteria and standard of 30 $\mu g/m^3$.

Table 5.8: Peak concentration observed in hourly concentrations over 100 year simulation under different stability classes on the 1 km boundary line (24 hour concentration)

Wind	Vinyl Chloride ($\mu g/m^3$)			H_2S ($\mu g/m^3$)		
Direction	A	D	F	A	D	F
0	0.06 (0.01)	0.78 (0.41)	2.16 (1.27)	0.10 (0.02)	1.24 (0.66)	3.43 (2.02)
90	0.07 (0.01)	0.6 (0.32)	1.63 (0.96)	0.10 (0.02)	0.96 (0.51)	2.61 (1.54)
180	0.06 (0.01)	0.78 (0.42)	2.22 (1.31)	0.10 (0.02)	1.25 (0.66)	3.53 (2.07)
247.5	0.06 (0.01)	0.62 (0.33)	1.72 (1.01)	0.09 (0.02)	0.99 (0.52)	2.76 (1.62)
270	0.07 (0.01)	0.6 (0.32)	1.63 (0.96)	0.10 (0.02)	0.96 (0.51)	2.62 (1.54)

The concentrations of the dispersed fluxes were examined at 4 boundary limits (100 m, 200 m, 500 m and 1000 m). The receptor points on these boundary limits were at the intersection of the boundary lines and the 247.5 degree line shown in Figure 5.27. A neutral stability (D) atmospheric condition with a wind velocity of 4 m/s was used for this simulation as these were the most frequent conditions observed around the landfill. Figures 5.31 and 5.32 present concentrations at the four (100 m, 200 m, 500 m and 1000 m) boundary limits over the 100 year simulation for vinyl chloride and H_2S respectively. As expected higher concentration of vinyl chloride and H_2S were observed at 100 m and 200 m from the edge of the landfill than at 500 m and 1000 m. The differences in peak width and peak time were a result of the dispersion coefficients. The σ_y and σ_z are a function of the downwind distance and increase in value as the downwind distance increases. As a result, the number of emitting sources impacting a receptor further downwind increases due to the wider σ_y (therefore increasing the width of the curve near the peak), although the concentration will be lower. The number of sources impacting a receptor along the 100 m boundary is fewer but the concentration is higher

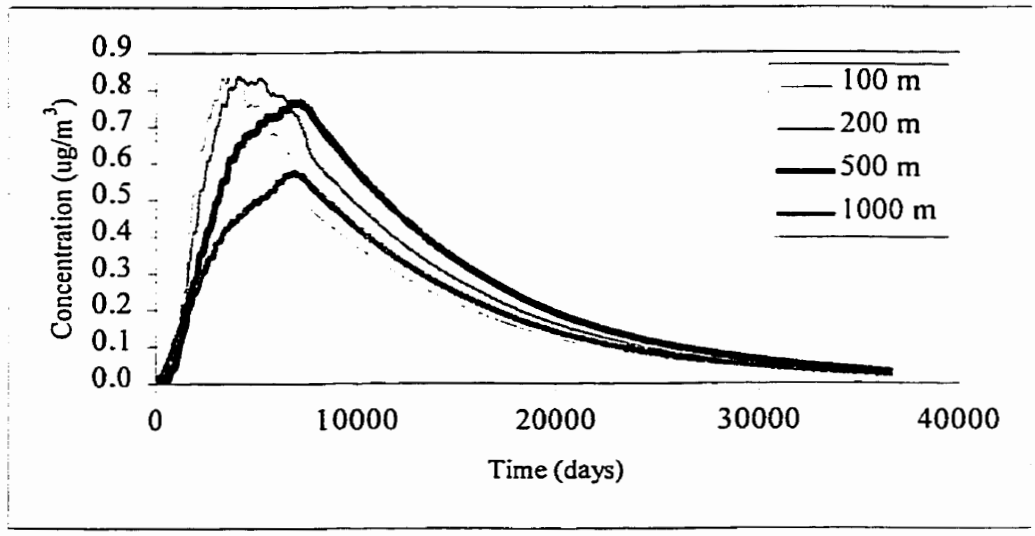

Figure 5.31: Hourly vinyl chloride concentrations at receptor A under neutral stability conditions at wind velocity of 4 m/s and a wind direction of 247.5 degrees.

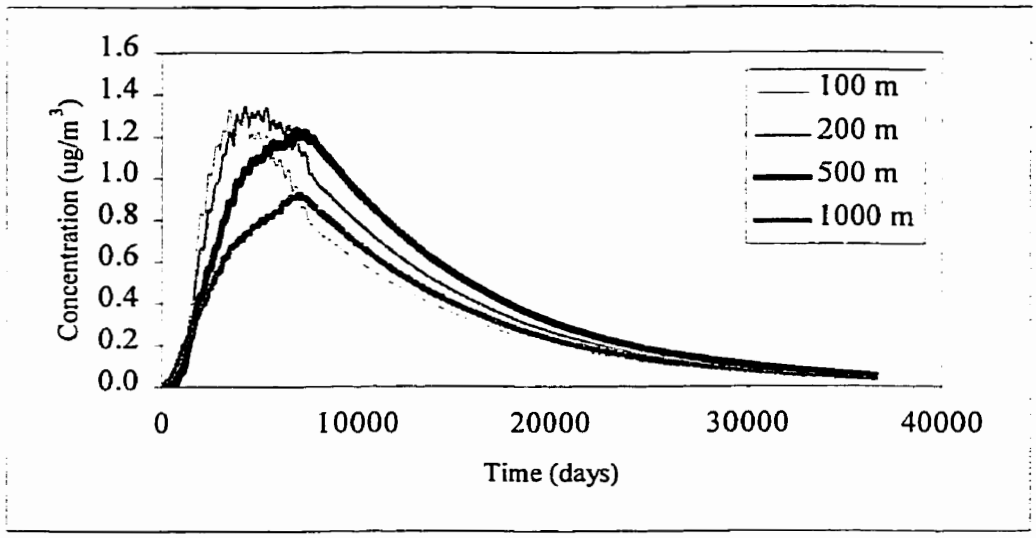

Figure 5.32: Hourly H_2S concentrations at receptor A under neutral stability conditions at wind velocity of 4 m/s and a wind direction of 247.5 degrees.

resulting in a narrower and higher peak. The peak time and concentration would correspond to the peak emission and time from the waste columns. None of the curves exceeded the ½ hour POI and 24 hour AAQC values for either the vinyl chloride or H_2S.

Figures 5.33(a) and 5.34(a) illustrate the down wind concentrations from the edge of the landfill to 4 km from the landfill and Figures 5.33(b) and 5.34(b) show the distribution of the concentration along the southern 1 km boundary line for vinyl chloride and H_2S respectively at 7700 days. The maximum concentrations occurred at approximately 7700 days in Figures 5.31

and 5.32. A wind speed of 2 m/s with a northerly wind direction (0 degrees) was used to generate the simulation. The down wind simulations were generated at receptors that were along a longitudinal axis through the centre of the landfill. In all the stability classes except for F, the peak concentration was observed prior to the 1 km boundary limit. Under stable

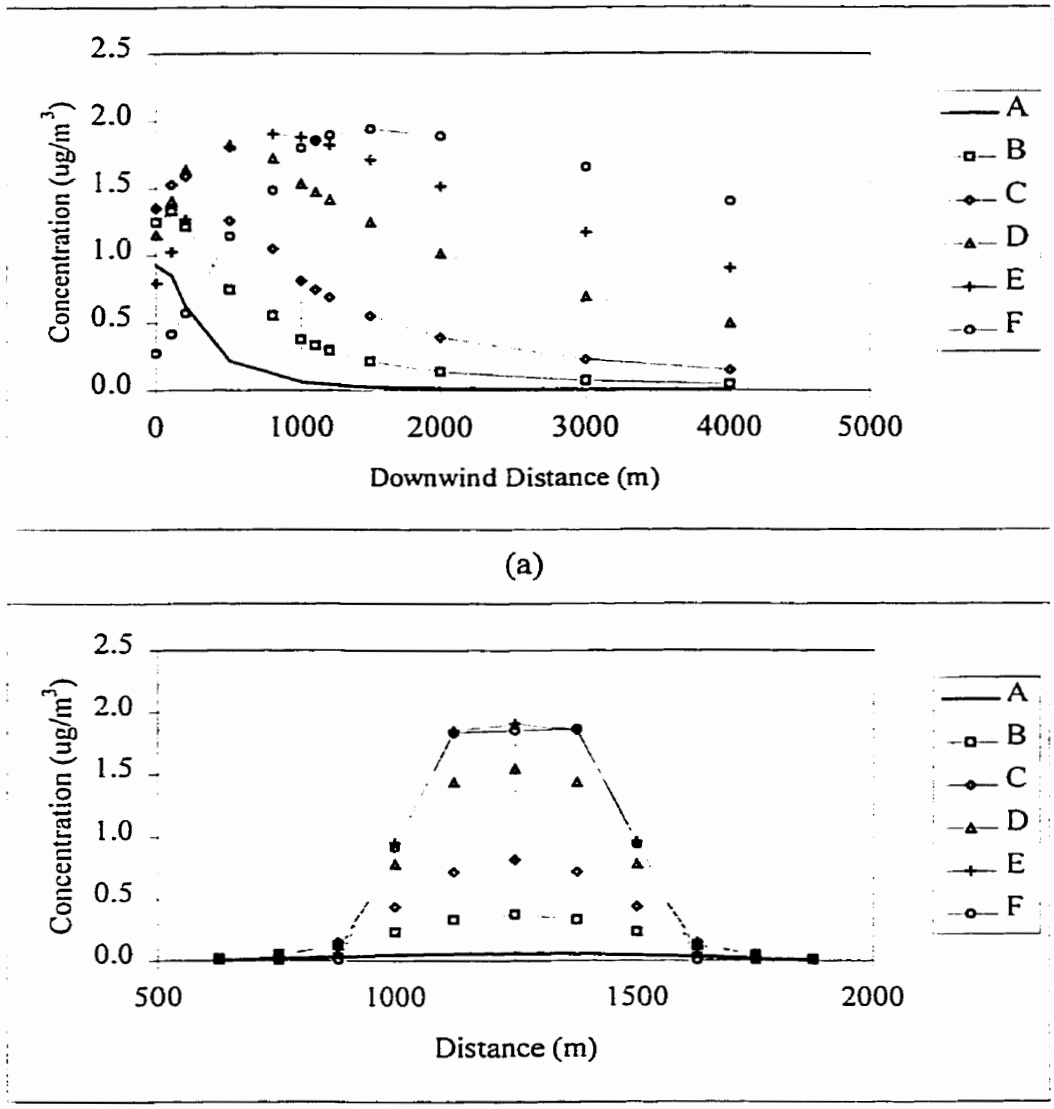

Figure 5.33: Hourly vinyl chloride concentration for all the stability classes and velocity of 2 m/s for a wind direction of 0 degrees at 7700 days. (a) centre line concentration downwind of the landfill (b) cross wind concentrations along the 1 km boundary line (dashed line in (a))

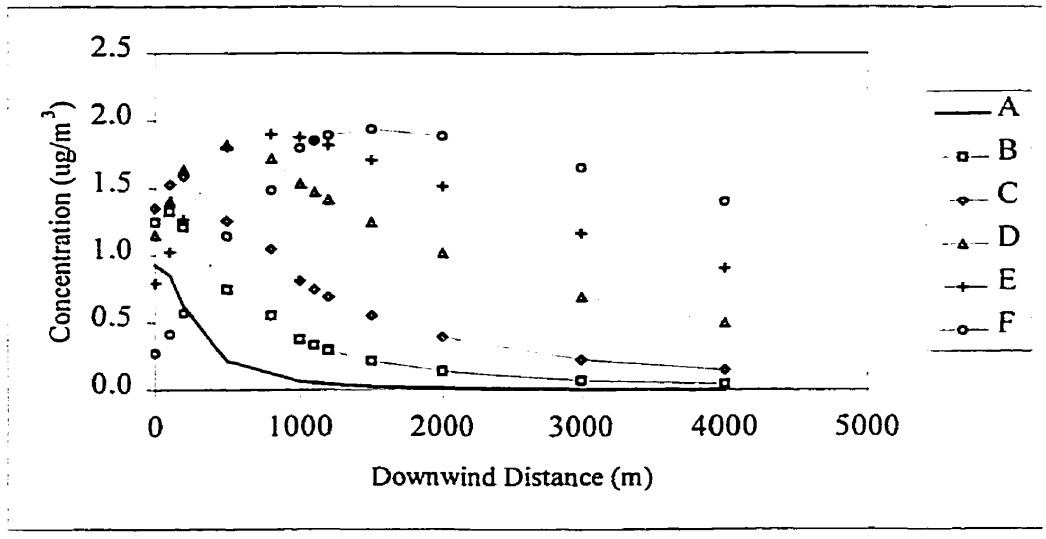

(a)

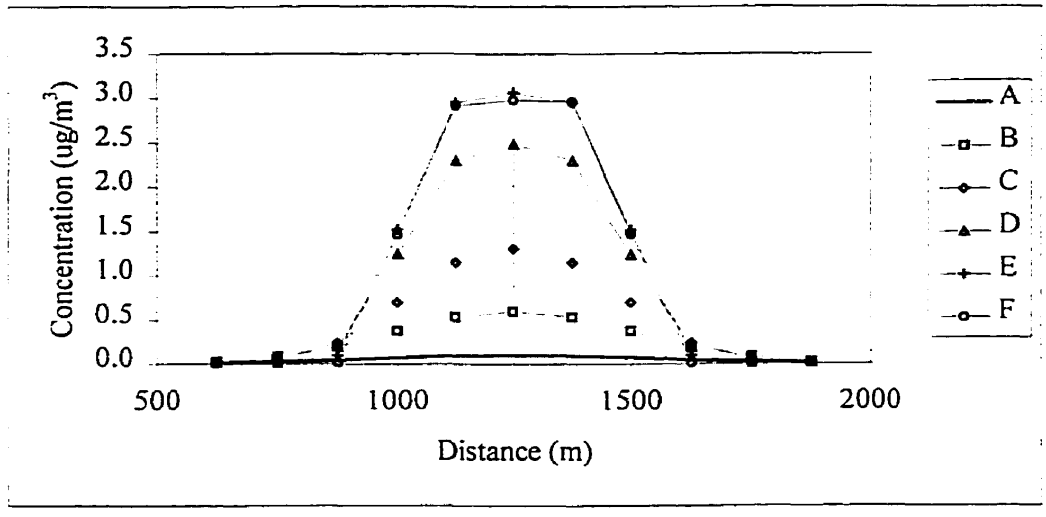

(b)

Figure 5.34: Hourly H_2S concentration for all the stability classes and velocity of 2 m/s for a wind direction of 0 degrees at 7700 days. (a) centre line concentration downwind of the landfill (b) cross wind concentrations along the 1 km boundary line (dashed line in (a))

conditions (F), the peak concentration occurred at 1.5 km. The distribution of the concentration along the 1 km boundary line indicates that the E stability class produces the highest concentration (worst case) (Figures 5.33(b), 5.34 (b)). This is a result of the stable conditions not peaking until the 1.5 km mark. However the peak concentration of both E and F curves is very close. None of the downwind concentrations curves exceed the ½ hour POI standard for vinyl chloride. From the landfill edge to the 1 km boundary, all but one stability

class had concentrations higher than 1 $\mu g/m^3$. The wind conditions in a 24 hour period will involve several stability classes and wind speeds. Therefore, given that between the edge of the landfill and 1 km boundary the hourly concentrations of vinyl chloride are greater than 1 $\mu g/m^3$, the daily average could exceed the 24 hour AAQC. Based on the Figure 5.33 (b), the area impacted could be approximately 500 m wide along the 1 km boundary, which is equivalent to 41 houses with 40 foot frontage.

The H_2S concentration would not exceed either the ½ POI standard or the 1 hour AAQC of 30 $\mu g/m^3$ as the highest concentration observed was 3 $\mu g/m^3$ under stable conditions.

5.8 Discussion

5.8.1 Modelling LFG Production and Emission

The LES model developed to simulate LFG production and emission in this research:

- is unique;
- allows LFG simulation during construction and can accommodate most landfill designs and filling sequences;
- incorporates the Scholl Canyon Model for LFG production and the Farquhar and Rovers (1973) phases of LFG production;
- can accommodate a wide range of input factors which affect LFG production and transport;
- incorporates the work of Bleiker (1992) that describes increases in waste density and reductions in waste permeability due to compaction as depth increases;
- predicts increases in gas pressure as the waste depth increases and accounts for changes in viscosity and other gas properties;
- accounts for the pressure driven LFG flow upward from the base to the surface and can handle staging of landfill lifts;
- can include various cover conditions, methane oxidation in the cover, and increased flux due to holes in the cover; and
- can also simulate vinyl chloride and H_2S production and emissions.

The LES model simulations of the base case produced realistic LFG concentrations and pressures with landfill depth. Simulations of variations in landfill gas composition with time at the base of the landfill were realistic and provided good comparisons with expected patterns as seen in Figure 5.11. The effect of increased placement of waste in lifts was simulated in Figures 5.12, 5.13 and 5.14.

The simulation of gas flux through a 1.0 inch diameter hole in the column surface area of 12.5 m by 12.5 m created a rapid increase in gas flux and a dramatic drop in the pressure within the landfill column. This is consistent with the high gas flux measurements made from holes in the intermediate cover of the Waterloo Landfill (Section 4.3)

Figures 5.35, 5.36 and 5.37 provide comparisons between methane, oxygen and carbon dioxide concentrations measured in the soil cover of a landfill (Lagerkvist *et al.*, 1997) with the model output. The model output fits the concentrations obtained in the literature fairly well. The literature values did not provide data close to the surface (depth 0.0 to 0.5 m); therefore it is difficult to compare above this point. However, the model output does appear to follow the trend in the literature data and indicates that the model provides realistic simulations of the gas concentration within a landfill waste column. The oxidation and no oxidation curves are similar for the length of the column until the top cell where the microbes are actively converting the CH_4 to CO_2. The oxidation of the CH_4 to CO_2 by the soil microbes is dependent on temperature and O_2 concentration therefore oxidation only occurred within the top cell of the model simulations.

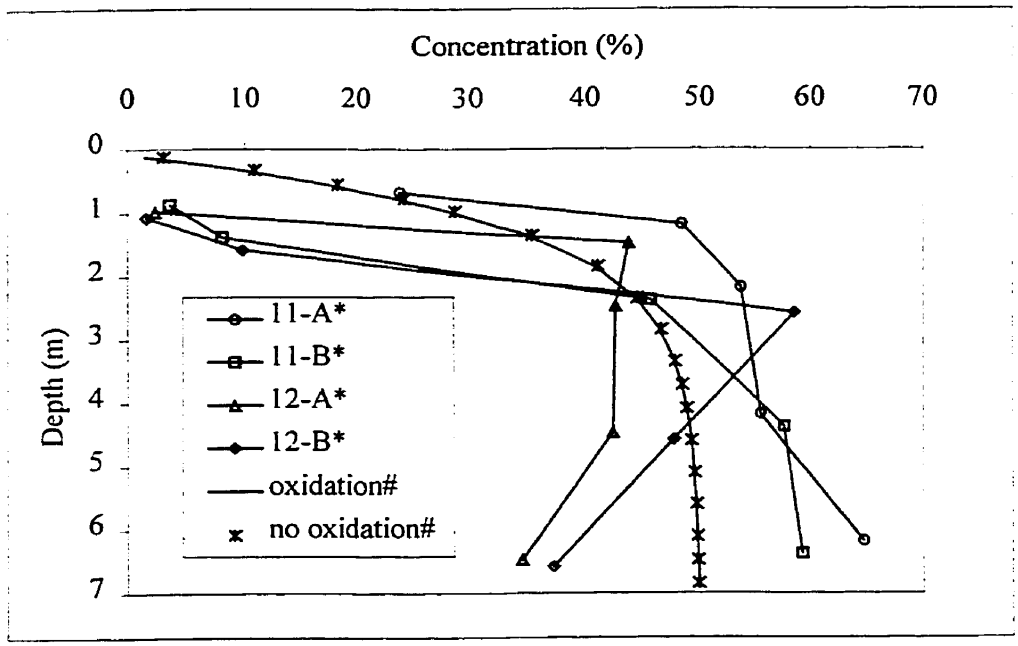

Figure 5.35: Comparison of model methane profile with literature methane concentrations (* Lagerkvist *et al.*, 1997, # LES Model)

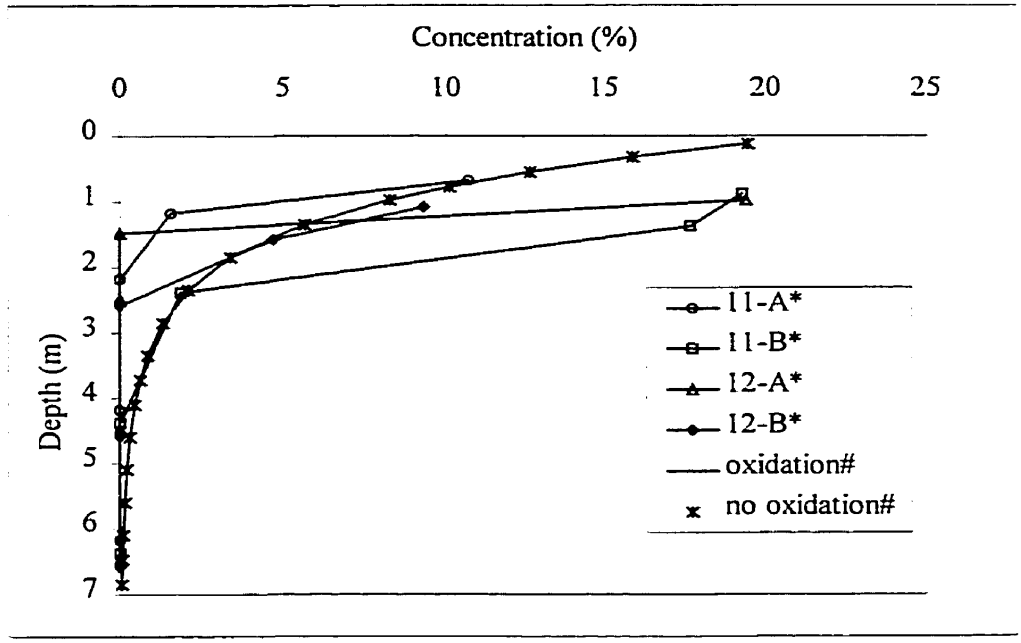

Figure 5.36: Comparison of model oxygen profile with literature oxygen concentrations (* Lagerkvist *et al.*, 1997, # LES Model)

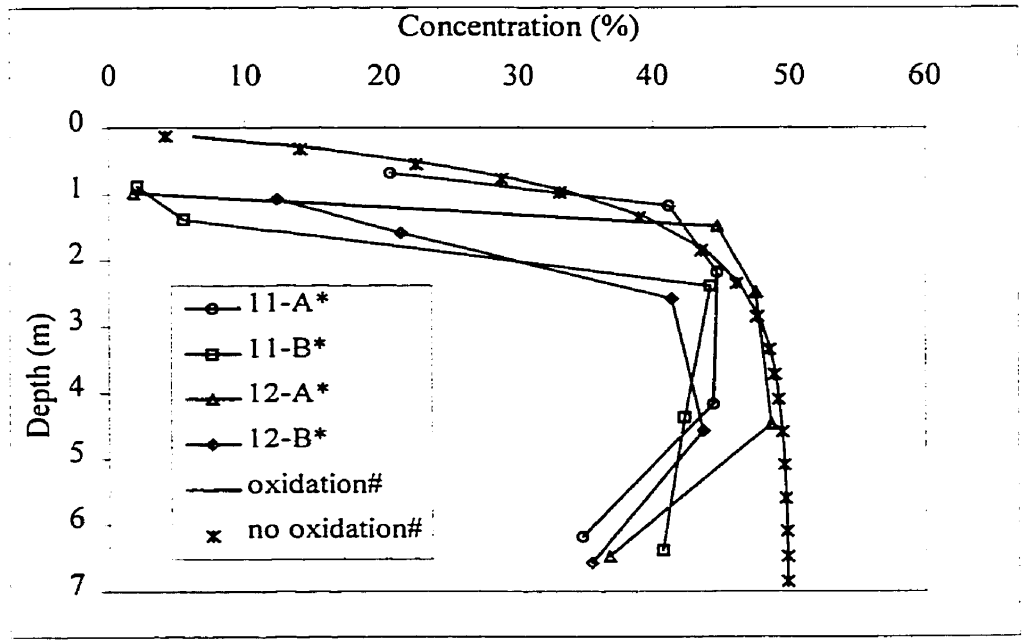

Figure 5.37: Comparison of model CO_2 profile with literature CO_2 concentrations (* Lagerkvist *et al.*, 1997, # LES Model)

Table 5.9 presents comparisons between the concentrations of LFG components of two Ontario landfills and the model output. The peak and end values from the model output are presented. The peak value corresponds to the highest concentration simulated in the bottom cell of the

waste column (6000 days) and the end concentration refers to the concentration at the end of the simulation (36525 days). LFG concentrations at the landfills were obtained from the main header in the gas collection systems at the Waterloo and Cambridge landfills. The CH_4 and CO_2 concentrations predicted by the model were higher than Cambridge values. Comparison with Waterloo's values indicates that the CH_4 values were very close to the field values: the measured CO_2 values were lower than those predicted by the model. The model used the assumption of a 50% CH_4 and 50% CO_2 production from the Scholl Canyon model and this could contribute to the differences. The Cambridge landfill had an average nitrogen gas concentration of 16.9% (V/V) as compared to 7.1% (V/V) at Waterloo. The higher nitrogen concentration means that air intrusion is diluting the gases. Another possible explanation is that gas production at Cambridge is further along the gas production curve than Waterloo. None the less the comparisons are reasonably good.

Emissions of vinyl chloride and other chlorinated compounds from the landfill may occur through reductive dehalogenation of other chlorinated organic compounds or due to

Table 5.9: Comparison of LFG components sampled at landfills with model output

Landfill	CH_4 mol/m^3 (%)	CO_2 mol/m^3 (%)	Vinyl Chloride mol/m^3 (mg/m^3)	H_2S mol/m^3 (mg/m^3)
Cambridge*	15.5 (37.8)	14.5 (35.3)	1.03 x10^{-4} (6.45)	1.7 x 10^{-3} (57.9)
Waterloo*	22.1 (54)	16 (39)	1.57 x10^{-4} (9.8)	1.9 x10^{-3} (64.1)
Model output (peak)	21.4 (50)	22.1 (50)	1.31 x10^{-3} (81.9)	3.89 x10^{-3} (132.6)
Model output (end)	10.6 (26)	12.6 (30)	9.26 x10^{-4} (57.9)	2.2 x10^{-3} (75)

Note:

* - Average of quarterly sampling (1997) from main header in gas collection system

volatilization of the free product (except for vinyl chloride) deposited in the landfill. Volatilization of free products will result in the emissions of vinyl chloride shortly after landfilling of the waste with the anaerobic biodegradation intermediates contributing to the later emissions (Thomas & Barlaz, 1999). The vinyl chloride concentrations simulated by the model were higher than the concentrations observed in the header of the gas collection system at the landfills (Table 5.9). The model output was generated using the default parameters (18.7 ppm) for vinyl chloride suggested by the MOE (1992). Lower concentrations of vinyl chloride

could be achieved by using a smaller default concentration. Kromann *et al.* (1998) found that variable degree of conversion of the chlorinated ethenes seems to be coupled with the level of methanogenesis and indicates that these compounds may not be completely converted in low organic or very stable landfills. The model output assumes all the emissions produced through volatilization and degradation are discharged to the surface. The vinyl chloride concentration predicted by the model is assumed to exit the landfill as a vapour. Some of the vinyl chloride gas present in the landfill will dissolve into the water and end up in the leachate in the landfill therefore reducing the gas concentration.

The model's predicted peak concentration for H_2S was approximately 2 times higher than the measured landfill gas concentrations; but simulated concentration were similar to the observed concentrations at the landfills at the end of the simulation. The simulated concentrations are reasonable close and indicate that the model works well. Sulfide generation has also been found to occur faster than methane production (Flynn, 1998). The model simulated the peak production of H_2S at 6 months with the methane peak at 1 year after waste placement. Construction and demolition (C&D) waste and wallboard ($CaSO_4$) are major sources of H_2S production (Fairweather & Barlaz, 1998). The amount of the C&D waste present will also contribute to the amount H_2S production. The model could allow operators to evaluate the impact of large areas of C&D waste on the emission of odourous compounds.

The methane flux measured at the Waterloo Landfill ranged from 0 to 321 $g/m^2/d$ for all surfaces including holes in the intermediate cover. The model simulations for the base case indicated that the methane flux from the surface would range from 0 to 98.8 $g/m^2/d$ from the start to the finish of the waste column. Another simulation with methane oxidation in the topsoil of the landfill cover resulted in a decrease in the peak methane flux from 98.8 $g/m^2/d$ to 48 $g/m^2/d$. The flux measurements estimated by the model for the base and the oxidation cases were within the range of values observed in the field and the literature.

H_2S fluxes measured at the Waterloo Landfill from imperfect cover conditions (hole) ranged from 3.43 to 23.7 $mg/m^2/d$. The H_2S fluxes predicted by the model ranged from 0 to 42.5 $mg/m^2/d$ for both an intact cover and a simulated hole, providing excellent agreement. The model's peak concentration occurred after the waste column was capped and 2148 tonnes of waste had been landfilled.

The upper part of methane field flux measurements range (31-321 $g/m^2/d$) was obtained from imperfect cover conditions including holes in the intermediate cover. Simulation of a hole in the final cover resulted in a decrease in the pressure within the waste column. The pressure decrease and reduction in the cover permeability combined to produce flux values similar to the intact clay cover simulation (base case) with higher gas pressures within the waste column. Gas flow between adjacent areas, not allowed for in the column simulations, will provide a gas supply to increase the flux though the imperfect cover and a reduction in the flux through the intact cover. A comparison between the base case and hole simulation indicates that similar fluxes can be obtained with a low intact permeable cover which allows the gas pressure to build or less permeable cover with less gas pressure. This indicates that the removal of gas by gas collection systems would reduce the pressure build up under the cover and reduce the surface emissions.

5.8.2 Modelling LFG Transport Off-site

The model for LFG transport off-site to a boundary point of impingement (POI) was accomplished through the use of a modified 1-D analytical Gaussian Plume Model. Although it is not unique, its coupling with a LFG production model as done in this research is unique.

The model was used to test the sensitivity of the model output to changes in distance from the source, wind direction and wind velocity using realistic parameter values. The model was then used to simulate the concentration of vinyl chloride and H_2S at various distances from the landfill under weather conditions typical of the Waterloo Landfill.

The air quality criteria set by the MOE for vinyl chloride and H_2S to minimize the public health impacts were used in this analysis for comparisons with the model simulations. Simulation of vinyl chloride and H_2S transport from the base case simulated landfill cover produced vinyl chloride concentrations at the 1 km boundary that exceed the 24 hour AAQC. MOE (1999) evaluated the risk associated with landfill emissions and found that 6.6 million tonnes of waste with gas collection starting in year 4 and operating for 20 years after closure had a combined cancer risk range of 4×10^{-6} to 1×10^{-5}, with no individual chemical risk exceeding 1×10^{-5}. MOE assumed that 70% of the landfill gas was recovered with the other 30% escaping to the atmosphere. The landfill simulation in this study had 4.8 million tonnes of waste without any gas collection. The vinyl chloride concentration was found to exceed the

24 hour AAQC only within a 1 km boundary surrounding the landfill. Although, no risk analysis was performed in this study, given the conditions defined the MOE (1999), this landfill would likely fall within or below the cancer risk range defined by the MOE. The emission model is adaptable to be used to perform risk analysis studies of a landfill.

The H_2S emissions from the landfill surface were found not to exceed any of the MOE's criteria or standards.

Dispersion modelling indicated that the north-south axis generated the highest atmospheric concentration of both vinyl chloride and H_2S for the boundary configuration used in this work. This modelling provides an indication of the impact of the landfill construction on the atmospheric concentration. Landfill operators will have no control over the wind direction or speed but they can modify the landfill configuration to take advantage of these variables when designing the landfill to help reduce the boundary level concentrations. The model would provide a means to evaluate different construction orientations and practices on the boundary level concentrations.

Chapter 6

6.0 Conclusions and Recommendations

Landfill emissions will impact the environment and the population living near by. The research conducted and presented in this thesis was done to provide a method and means of evaluating the emissions from the landfill surface and the impact on the population and environment.

6.1 Conclusions

A flux chamber for measuring gas emissions from soil surfaces was designed and tested as a part of this research. The design was based on principles learned from early designs reported in the literature but with attention paid to improving inconsistent results obtained with the earlier versions. Controlling the pressure differential between the atmosphere and the chamber interior through continuous pressure measurement and effluent gas flow adjustment, proved to be the key design feature. The following conclusions were drawn from the laboratory test results:

1. The flux chamber was capable of maintaining average pressure differentials below 0.04 mm H_2O for several hours although standard deviations up to 0.2 mm H_2O were observed due to the pulsating behaviour of the peristaltic pumps used to control the gas flow.
2. The recovery of methane gas flux through the soil layer was excellent with recovery efficiency ratios ranging from 0.99 to 1.08. The inflow of methane beneath the soil layer was maintained at rates considered to be typical of landfill behaviour.

3. When pressure differentials were allowed to reach approximately ±1.8 mm H_20. large errors in methane flux measurements occurred with the methane recovery efficiency ratio ranging from 0.07 to 2.74. Although this is a very small pressure differential when compared to barometric or landfill pressure fluctuations, it induced a profound bias in the gas recovery efficiency.

4. ORBO tubes added to the chamber effluent lines, permitted the flux measurements of TCE and PCE to be made with capture efficiency ratios near 1.0. A lag in recovery when compared to methane was attributed to sorption and dissolution into soil moisture.

The flux chamber was tested at three local landfills to assess field performance. Average pressure differentials of 0.023 mm H_2O were maintained and thus, based on the laboratory results, realistic flux measurements were assumed to be possible since the actual gas flux rates through the surfaces investigated were unknown. The following conclusions were drawn from the field experiments:

5. Although the surface area of the chamber was small, measurements of methane, TCE, PCE and H_2S flux were within realistic ranges.

6. Small holes a few millimeters in diameter, in the intermediate cover, produced increases in gas flux rates up to three orders of magnitude when compared to intact cover material and yielded methane concentrations up to 26.7% V/V. One hole approximately 5 cm in diameter produced a gas flow of 19.2 L/min and a methane concentration of 54% V/V. It is expected that even imperfections of this magnitude in cover materials have the potential to release gas from large areas beneath the cover.

7. TCE, PCE and H_2S emissions were detected at several sampling locations. Only H_2S concentrations exceeded air quality standards; however, comparison with air quality standards is normally done only after transport to some distant point of impact during which dilution and dispersion will have occurred to reduce the concentrations.

Laboratory experiments were conducted to evaluate further, the impact of imperfections in cover materials on gas emissions from landfills. Under conditions of typical landfill pressures and gas composition, a 17 cm thick layer of clay cover material and a hole with nominal diameter of 0.16 cm diameter, measurements of gas discharge were made in several

experiments. Discharge from the hole was modelled with the Hagen-Pousielle and the Darcy-Weisbach equations.

8. One 0.16 cm diameter hole can emit the same flux as approximately 212 m^2 of competent clay cover with the same pressure differential across the clay layer.

A unique numerical model was developed to simulate landfill gas production and release through the landfill surface. It incorporated the construction sequence of the landfill, changes in waste density due to compaction, increases in mass flux due to additional waste lifts, variations in cover conditions including holes and methane oxidation, typical production rate kinetics and the changing phases of landfill gas production. The simulation results from this model were used as a source for a Gaussian plume model to simulate gas transport off site. Although insufficient field data were available for comparison, a realistic base case plus parameter modifications were used for simulations. Several conclusions were drawn from this work:

9. The model produced gas production patterns and gas flux rates consistent with previous field and laboratory experience. Measured methane concentration profiles due to oxidation in cover materials from Lagerkvist *et al.* (1997) were well matched with the model predicted profiles.

10. The base case produced methane flux values which ranged up to 98 $g/m^2/d$ without methane oxidation in the cover and 48 $g/m^2/d$ with oxidation. These compared favourably to flux chamber measurements made at the Waterloo Landfill which ranged up to 31 $g/m^2/d$ through competent intermediate cover and up to 321 $g/m^2/d$ through cover with small holes in it.

11. The base case provided estimates of H_2S flux, which compared favourably with measurements made at the Waterloo Landfill site.

12. Simulation of landfill gas transport off site from the base case using weather conditions measured at the Waterloo Landfill site, showed that health risks due to vinyl chloride and hydrogen sulphide would be small in the context of Ontario MOE Guidelines.

6.2 Recommendations

Results from this research could be expanded in scope for future projects. Specifically, recommended studies for future research include:

- Although, the present flux chamber design successfully monitored the flux from the landfill surface, given the heterogeneity of gas emissions from the landfill surface it is to be expected that a larger chamber surface area would reduce the number of flux measurement required to define the LFG emissions from the landfill surface. A larger chamber surface area may be more cost effective. The construction of a larger prototype that scales up the principles and equipment configurations used in this design should be done. However, the small scale of the heterogeneities compared to the large surface area of a landfill will require that many measurements at many locations be done in order to quantify the overall gas flux from a landfill.

- At present the emission model assumes constant atmospheric pressure and temperature. Emissions are affected by changes in atmospheric pressure. Daily and seasonal temperature changes will affect the oxidation potential of the cover and microbial degradation of waste near the landfill surface. The incorporation of changes in atmospheric temperature and pressure to evaluate the changes on the production and flux of the landfill gas components would provide insight to the impact of seasonal changes on the landfill emissions. Aerobic and anaerobic decay of the waste also generate heat that will influence the pressure within the landfill and ultimately the movement of the landfill gas to the surface. Adding heat generation effect to the gas production and emission model should be done.

- The landfill generated for the dispersion modelling was a flat elevated surface without any side slopes to contribute to the atmospheric concentration. The configuration of the model should be modified to produce shorter columns to simulate the side slopes of the landfill. This configuration may provide more realistic simulations.

- The simulation of holes in cover materials indicated that the surrounding waste columns might contribute to the emission from the less permeable column surface. Further development of the model to incorporate 2 or 3 dimensional gas transport throughout the

landfill and its impact on the flux out of the surface would provide a better means to evaluate the impact of these "holes" on the overall emission from the landfill.

- Gas recovery for utilization and migration control will impact the emission of the gases from the landfill surface. A gas removal component should be added to the gas transport equation within each cell to evaluate the impact on the pressure distribution within the landfill and the emission of gases from the landfill surface.
- Risk of landfill emission on the public is always a major concern. The simulation results from the model were found to provide realistic estimates of the flux from the landfill surface. Therefore, the use of the model should be encouraged to provide estimates of the concentrations of the NMOCs at the landfill boundary to evaluate the risk of emission of several NMOCs from the landfill surface on the surrounding public.

References

Asante-Duah, D.K., (1993), Risk Assessment Techniques and Methods of Approach. In: *Hazardous Waste Risk Assessment*, Ann Arbor: Lewis Publishers, p. 113-119.

Assmuth, T. and Kalevi, K., (1992), Concentrations and Toxicological Significance of trace organic compounds in Municipal Solid Waste Landfill Gas. *Chemosphere* 24(9): 1207-1216.

Augenstein, D., and Pacey, J., (1991), Modeling landfill methane generations. *Proceedings of Sardinia 91, Sixth International Landfill Symposium*, Cagliari, Italy; October 14-18, 1991 pages 115-148.

Balfour, W.D., Schmidt, C.E., and Eklund, B.M., (1987), Sampling Approaches for the Measurement of Volatile Compounds at Hazardous Waste Sites. *Journal of Hazardous Materials*, 14: 135-148.

Baker, L.W. and Mackay, K.P., (1985), Screening Models for Estimating Toxic Air Pollution Near a Hazardous Waste Landfill. *Journal of the Air Pollution Control Association* 35(1): 1190-1195.

Bear, J., (1972), *Dynamics of Fluids in Porous Media.* American Elsevier, New York.

Bennett, G.F., (1987), Air quality aspects of hazardous waste landfills. *Journal of Hazardous Waste and Hazardous Materials* 4(2): 119

Bird, R.B., Stewart, W.E., and Lightfoot, E.N. (1960) *Transport Phenomena*, John Wiley & sons, Inc., New York.

Bleiker, D.E., (1992), *Landfill Performance: Leachate Quality Prediction and Settlement Implications*. MASc. thesis University of Waterloo.

Bogner, J.E., Spokas, K.A., and Burton, E.A., (1997a), Kinetics of Methane Oxidation in a Landfill Cover Soil: Temporal Variation, a Whole-Landfill Oxidation Experiment, and Modeling of Net CH_4 Emissions. *Environmental Science and Technology* 31(9): 2504-2514.

Bogner, J., Meadows, M., and Czepiel, P., (1997b), Fluxes of methane between landfills and the atmosphere: natural and engineering controls. *Soil Use and Management* 13: 268-277.

Bogner, J., Spokas, K., Niemann, M., Niemann, L., and Baker, J., (1997c), Emissions of Non-Methane Organic Compounds at an Illinois (USA) Landfill Site: Preliminary Field. *Proceedings of Sardinia 97, Sixth International Landfill Symposium*, Cagliari, Italy; October 13-17, 1997 volume 4: 126-138.

Börjesson, G. and Svensson, B.H. (1997a), Measurements of landfills gaseous emissions and investigations on methane oxidation in the cover soils. *Proceedings of Sardinia 97, Sixth International Landfill Symposium*, Cagliari, Italy; October 13-17, 1997 volume 4:45-52.

Börjesson, G. and Svensson, B.H. (1997b), Effects of a Gas Extraction Interruption on Emissions of Methane and Carbon Dioxide from a Landfill, and on Methane Oxidation in the Cover Soil. *Journal of Environmental Quality* 26(4): 1182-1190.

Brosseau, J. and Heitz, M., (1994), Trace Gas Compound Emissions from Municipal Landfill Sanitary Sites. *Atmospheric Environment* 28(2): 285-293.

CCME, (1998), 23% National Reduction in Solid Waste from 1988 to 1994. www.ccme.ca/5e_othertopics/5ec.html (website).

Chitgopekar, N.P., Reible, P.D., and Thibodeaux, L.J., (1990), Modelling Short Range Air Dispersion from Area Sources of Non-buoyant Toxics. *J. Air Waste Manage Assoc* 40(8): 1121-1128.

Christensen, T.H., Kjeldsen, P., and Lindhardt, B., (1996), Gas-Generating Processes in Landfills, in *Landfilling of Waste: Biogas*. Edited by T.H. Christensen, R. Cossu and R. Stegmann, E & FN Spon, London

Cook, C.M., Grefe, R.P., and Kuehling, H.H., (1991), The Role of Active Gas Extraction Systems in Capturing VOCs from Municipal Landfill Waste and Leachate: A Preliminary Assessment. *Univ. of Wis. Munic & Ind Waste Res. & Practice 14th Conf. Madison, Sep 25-26* 191-220.

Cossu, R., Andreottola, G., and Muntoni, A., (1996), Modelling Landfill Gas Production in *Landfilling of Waste: Biogas*. Edited by T.H. Christensen, R. Cossu and R. Stegmann, E &FN Spon, London p 237-268

Cossu, R., Muntoni, A., Chiarantini, L., Massacci, G., Serra, P., Scolletta, A., and Sterzi, G., (1997), Biogas Emissions Measurement using Static and Dynamic Flux Chambers and Infrared Method. *Proceedings of Sardinia 97, Sixth International Landfill Symposium*, Cagliari, Italy; October 13-17, 1997 volume 4:103-114.

Crooks, G. and Ramsay, S., (1993), A Wind Tunnel Study of Mean and Fluctuating Concentrations in a Plume Dispersing over a Two-Dimensional Hill. *Boundary-Layer Meteorology* 66:155-172.

Crouch, E.A.C., Green, L.C., and Zemba, S.G., (1990), Estimation of Health Risk from Landfill Gas Emissions. *Proceedings of the 13th Annual International Landfill Gas Symposium March 27-29 Lincolnshire, Illinosis* 87-94.

Denmead, O.T., (1979), Chamber Systems for Measuring Nitrous Oxide Emission from Soils in the Field. *Soil Sci. Soc. Am. J.* 43: 89-95.

Dupont, R.R., (1987), Measurement of Volatile Hazardous Organic Emissions from Land Treatment Facilities. *J. Air Pollut. Control Assoc.* 37(2): 168-176.

El-Fadel, M., Findikakis, A.N., and Leckie, J.O., (1989), A numerical model for methane production in managed sanitary landfills. *Waste Management & Research* 7:31-42.

El-Fadel, M., Findikakis, A.N., and Leckie, J.O., (1995), Migration and Atmospheric Emission of Landfill Gas. *Hazardous Waste & Hazardous Materials* 12(4): 309-327.

Eklund, B.M., Balfour, W.D., and Schmidt, C.E., (1985), Measurement of Fugitive Volatile Organic Emission Rates. *Environmental Progress* 4(3): 199-202.

Eklund, B., (1992), Practical Guidance for Flux Chamber Measurements of Fugitive Volatile Organic Emission Rates. *J. Air Waste Manage. Assoc.* 42:1583-1591.

Emcon Associates, (1980), *Methane Generation and Recovery from Landfills* Ann Arbor-Science, Ann Arbor.

Fairbanks, D.F., and Wilke, C.R., (1950). Diffusion Coefficients in Multicomponent Gas Mixtures. *Industrial and Engineering Chemistry* 42(3): 471-475.

Fairweather, R.J. and Barlaz, M.A., (1998). Hydrogen Sulfide Production during Decomposition of Landfill Inputs. *Journal of Environmental Engineering* 124(4): 353-361.

Farquhar, G.J. and Rover, F.A., (1973), Gas Production During Refuse Decomposition. *Water Air and Soil Pollution* 2(10): 483-499.

Finlayson, B.A., (1992), *Numerical Methods for Problems with Moving Fronts*, Ravenna Park Publishing, Inc. Seattle, Washington 605p.

Finley, B. and Paustenbach, D., (1994), The Benefits of Probabilistic Exposure Assessment: Three Case Studies Involving Contaminated Air, Water, and Soil. *Risk Analysis* 14(1): 53-73.

Flynn, B.E., (1998), Invisible Threat: Odours & Landfill Gas from C&D Waste. *Waste Age* 29(1): 91-97

Freeze, R.A. and Cherry, J.A. (1979), *Groundwater*. Prentice-Hall, Inc., Englewood Cliffs, New Jersey.

Gao, F., Yates, S.R., Yates, M.V., Gan, J., and Ernst, F.F., (1997), Design, Fabrication, and Application of a Dynamic Chamber for Measuring Gas Emissions from Soil. *Environmental Science & Technology* 31(1): 148-153.

Gholson, A.R., Albritton, J.R., and Jayanty, R.K.M, (1989), *Evaluation of the Flux Chamber Method for Measuring Volatile Organic Emissions from Surface Impoundments*. Research Triangle Institute, Research Triangle Park, NC 2779 EPA/600/3-89/008. January 65p

Goldberg, M.S., Siemiatyck, J., DeWar, R., Désy, M., and Riberdy, H., (1999), Risks of Developing Cancer Relative to Living near a Municipal Solid Waste Landfill Site in Montreal, Quebec, Canada. *Archives of Environmental Health* 54(4): 291-296.

Gregory, R., Revans, A., Hill, M., Meadows, M., Ferguson, C., and Gronow, J., (1999), A Framework to Model Human Health and Environmental Risks from Landfill Gas. *Proceedings of Sardinia 99, Seventh International Landfill Symposium*, Cagliari, Italy; October 4-8, 1999 volume 2: 605-612.

Guo, H., Murray, F., and Wilkinson, S., (2000), Evaluation of Total Volatile Organic Compound Emissions from Adhesives Based on Chamber Tests. *Journal of Air & Waste Management Association* 50(2): 199-206.

Höring, K., Kruempelbeck, I., and Ehrig, H.-J., (1999), Long-Term Emission Behaviour of Mechanical-Biological Pretreated Municipal Solid Waste *Proceedings of Sardinia 99, Seventh International Landfill Symposium*, Cagliari, Italy; October 4-8, 1999 volume 1:409-418.

Humer, M. and Lechner, P., (1999), Methane oxidation in compost cover layers on landfills. *Proceedings of Sardinia 99, Seventh International Landfill Symposium*, Cagliari, Italy; October 4-8, 1999 volume 3:403-410.

Jones, K.H., (1994), Comparing Air Emissions from Landfills and WTE Plants. *Solid Waste Management* 8(2): 28-39.

Kanemasu., E.T., Powers, W.L., and Siji, J.W., (1974), Field chamber measurements of CO_2 flux from soil surface. *Soil Science*. 118(4): 233-237.

Karimi, A., Ravindran, V., and Pirbazari, M., (1988), A Laboratory Experiment and Predictive Model for Evaluating Landfill Cover Controls of Emissions of Volatile Organic Chemicals to Air. *Hazardous Waste & Hazardous Materials* 5(3):203-218.

Kienbusch, M.R., (1986), *Measurement of Gaseous Emission Rates from Landfill Surfaces using an Emission Isolation Flux Chamber: User's Guide*, Environmental Monitoring Systems Laboratory, Office of Research and Development, USEPA. EPA/600/8-86/008 February.

Kightley, D., Nedwell, D.B., and Cooper, M., (1995), Capacity for Methane Oxidation in Landfill Cover Soils Measured in Laboratory-Scale Soil Microcosms. *Applied and Environmental Microbiology* 61(2): 592-601.

Kjeldsen, P., (1996), Landfill Gas Migration in Soil, in *Landfilling of Waste: Biogas*. Edited by T.H. Christensen, R. Cossu and R. Stegmann, E & FN Spon, London

Kjeldsen, P., Dalager, A., and Broholm, K., (1996), Degradation of landfill gas constituents in soil. *19th Annual Landfill Gas Symposium SWANA* March 19-21, 1996 p117-132.

Kromann, A., Ludvigsen, L., Albrechtsen, H-J., Christensen, T.H., Ejlertsson, J., and Svensson, B.H., (1998), Degradability of chlorinated aliphatic compounds in methanogenic leachates sampled at eight landfills. *Waste Management Research* 16(1): 54-62.

Lagerkvist, A., (1997), *Biogas fran deponiceller* Samordnad Deponigas Forskning, Utveckling, Demonstration RVF Rapport 97:7.

Lamborn, J.M., (1997), Landfills gas generation at the Narre Warren Landfill site, Australia. *Proceedings of Sardinia 97, Sixth International Landfill Symposium*, Cagliari, Italy; October 13-17, 1997 volume 2:507-514.

Lang, R. and Tchobangoblous, G., (1989), Modelling Emissions of Trace Gases from Landfills. *Proceedings of 82nd A&WMA Annual Meeting June 25-30 Anaheim, California* 4.

Lin, J.-S. and Hildemann, L.M., (1995), A nonsteady-state analytical model to predict gaseous emissions of volatile organic compounds from landfills. *Journal of Hazardous Materials* 40:271-295.

Luckner, L. and Schestakow, W.M., (1991), *Migration Processes in the Soil and Groundwater Zone* Lewis Publishers, Inc, Michigan, 485p

Matthias, A.D., Yarger, D.N., and Weinback, R.S., (1978) A numerical evaluation of chamber methods for determination of gas fluxes. *Geophysical Research Letters*. 5(9): 765-768.

Maurice, C. and Lagerkvist, A., (1997), Seasonal variation of landfill gas emissions. *Proceedings of Sardinia 97, Sixth International Landfill Symposium*, Cagliari, Italy; October 13-17, 1997 volume 4:87-93.

McBean, E.A., Rovers, F.A., and Farquhar, G.J., (1995), *Solid Waste Landfill Engineering and Design*, Prentice Hall New Jersey, p. 73-82.

McBean, E.A., Rovers, F. and Schmidtke K., (1990), Risk Assessment Using Relatively Simple Mathematical Models. In: *Risk Assessment for Groundwater Pollution Control*, edited by McTernan, W.F. and Kaplan, E. New York: ASCE, p. 158-186.

Millington, R.J., (1959), Gas diffusion in porous media. *Science* 130: 100-102

Millison, D., Marcotte, B., Rudolph, C., and Randles, K., (1991), Applications and Comparison of Soil Gas, Flux Chamber and Ambient Air Sampling Results to Support Risk Assessment at a Hazardous Waste Site *Hazardous Materials Controls* 4(4): 51-59.

MOE, (1992), *Interim Guide to Estimate and Assess Landfill Air Impacts*. Air Resources Branch, October

MOE, (1994a), *Summary of Point of Impingement Standards, Ambient Air Quality Criteria (AAQCs), and Approvals Screening Levels (ASLs)*, Standards Development Branch. June.

MOE, (1994b), *Land Use on or Near Landfills and Dumps*, MOE Policy Manual, Guideline D-4, April.

MOE (1999), *Environmental Risks of Municipal Non-Hazardous Waste Landfilling and Incineration, Technical Report Summary*, Standards Development Branch, Environmental Sciences and Standards Division, July

Mortazavi, R., and Williams, J., (1995), *Characterization of Greenhouse Gases and Volatile Organic Compounds from Vented Landfill Gases*. Environment Canada (Report PMD/95-5) August 1995

Mosher, B.W., Czepiel, P.M., Harriss, R.C., Shorter, J.H., Kolb, C.E., McManus, J.B., Allwine, E., and Lamb, B.K., (1999), Methane Emissions at Nine Landfill Sites in the Northeastern United States. *Environmental Science and Technology*, 33(12): 2088-2094

Neitzert, F., Olsen, K., and Collas, P., (1999), *Canada's Greenhouse Gas Inventory 1997 Emissions and Removals with Trends*. Environment Canada Greenhouse Gas Division Pollution Data Branch April 1999

Neufeld, P.D., Janzen, A.R., and Aziz, R.A., (1972), Empirical Equations to Calculate 16 of the Transport Collision Integrals $\Omega^{(l,s)^*}$ for the Lennard-Jones (12-6) Potential. *Journal of Chemical Physics* 57(3): 1100-1102.

Paladugu, S.N., (1994), *Measurement of Landfill Gas Emission Rates using the Flux Tube Technique.* Master Thesis University of Central Florida, Orlando, Florida

Page, N.P. and Donahoe, S., (1993) Health Risk Assessment of Toxic Wastes. In: *Effective and Safe Waste Management*, Lewis Publishers, p. 293-313.

Perera, M.D.N., Hettiaratchi, J.P.A., and Achari, G., (1999), A mathematical model to improve the accuracy of gas emission measurements from landfill. *Proceedings of Sardinia 99, Seventh International Landfill Symposium*, Cagliari, Italy, October 4-8, 1999 volume 4:55-62.

Perry, R.H. and Green D., (1984), *Perry's Chemical Engineers' Handbook* 6th Ed.

Phyper, J.D. and Ibbotson, B., (1991), *The Handbook of Environmental Compliance in Ontario* McGraw-Hill Ryerson, Toronto.

Pohland, F.G. and Harper, S.R., (1986), *Critical Review and Summary of Leachate and Gas Production From Landfills.* EPA/600/2-86/073. U.S. Environmental Protection Agency, Cincinnati.

Popov, V. and Power, H., (1994), Gases emission to the atmosphere from a multi-layer landfill. *Proceedings of the 2nd International Conference on Air Pollution.* Barcelona, Spain Part 2 (of 2): 81-89

RWDI (Rowan Williams Davies & Irwin Inc.), (1993), *Final Report Ambient Air Quality Impact Assessment* Eastview Landfill Site Guelph, Ontario.

Rash, F.D., (1992), *Landfill Gas Emission Rate Measurement Using an Emission Isolation Flux Chamber*, Master Thesis, University of Central Florida, Orlando, Florida.

Regional Municipality of Waterloo (ROW), (1990), *Waterloo Landfill Site Hydrogeologic Investigation Final Report*. Prepared by Conestoga-Rovers & Associates, June

Regional Municipality of Waterloo, (1994), *Landfill Gas Utilization, Waterloo Landfill Site*. Request for Proposal, P-94016.

Reid, R.C., Prausnitz, J.M., and Sherwood, T.K., (1977), *The Properties of Gases and Liquids* 3rd Edition McGraw-Hill, New York.

Reinhart, D.R., Cooper, D.C., and Walker, B.L., (1992), Flux Chamber Design & Operation for the Measurement of Municipal Solid Waste Landfill Gas Emission Rates. *J. Air Waste Manage Assoc* 42(8):1067-1070.

Reinhart, D.R., (1993), A Review of Recent Studies on the Sources of Hazardous Compounds Emitted from Solid Waste Landfills: A U.S. Experience. *Waste Management & Research* 11:257-268.

Richards, K.M., Maunder, D.H., and Gorman, J.F., (1992) Landfill Gas: The Energy Environment Paradox. In: *Renewable Energy Technology and the Environment Volume 3*, edited by Sayigh, A.A.M. Oxford: Pergamon Press, p. 1200-1219.

Roelle, P., Aneja, V.P., O'Connor, J. Robarge, W., Kim, D-S., and Levine, J.S., (1999), Measurement of nitrogen oxide emissions from an agricultural soil with a dynamic chamber system. *Journal of Geophysical Research* 104(D1): 1609-1619.

Sadek, S.E., Lee, T.C., Smith, J.D., and Gebel, R., (1998), Flux Chamber Measurements of Mass Transfer Rates. *Journal of Environmental Engineering* 124(2): 111-121.

Savanne, D., Arnaud, A., Beneito, A., Berne, P., Burkhalter, R., Cellier, P., Gonze, M.A., Laville, P., Levy, F., Milward, R., Pokryszka, Z., Sabroux, J.C., Tauziede, C., and Tregoures, A., (1997), Comparison of different methods for measuring landfill methane emissions. *Proceedings of Sardinia 97, Sixth International Landfill Symposium*, Cagliari, Italy; October 13-17, 1997 volume 4:81-85.

Scharff, H. and Hensen, A. (1999), Methane emission estimates for two landfills in the Netherlands using mobile TDL measurements. *Proceedings of Sardinia 99, Seventh International Landfill Symposium*, Cagliari, Italy; October 4-8, 1999 volume 4:71-78.

Schnelle, K.B. and Dey, P.R., (2000), *Atmospheric Dispersion Modeling Compliance Guide*. McGraw-Hill, New York.

Seigneur, C., Wegrecki, A., Nair, S., and Longwell, D., (1989), Mathematical Modelling of Air Toxic Emission from Landfill Sites. In: *Intermedia Pollutant Transport Modelling & Field Measurements*, edited by Allen, D., Cohen, Y. and Kaplan, I.R. New York: Plenum Press.

Shen, T.T., Nelson, T.P., and Schmidt, C.E., (1990), Assessment and Control of VOC Emissions from Waste Disposal Facilities. *Critical Reviews in Environmental Control* 20(1):43-76.

Streeter, V.L. and Wylie, E.B., (1985), *Fluid Mechanics*. 8th Edition McGraw-Hill Book Company, New York, 586 pages.

Tanaka, N., Matsuto, T., and Lee, H-S., (1997) On-Site Survey of Methane and Carbon Dioxide Flux from MSW Landfills in Japan, *Proceedings of Sardinia 97, Sixth International Landfill Symposium*, Cagliari, Italy; October 13-17, 1997 volume 4:71-80.

Taylor, P.A., Mason, P.J., and Bradley, E.F., (1987), Boundary-Layer Flow Over Low Hills. *Boundary-Layer Meteorology* 39:107-132.

Thibodeaux, L.J., (1981), Estimating the Air Emissions of Chemicals from Hazardous Waste Landfills. *Journal of Hazardous Materials* 4:235-244.

Thibodeaux, I.J., Springer, C., and Riley, L.M., (1982), Models of Mechanisms for the Vapor Phase Emission of Hazardous Chemicals from Landfills. *Journal of Hazardous Materials* 7:63-74.

Thoits, F., (1989), Landfill Air Emissions Data and Risk Assessment Determination in the Monterey Bay Unified Air Pollution Control District. *12th GRCDA* 46-61.

Thomas, C.L. and Barlaz, M.A., (1999), Production of non-methane organic compounds during decomposition in a laboratory-scale landfill. *Waste Management & Research* 17:205-211.

Turner, D.B., (1994), *Workbook of Atmospheric Dispersion Estimates An Introduction to Dispersion Modeling* 2nd Edition Lewis Publishers, Boca Raton.

USEPA, (1987) *On-Site Meteorological Program Guidance for Regulatory Modeling Applications.* Office of Air Quality Planning and Standards, Office of Air and Radiation. Research Triangle Park, N. Carolina. Report No. EPA-450/4-87-013, June.

USEPA, (1991) *Air Emissions from Municipal Solid Waste Landfills - Background Information for Proposed Standards and Guidelines.* Office of Air Quality Planning and Standards, Office of Air and Radiation. Research Triangle Park, N. Carolina. Report No. EPA-450/3-90-011a, March.

Van Geel, P.J. (1994), *Laboratory and numerical simulation of a LNAPL spill in a sand porous medium.* Ph.D. thesis University of Waterloo.193 pages

Venkatram, A. and Seigneur, C., (1993), Review of mathematical models for health risk assessment: II. Atmospheric chemical concentrations. *Environmental Software* 8:75-90.

Vogel, T.M. and McCarty, P.L. (1985) Biotransformation of Tetrachloroethylene to Trichoroethylene, Dichloroethylene, Vinyl Chloride, and Carbon Dioxide under Methanogenic Conditions. *Applied and Environmental Microbiology* 49(5): 1080-1083.

Walker, B.L. (1991), *Flux Chamber Design and Operation for the Measurement of Municipal Solid Waste Landfill Gas Emission Rates.* Master Thesis University of Central Florida, Orlando, Florida.

Wark, K. and Warner, C.F., (1981), Dispersion of Pollutants in the Atmosphere Ch4 in *Air Pollution. Its Origin and Control.* 2nd Ed. Harper & Row Publishers, New York.

Whalen, S.C., Reeburgh, W.S., and Sandbeck, K.A., (1990), Rapid Methane Oxidation in a Landfill Cover Soil. *Applied and Environmental Microbiology* 56(11): 3405-3410.

Williams, B. and Williams, J. (1995), *Measurement of Emission Rates of Selected Landfill Gases from Municipal Solid Waste Landfills*, Pollution Measurement Division, Environment Canada, Report PMD/95-4, 34p

Yoshida, H., Tanaka, N., and Hozumi, H., (1999), Theoretical Study on Temperature Distribution in Landfills by Three-Dimensional Heat Transport Model. *Proceedings of Sardinia 99, Seventh International Landfill Symposium*, Cagliari, Italy; October 4-8, 1999 volume 1:85-94.

Young, P.J. and Parker, A., (1983), The Identification and Possible Environmental Impact of Trace Gases and Vapours in Landfill Gas. *Waste Management & Research* 1:213-226.

Zeiss, C. and Atwater, J., (1993), A Case Study of Nuisance Impact Screening for Municipal Waste Landfill Planning. *Environmental Technology* 14:1101-1115.

Appendix A
Calibration Curves for Pressure Transducers

Appendix A: Calibration Curves for Pressure Transducers

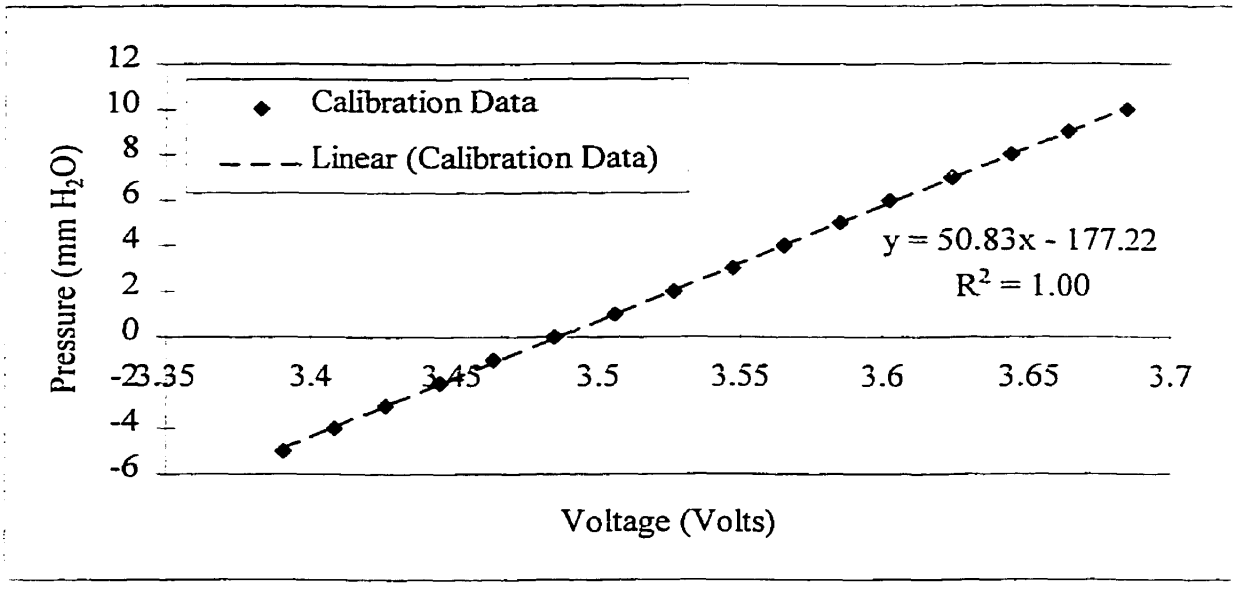

Figure A.1: Calibration of pressure transducer with Betz manometer (July, 1997)

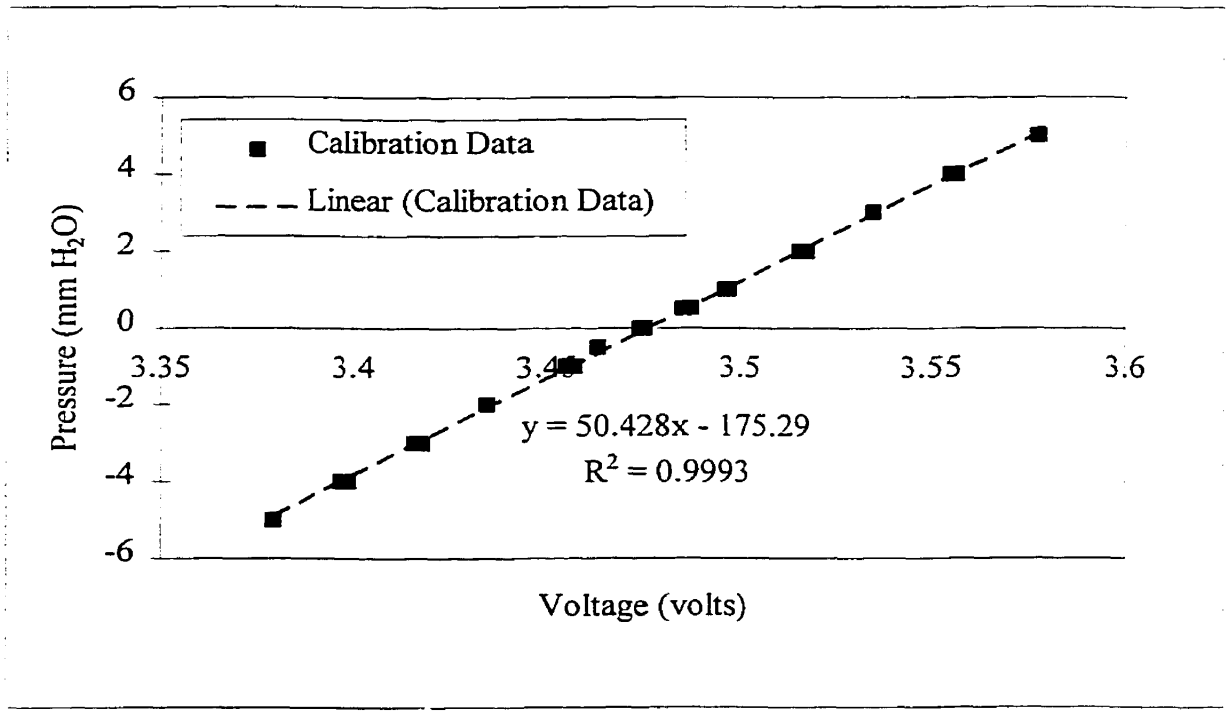

Figure A.2: Calibration of Pressure Transducer with Betz manometer (October 1997)

Appendix B

Methane Calibration Curve of GC-FID and Methane MDL

Appendix B: Methane Calibration Curve of GC-FID and Methane MDL

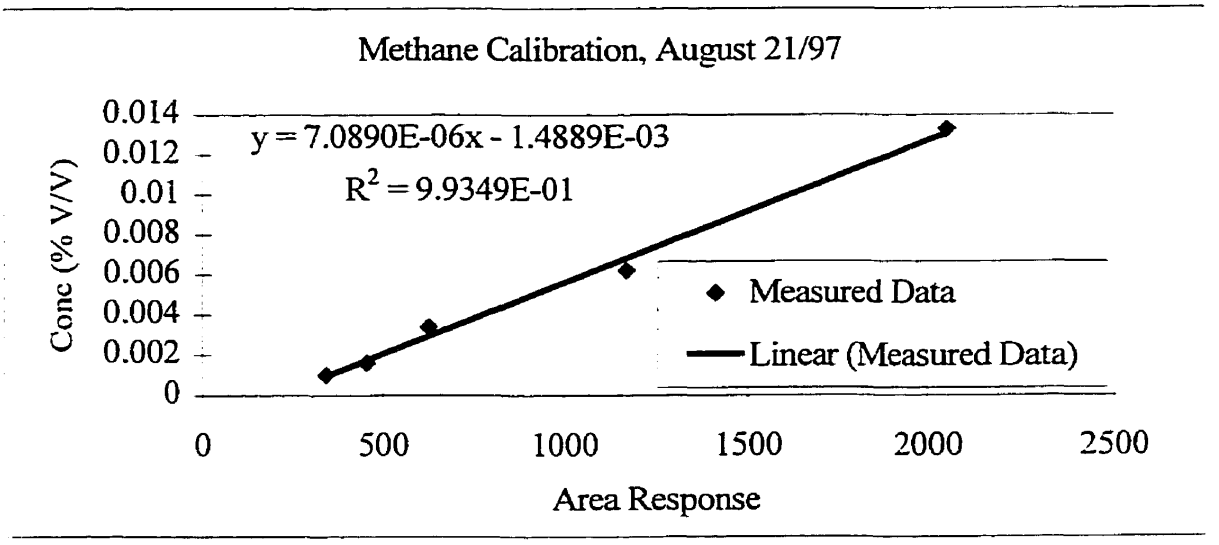

Figure B.1: Methane Calibration curve for GC-FIC on August 21/97

Method Detection Level (MDL) was determined following the procedure indicated in Standard Methods (20th edition).

Table B.1: Method Detection Level for GC-FID

Methane Concentration (% V/V)	GC Area Response	Corrected Area Response	Methane Concentration from Calibration Curve (% V/V)	Standard Deviation of 7 methane concentration values
0.001	689	304.25	6.68E-04	4.87E-04
	752	367.25	1.11E-03	
	826	441.25	1.64E-03	
	823	438.25	1.62E-03	
	750	365.25	1.10E-03	
	767	382.25	1.22E-03	
	635	250.25	2.85E-04	

One-sided *t* distribution for 6 degrees of freedom (7 – 1 = 6) at the 99% level = 3.14

$$MDL = 3.14 \times s$$

Therefore, the MDL is equal to $4.87 \times 10^{-4} \times 3.14 = 1.53 \times 10^{-3}$ % V/V

Converting to $\mu g/m^3$, the MDL is 10,200 $\mu g/m^3$ assuming 1 atm and 20° C.

Appendix C
Data from laboratory experiments

Appendix C: Data from laboratory experiments

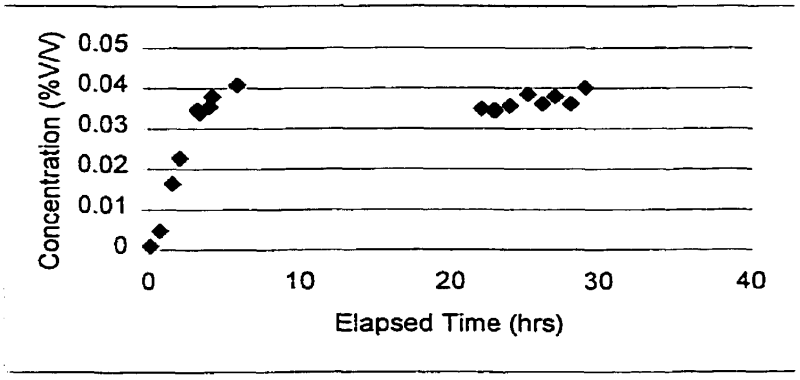

Figure C.1: CH_4 concentration in the chamber effluent versus elapsed time in experiment #1

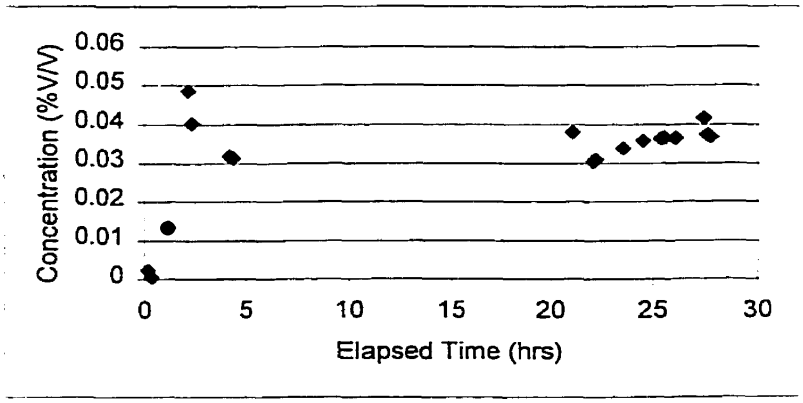

Figure C.2: CH_4 concentration in the chamber effluent versus elapsed time in experiment #2

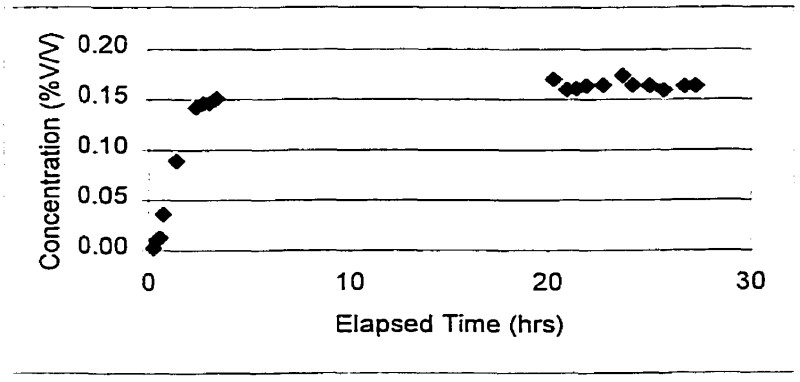

Figure C.3: CH_4 concentration in the chamber effluent versus elapsed time in experiment #3

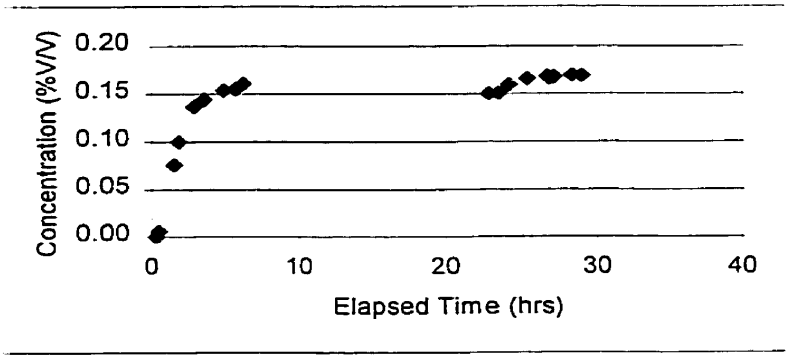

Figure C.4: CH_4 concentration in the chamber effluent versus elapsed time in experiment #4

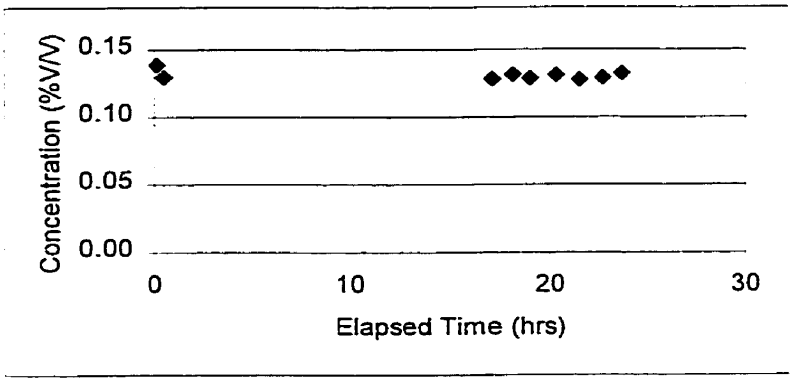

Figure C.5: CH_4 concentration in the chamber effluent versus elapsed time in experiment #5

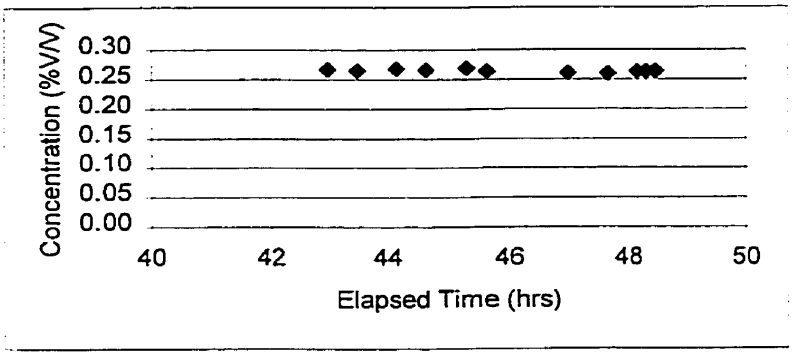

Figure C.6: CH_4 concentration in the chamber effluent versus elapsed time in experiment #6

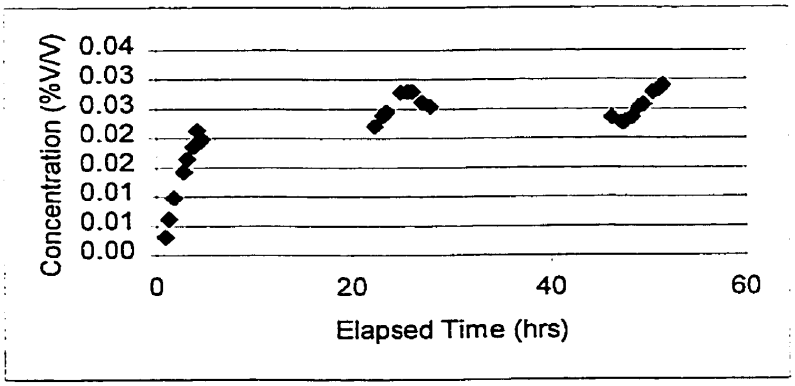

Figure C.7: CH_4 concentration in the chamber effluent versus elapsed time in experiment #7

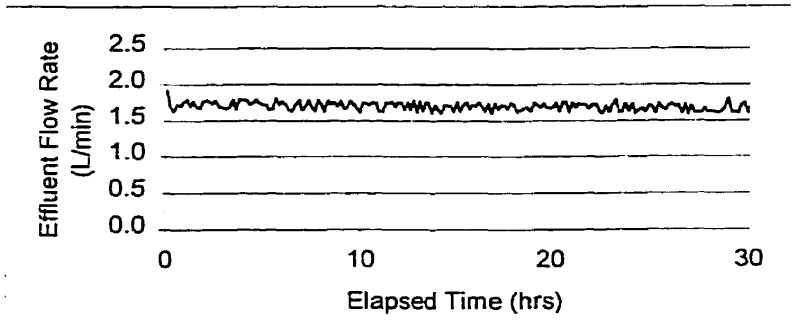

Figure C.8: Effluent flow rate from flux chamber versus elapsed time in experiment #1

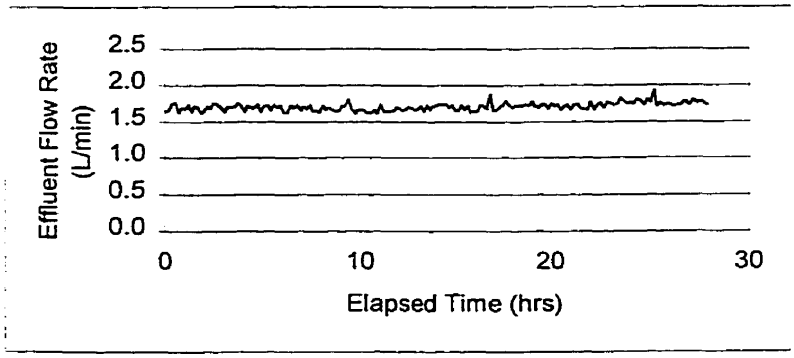

Figure C.9: Effluent flow rate from flux chamber versus elapsed time in experiment #2

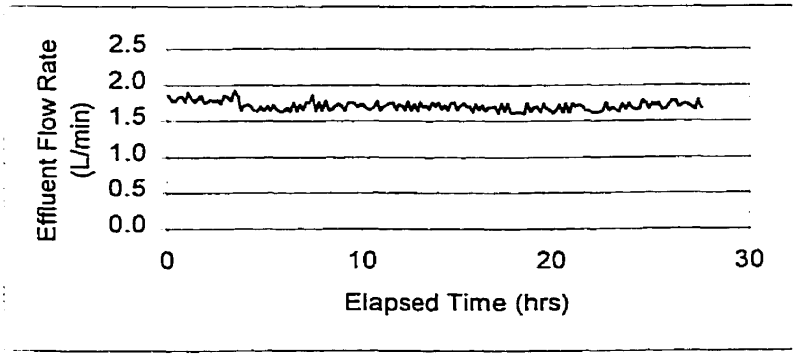

Figure C.10: Effluent flow rate from flux chamber versus elapsed time in experiment #3

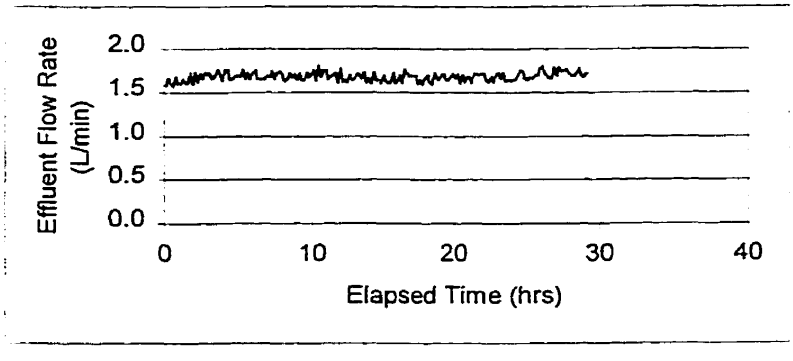

Figure C.11: Effluent flow rate from flux chamber versus elapsed time in experiment #4

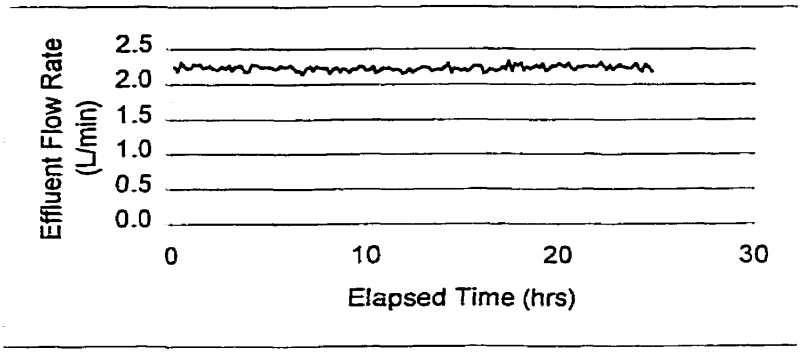

Figure C.12: Effluent flow rate from flux chamber versus elapsed time in experiment #5

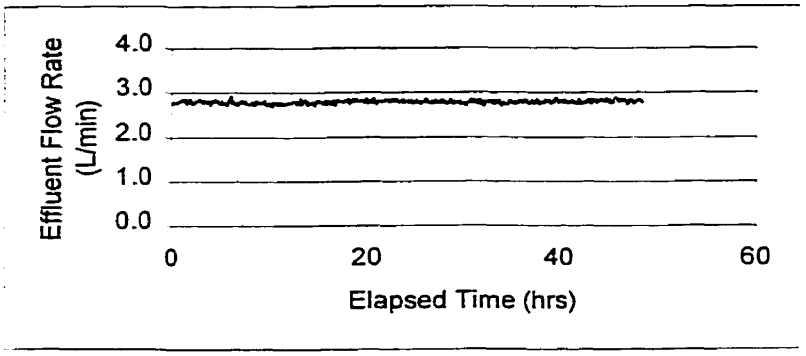

Figure C.13: Effluent flow rate from flux chamber versus elapsed time in experiment #6

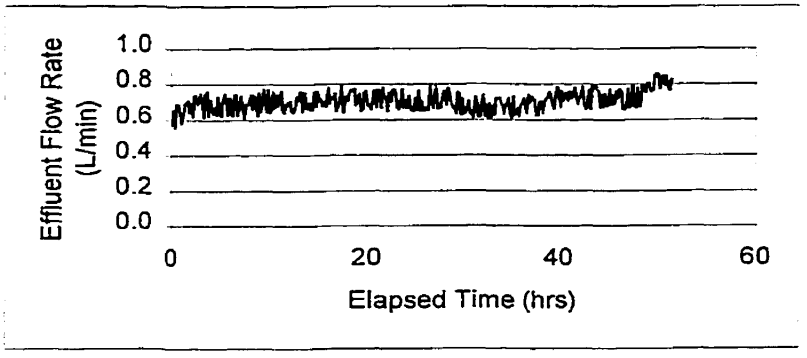

Figure C.14: Effluent flow rate from flux chamber versus elapsed time in experiment #7

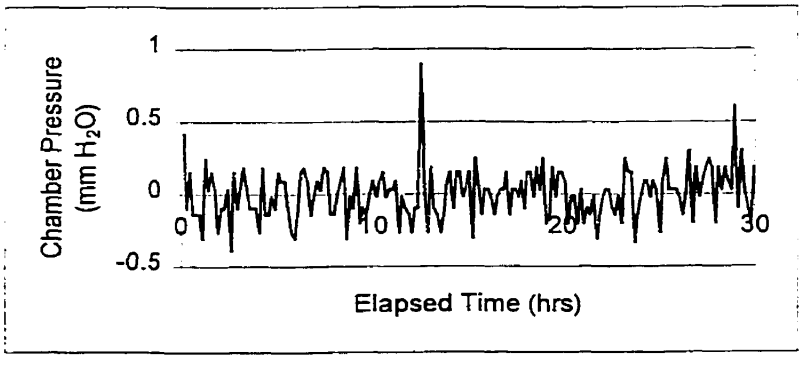

Figure C.15: Chamber pressure transducer data from experiment #1 versus elapsed time

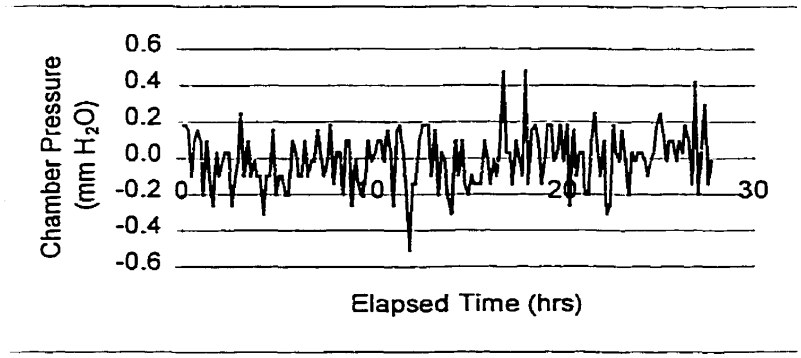

Figure C.16: Chamber pressure transducer data from experiment #2 versus elapsed time

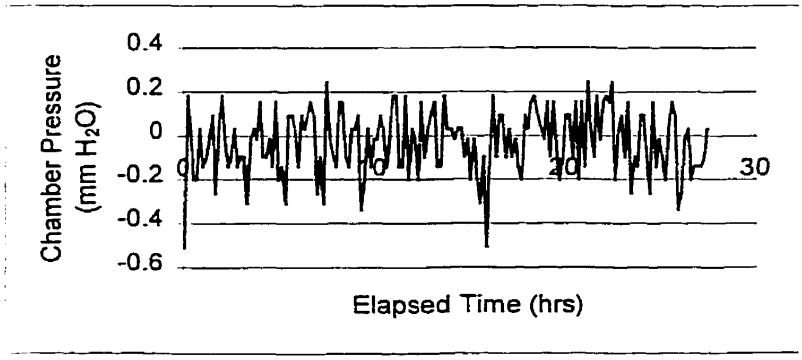

Figure C.17: Chamber pressure transducer data from experiment #3 versus elapsed time

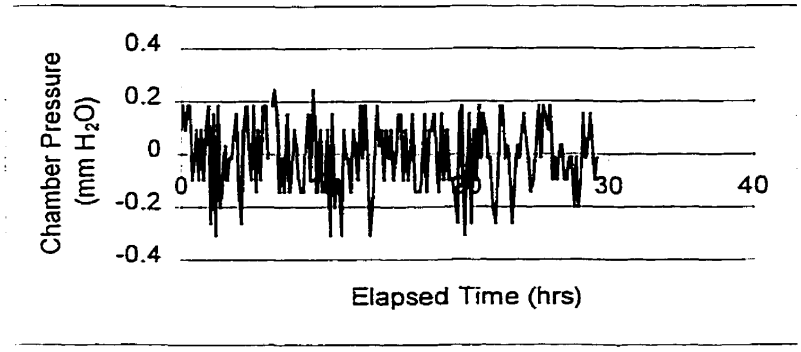

Figure C.18: Chamber pressure transducer data from experiment #4 versus elapsed time

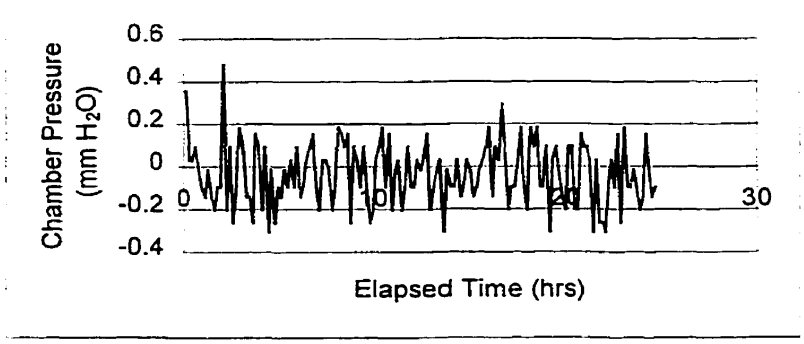

Figure C.19: Chamber pressure transducer data from experiment #5 versus elapsed time

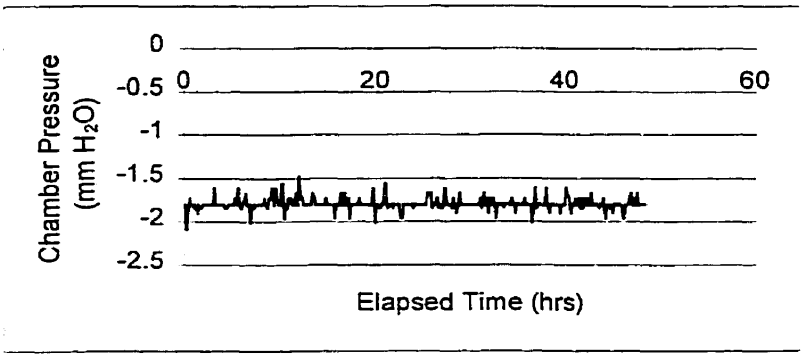

Figure C.20: Chamber pressure transducer data from experiment #6 versus elapsed time

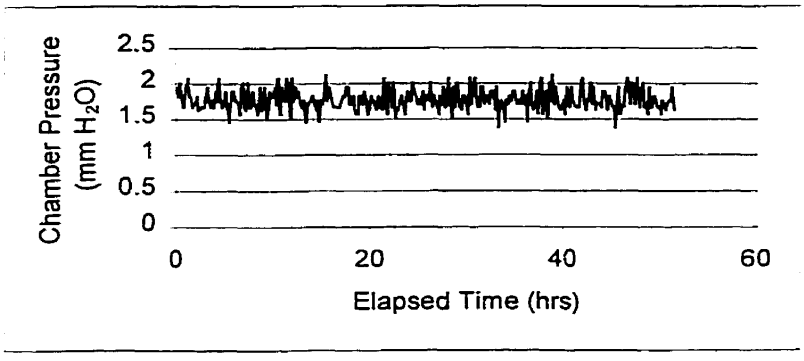

Figure C.21: Chamber pressure transducer data from experiment #7 versus elapsed time

Appendix D
Data from field flux experiments

Appendix D: Data from field flux experiments

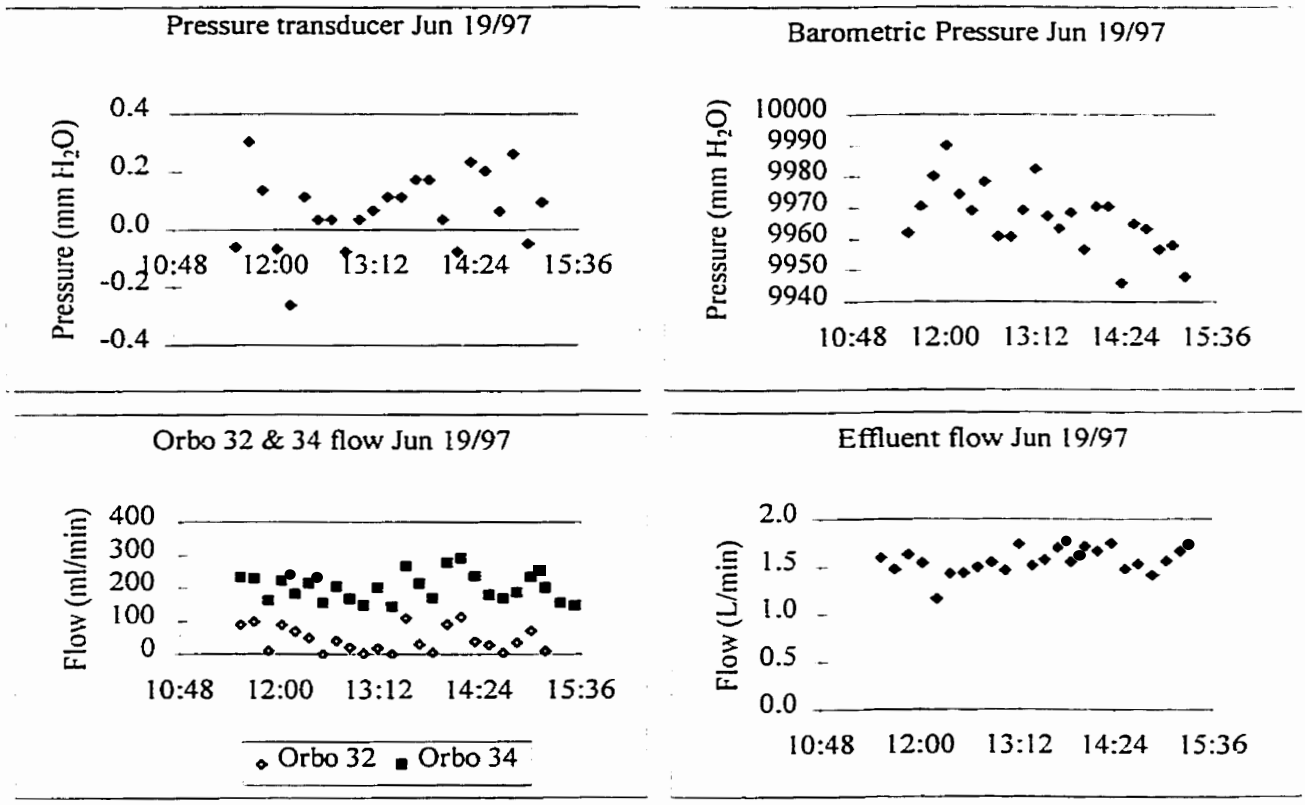

Figure D.1: Data from Waterloo Landfill flux measurements on Jun 19/97

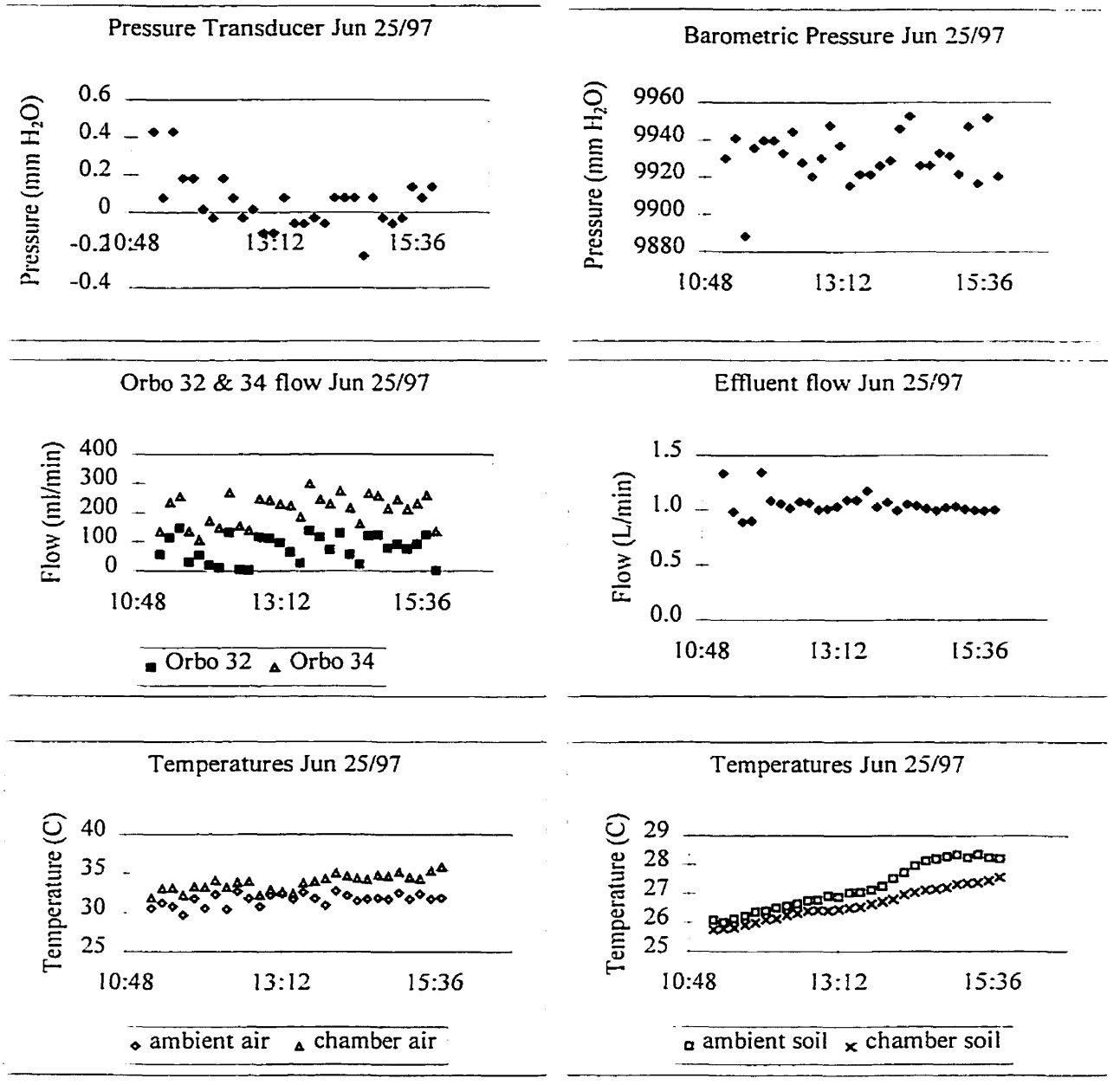

Figure D.2: Data from Waterloo Landfill flux measurements on Jun 25/97

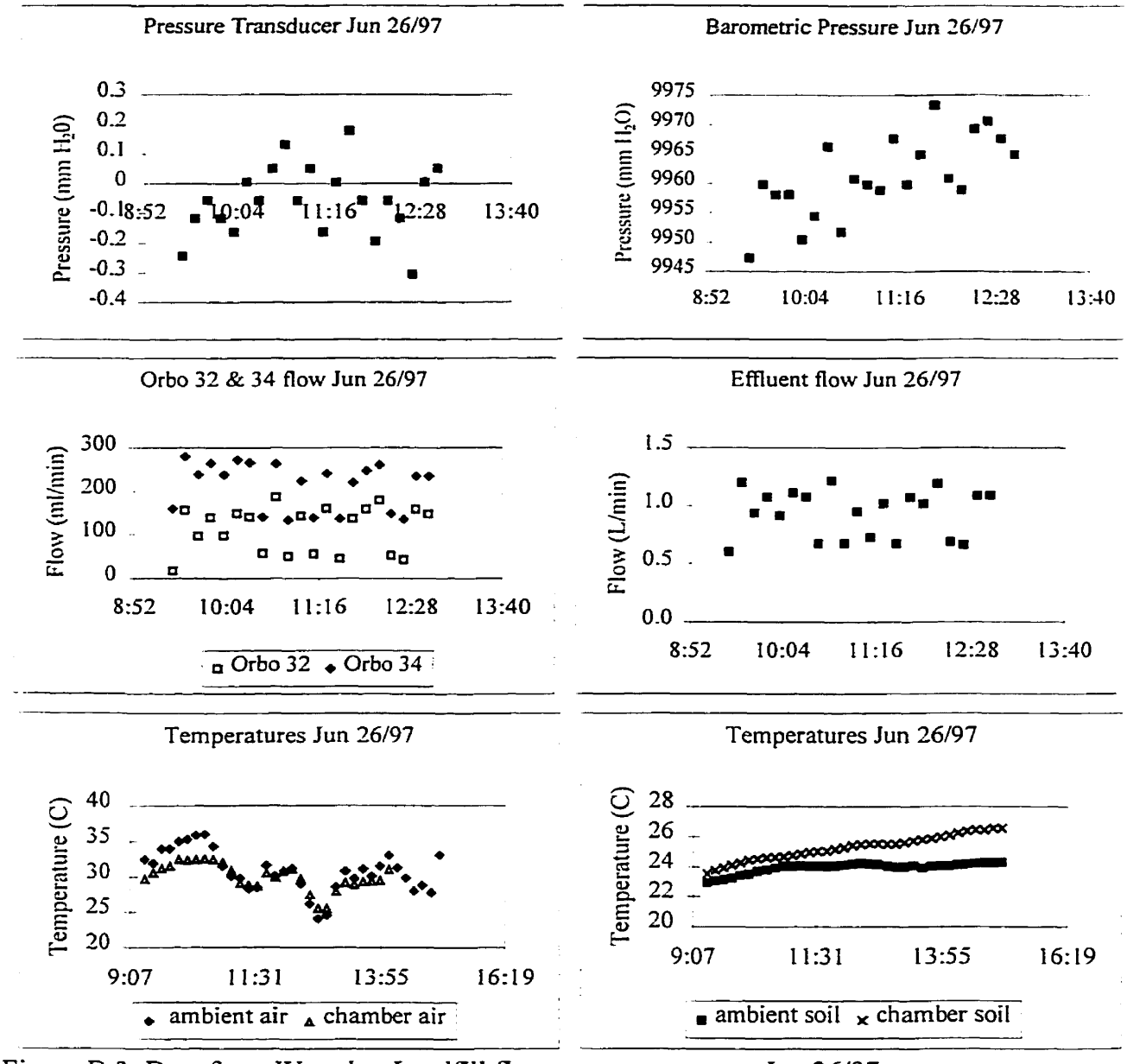

Figure D.3: Data from Waterloo Landfill flux measurements on Jun 26/97

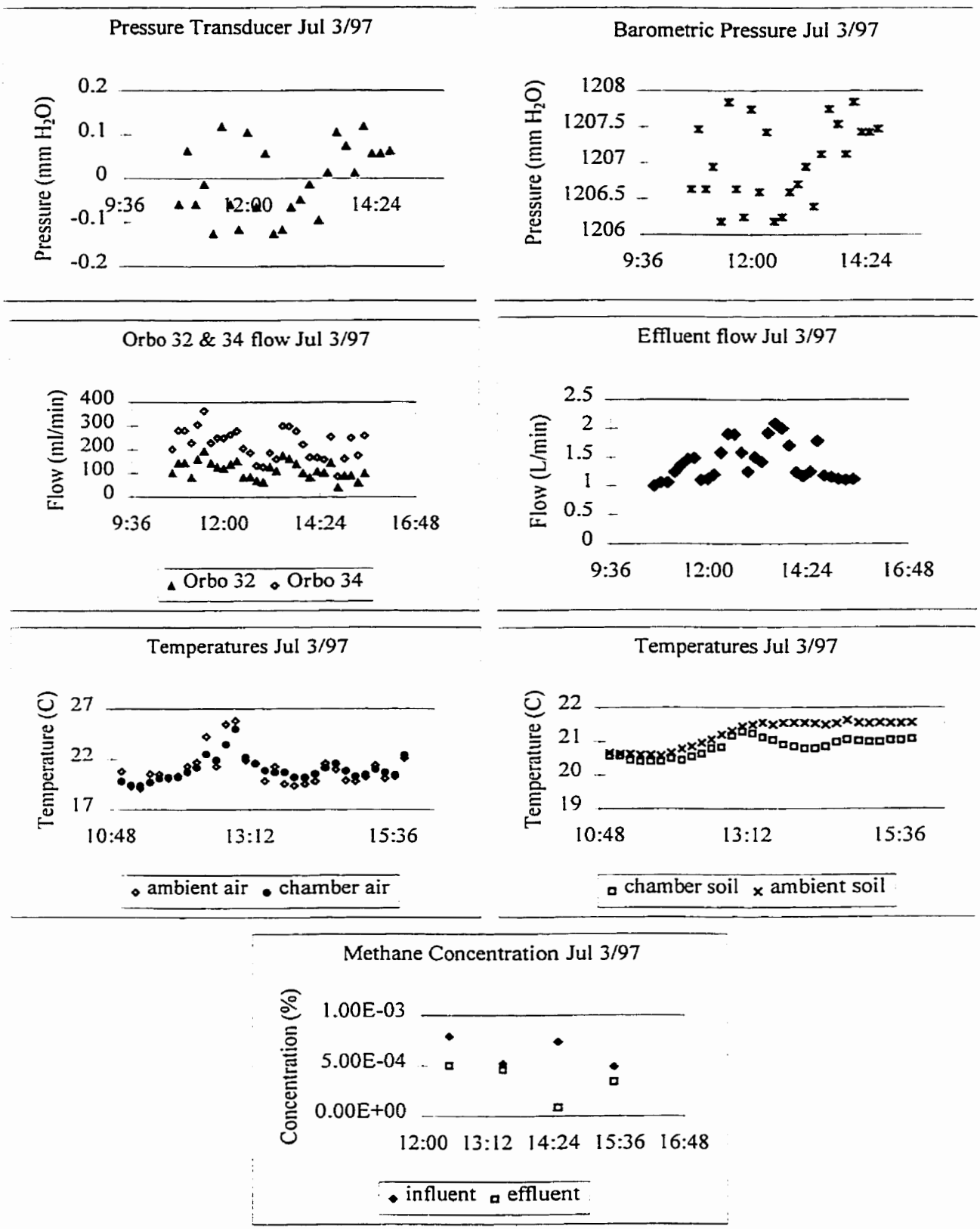

Figure D.4: Data from Waterloo Landfill flux measurements on Jul 3/97

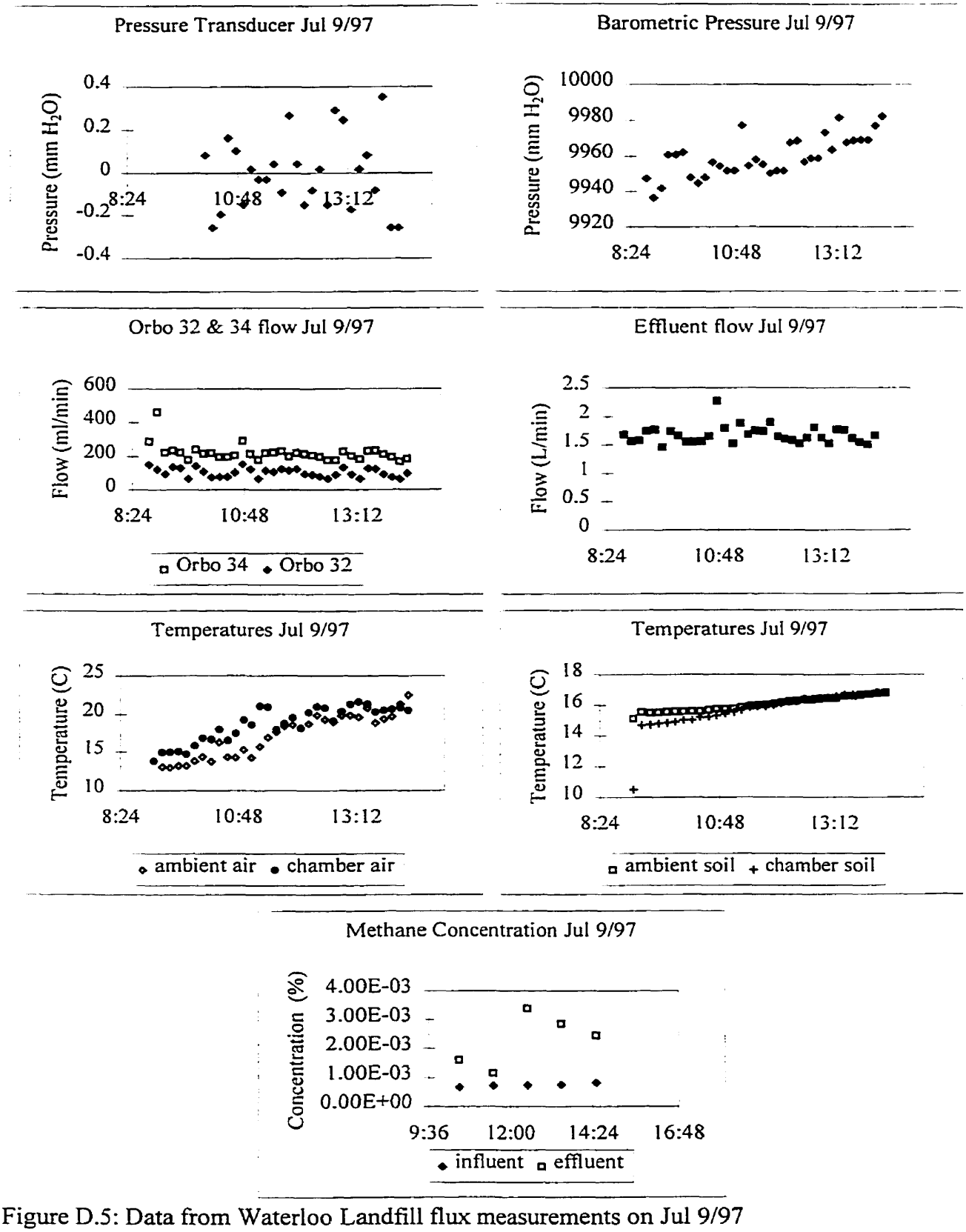

Figure D.5: Data from Waterloo Landfill flux measurements on Jul 9/97

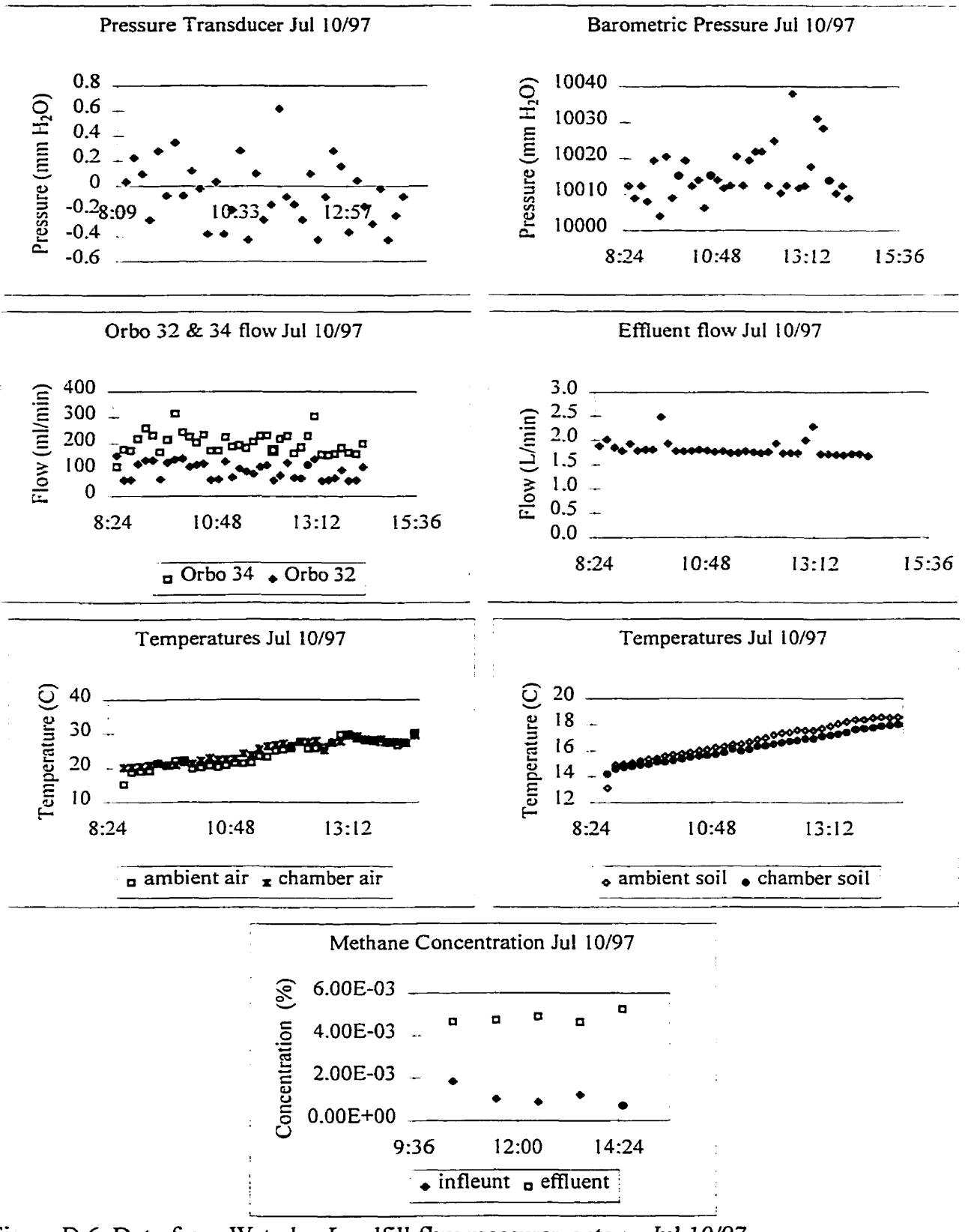

Figure D.6: Data from Waterloo Landfill flux measurements on Jul 10/97

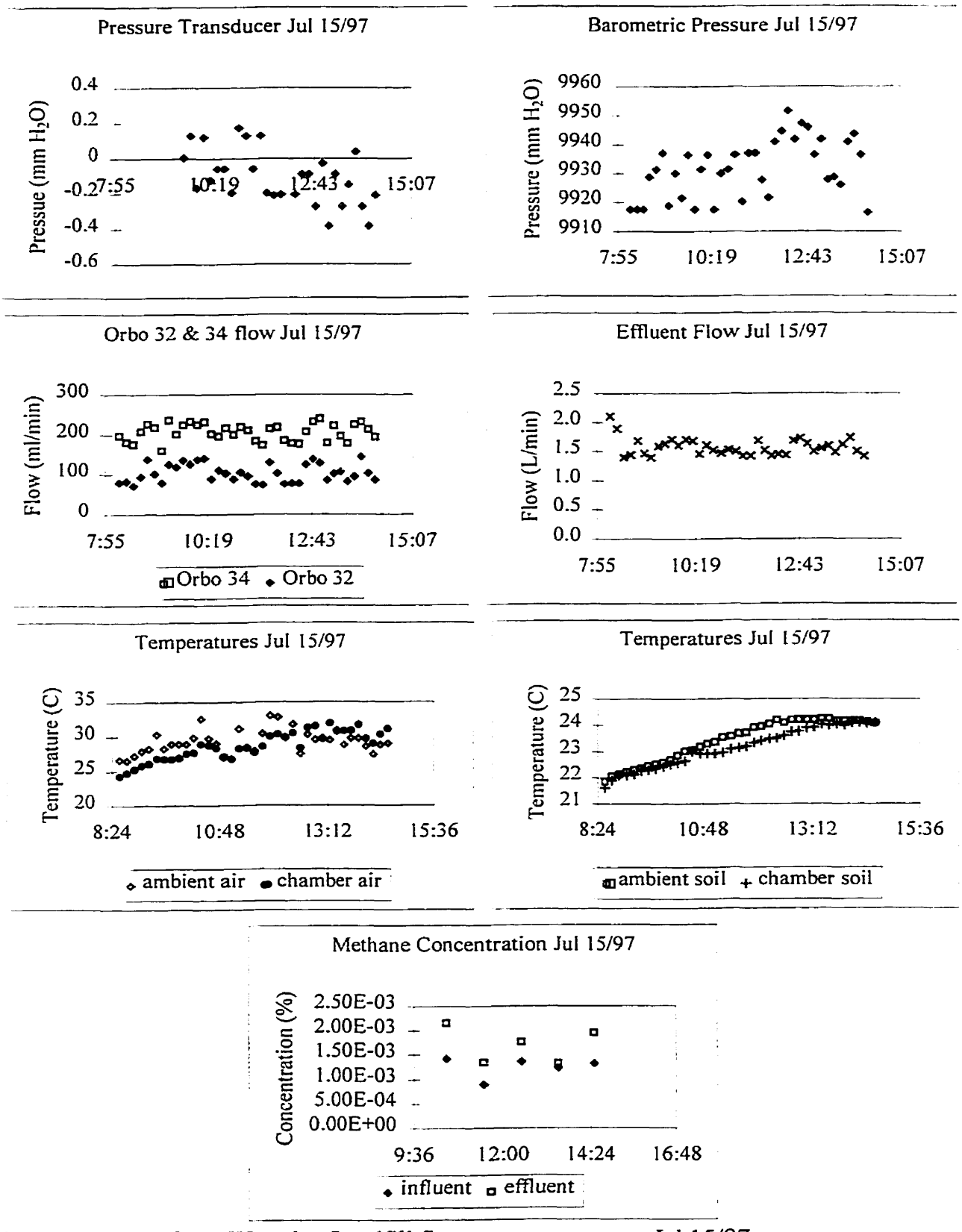

Figure D.7: Data from Waterloo Landfill flux measurements on Jul 15/97

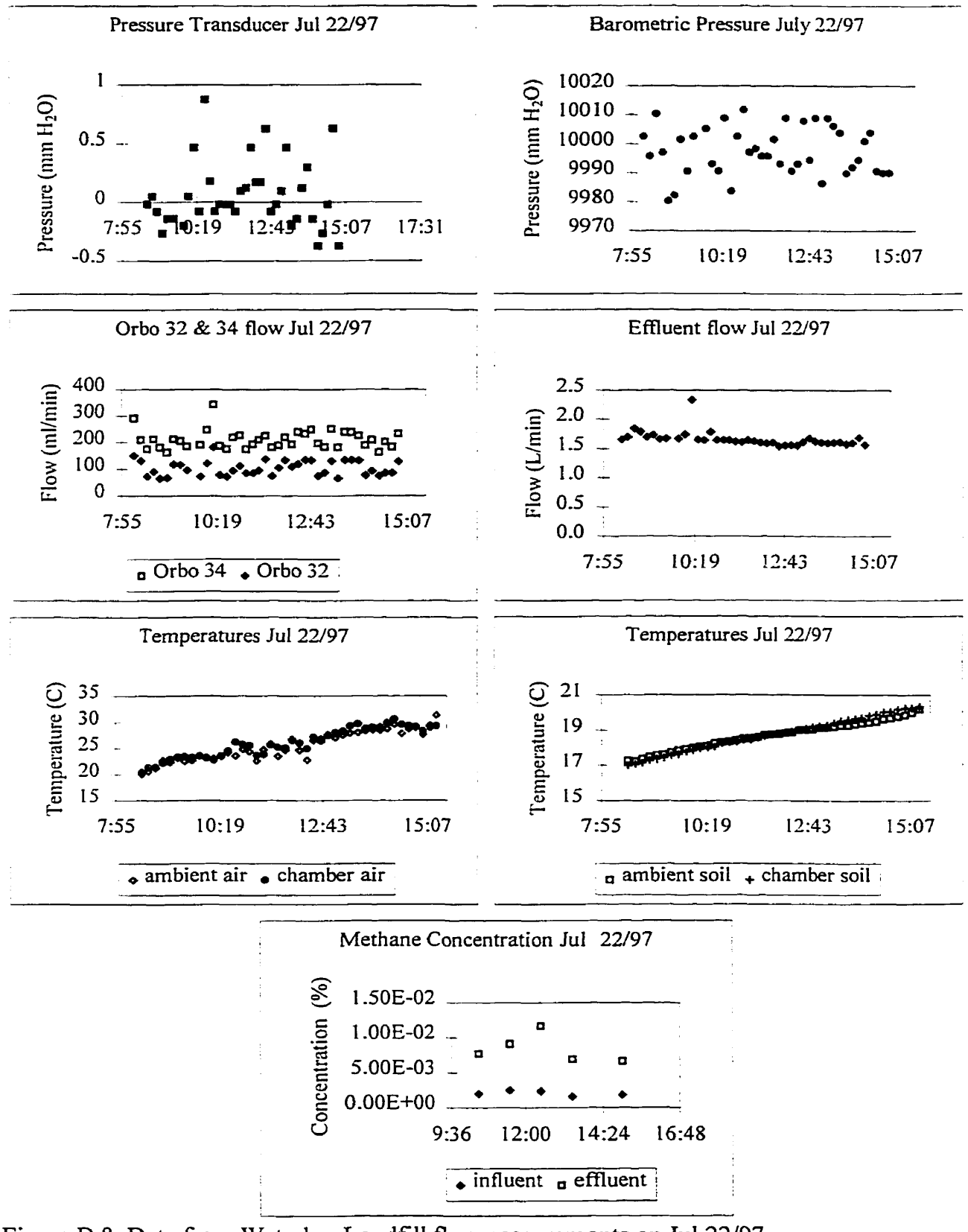

Figure D.8: Data from Waterloo Landfill flux measurements on Jul 22/97

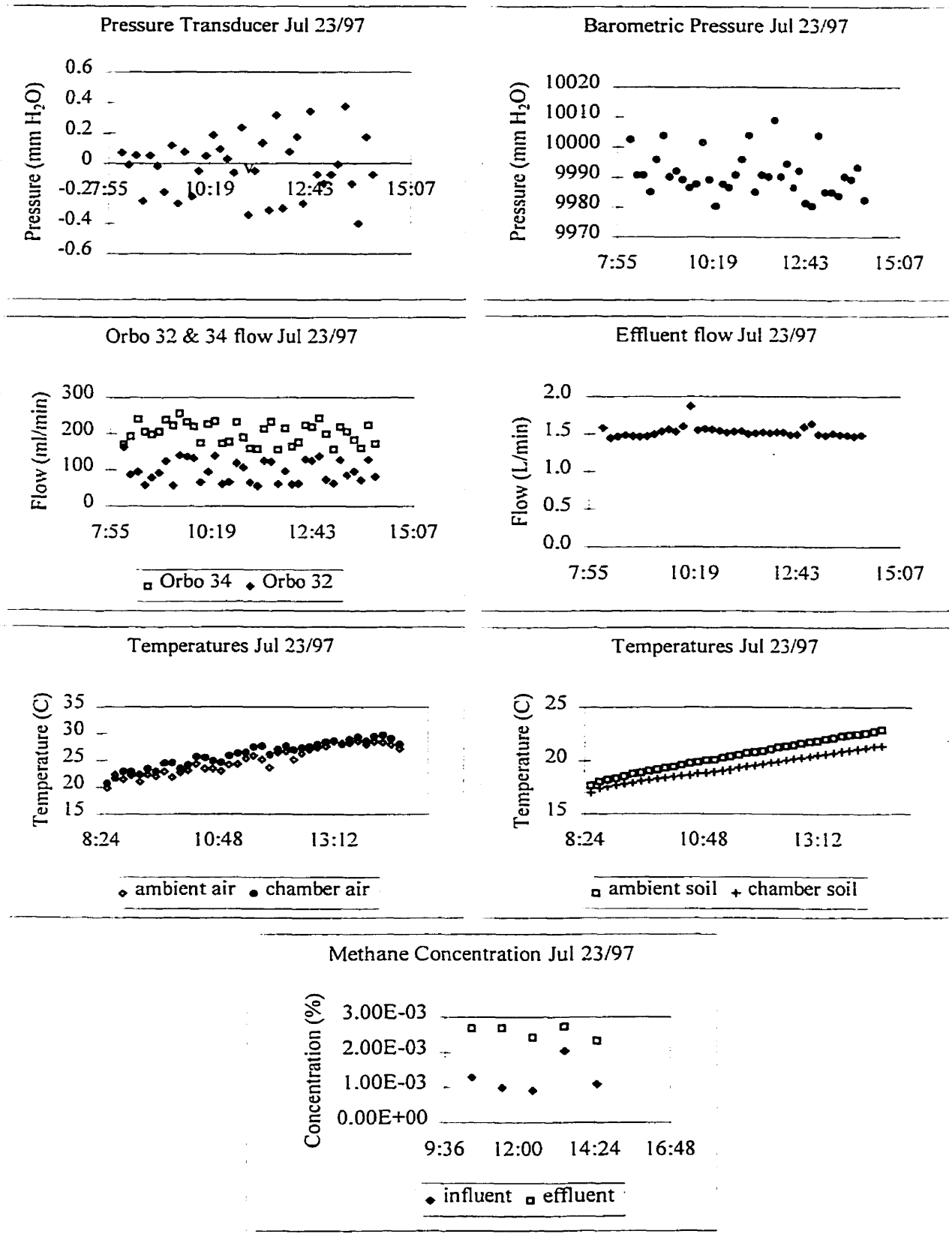

Figure D.9: Data from Waterloo Landfill flux measurements on Jul 23/97

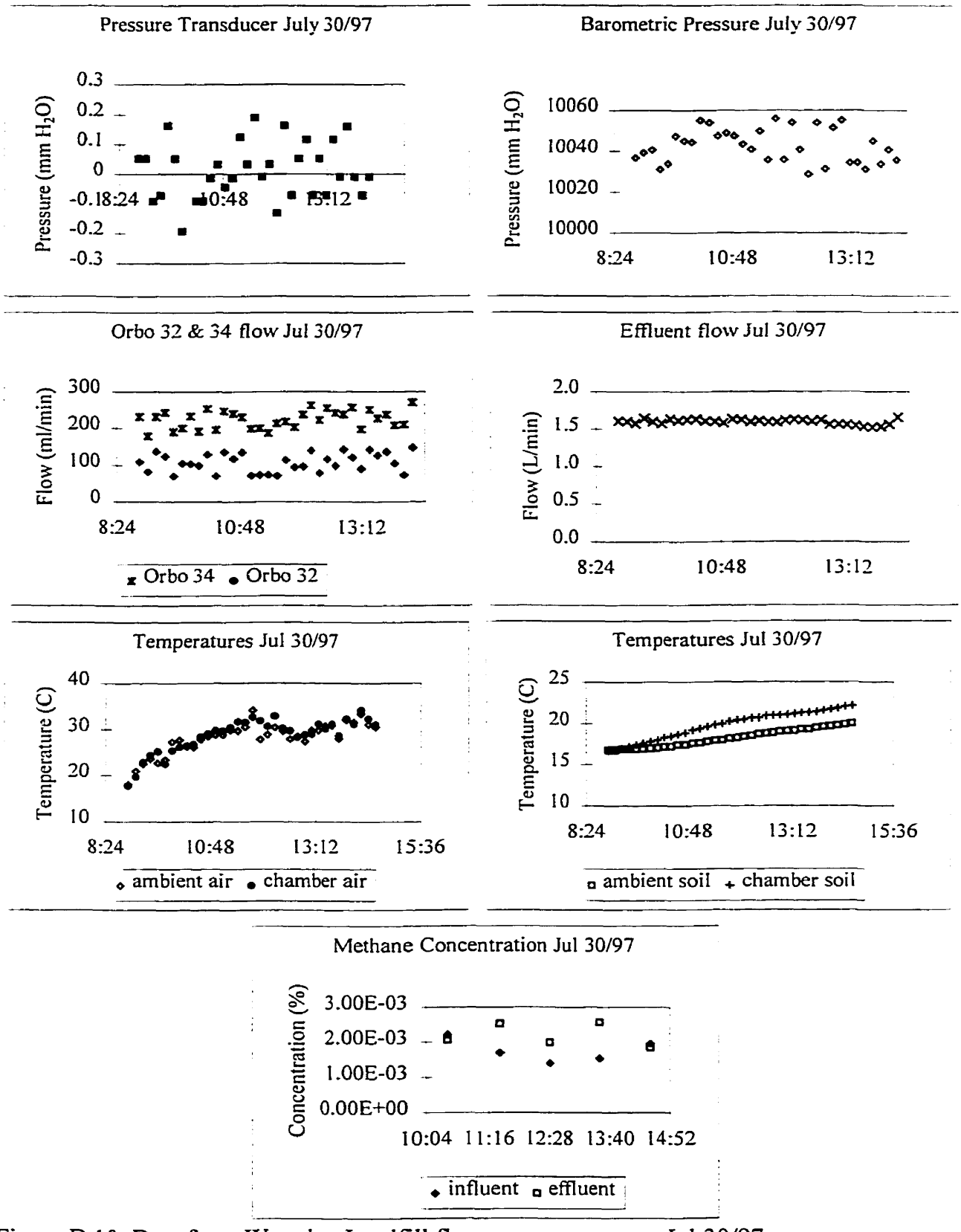

Figure D.10: Data from Waterloo Landfill flux measurements on Jul 30/97

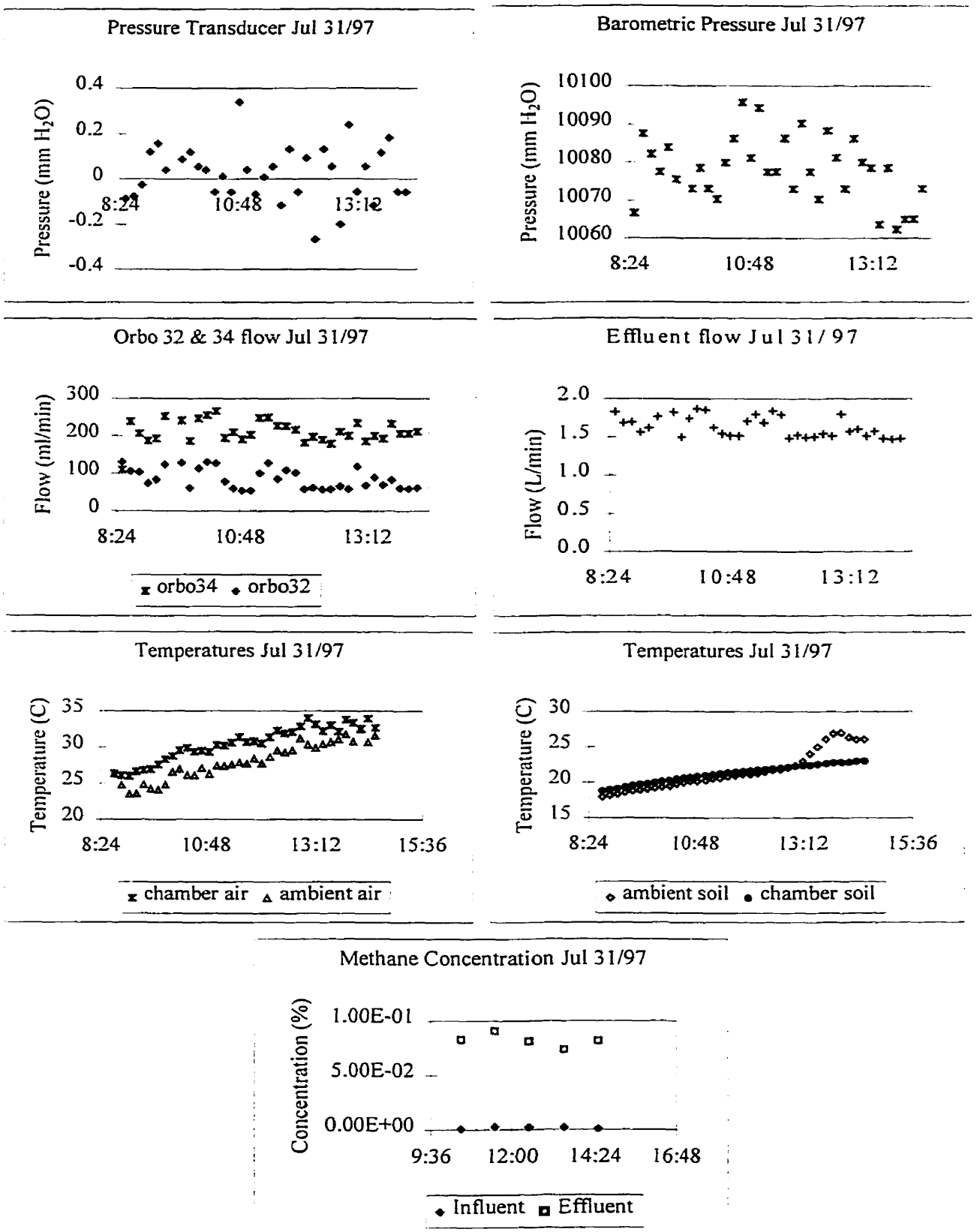

Figure D.11: Data from Waterloo Landfill flux measurements on Jul 31/97

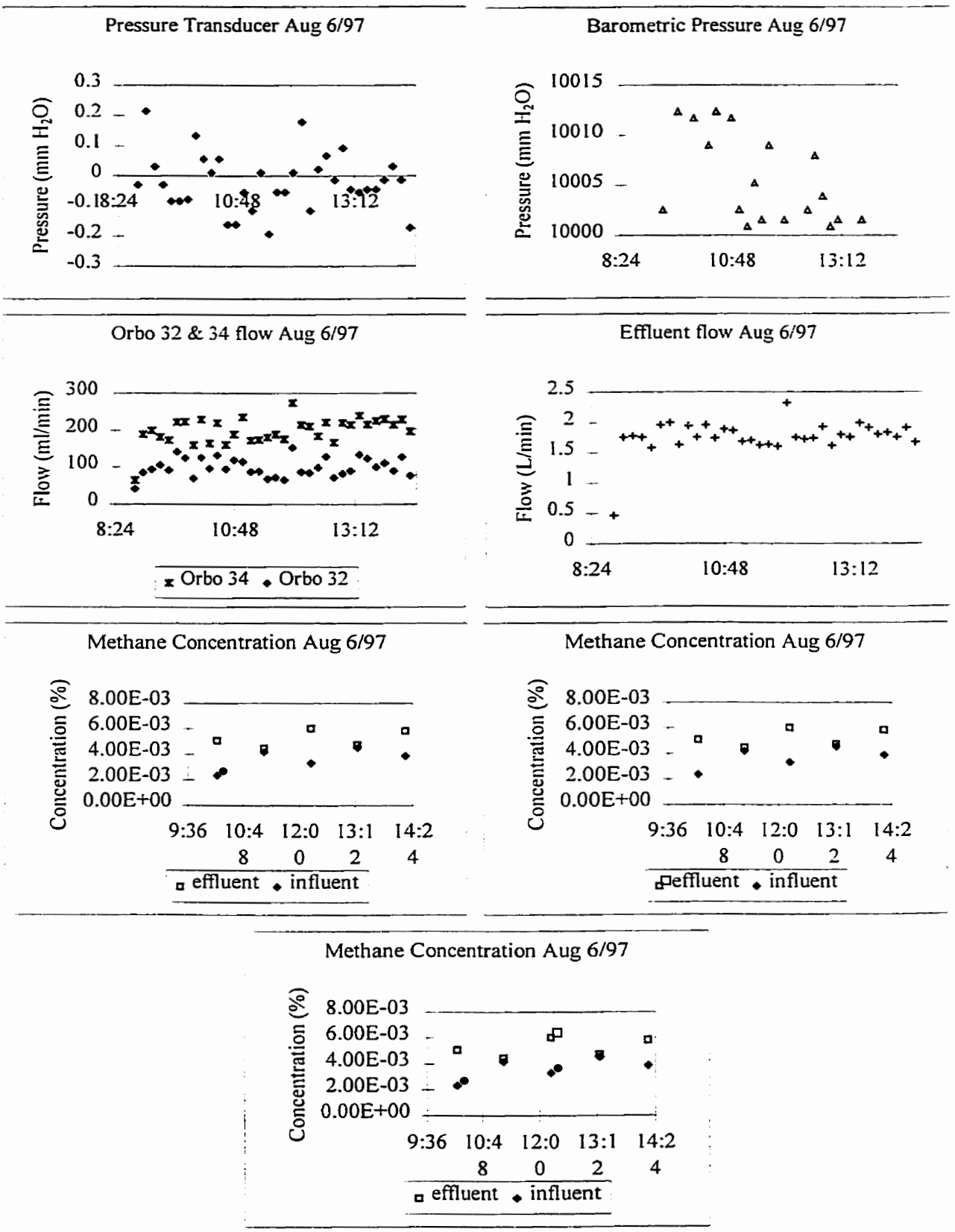

Figure D.12: Data from Waterloo Landfill flux measurements on Aug 6/97

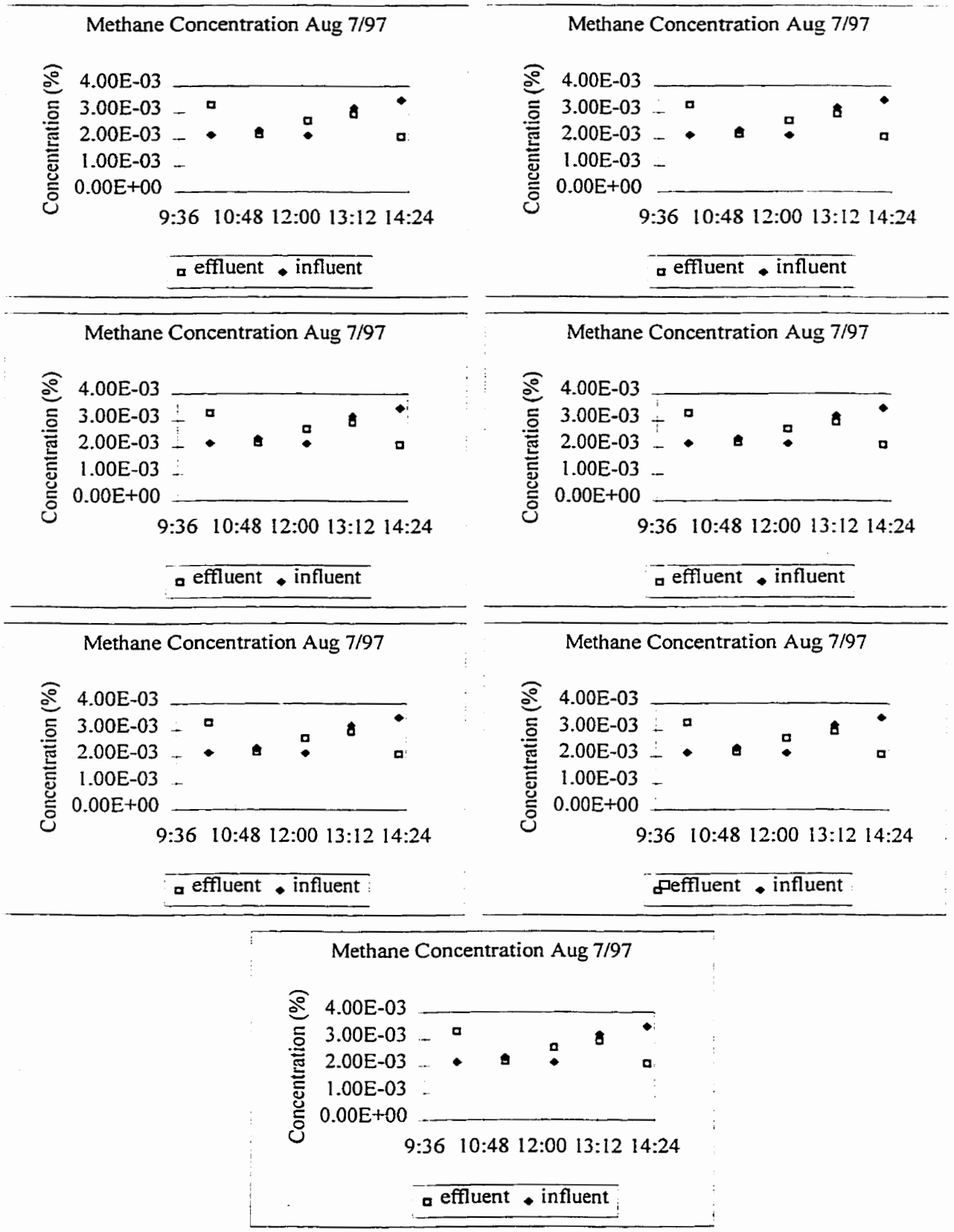

Figure D.13: Data from Waterloo Landfill flux measurements on Aug 7/97

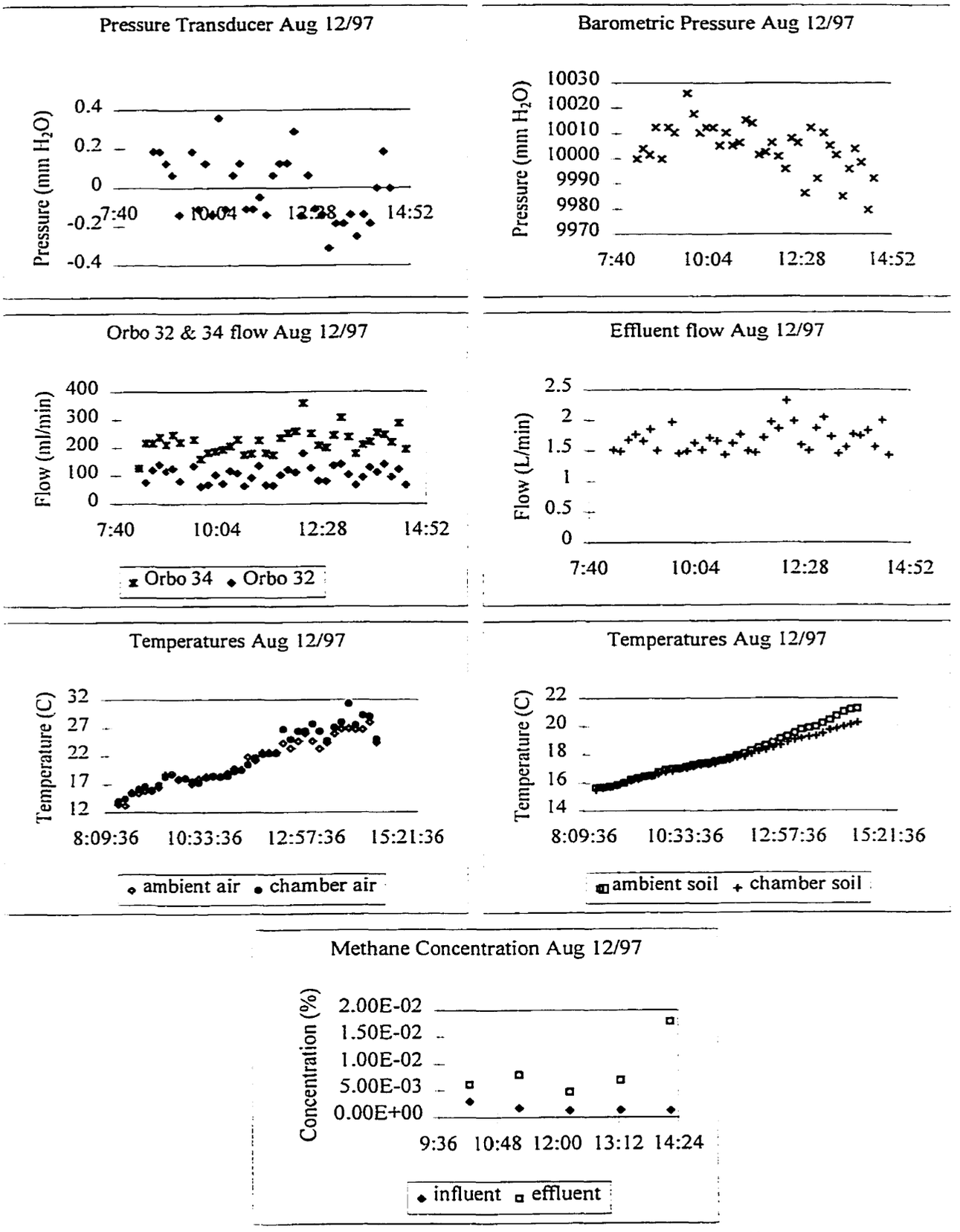

Figure D.14: Data from Waterloo Landfill flux measurements on Aug 12/97

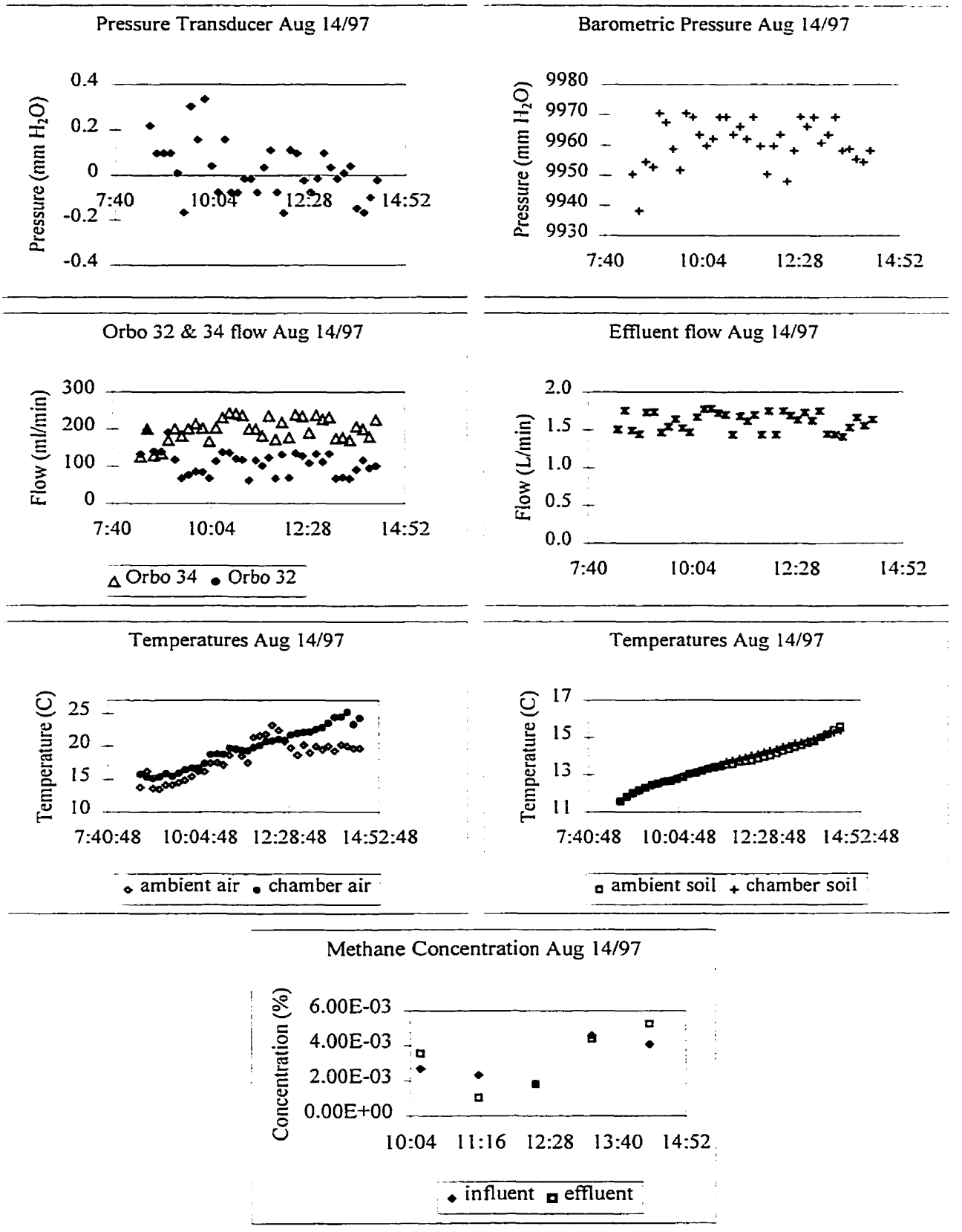

Figure D.15: Data from Waterloo Landfill flux measurements on Aug 14/97

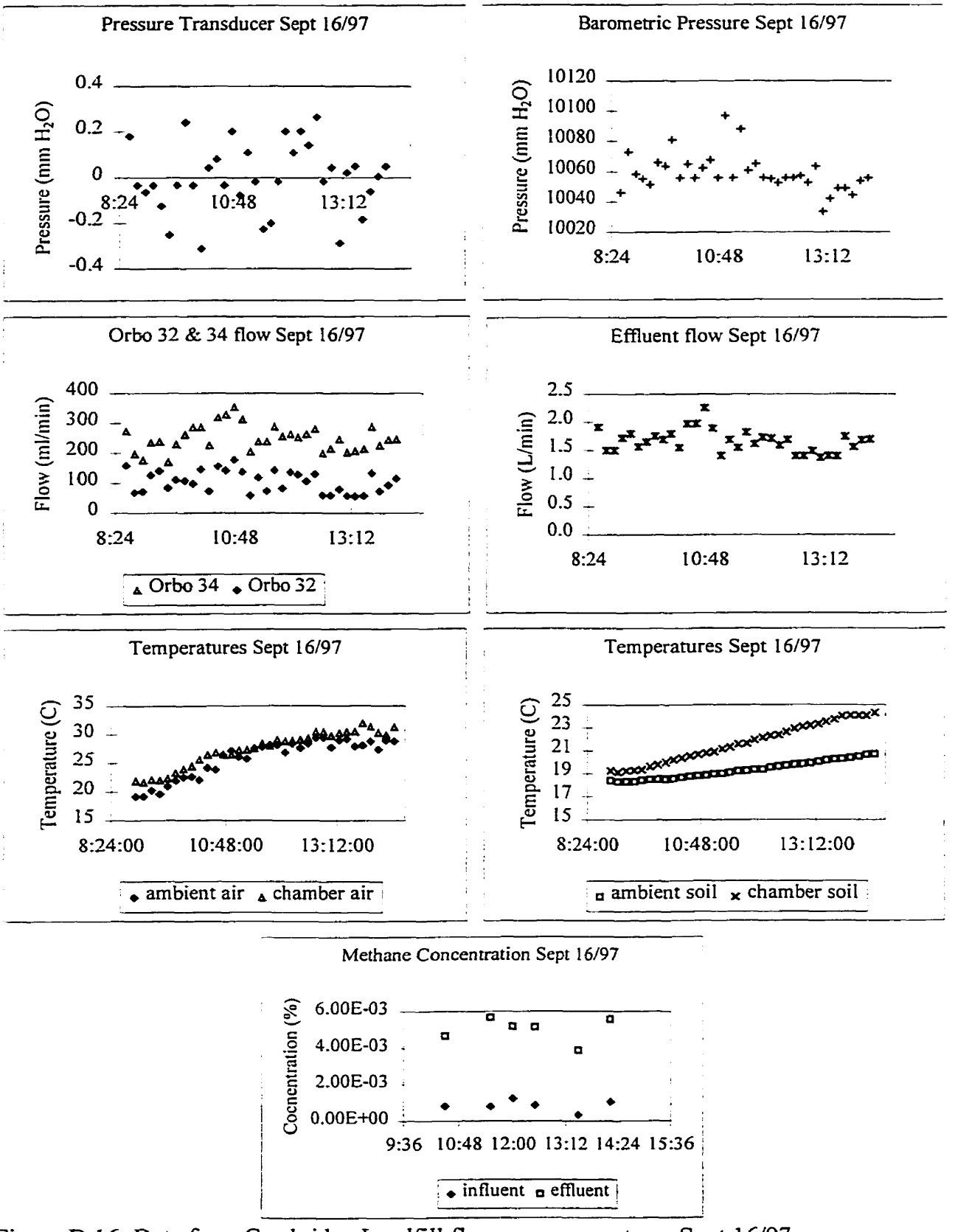

Figure D.16: Data from Cambridge Landfill flux measurements on Sept 16/97

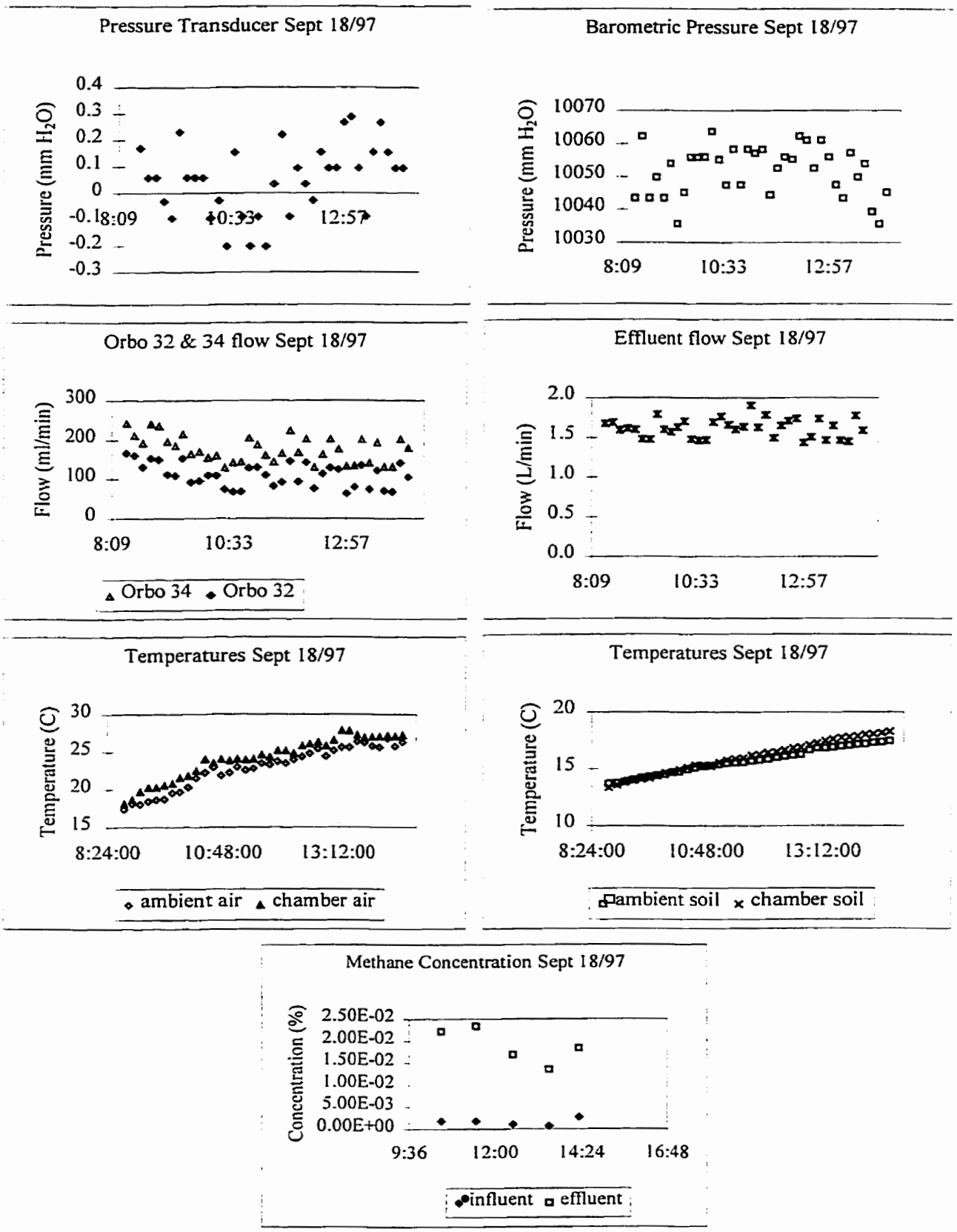

Figure D.17: Data from Cambridge Landfill flux measurements on Sept 18/97

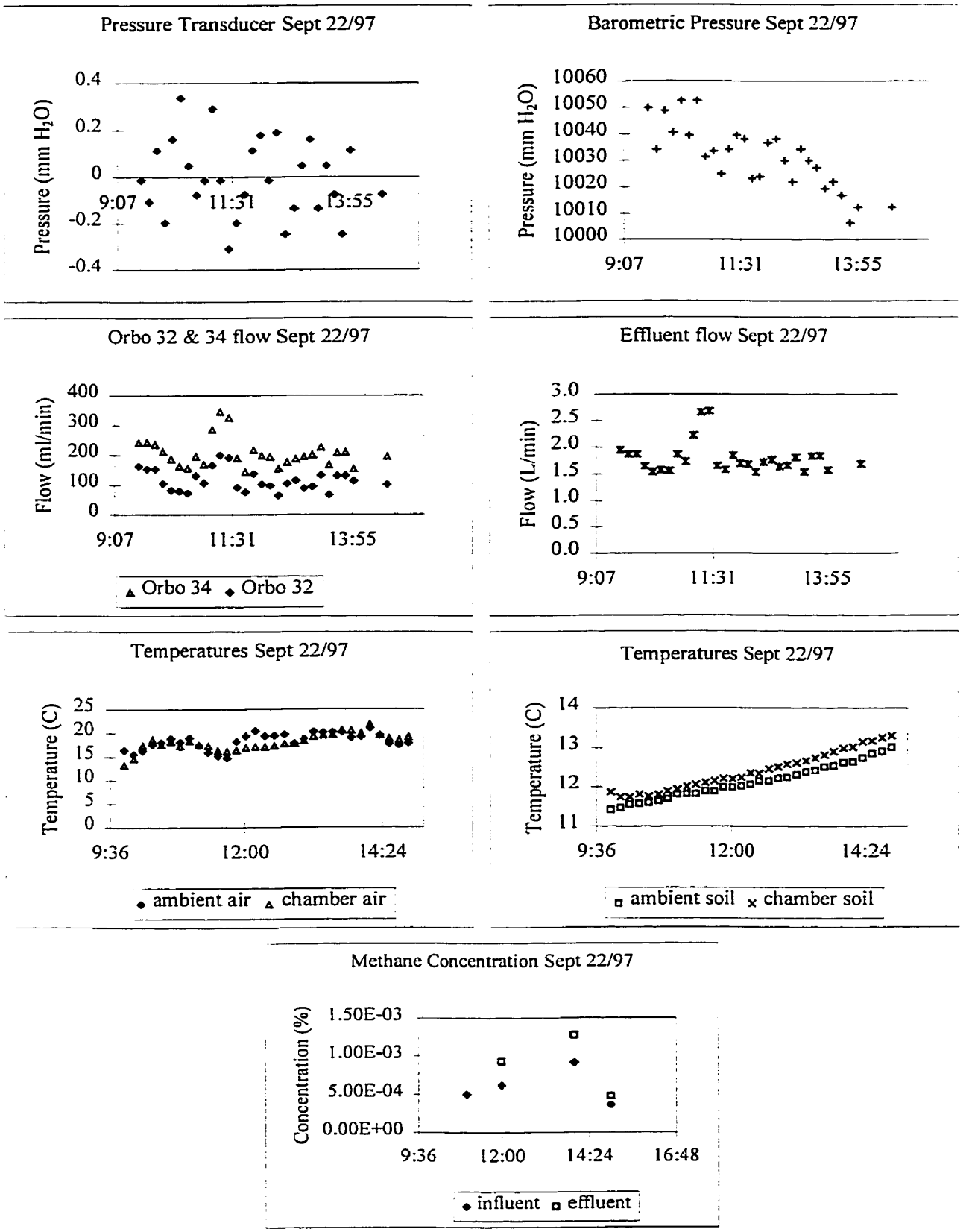

Figure D.18: Data from Stratford Landfill flux measurements on Sept 22/97

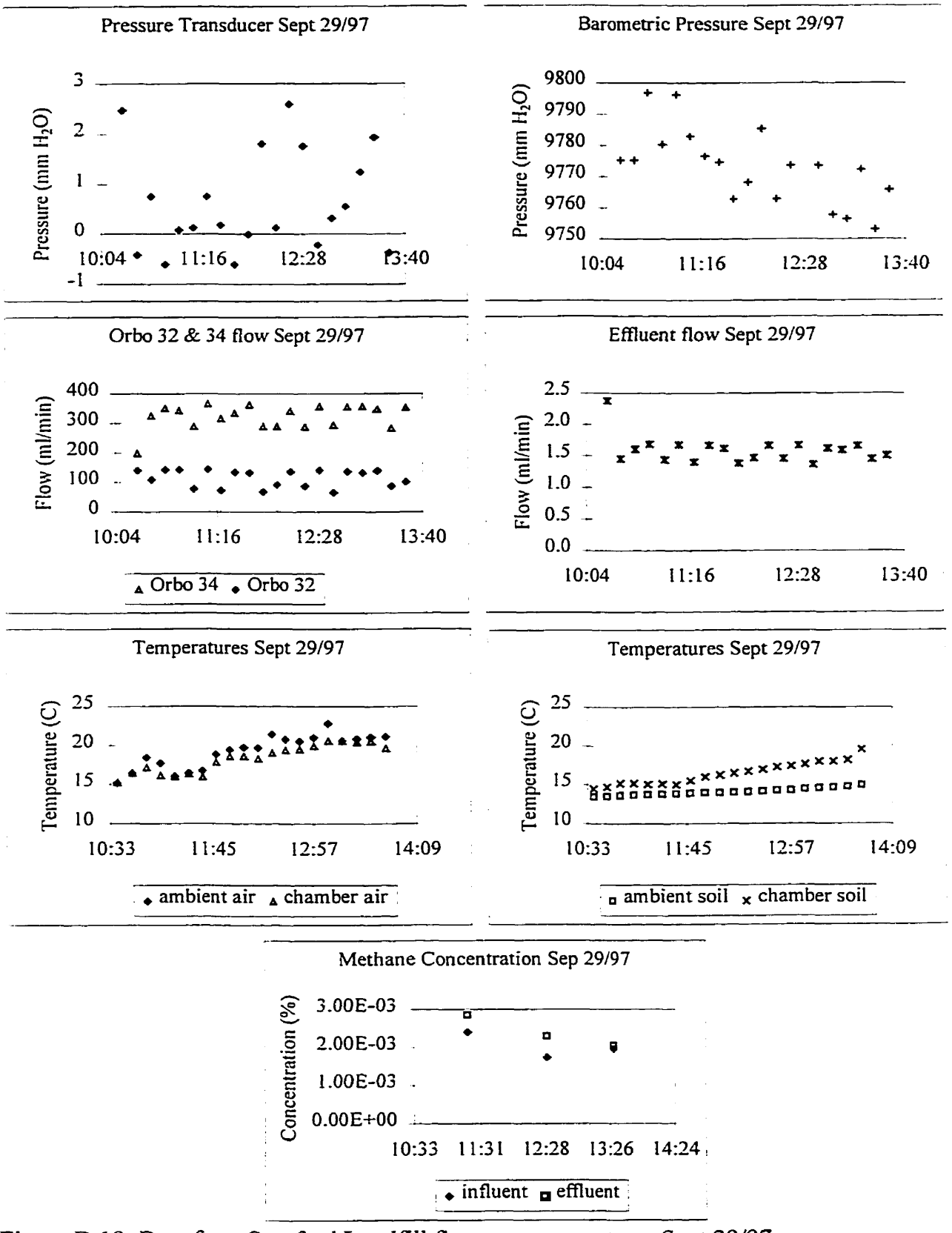

Figure D.19: Data from Stratford Landfill flux measurements on Sept 29/97

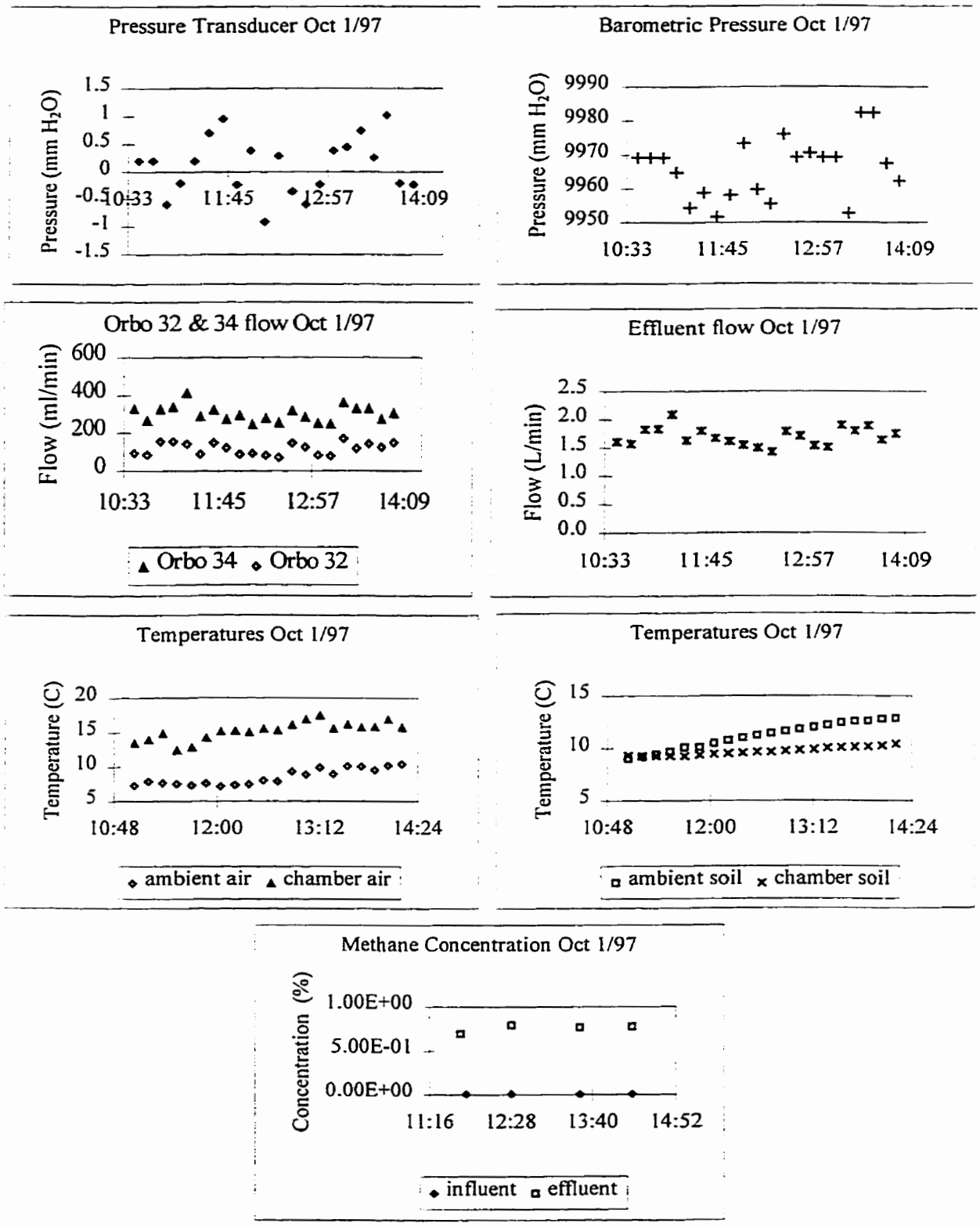

Figure D.20: Data from Waterloo Landfill flux measurements on Oct 1/97

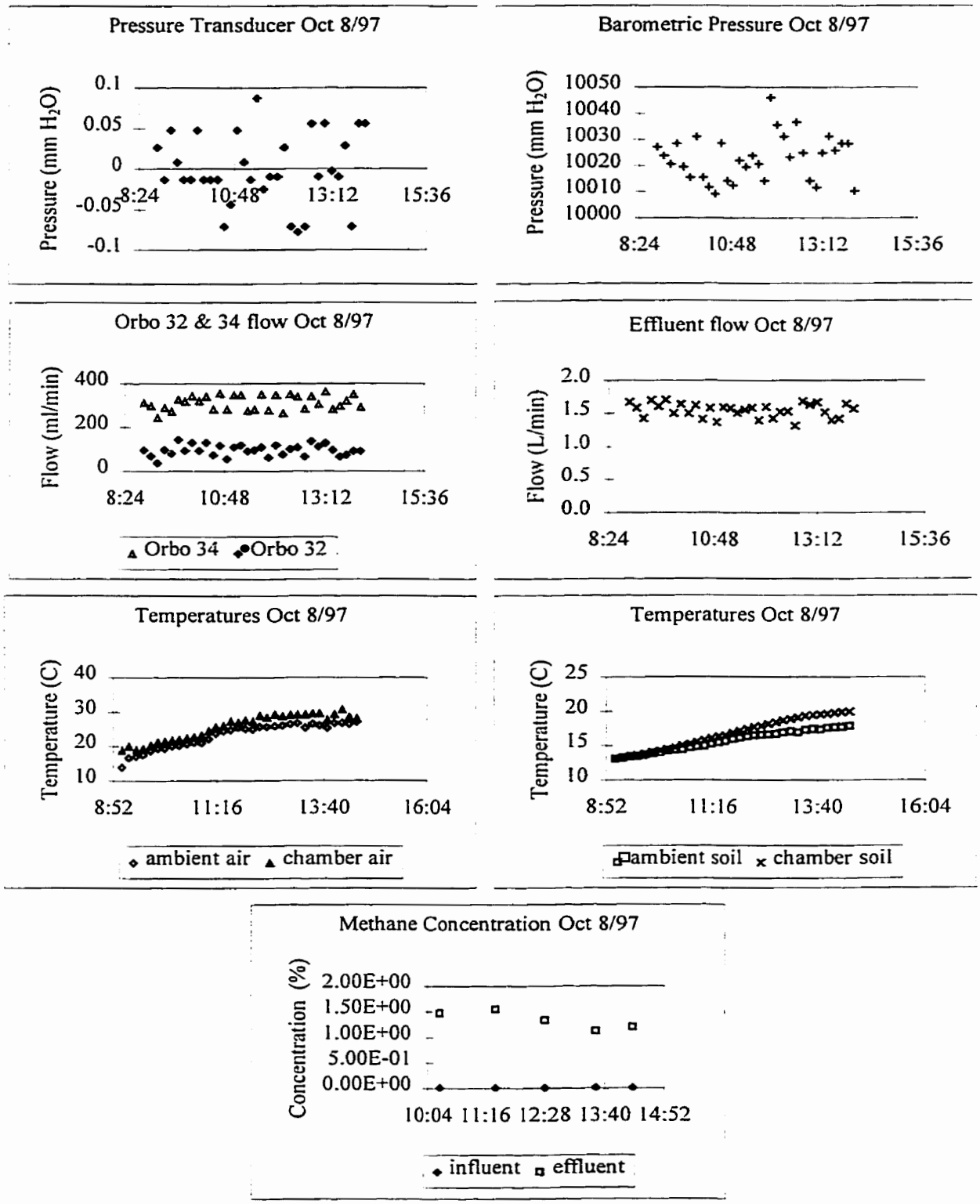

Figure D.21: Data from Waterloo Landfill flux measurements on Oct 8/97

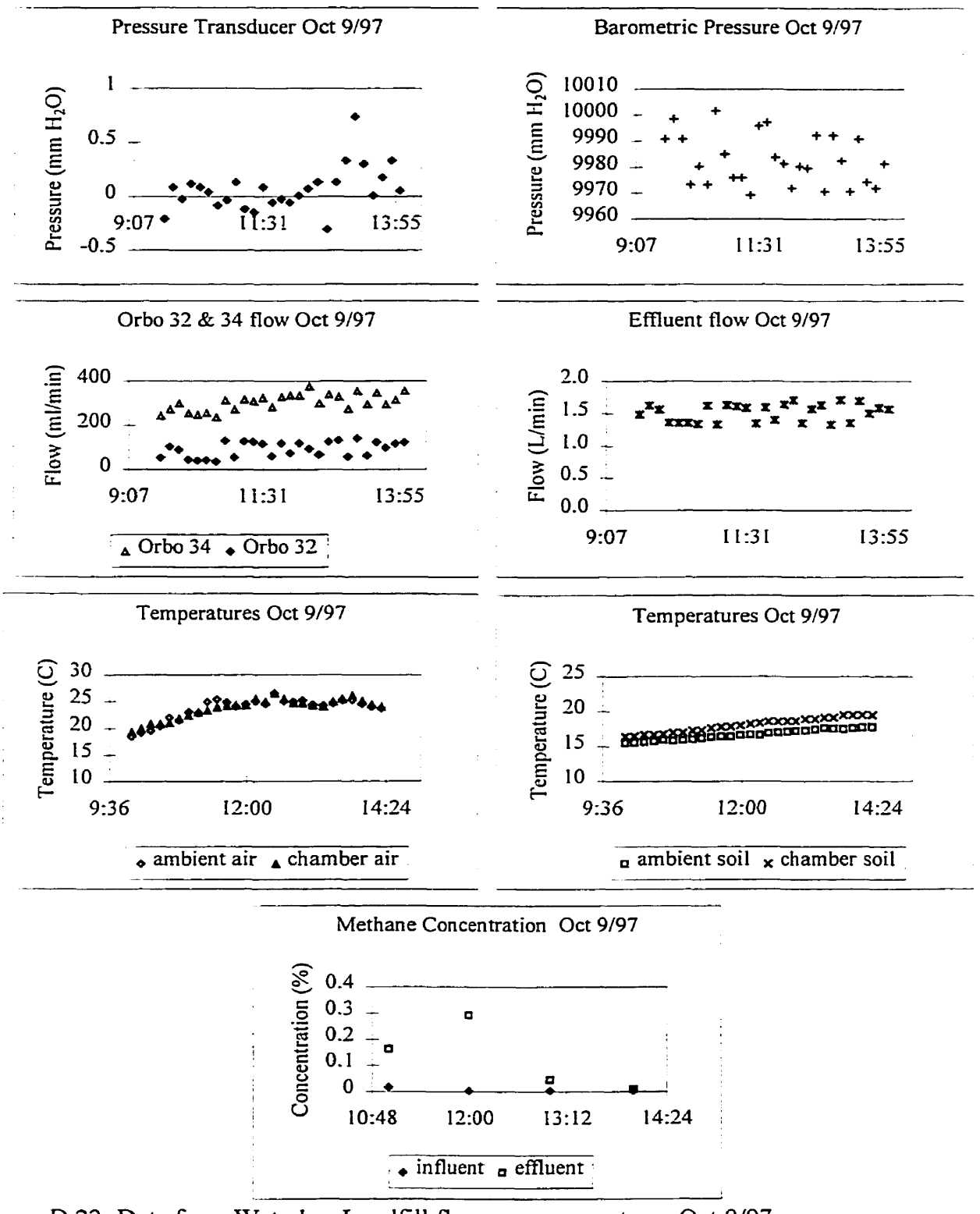

Figure D.22: Data from Waterloo Landfill flux measurements on Oct 9/97

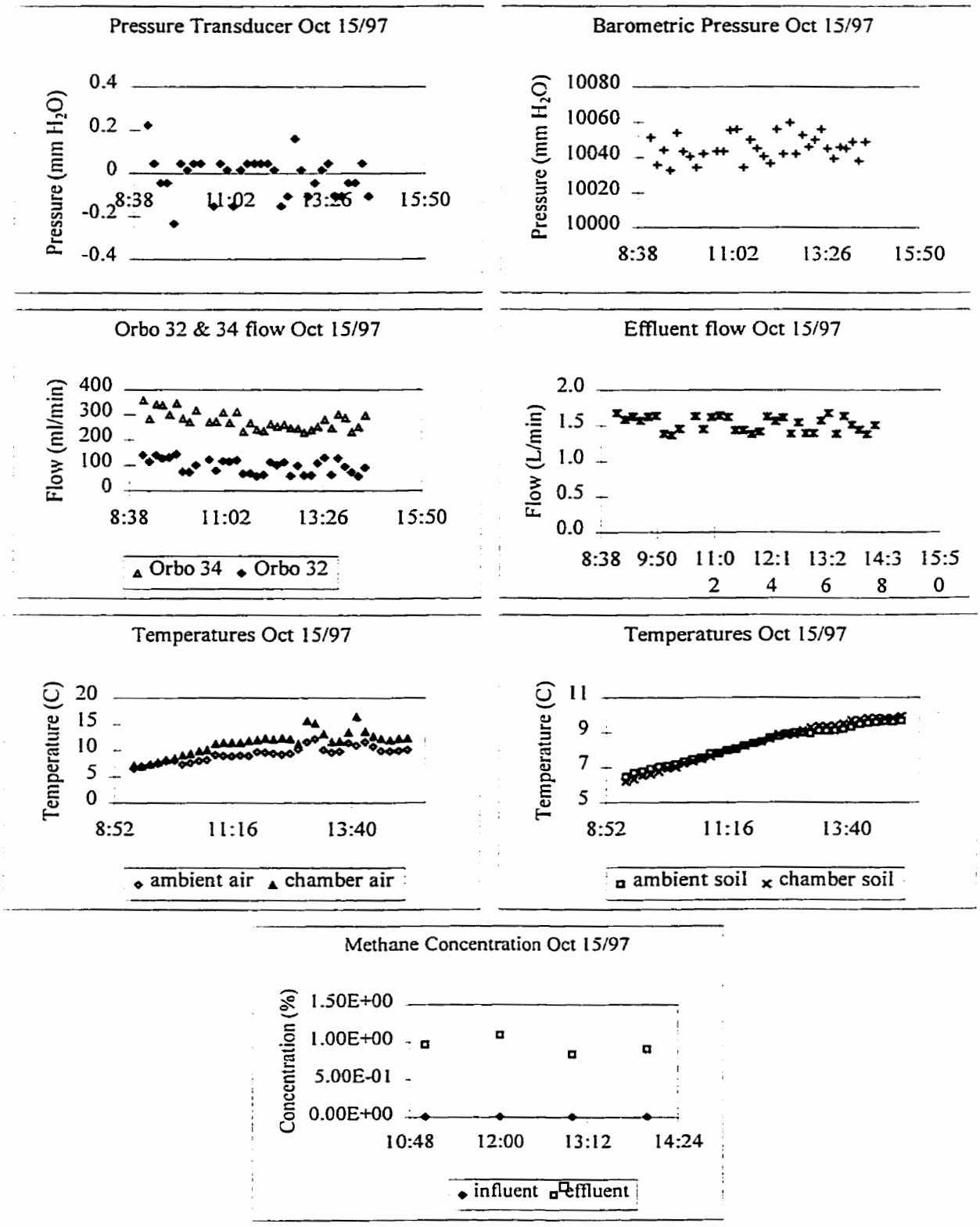

Figure D.23: Data from Waterloo Landfill flux measurements on Oct 15/97

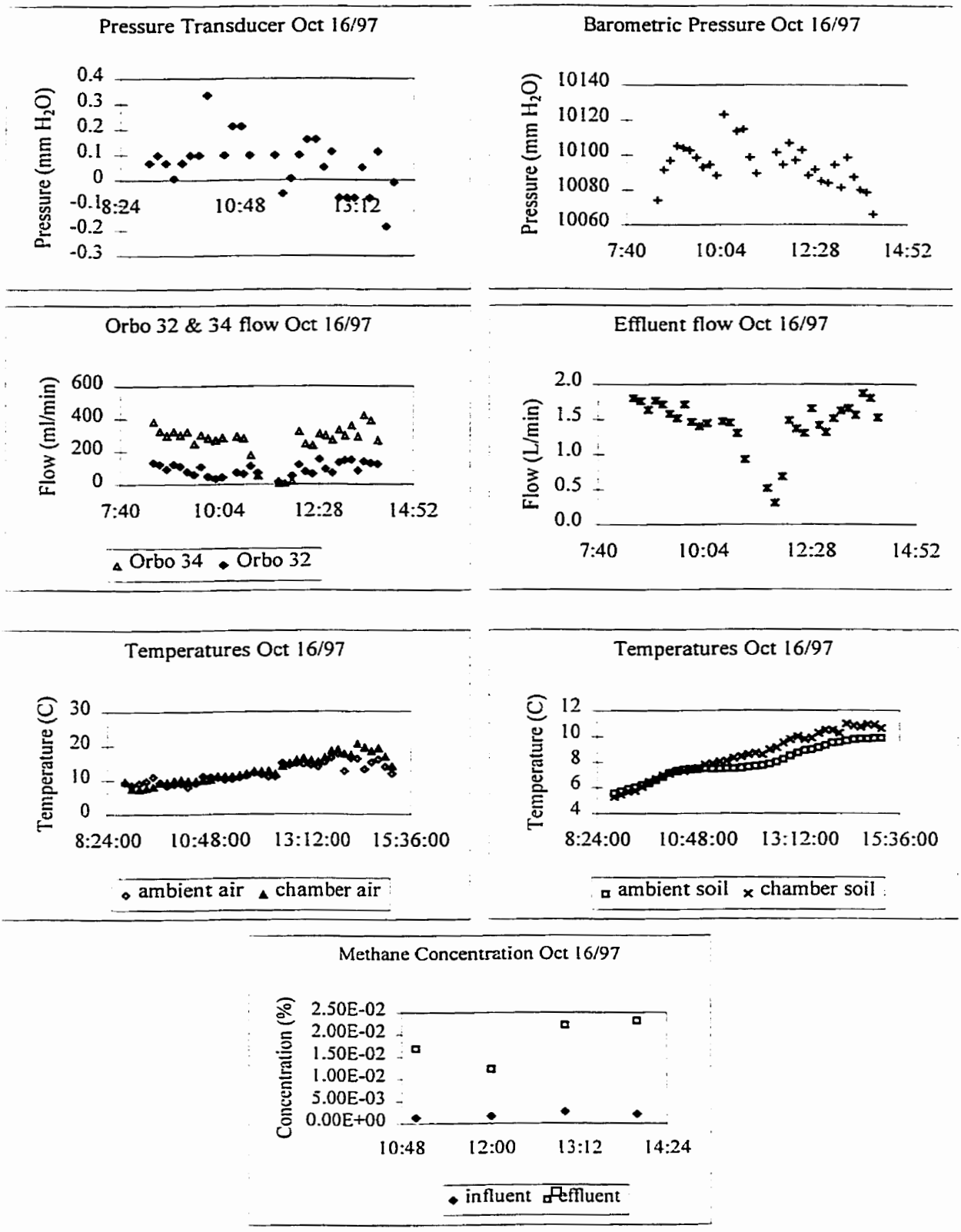

Figure D.24: Data from Waterloo Landfill flux measurements on Oct 16/97

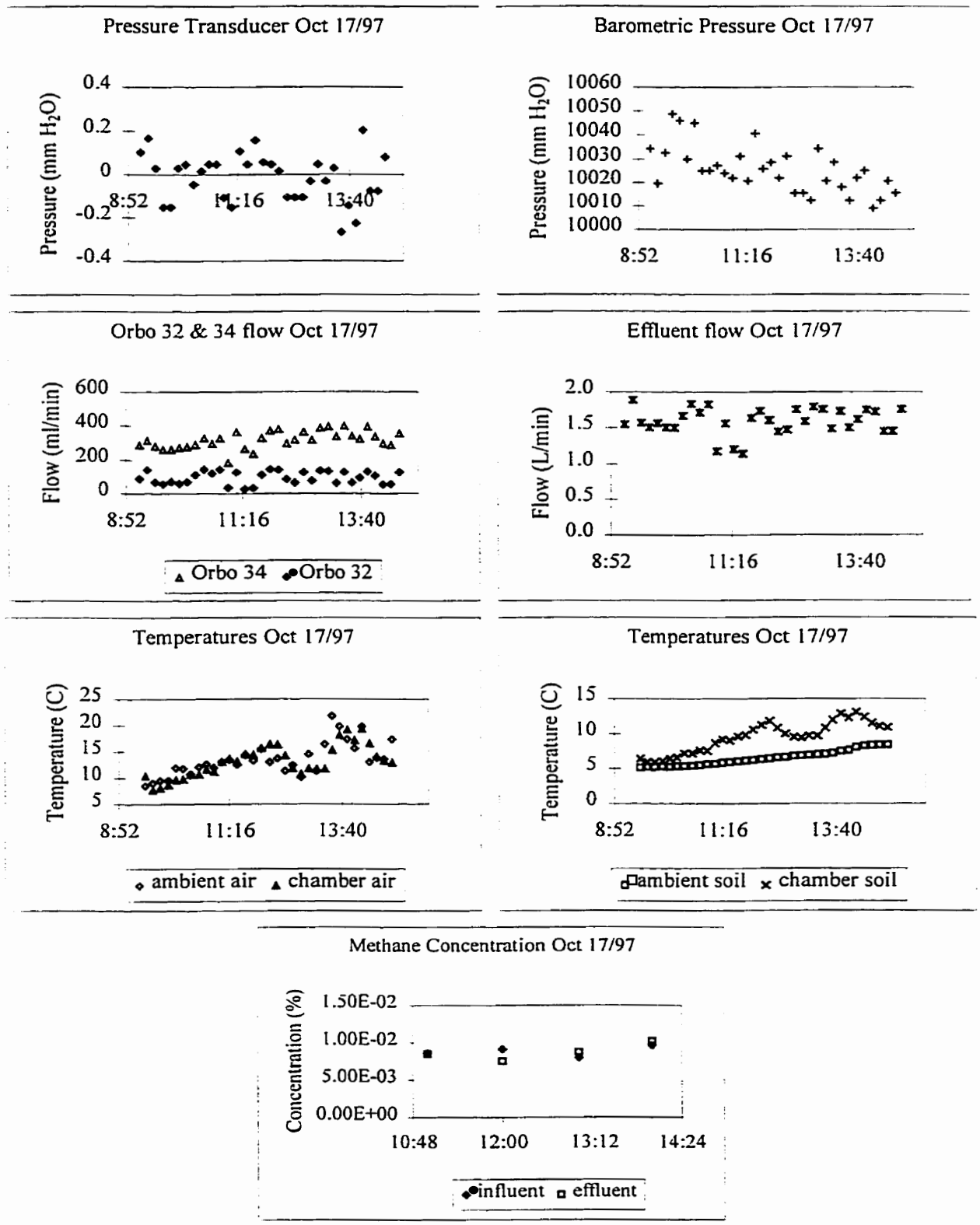

Figure D.25: Data from Waterloo Landfill flux measurements on Oct 17/97

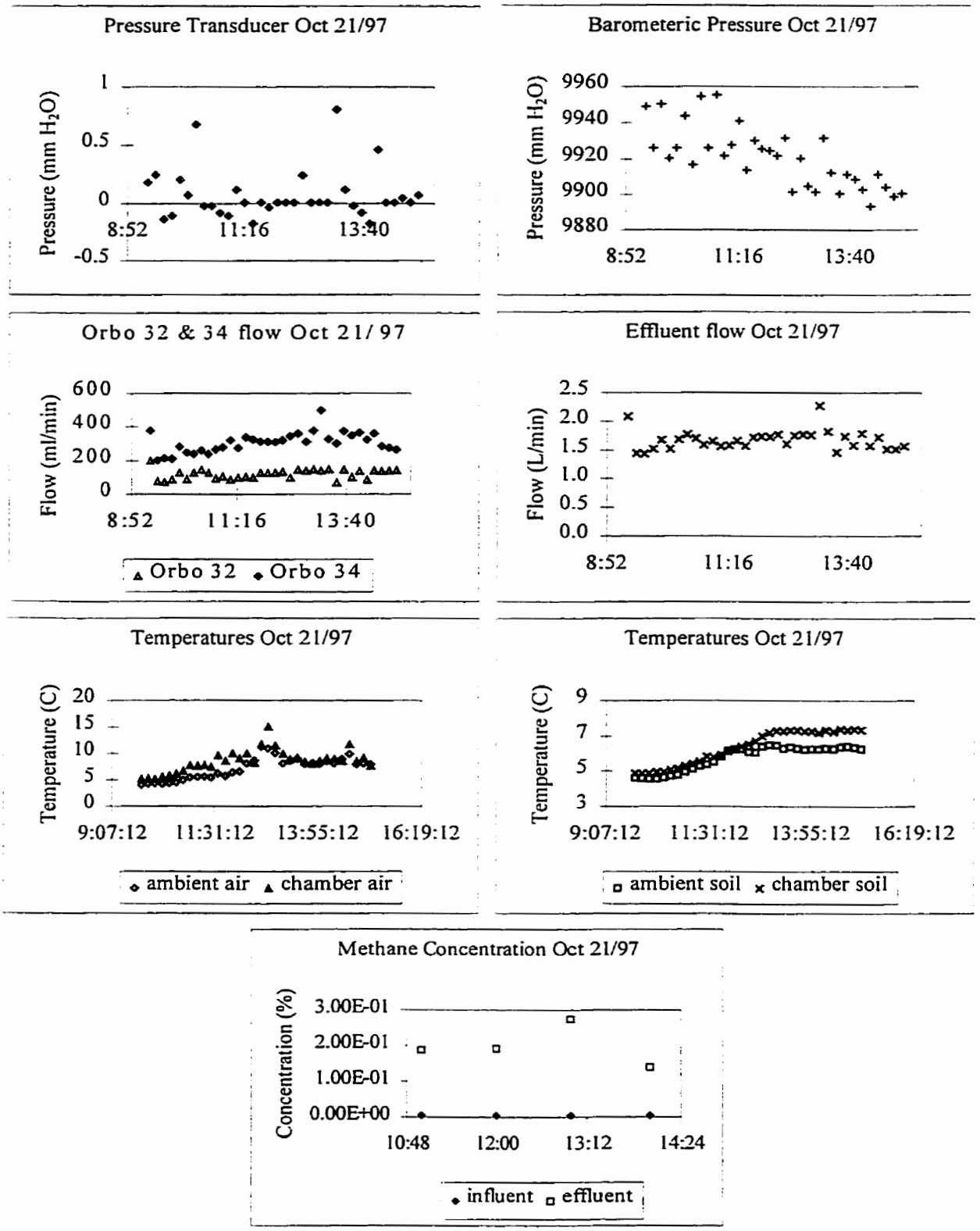

Figure D.26: Data from Waterloo Landfill flux measurements on Oct 21/97

Appendix E

Conversion of the VOC and H_2S values to ½ hour and 24 hour average values

Appendix E: Conversion of the VOC and H_2S values to ½ hour and 24 hour average values.

The conversion of the VOCs and H_2S values to ½ hour and 24 hour values was performed using the following equation and table. The equation is

$$X_s = X_l(t_l/t_s)^p$$

where:

X_s = concentration for the shorter averaging time

X_l = concentration for the longer averaging time

t_l = longer averaging time

t_s = shorter averaging time

p = exponent as follows:

Atmospheric Stability	Exponent p
A –convective	0.5
B	0.5
C- neutral	0.33
D	0.2
E	0.167
F – very stable	0.167

The atmospheric stability class for each sample date was determined from the average wind velocity over the sample time frame. The average wind velocity was determined from the hourly data obtained from the Waterloo and Cambridge Landfill's weather stations. Some of the missing wind velocities were approximated from Enviroment Canada's weather website or assuming an "A" atmospheric stability class. Using the wind velocity and strong insolation, the stability classes were selected. The wind velocity and stability class for each sample date are shown in the following table. The collection time for each sample are also shown in the following table.

Sample Calculation:

Using sample date: Jun 25/97, and TCE influent concentration

X_l = 1 ug/m3, t_l = 4.4 hours, t_s = ½ hour, p = 0.33 (Stability Class – C)

$$X_s = 1(4.4/0.5)^{0.33}$$

$$X_s = 2.06 ug/m^3$$

Table E.1: Wind velocities and stability classes used during field sampling periods

Date	Wind velocity (m/s)	Stability Class	Influent VOC & H_2S (min)	Effluent VOC (hrs)	Effluent H_2S (hrs)
Waterloo Landfill					
19-Jun-97	1.8	A	284	4.38	4.38
25-Jun-97	6.6	C	271	4.40	4.45
26-Jun-97	3.3	B	336	5.00	4.97
3-Jul-97	4.6	B	280	4.10	4.03
9-Jul-97	3.6	B	309	4.62	4.60
10-Jul-97	2.6	A-B	323	5.22	5.28
15-Jul-97	2.4	A	326	5.07	5.17
22-Jul-97		Assummed A for Jul 22-Aug 7	361	5.40	5.47
23-Jul-97			294	4.98	4.98
30-Jul-97			304	4.68	4.68
31-Jul-97			316	4.87	4.85
6-Aug-97			301	4.82	4.83
7-Aug-97			326	5.08	5.10
12-Aug-97	4.6	B	335	5.13	5.08
14-Aug-97	2.6	A	322	5.05	5.03
1-Oct-97	5.2	C	187	2.60	2.58
8-Oct-97	2.1	B	300	4.53	4.52
9-Oct-97	4.9	C	240	3.37	3.35
15-Oct-97	1.9	A	307	4.20	4.13
16-Oct-97	3.7	B	281	3.77	3.73
17-Oct-97	2.2	A	250	4.43	4.40
21-Oct-97	4.3	B	208	3.48	3.50
Cambridge Landfill					
16-Sep-97	1.6	A	314	4.58	4.55
18-Sep-97	3.2	B	215	4.78	4.73
Stratford Landfill					
22-Sep-97	4.9	B	299	4.00	4.00
29-Sep-97	6.2	C	196	2.85	2.80

Reference:
MOE, 1996, Technical Bulletin, Odour Impacts- An Overview Science and Technology branch, environmental engineering services STB Technical Bulletin No. EES-1 February, 1996.

Appendix F

Constants used to calculate viscosity and diffusion coefficients for the gas mixture in the model

Appendix F: Constants used to calculate viscosity and diffusion coefficients for the gas mixture in the model

Table F.1: Constants used to calculate viscosity and diffusion coefficients for the gas mixture in the model

Gas	Molecular Weight g/mole	Characteristic length, σ A°	ε/k K
Methane (CH_4)	16.0426	3.758	148.6
Nitrogen (N_2)	28.0134	3.798	71.4
Oxygen (O_2)	31.9988	3.467	106.7
Carbon Dioxide(CO_2)	44.0098	3.941	195.2
Vinyl Chloride	62.4987	4.644	348.9
Hydrogen Sulphide (H_2S)	34.0758	3.623	301.1

Values obtained from Reid *et al.*, (1977)

Appendix G
Model Validation against Analytical Equation

Appendix G Model Validation against Analytical Equation

Model validation consisted of comparing the LES model output with an analytical equation. The LES model was simplified so that only the bottom cell of the waste column was producing gas at a constant rate over time. The analytical equation was an analytical solution to the advection-dispersion equation with the following assumptions (van Genuchten & Alves. 1982). The initial and boundary conditions are

$$c(x,0) = C_i$$

$$(-D\frac{\partial c}{\partial x} + vc)\Big|_{x=0} = \begin{cases} vC_o & 0 < t \le t_o \\ 0 & t > t_o \end{cases}.$$

$$\frac{\partial c}{\partial x}(\infty, t) = 0$$

The analytical solution is

$$c(x,t) = \begin{cases} C_i + (C_o - C_i)A(x,t) & 0 < t \le t_o \\ C_i + (C_o - C_i)A(x,t) - C_o A(x, t - t_o) & t > t_o \end{cases}$$

where

$$A(x,t) = \frac{1}{2}erfc\left[\frac{Rx - vt}{2(DRt)^{1/2}}\right] + (\frac{v^2 t}{\pi DR})^{1/2}\exp\left[-\frac{(Rx - vt)^2}{4DRt}\right]$$
$$-\frac{1}{2}(1 + \frac{vx}{D} + \frac{v^2 t}{DR})\exp(\frac{vx}{D})erfc\left[\frac{Rx + vt}{2(DRt)^{1/2}}\right]$$

R = retardation factor (assummed to be one),

v = darcy's velocity (m/s),

D = disperison coefficient (m/s),

t = time (s),

x = distance or depth (m),

$$C_o = \frac{P}{A\phi_g v},$$

A = surface area of cell (m^2),

P = production rate of gas (mol/s),

c = concentration (mol/m^3), and

ϕ_g= gas porosity (dimensionless).

Figure G.1 shows comparison between the LES model output and the analytical equation at three different time intervals (50 days, 100 days and 200 days). The comparisons are excellent and thus the LES model is validated under the conditions selected for this case.

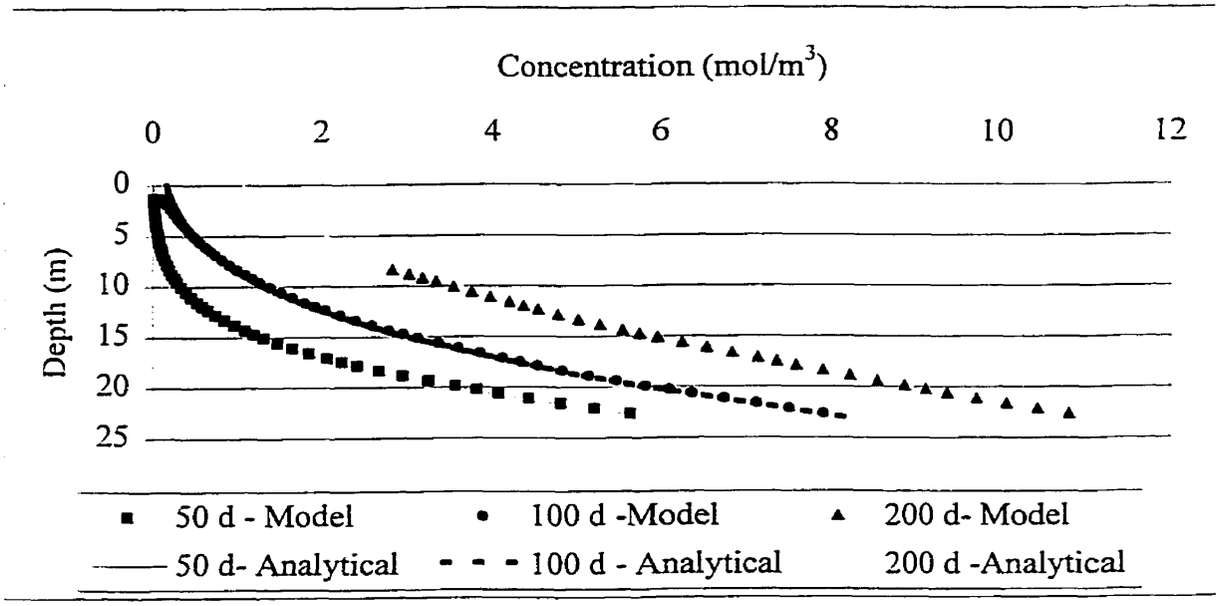

Figure G.1: Comparison between model output and analytical equation at 3 time intervals

Reference

van Genuchten, M. Th., and Alves. W. J., (1982), *Analytical Solutions of the One-Dimensional Convective-Dispersive Solute Transport Equation.* U.S.Department of Agriculture, Technical Bulletin No. 1661.

Appendix H

Profiles of CO_2, vinyl chloride and H_2S concentrations with depth at three time intervals

Appendix H: Profiles of CO_2, vinyl chloride and H_2S concentrations with depth at three time intervals

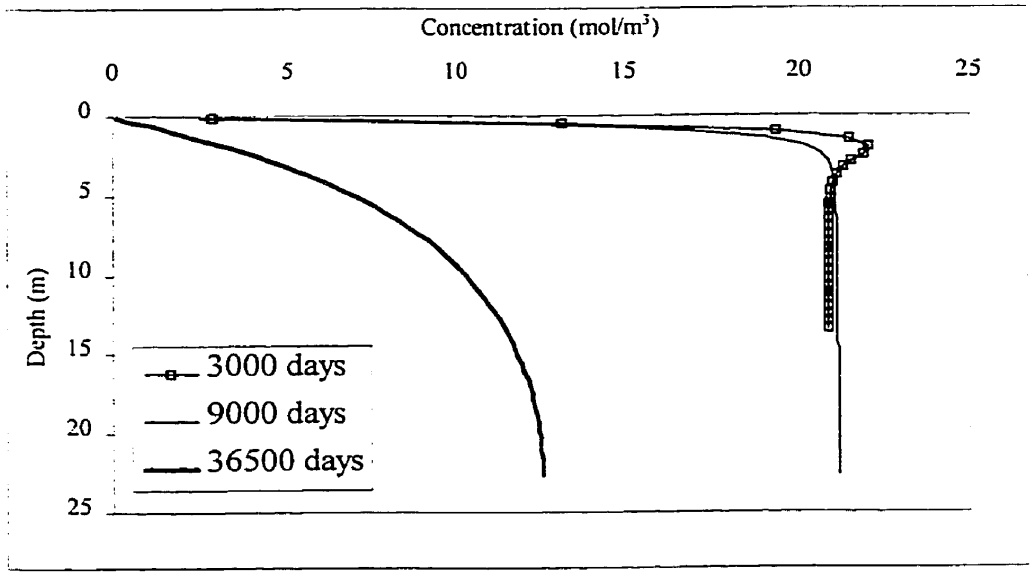

Figure H.1: CO_2 profile in waste column for the base case at three different time intervals.

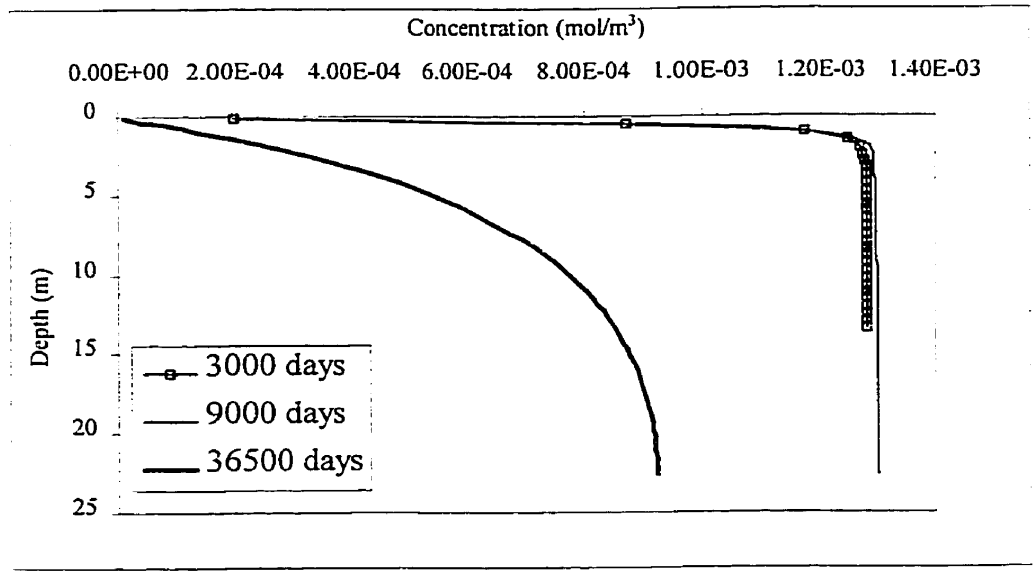

Figure H.2: Vinyl chloride profile in waste column for the base case at three different time intervals.

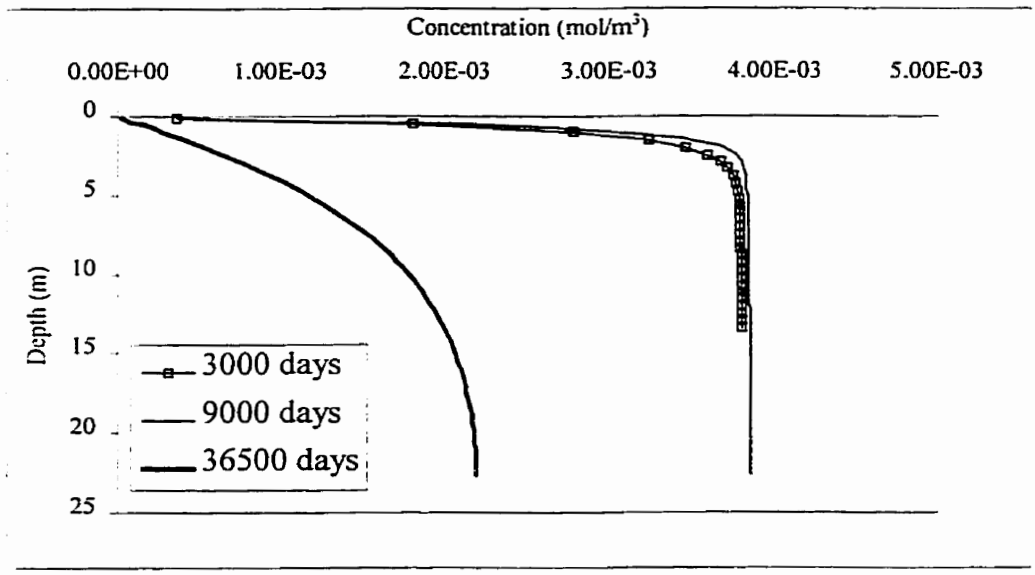

Figure H.3: H_2S profile in waste column for the base case at three different time intervals

Appendix I

Stability curves and weather data used in dispersion calculations

Appendix I: Stability curves and weather data used in dispersion calculations

The downwind position, x, as well as the atmospheric stability conditions determine the horizontal and vertical deviations (σ_y, σ_z) or dispersion of the emitted plume. One widely accepted set of curves correlating the deviation and x-distance is shown in Figures I.1 and I.2.

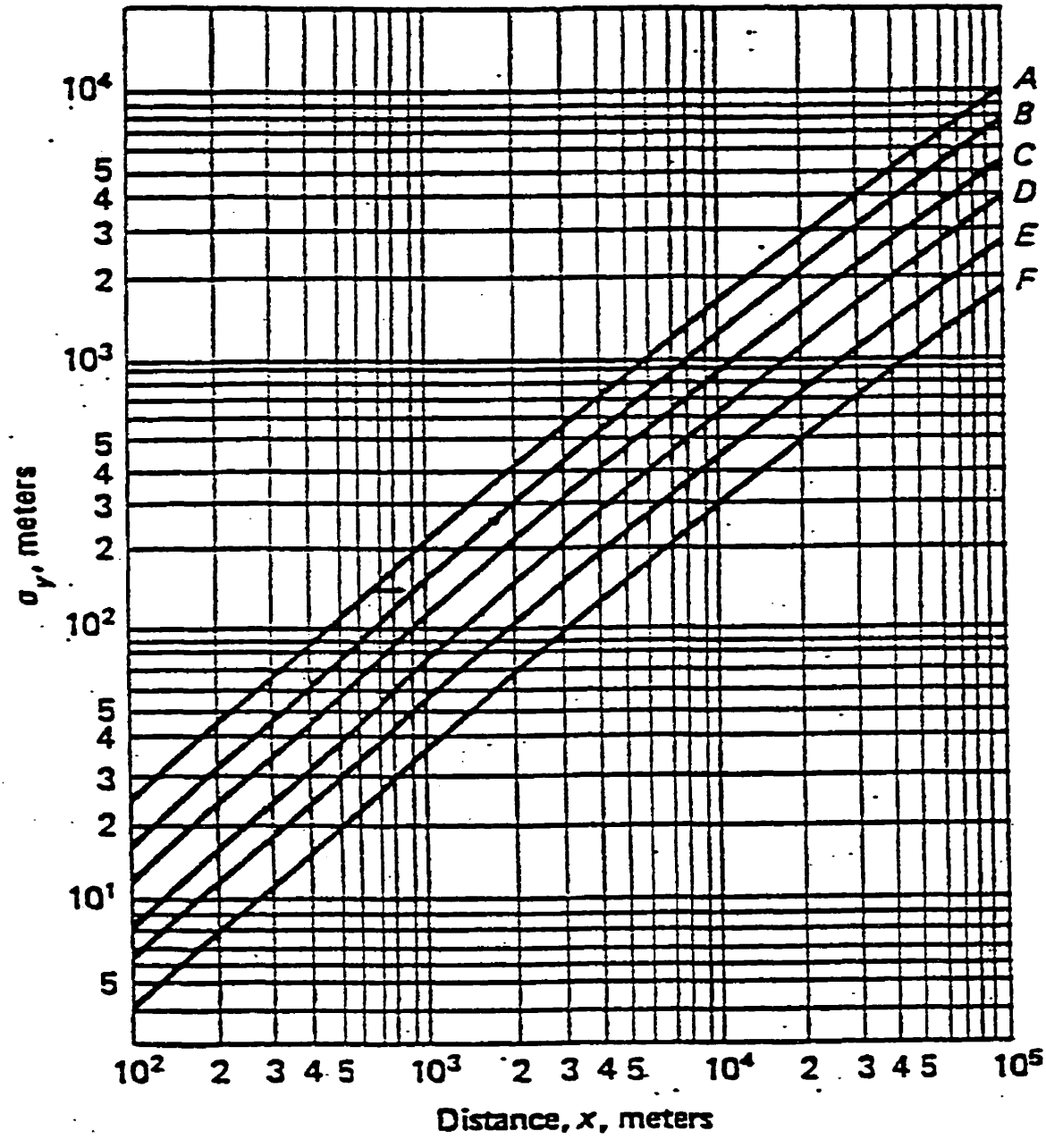

Figure I.1: Standard deviation σ_y, in the crosswind direction as a function of distance downwind (Wark & Warner, 1981)

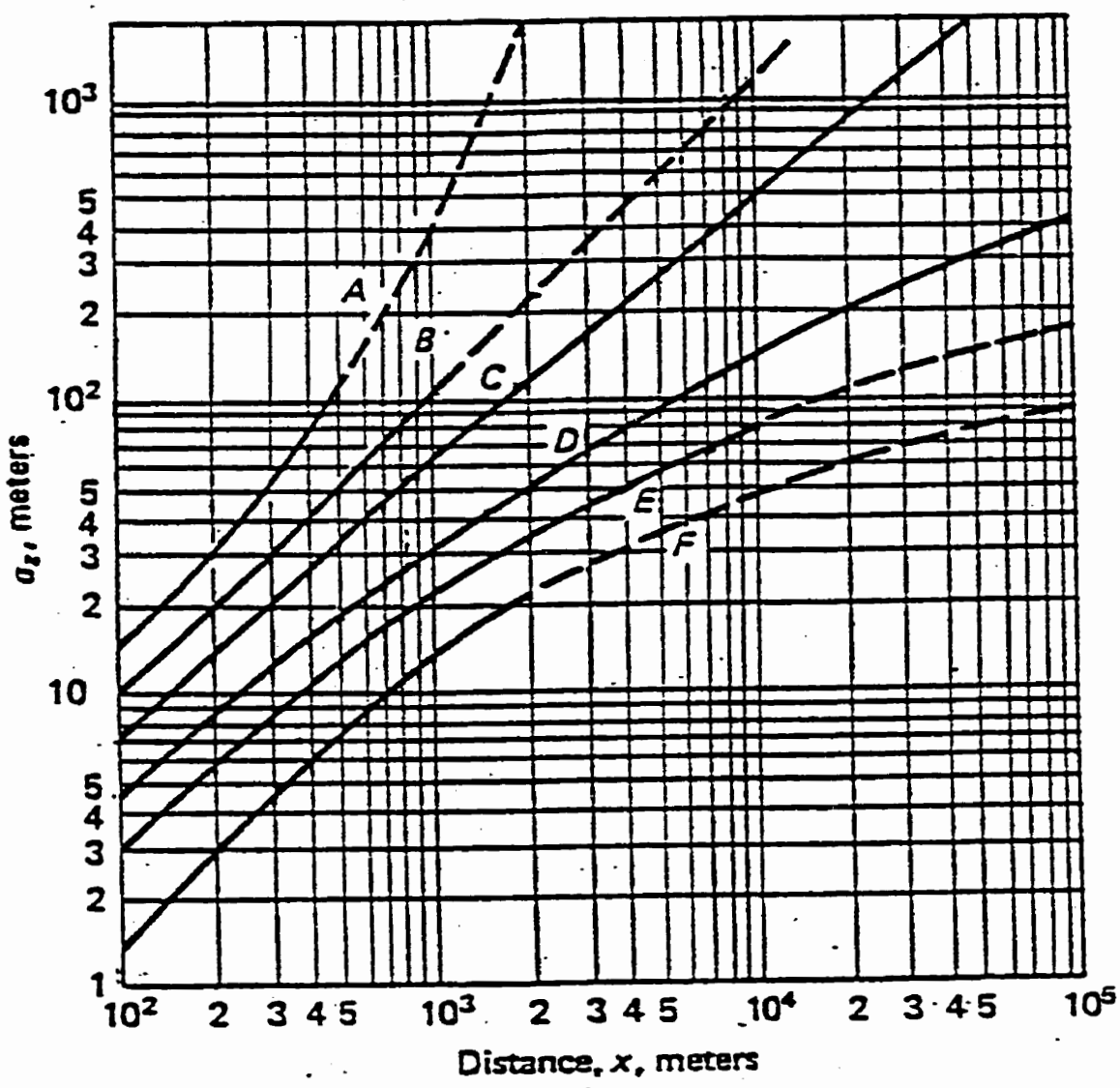

Figure I.2: Standard deviation σ_z, in the vertical direction as a function of distance downwind (Wark & Warner, 1981)

The wind direction, velocity and standard deviation were obtained from the Waterloo Landfill weather station. The data was from 1995 to 1997. Frequency distributions of these three parameters were created to generate the wind rose and joint probabilities of the direction, speed and stability. The Pasquill stability classes were determined by following the procedure presented by the USEPA (1987). The horizontal wind direction deviation and horizontal wind velocity were also obtained from the weather station at the Waterloo Landfill. Figure I.3 is the wind rose of Waterloo Landfill wind direction from 1995 to 1997. The figure indicates the prevailing wind direction (22%) at the landfill is south west (225 degrees) which is consistent with this area. Tables I.1 and I.2 show the frequency distribution for the wind speed and stability class in each wind direction sector (22.5 degrees) and the joint probability of wind direction, velocity and stability.

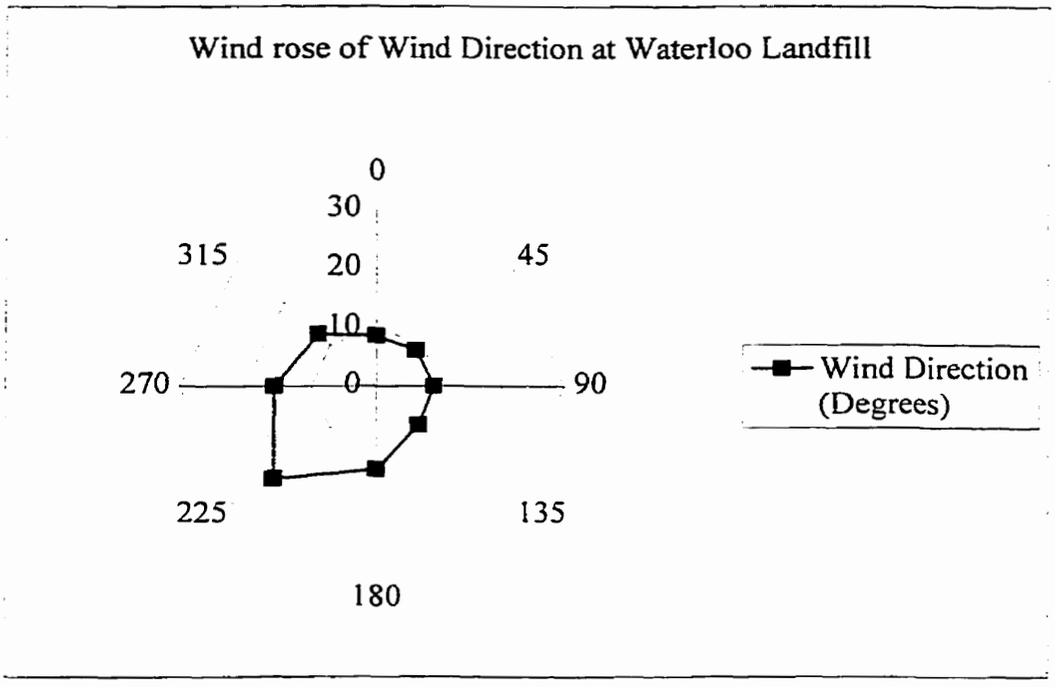

Figure I.3: Wind rose of wind direction at the Waterloo Landfill.

Table I.1 Frequency distribution and percentage of velocities (m/s) and stability classes for each wind direction sector

0-45

Velocity	*Frequency*	*Percent*
<2	398	28
2-3	350	24
3-5	495	34
5-6	117	8
>6	80	6
	1440	

Stability	*Frequency*	*Percent*
A	58	4
B	50	3
C	106	7
D	855	59
E	155	11
F	216	15
	1440	

45-90

velocity	*Frequency*	*Percent*
<2	265	19
2-3	237	17
3-5	515	38
5-6	152	11
>6	196	14
	1365	

Stability	*Frequency*	*Percent*
A	58	4
B	59	4
C	172	13
D	971	71
E	58	4
F	47	3
	1365	

90-135

velocity	*Frequency*	*Percent*
<2	291	20
2-3	344	24
3-5	551	39
5-6	142	10
>6	100	7
	1428	

Stability	*Frequency*	*Percent*
A	67	5
B	58	4
C	154	11
D	950	67
E	152	11
F	47	3
	1428	

135-180

Velocity	*Frequency*	*Percent*
<2	214	15
2-3	337	23
3-5	653	44
5-6	128	9
>6	137	9
	1469	

Stability	*Frequency*	*Percent*
A	83	6
B	89	6
C	193	13
D	950	65
E	118	8
F	36	2
	1469	

180-225

Velocity	*Frequency*	*Percent*
<2	337	15
2-3	544	24
3-5	843	38
5-6	258	12
>6	248	11
	2230	

Stability	*Frequency*	*Percent*
A	105	5
B	215	10
C	771	35
D	875	39
E	155	7
F	109	5
	2230	

225-270

Velocity	*Frequency*	*Percent*
<2	330	9
2-3	517	15
3-5	1100	32
5-6	517	15
>6	1022	29
	3486	

Stability	*Frequency*	*Percent*
A	90	3
B	85	2
C	472	14
D	2528	73
E	228	7
F	83	2
	3486	

Table I.1: cont'd

270-315 315-360

Velocity	*Frequency*	*Percent*	Velocity	*Frequency*	*Percent*
<2	332	14	<2	486	25
2-3	412	17	2-3	394	21
3-5	902	37	3-5	631	33
5-6	309	13	5-6	211	11
>6	504	20	>6	193	10
	2459			1915	

stability	*Frequency*		stability	*Frequency*	
A	99	4	A	104	5
B	105	4	B	83	4
C	509	21	C	244	13
D	1608	65	D	1162	61
E	81	3	E	205	11
F	57	2	F	117	6
	2459			1915	

Table I.2: Joint probabilities for each wind direction, wind speed and stability class for each wind direction sector

0-45			speed (m/s)			total
stability	<2	2-3	3-5	5-6	>6	
A	0.0010	0.0008	0.0012	0.0003	0.0002	0.0035
B	0.0008	0.0007	0.0010	0.0002	0.0002	0.0030
C	0.0018	0.0015	0.0022	0.0005	0.0004	0.0063
D	0.0141	0.0124	0.0176	0.0042	0.0028	0.0512
E	0.0026	0.0023	0.0032	0.0008	0.0005	0.0093
F	0.0036	0.0031	0.0044	0.0011	0.0007	0.0129
45-90			speed (m/s)			
stability	<2	2-3	3-5	5-6	>6	
A	0.0007	0.0006	0.0014	0.0004	0.0005	0.0037
B	0.0007	0.0007	0.0014	0.0004	0.0005	0.0038
C	0.0021	0.0019	0.0041	0.0012	0.0016	0.0110
D	0.0120	0.0107	0.0233	0.0069	0.0089	0.0618
E	0.0007	0.0006	0.0014	0.0004	0.0005	0.0037
F	0.0006	0.0005	0.0011	0.0003	0.0004	0.0030
90-135			speed (m/s)			
stability	<2	2-3	3-5	5-6	>6	
A	0.0009	0.0010	0.0016	0.0004	0.0003	0.0042
B	0.0007	0.0009	0.0014	0.0004	0.0003	0.0037
C	0.0020	0.0023	0.0037	0.0010	0.0007	0.0097
D	0.0122	0.0144	0.0231	0.0059	0.0042	0.0598
E	0.0020	0.0023	0.0037	0.0010	0.0007	0.0096
F	0.0006	0.0007	0.0011	0.0003	0.0002	0.0030
135-180			speed (m/s)			
stability	<2	2-3	3-5	5-6	>6	
A	0.0008	0.0012	0.0023	0.0005	0.0005	0.0053
B	0.0008	0.0013	0.0025	0.0005	0.0005	0.0056
C	0.0018	0.0028	0.0054	0.0011	0.0011	0.0122
D	0.0088	0.0138	0.0268	0.0052	0.0056	0.0602
E	0.0011	0.0017	0.0033	0.0007	0.0007	0.0075
F	0.0003	0.0005	0.0010	0.0002	0.0002	0.0023

Table I.2: cont'd

180-225			speed (m/s)			
stability	<2	2-3	3-5	5-6	>6	
A	0.0010	0.0016	0.0025	0.0008	0.0007	0.0067
B	0.0021	0.0033	0.0052	0.0016	0.0015	0.0136
C	0.0074	0.0119	0.0185	0.0057	0.0054	0.0489
D	0.0084	0.0135	0.0210	0.0064	0.0062	0.0555
E	0.0015	0.0024	0.0037	0.0011	0.0011	0.0098
F	0.0010	0.0017	0.0026	0.0008	0.0008	0.0069
225-270			speed (m/s)			
stability	<2	2-3	3-5	5-6	>6	
A	0.0005	0.0008	0.0018	0.0008	0.0017	0.0057
B	0.0005	0.0008	0.0017	0.0008	0.0016	0.0054
C	0.0028	0.0044	0.0094	0.0044	0.0088	0.0299
D	0.0152	0.0238	0.0506	0.0238	0.0470	0.1604
E	0.0014	0.0021	0.0046	0.0021	0.0042	0.0145
F	0.0005	0.0008	0.0017	0.0008	0.0015	0.0053
270-315			speed (m/s)			
stability	<2	2-3	3-5	5-6	>6	
A	0.0008	0.0010	0.0023	0.0008	0.0013	0.0063
B	0.0009	0.0011	0.0024	0.0008	0.0014	0.0066
C	0.0043	0.0054	0.0118	0.0040	0.0066	0.0321
D	0.0137	0.0170	0.0372	0.0128	0.0208	0.1015
E	0.0007	0.0009	0.0019	0.0006	0.0010	0.0051
F	0.0005	0.0006	0.0013	0.0005	0.0007	0.0036
315-360			speed (m/s)			
stability	<2	2-3	3-5	5-6	>6	
A	0.0017	0.0014	0.0023	0.0008	0.0007	0.0068
B	0.0014	0.0011	0.0018	0.0006	0.0006	0.0055
C	0.0041	0.0033	0.0053	0.0018	0.0016	0.0161
D	0.0194	0.0157	0.0252	0.0084	0.0077	0.0765
E	0.0034	0.0028	0.0044	0.0015	0.0014	0.0135
F	0.0020	0.0016	0.0025	0.0008	0.0008	0.0077
					total	1

Appendix J
Additional hourly concentration in other wind directions

Appendix J: Hourly concentration in other wind directions

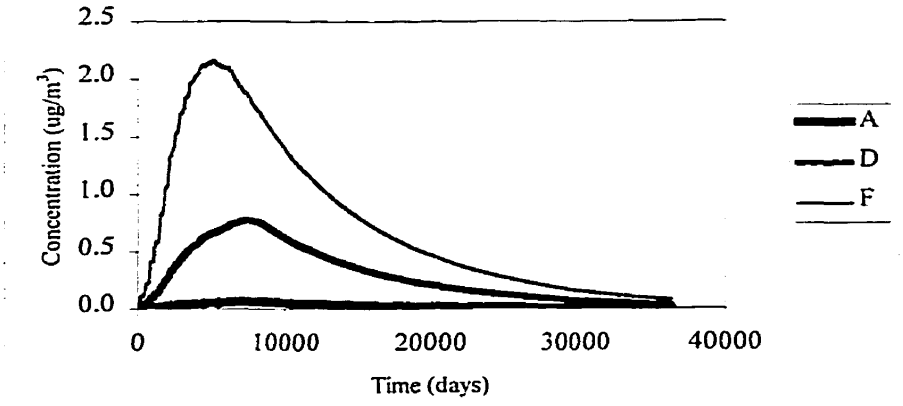

Figure J.1: Hourly vinyl chloride concentration at 3 stability classes and wind direction of 0 degrees on 1 km boundary line.

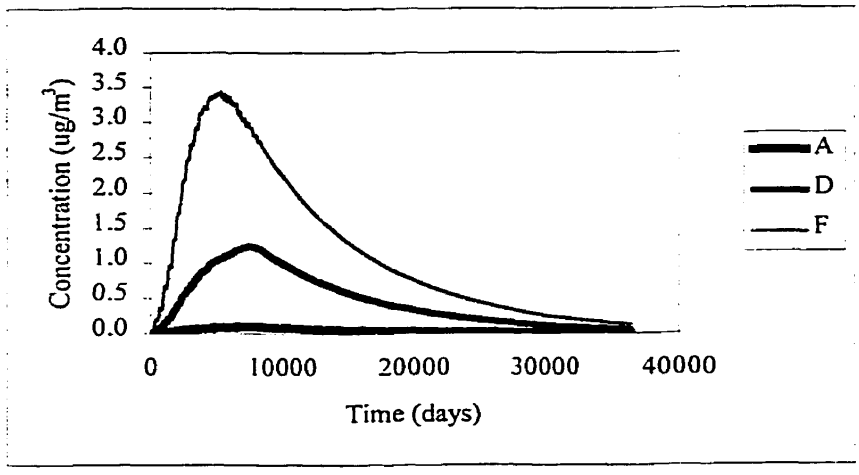

Figure J.2: Hourly H_2S concentration at 3 stability classes and wind direction of 0 degrees on 1 km boundary line.

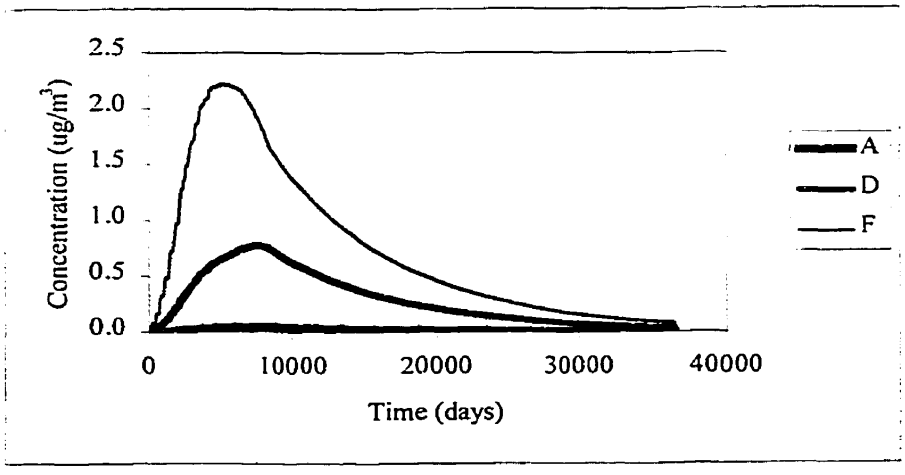

Figure J.3: Hourly vinyl chloride concentration at 3 stability classes and wind direction of 90 degrees on 1 km boundary line.

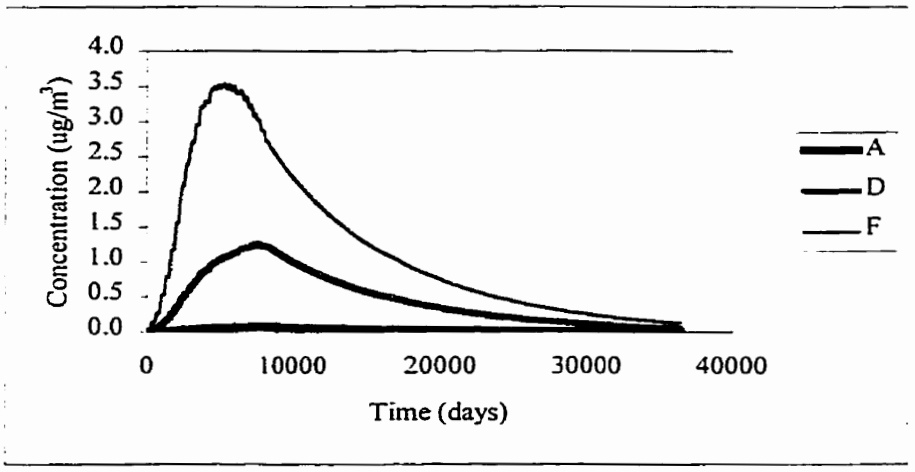

Figure J.4: Hourly H_2S concentration at 3 stability classes and wind direction of 90 degrees on 1 km boundary line.

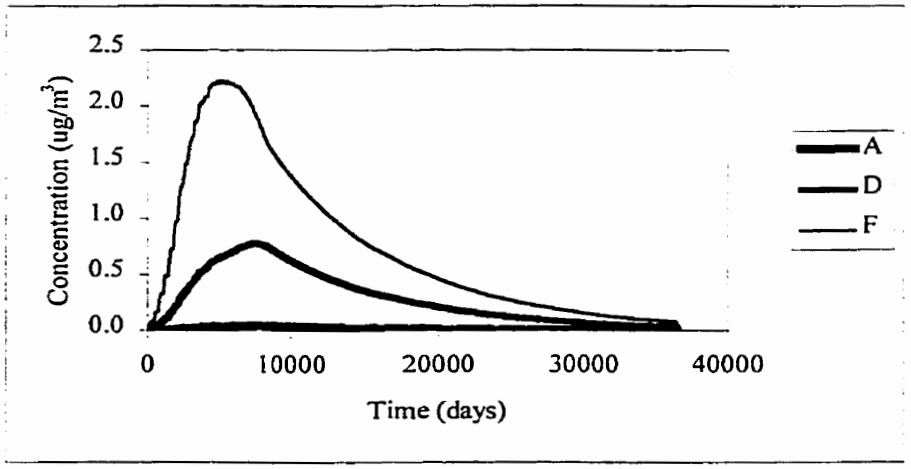

Figure J.5: Hourly vinyl chloride concentration at 3 stability classes and wind direction of 180 degrees on 1 km boundary line.

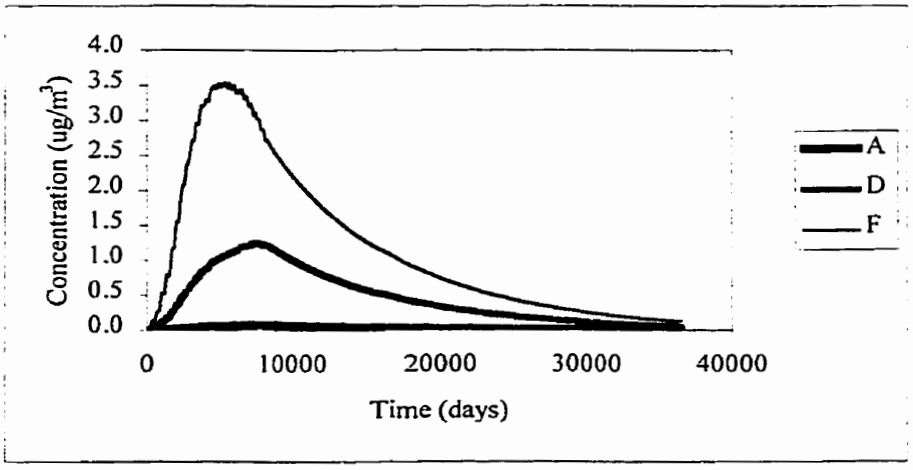

Figure J.6: Hourly H_2S concentration at 3 stability classes and wind direction of 180 degrees on 1 km boundary line.

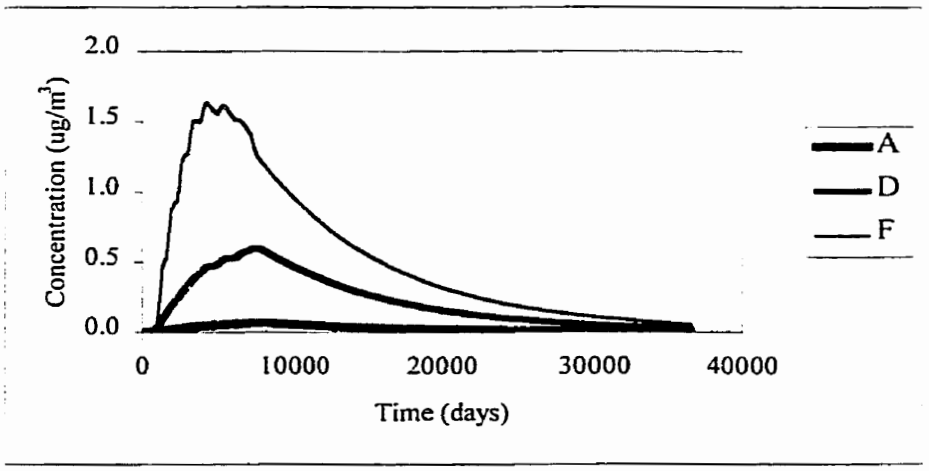

Figure J.7: Hourly vinyl chloride concentration at 3 stability classes and wind direction of 270 degrees on 1 km boundary line.

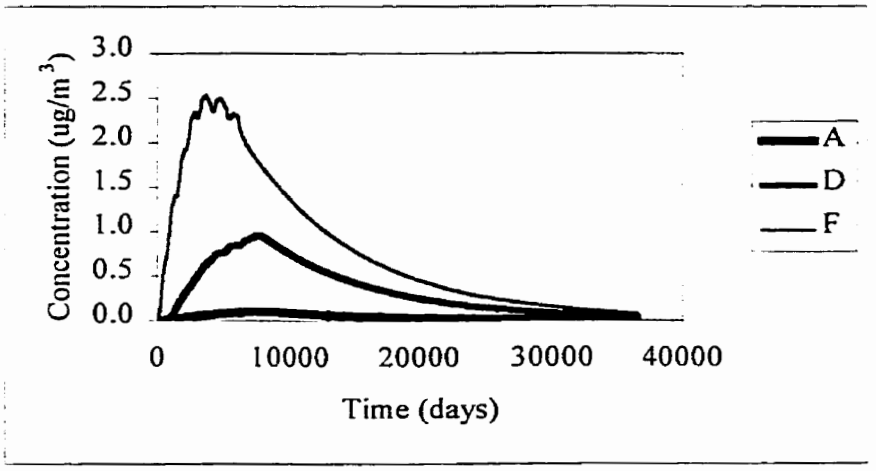

Figure J.8: Hourly H_2S concentration at 3 stability classes and wind direction of 270 degrees on 1 km boundary line.